Polymer, Particle, Surfactant Interactions

Sarah Jane Mears.

A thesis submitted to the University of Bristol in accordance with the requirements for the degree of Doctor of Philisophy in the Faculty of Science, School of Chemistry.

November 1996.

Abstract

Dynamic light scattering, small-angle neutron scattering and nuclear magnetic resonance spectroscopy measurements have been performed on aqueous silica and polystyrene latex dispersions containing physisorbed poly(ethylene oxide) in the presence of the surfactant sodium dodecyl sulphate. From the dynamic light scattering measurements, it appeared that near complete desorption of the polymer occurred around the normal critical micelle concentration of the pure surfactant. However, at very high surfactant concentrations, the apparent hydrodynamic thickness returned to its initial value in the absence of surfactant. Similarly, the small-angle neutron scattering measurements suggested that as the normal critical micelle concentration of the surfactant was approached, very thin layers were formed. It was possible to obtain the volume fraction profiles of the adsorbed polymer layer, along with information on the structure of the surfactant micelles. Two types of SDS structure were observed, one corresponding to SDS existing bound to bulk polymer and the other to SDS bound to adsorbed polymer.

Small-angle neutron scattering measurements were performed on an aqueous polymeric microgel in the presence of the surfactant sodium dodecyl sulphate. Two surfactant concentrations were used. Through selective deuteration of the solvent, the different components of the system could be made 'invisible' to the neutrons. It was found that the microgel was swollen in the presence of surfactant, whilst the incorporated surfactant micelles tended to be smaller in size. At the lower surfactant concentration it is suggested that in the presence of the microgel, the surfactant exists in monomeric form rather than in micellar form.

A preliminary investigation into the solution and adsorption properties of the commercial polyelectrolyte Quatrisoft LM in the presence of surfactant has been performed using small angle neutron scattering measurements. These measurements showed that the structure of SDS micelles in the bulk were significantly affected by the presence of the polyelectrolyte. The micellar radius was significantly increased. It was also observed that the presence of surfactant significantly disrupted the adsorbed layer.

Declaration.

Except in cases where due acknowledgement has been made, the work presented in this thesis is the sole work of the author carried out between October 1993 and November 1996. It has not been presented for any other degree.

Sarah Mears.

Sarah Mears.

As a result of this study, the following publications have been made;

Adsorption Studies on Mixed Silica, Polymer, Surfactant Systems
T. Cosgrove, S. J. Mears, L. Thompson, I. Howell
ACS Symposium Series **1995** 615 196

The Structure of Sodium Dodecyl Sulphate Bound to a Poly(NIPAM) Microgel.
S. J. Mears, Y. Deng, T. Cosgrove, R. Pelton
Accepted by Langmiur

Dynamic Light Scattering and Small-Angle Neutron Scattering Studies on the Poly(ethylene oxide), Sodium Dodecyl Sulphate, Polystyrene Latex System.
S. J. Mears, T. Cosgrove, T. Obey, L. Thompson, I. Howell.
Submitted to Colloids and Surfaces.

Acknowledgements.

I would firstly like to thank my advisor, Dr. T. Cosgrove for all of his help, support and constant belief that I really did know what I was doing.

Thanks must also go Unilever, Port Sunlight for funding this project and in particular to Laurie Thompson and Ian Howell for all of their interest and input. A mention must go to Jeff, Ed and the NMR department for not strangling me when every piece of equipment I approached became fatally ill!

My appreciation goes to Steve King at the Rutherford Appleton Laboratories, Didcot for his endless help and enthusiasm during neutron scattering experiments.

Finally, I would like to acknowledge all of the people here in Bristol, past and present, who've helped make my last three years so enjoyable; especially Nick, Tim, Juliet, Cheryl, Pete, Siân, John, Ian, Robin and the BV-Boys for being so BV-ish!

Contents

List Of Tables and Figures ix)

List of Symbols xvi)

Chapter 1. - Introduction.

1.1 Colloidal dispersions. 2
1.1.1 Colloidal silica. 2
1.1.2 Polystyrene latex. 2
1.2. Surfactants. 3
1.2.1 Sodium dodecyl sulphate. 3
1.3 Polymers. 4
1.3.1 Homopolymers. 4
1.3.2. Polyelectrolytes. 4
1.3.3 Copolymers. 5
1.3.4 Polymer microgels. 6
1.4 Polymer Surfactant interactions. 6
1.4.1 Poly(ethylene oxide) / SDS 8
1.4.2 Polyelectrolytes/SDS 12
1.4.3 Poly(NIPAM)/SDS. 13
1.5 Adsorption to a solid substrate. 14
1.5.1 Adsorption of PEO 15
1.5.2 Adsorption of Quatrisoft LM. 16
1.5.3. Mixed adsorption. 17
References 22

Chapter 2. - Polymer And Surfactant Theory

2.1 Polymers in solution 23
2.1.1 Dilute polymer solutions 23
2.1.1.1 Conformation. 23
2.1.2 Models for polymer chains in solution. 24
2.1.2.1 Lattice model. 24
2.1.2.2 Continuum model. 25
2.1.3 Chain dimensions. 25
2.1.4 Semi-dilute polymer solutions. 29
2.1.4.1 Flory-Huggins theory 30
2.1.4.2 De Gennes scaling theory 33
2.1.5 Gels. 34
2.1.6 Polyelectrolytes 34

2.2 Surfactants in solution 35
2.2.1 Classification of surfactants. 35
2.2.2 Interfacial properties at the air/water interface. 36
2.2.3 The formation of micelles. 37
2.3 Polymers at interfaces. 38
2.3.1 The process of adsorption. 38
2.3.2 Adsorption isotherms. 39
2.3.3 Volume fraction profiles. 42
2.3.4 Variation of measured/theoretical parameters. 43
2.3.5 Polyelectrolyte adsorption 44
2.3.6 Models of adsorption. 44
2.4 Surfactant adsorption. 49
References 52

Chapter 3 - Nuclear Magnetic Resonance Spectroscopy.
3.1 Properties of the nucleus. 54
3.2 Application of an external magnetic field. 55
3.3 The Bloch equations. 58
3.4 The rotating frame of reference. 60
3.5 The origin of relaxation. 62
3.6 Relaxation mechanisms 63
3.7 Free induction decay. 64
3.8 The measurement of T_1 by the inverse recovery method 65
3.9 Measurement of T_2 by the spin-echo technique. 65
3.10 The Carr-Purcell sequence. 66
3.11 The CPMG Sequence. 67
3.12 The application of NMR to solvent relaxation measurements. 67
3.13 Pulsed field gradient methods. 68
3.13.1 Derivation 69
3.13.2 Effect of pulse sequence on Nuclear Spins 72
3.13.3 LED sequence 75
3.13.4 Restricted diffusion 75
References 76

Chapter 4. - Small-Angle Neutron Scattering.
4.1 The neutron. 78
4.2 The scattering vector. 79
4.3 Neutron scattering length density. 80
4.4 Neutron instrumentation and data reduction. 81
4.5 Scattering from spherical particles. 83
4.5.1 Polydispersity effects. 84
4.5.2 Guinier analysis. 85
4.5.3 Porod's law. 86
4.5.4 Concentrated dispersions. 86
4.6 Particles with adsorbed layers. 87
4.7 Fluctuations in the adsorbed layer. 88

4.8 The incoherent background. 90
4.9 Data analysis. 90
4.9.1 At zero contrast for the particle. 90
4.9.2 Data analysis when all components are visible. 94
References 96

Chapter 5. - Experimental
5.1 Materials. 97
5.1.1 Substrates. 97
5.1.2 Polymers. 99
5.1.3 Surfactant. 100
5.1.4 Poly(NIPAM). 100
5.2 Adsorption isotherms. 101
5.3 Photon correlation spectroscopy. 104
5.3.1 Correlation times, choice of sample time (τ) 106
5.4 Nuclear magnetic resonance spectroscopy. 107
5.5 Small-angle neutron scattering. 110
References 113

Chapter 6. - Adsorption and Hydrodynamic Thickness Results on PEO and SDS.
6.1. Adsorption isotherms. 114
6.2. Background PCS experiments. 117
6.3 Hydrodynamic thickness measurements on PEO, SDS and silica 123
6.4 Measurements on PEO, SDS and polystyrene latex 129
6.5 Interpretation and discussion of results. 132
References 134

Chapter 7. - NMR Results on PEO and SDS.
7.1 Solvent relaxation measurements. 135
7.1.1. Individual components. 135
7.1.2 Binary mixtures. 140
7.1.3 Mixtures of all three components 145
7.2 Self-diffusion measurements. 147
7.2.1 Pure SDS solutions. 147
7.2.2 SDS and PEO in solution. 152
7.2.2.1 Self-diffusion of SDS 152
7.2.2.2 Self-diffusion of PEO 155
7.2.3 Mixtures of all three components 158
7.2.3.1 Self-diffusion of SDS 158
References 164

Chapter 8. - SANS Results on PEO and SDS.
8.1 Introduction 165
8.2 Pure components. 166
8.2.1 Silica dispersions. 166
8.2.2 PEO in solution 170
8.2.3 SDS in solution. 173
8.3 Binary mixtures 178
8.3.1 Mixtures of PEO and particles. 178
8.3.2 Mixtures of PEO and SDS in D_2O 183
8.3.3 Dispersions of PSL and SDS. 188
8.4 Mixtures of PEO, SDS and PSL. 190
8.4.1 PEO visible, SDS and PSL invisible. 190
8.4.2 PSL matched, PEO and SDS visible 194
8.4.3 PEO and PSL visible, with SDS 197
8.5 Mixtures of PEO, SDS and silica 199
8.6 Conclusions 202
References 203

Chapter 9. - Comparisons with Other Systems.
9.1 Poly(NIPAM) microgel and SDS 204
9.1.1. Scattering theory relevant to the poly(NIPAM) microgel 204
9.1.2 Binding isotherms 206
9.1.3 SANS measurements on the pure microgel 208
9.1.4 Mixtures of SDS and poly(NIPAM) microgel - poly(NIPAM microgel visible., SDS invisible 208
9.1.5 Mixtures of SDS and poly(NIPAM) microgel - poly(NIPAM microgel visible., SDS visible 212
9.2 Quatrisoft LM, SDS and PSL 216
9.3 Polystyrene / poly(vinylpyridine) and SDS 223
9.3.1 UV absorbance studies 223
9.3.2 Photon correlation spectroscopy measurements 225
9.3.3. Small-angle neutron scattering measurments 228
References 232

Chapter 10. - Conclusions.
10.1 PEO/SDS Systems. 233
10.2 The Structure of SDS Bound to Poly(NIPAM) 234
Suggestions for further Work 235

Appendix A - Raw NMR self-diffusion data 235

List of Tables and Figures.

Table 5.1. Calibration data for PEO and SDS using the tannic acid method.

Table 5.2. Scattering length densities of the individual components examined in this thesis.

Table 6.1. Effect of various alcohol's on the hydrodynamic thickness of adsorbed PEO layers.

Table 7.1. Measured and calculated values for the diffusion coefficient of SDS as a function of concentration.

Table 7.2. Values for the diffusion coefficient of micellar SDS in the presence of 0.5 % w/w PEO as a function of concentration.

Table 7.3. Variation in parameters obtained for data fitting dependant upon imposed constraints.

Table 8.1. Parameters used to model the SDS scattering.

Table 8.2. Typical fitted parameters for SDS using the Hayter-Penfold model.

Table 8.3. Comparison of techniques for the parameters obtained for an adsorbed PEO layer.

Table 8.4. Comparison of parameters for adsorbed polymer layers in the presence of SDS.

Table 9.1. Binding Data for the two SDS concentrations used in the SANS Experiments.

Table 9.2. Typical Fitted Parameters for poly(NIPAM) using the Debye Model.

Table 9.3. Effect of SDS on the UV absorbance of PS-PVP^+.

Table 9.4. Hydrodynamic thickness as a function of initial polymer concentration measured by PCS.

Table 9.5. Hydrodynamic thickness as a function of initial polymer concentration at low coverages - measured by PCS.

Table 9.6. Parameters for adsorbed PS-PVP^+ as a function of SDS concentration.

Figure 1.1. Schematic representation of a polymer-surfactant interaction
Figure 1.2. "Phase diagram" for the PEO/SDS system in aqueous solution.

Figure 2.1. Schematic representation of a lattice model for polymer chains.
Figure 2.2. Schematic representation of a continuum model for polymer chains.
Figure 2.3. Schematic representation of the mixing of polymer segments.
Figure 2.4. Schematic representation of the hydrodynamic radius of a polymer chain
Figure 2.5. Effect of temperature on χ.
Figure 2.6. Effect of temperature on χ; Incorporating free volume effects
Figure 2.7. Scaling for a polymer where N=40.
Figure 2.8. The processes which lead to polymer adsorption
Figure 2.9. The structure of an adsorbed polymer layer.
Figure 2.10. An adsorption isotherm for a polymer adsorbed onto a surface
Figure 2.11. Schematic representation of a typical volume fraction profile
Figure 2.12. Comparison of adsorption isotherms of monodisperse and polydisperse polymers.
Figure 2.13. Adsorption isotherm of a surfactant

Figure 3.1. The precession of a magnetic moment $\bar{\mu}$ about a fixed magnetic field, B_0.
Figure 3.2. The precession of an ensemble of identical magnetic moments of nuclei with $I = ½$. The net macroscopic magnetisation is orientated along the z axis.
Figure 3.3. The Stejskal and Tanner sequence for measuring diffusion coefficients.
Figure 3.4. Effect of the diffusion experiment on nuclear spins.

Figure 4.1. Schematic representation of the scattering from a particle
Figure 4.2. logI(Q) against Q^2 for spherical particles calculated using equation 4.11 for 25 nm and 100 nm spheres
Figure 4.3. A schematic diagram of a coherent scattering event.
Figure 4.4. Schematic diagram of an adsorbed polymer chain and the corresponding volume fraction profile.

Figure 5.1. TEM micrograph of Snowtex ZL.
Figure 5.2. TEM micrograph of polystyrene latex.
Figure 5.3. Calibration data for PEO using the tannic acid method
Figure 5.4. Calibration data for Quatrisoft LM.
Figure 5.5. Schematic diagram of the PCS equipment used in this study.
Figure 5.6. Stack plot of intensity as a function of δ for 0.4 % w/w SDS and 0.5 % w/w PEO in D_2O.
Figure 5.7. Plot of ln attenuation against β for 1.0 % w/w SDS.
Figure 5.8. Schematic layout of the D17 instrument at the ILL facility.

Figure 6.1. The conventional adsorption isotherms for PEO on silica determined using the phosphomolybic acid method. The isotherm is depicted in the absence of surfactant (○) and with an added SDS concentration of 30 ppm (●).

Figure 6.2. The conventional adsorption isotherm for PEO on polystyrene latex determined using the phosphomolybic acid method.

Figure 6.3. A typical decay profile of polystyrene latex as a function of correlator channel.

Figure 6.4. The diffusion coefficient of a silica dispersion as a function of concentration at 25 °C.

Figure 6.5. The hydrodynamic diameter of SDS adsorbed onto polystyrene latex and onto silica as a function of SDS concentration. The diameter of the bare silica particle was 94.09 ± 1.00 nm and the bare polystyrene latex particle was 162.60 ± 1.00 nm.

Figure 6.6. The hydrodynamic thickness (δh) as a function of adsorbed amount for 200,000 molecular weight PEO on silica. The values of adsorbed amount were extracted from the data in figure 6.1.

Figure 6.7. The effect on the hydrodynamic thickness of an aqueous dispersion of silica and PEO by the addition of SDS. The concentration of both the silica and the polymer remained fixed, whilst the surfactant concentration was varied up to 10,000 ppm.

Figure 6.8. The hydrodynamic thickness of an adsorbed PEO layer as a function of time for various fixed SDS concentrations

Figure 6.9. The effect of temperature on the adsorbed layer was investigated. In all of these samples, the concentrations of each of the components remained fixed. SDS in the absence of polymer (○). PEO in the absence of SDS (□). PEO with 2,000 ppm added SDS (Δ).

Figure 6.10. The effect on the hydrodynamic thickness of an aqueous dispersion of silica and PEO by the sequential addition of SDS.

Figure 6.11. The effect on the hydrodynamic thickness of an aqueous dispersion of PSL and PEO by the addition of SDS. The concentration of both the PSL and the polymer remained fixed, whilst the surfactant concentration was varied up to 10,000 ppm.

Figure 6.12 The effect of SDS on the hydrodynamic diameter of a grafted PEO layer. The substrate is a polystyrene latex, the concentration of which is maintained constant

Figure 7.1. Shows both the specific longitudinal (R_1^{sp}) and specific transverse (R_2^{sp}) relaxation rates of the solvent for aqueous dispersions of the silica Snowtex 50 as a function of solids concentration in H_2O. All of the T_1 measurements were performed at 40°C due to instrumental limitations. The relaxation rates have been normalised against H_20 for all of these measurements. Also shown is the transverse relaxation rate of the solvent for

Snowtex 40 which is identical in composition to Snowtex 50 but with a much smaller radius.

Figure 7.2 Specific area against relaxation rate enhancement for two different sized silica particles.

Figure 7.3 The specific longitudinal and transverse relaxation rates of the solvent in the presence of the surfactant SDS as a function of concentration in H_2O. The data have been normalised against water.

Figure 7.4 The specific transverse relaxation rate of the solvent for 114,000 molecular weight PEO in H_2O as a function of polymer concentration (●). Also shown is the corresponding data for PEO (○) in the presence of 5.0 % w/w Snowtex 40 as a function of initial polymer concentration. The data for the adsorbed PEO have been normalised against the silica dispersion.

Figure 7.5 Shows the specific relaxation rate data for the adsorbed polymer from Figure 7.4 plotted against the adsorbed amount of the polymer.

Figure 7.6 The bound fraction against adsorbed amount for 114,000 molecular weight PEO adsorbed onto 5.0 % w/w Snowtex 40.

Figure 7.7 The specific relaxation rate of the solvent for SDS with 5.0 % w/w silica as a function of SDS concentration. Also shown is the data for SDS alone as a function of SDS concentration.

Figure 7.8 The effect of mixtures of PEO and SDS on the specific transverse relaxation rate of the solvent (●). The polymer concentration is maintained at 0.5 % w/w and the SDS concentration varied. Also shown is the data for SDS alone (○).

Figure 7.9 The specific relaxation rate of the solvent for mixtures of PEO, SDS and silica (○). In all of these samples the polymer concentration is maintained at 0.5 % w/w, the silica at 5.0 % w/w and the SDS concentration varied from 0 - 1.0 % w/w.

Figure 7.10 The measured self-diffusion coefficients (D_s) of SDS a function of concentration. The solvent in all instances was D_2O and these diffusion coefficients were calculated using a value of Ds for water of 2.23×10^{-9} m^2s^{-1}.

Figure 7.11 The measured self-diffusion coefficients for SDS in the presence of 0.5 % w/w PEO of molecular weight 100,000. The solvent in all instances was D_2O. Also shown for comparison is the data for SDS alone.

Figure 7.12 The viscosity data for 0.5 % w/w PEO of molecular weight 100,000 as a function of molecular weight.

Figure 7.13 The measured values of D_s for PEO of molecular weight 100,000 as a function of surfactant concentration. The solvent was D_2O.

Figure 7.14 The measured diffusion coefficient of SDS as a function of concentration in the presence of 0.5 % w/w PEO of molecular weight 100,000 Snowtex 50. The silica is at 5.0 % w/w and the solvent is D_2O.

Figure 7.15 The measured diffusion coefficient of 0.5 % w/w PEO of molecular 100,000 in the presence of SDS and 5.0 % w/w silica as a function of SDS concentration.

Figure 7.16 DLS data on the same sample used for the PFG-NMR measurements.

Figure 8.1. The scattering pattern arising from a series of silica dispersions at 5.0 % w/w as a function of H_2O/D_2O ratio.

Figure 8.2 Plot of $Q^6I(Q)$ against Q^6 to obtain the incoherent background level

Figure 8.3 The square root of the initial intensities from figure 8.1 plotted as a function of H_2O/D_2O ratio

Figure 8.4 The scattering from a silica dispersion at a H_2O/D_2O ratio of 30/70. Also shown in this figure are the Guinier region and the Porod region from which estimates can be made of the radius of gyration of the particle and the surface area to volume ratios respectively.

Figure 8.5 The scattering from 0.5 % w/w PEO in D_2O.

Figure 8.6 Modelled scattering from a 1.0 % w/w H-SDS in D_2O broken down into its form factor and structure factors.

Figure 8.7 Models of the scattering obtained for H-SDS in D_2O as a function of volume fraction (ϕ).

Figure 8.8 Modelled scattering from H-SDS in D_2O as a function of micellar radius.

Figure 8.9 Scattering from H-SDS in D_2O at 0.3 % w/w and 1.0 %w/w. Also shown are the fits obtained from these data using the Hayter-Penfold model.

Figure 8.10. SANS data for a silica particle with adsorbed PEO layer under "contrast match" conditions for the particle. Under these conditions the particle is effectively invisible to the neutrons and only the scattering pattern arising from the adsorbed layer can be seen.

Figure 8.11 SANS data for PEO adsorbed onto PSL. Also shownis the fit to this data set, according to equation 4.22 given in the SANS theory chapter (Chapter 4). This fit was obtained by fixing the fluctuation exponent to $-\frac{4}{3}$ and fits were repeated until a minimum in the standard deviation of the fit was obtained.

Figure 8.12 Plot of $Q^{4/3}I(Q)$ against $Q^{4/3}$ for PEO adsorbed onto PSL under conditions of "contrast match" for the particle. The slope of this plot corresponds to the incoherent background level and the intercept on the $Q^{4/3}I(Q)$ axis to the fluctuation intensity.

Figure 8.13 The corresponding volume fraction profiles, dependant upon the choice of fluctuation exponent obtained from the data in **Figure 8.11.**

Figure 8.14 SANS from the PEO and D-SDS in D_2O as a function of SDS

concentration plotted on a log-log scale.

Figure 8.15 Shows is the scattering pattern from H-SDS and PEO in solution as a function of surfactant concentration

Figure 8.16 Gives a measure of the effect of SDS on PEO can be obtained by subtracting the data in **figure 8.14** from that in **figure 8.15**. Also shown on **figure 8.16** are the fits obtained from the data fitting of the 0.3 % w/w and 1.0 % w/w SDS in D_2O.

Figure 8.17 SANS of "adsorbed" SDS;

Figure 8.18 Shows the SANS from the adsorbed polymer layer as a function of SDS concentration. The SDS used for these samples is a mixture of H-SDS and D-SDS to the same scattering length density as the solvent (and indeed the PSL); thus only the scattering from the layer is visible. The error bars are not shown on these plots in an attempt to clarify the chart data. The scattering at very low values of Q is shown in the insert. The incoherent background has been subtracted from all of these data sets. Also shown in the main figure are the fits obtained for these data.

Figure 8.19 The corresponding volume fraction profiles for the scattering in **figure 8.18.** Absent from this plot is the volume fraction profile for the sample with 1.0 % w/w SDS due to problems with fitting the data.

Figure 8.20 The scattering from the surfactant in the presence of an adsorbed polymer layer. The surfactant concentration is 1.0 % w/w. The substrate has been "matched out" and the scattering from the polymer layer subtracted (data in **figure 8.11**). Unfortunately, no allowance can be made for any interference term between the layer and the surfactant and therefore in this instance it must be assumed to be insignificant. Also present in **figure 8.20** is the scattering pattern from SDS

Figure 8.21 The scattering from the surfactant in the presence of an adsorbed polymer layer as a function of surfactant concentration.

Figure 8.22 The scattering of PEO, D-SDS and PSL as a function of D-SDS concentration. The solvent is D_2O.

Figure 8.23 The scattering of PEO, H-SDS and PSL as a function of D-SDS concentration. The solvent is D_2O.

Figure 8.24 The scattering of PEO, SDS and silica as a function of SDS concentration.

Figure 9.1 The binding curve of SDS to a poly(NIPAM) microgel at 23 °C. Shown in the inset is the same data plotted on a log-log scale to accentuate the effects at low concentrations. The position of the concentrations of SDS used for the SANS experiment are also shown.

Figure 9.2 The scattering pattern arising from the poly(NIPAM) as a function of SDS concentration. The SDS is deuterated, the

poly(NIPAM) hydrogenous and the solvent is D_2O. Under these conditions the scattering from the SDS is invisible

Figure 9.3 SANS data for poly(NIPAM) in the absence of SDS plotted as log I(Q) against log Q. Shown on this figure is the Q^{-4} and Q^{-2} dependence.

Figure 9.4 .The effect of poly(NIPAM) on 0.3 % w/w SDS. The SDS is deuterated and the poly(NIPAM) is hydrogenous. The solvent is 82 % H_2O/ 18 % D_2O. Under these conditions the scattering from the poly(NIPAM) is invisible. Also shown for comparison is the scattering from SDS alone at this contrast.

Figure 9.5 The effect of poly(NIPAM) on 1.0 % w/w SDS. The SDS is deuterated and the poly(NIPAM) is hydrogenous. The solvent is 82 % H_2O/ 18 % D_2O. Under these conditions the scattering from the poly(NIPAM) is invisible. Also shown for comparison is the scattering from SDS alone at this contrast.

Figure 9.6 Adsorption isotherm of Quatrisoft LM physically adsorbed onto polystyrene latex.

Figure 9.7 SANS of Quatrisoft LM in D_2O with and without D-SDS

Figure 9.8 SANS of Quatrisoft LM in D_2O with and without H-SDS

Figure 9.9 SANS of Quatrisoft LM physically adsorbed onto PSL.

Figure 9.10 SANS of Quatrisoft LM physically adsorbed onto PSL as a function of SDS concentration

Figure 9.11 Adsorption isotherm of PS-PVP^+ on Snowtex ZL

Figure 9.12 SANS of PS-PVP^+ physically adsorbed onto PSL as a function of SDS concentration

Figure 9.13 Volume fraction profiles of PS-PVP^+ physically adsorbed onto PSL as a function of SDS concentration.

List of Symbols and Abbreviations

Chapter 1.

CMC	Critical micelle concentration.
DLS	Dynamic light scattering
M	Molar
PCS	Photon correlation spectroscopy
PEO	Poly(ethylene oxide)
PFGSE-NMR	Pulsed field-gradient spin echo NMR
PSL.	Polystyrene latex
NMR	Nuclear magnetic resonance
SANS	Small-angle neutron scattering
SDS	Sodium dodecyl sulphate
χ	Flory parameter
χ_s	Flory-surface parameter

Chapter 2

A	Surface area
C	Concentration
c(m)	The number of self-avoiding walks with m contacts with surface.
the CMC	Critical micelle concentration
E_1^a	Adsorption energy of a solvent molecule
E_2^a	Adsorption energy of a polymer segment
E_{pp}	Energy of polymer-polymer interactions.
E_{ps}	Energy of polymer-solvent interactions.
E_{ss}	Energy of solvent-solvent interactions.
F	Free energy
G_{ads}	Gibbs free energy of adsorption
K	Equilibrium constant
K^*	Constant related to the heat of adsorption
k_B	Boltzmann's constant
l	Bond length
m	Number of monomer units
<m>	The average number of contacts with the surface
M	Mass of polymer at the interface
M_z	The Mark-Houwink parameter
n	Constant related to the distribution of surface site energies.
N	Number of bonds
r	End-to-end distance of a polymer chain
R	Molar gas constant
R_g	Radius of gyration
R_g°	Unperturbed radius of gyration
R_h	Hydrodynamic radius

RMS	Root-mean square dimensions
s	Distance from the centre of mass of a polymer chain
S	Entropy
T	Temperature
U	Internal energy
V	Volume
x	Chain length of polymer
x_2	Mole fraction of polymer
Z	Co-ordination of the lattice
α	An expansion factor which can relates R_g and R_g°
γ	Surface tension
Γ	Adsorbed amount
Γ_x	Surface concentration of species x
Γ^*	Adsorbed amount at which polymer chains begin to touch.
$[\eta]$	Measured intrinsic viscosity
θ	Bond angle
λ_1	Lattice parameter; $\lambda_1 Z$ is the number of neighbours a site has in each of the adjacent layers.
μ	Chemical potential
$\mu^\varnothing$	Standard chemical potential
ν	Scaling exponent
ρ	Density
σ	Steric factor
ϕ	Volume fraction
ϕ^*	Volume fraction at which polymer coils just begin to touch.
χ	Flory parameter
χ_e	The contact energy of a chain
χ_s	The Flory-surface parameter
Ω	The number of conformations a polymer chain may attain.
Φ	Viscosity empirical constant which = 3×10^{22} if R_h is in nm

Chapter 3

A	Amplitude
B	Magnetic field
E	Energy
G_z	Magnetic field gradient across the sample
h	Plank's constant
I	Nuclear spin
$\tilde{I}$	Angular momentum
k_B	Boltzmann constant
M	Bulk magnetisation
m_z	Spin quantum number
N	Numbers of nuclei
P_b	Fraction of protons in the bound environment
R_1	Longitudinal relaxation rate

R_2	Transverse relaxation rate
T	Absolute temperature.
T_1	Longitudinal relaxation time
T_2	Transverse relaxation time
t_p	Time for which pulse is applied
Δz	Position of the nuclear spin from the centre of the sample tube
δ	Time during which a field gradient pulse is applied
γ	Magnetogyric ratio
Δ	Time over which a PFG experiment is performed.
θ	Angle.
$\bar{\mu}$	magnetic moment
τ	Time delay
ω	frequency
ω_o	Larmor precession frequency

Chapter 4

A	Instrument constant
A_s	Surface area per unit volume
b	Scattering length
b_{inc}	The incoherent background
d	Sample thickness.
h	Plank's constant.
$\tilde{I}$	Scattering arising from fluctuations in the adsorbed layer
I_{corr}	Corrected intensity
$I_{ll}(Q)$	Scattering intensity arising from an adsorbed layer
$I_{pl}(Q)$	Particle-layer interference term.
$I_{pp}(Q)$	Scattering intensity from a particle
I_s	Intensity from the sample
I_w	Intensity from the standard sample
m	Molar mass.
M_s	Sample monitor count
M_w	Standard monitor count
N_p	Number of particles
P(Q)	Geometric interference factor (or form factor)
Q	Scattering vector
r	Particle radius
R_g	Radius of gyration
S(Q)	Structure factor
t	Maximum extent of the adsorbed layer.
T_s	Transmission of the sample
T_w	Transmission of water
V	Molecular volume.
V_p	Volume of the particle.
V_R	Electrostatic repulsive potential
z	Distance normal to the surface.

Γ	Adsorbed amount
ε_o	Permittivity of a vacuum
ε_r	Relative permittivity of the medium
θ	Angle
κ	Reciprocal Debye Huckel electrical double layer thickness
λ	Wavelength.
ν	Velocity
ξ	Characteristic correlation length.
ρ	Scattering length density
ρ_m	Physical density
σ	Second moment of an adsorbed layer
$\phi(z)$	Volume fraction of polymer at a distance z from the interface
ψ_S	Surface electrostatic potential.

Chapter 5

A	Surface area
A_0	Integrated intensity in the absence of a field gradient pulse
A_δ	Integrated intensity for a given field gradient pulse.
C_{eqm}	Equilibrium concentration
C_{init}	Initial concentration
D_s	Self diffusion coefficient.
G	Field gradient strength.
G'	Auto correlation function
I(t)	Fluctuating light intensity as a function of time
γ	Magnetogyric ratio
Γ	Excess adsorbed amount
δ	Length of field gradient pulse
Δ	Time between field gradient pulses
τ	Sample time

Chapter 6.

CMC	Critical Micelle Concentration
g-PEO	Grafted PEO
PEO	Poly(ethylene oxide)
ppm	Parts per million.
PSL	Polystyrene Latex
SDS	Sodium Dodecyl Sulphate.
T	Temperature
δh	Hydrodynamic thickness
τ	Sample time

Chapter 8.

CMC	Critical Micelle Concentration
I(Q)	Scattering Intensity as a function of Q
PEO	Poly(ethylene oxide)
P(Q)	Form Factor
PSL	Polystyrene Latex
Q	Scattering Vector
r	Radius
r_{of}	Radius for a Freely Rotating Chain
R_g	Radius of Gyration
SANS	Small-Angle Neutron Scattering
SDS	Sodium Dodecyl Sulphate.
S(Q)	Structure Factot
ϕ	Volume Fraction
ρ	Scattering Length Density
ξ	Characteristic Correlation Length, (or mesh size).

Chapter 9.

CMC	Critical Micelle Concentration
DLS	Dynamic Light Scattering
I(Q)	Scattering Intensity
N_p	Number of Particles per Unit Volume
Q	Scattering Vector
r	Radius
poly(NIPAM)	poly(N-isopropylacrylamide)
P(Q)	Form Factor
ppm	Parts per Million
SDS	Sodium Dodecyl Sulphate
V	Volume
$\Delta\rho$	Difference in Scattering Length Density Between the Solvent and the Particle
ϕ	Volume Fraction.
φ.	Size of Solid-like Inhomogenieties
ξ	Correlation length.

Chapter 1

Introduction.

Certain water soluble polymers such as poly(ethylene oxide) (PEO) can form self-assembled complexes with anionic surfactants, *for example,* sodium dodecyl sulphate (SDS), in aqueous solution and these complexes can play an important role in key industrial applications such as colloid stabilisation and destabilisation, enhanced oil recovery and detergency[1,2]. A central factor in all of these applications is the conformation of the polymer at the interface between the dispersed and continuous phases. In general, the structure of the polymer is to a large extent determined by interactions between the polymer molecule, its environment and the surfactant molecules. Structural perturbations may occur as a result of adsorption[3] and thus an understanding of polymer adsorption is of significant importance. It is therefore paramount to identify both the structure of these complexes in solution and also the effects of the complexation at interfaces. Industrially, polymers are used to aid the deposition of silicone oil emulsions onto skin and hair from shower gel and shampoo formulations. However, this action is subject to interference from the surfactant system which, by virtue of its interaction with the polymer, can either promote or prevent deposition. By studying the interaction between polymers and surfactants, both in solution and at the interface, the deposition properties can be determined and related to the structure of the interfacial layer.

The aim of this thesis is to investigate the solution and adsorption properties of a range of polymers (these being charged, uncharged or composed of different blocks) in the presence of SDS. This is in order to gain a greater understanding of

the factors involved in mixed adsorption systems and to relate this, in the future, to the deposition properties of these same systems.

1.1 Colloidal Dispersions.

A colloidal dispersion is a two phase system with dimensions in the nanometre (nm) to micrometer (μm) range. Dispersions may be solid in liquid (*e.g.* a sol such as polystyrene latex in water), liquid in liquid (*e.g.* an emulsion) or liquid in gas (*e.g.* an aerosol). The main dispersions used in this study both fall into the solid in liquid category, although they have very different properties and uses.

1.1.1 Colloidal Silica.

The silica dispersions used in this study were aqueous dispersions of silica (SiO_2) with diameters ranging from 12 nm to 120 nm. The small diameter results in a high specific surface area which accounts for the surface properties of these dispersions and their wide ranging applications including;

- Binder in casting of metals.
- Coating agent for antiblocking in plastic films
- Bonding improver in adhesives
- As a dye acceptor in photographic emulsions.

The silica particles are dispersed in an alkali medium which leads to a net negative charge on the particle. The negative charge on the particles causes a repulsive interaction between the particles and results in a stable dispersion.

1.1.2 Polystyrene Latex.

The second dispersion used in this study was a polystyrene latex. These polystyrene latices are produced by emulsion polymerisation[4] and are hydrophobic in nature. The charge on a polystyrene latex arises from the reaction with the initiator and can therefore be either positive or negative. Since

polystyrene latices can be prepared highly monodispersed these make ideal model systems.

1.2. Surfactants.

A surfactant, or to give it its full title a '*surface active agent*' is a molecule which contains both a hydrophilic and a lipophilic (oil-loving) region. As a consequence surfactants tend to have a high affinity for interfaces, be they air-liquid, oil-water or solid-liquid. Surfactants form micelles in solution providing that the concentration is above a critical value called the critical micelle concentration (CMC). Below this critical concentration the surfactant molecules are unassociated, but at the CMC the monomers associate into structures which are generally roughly spherical in shape, called micelles. A further increase in concentration may lead to other structures, *for example* rods or lamellae. At very high surfactant concentrations the structure may even become liquid crystalline.

1.2.1 Sodium Dodecyl Sulphate.

Probably the most common and widely studied surfactant is sodium dodecyl sulphate (SDS). Other names for SDS include sodium lauryl sulphate or dodecyl sulphate, sodium salt. SDS is an anionic surfactant of molecular weight 288 g and in pure water exhibits a CMC of approximately 8.3×10^{-3} M at a temperature of 25 °C[5]. The aggregation number of SDS is around 80 with about 25 % of the sodium counter ions in close proximity to the micelle. SDS has many diverse applications ranging from the detergent and cosmetics industry, (*for example*, bath foams and washing powder) to the photographic industry as a complexing agent with gelatin. The major drawback with SDS is the fact that it readily hydrolyses to form dodecanol which is more surface active than SDS and may be an unwanted by-product.

1.3 Polymers.

A polymer is defined as a large molecule made up of many relatively simple repeat units called monomers.

1.3.1 Homopolymers.

A simple homopolymer contains identical repeat units and common examples include, poly(ethylene oxide), poly(styrene) and poly(vinyl alcohol).

The homopolymer used in this study was poly(ethylene oxide) or PEO. PEO is a water soluble homopolymer which has been studied extensively in the literature[6,7]. Recent light scattering studies[8] on the aqueous PEO system have revealed that PEO-PEO interactions in dilute solution are unusually strong, perhaps even anomalous in character, when compared to the behaviour of other linear flexible homopolymers in a good solvent. Viscometry measurements on PEO in aqueous solution[9] have indicated that the intrinsic viscosity of PEO is consistently higher than for other similar polymers. Furthermore, PEO coils tend to have unusually large coil and hydrodynamic radii. Even so, PEO is well suited as a model system since it can be prepared with a very low polydispersity and the χ and χ_s parameters (the Flory and Flory-surface parameters) are such that the polymer adsorbs from aqueous solutions onto a variety of surfaces such as polystyrene latex and silica.

1.3.2. Polyelectrolytes.

A simple polyelectrolyte may be defined as a homopolymer, where each monomer unit carries an ionisable group. Such a group may be a strong acid or base so that its charge is virtually independent of changes in pH. These are known as strong polyelectrolytes. Similarly, a weak polyelectrolyte will have weak acid or base groups and have a charge which is strongly pH dependent.

As a polyelectrolyte is dissolved in water it acquires a certain degree of charge. As a direct effect of this charge a strong electrostatic repulsion builds up along the

chain which is dependent upon the distance between charged units. The chain will therefore become rigid and stretched minimising the internal repulsion. This effect is dependent upon ionic strength; at high ionic strength all of the charges may be "screened out" and the polyelectrolyte chain may revert back to a homopolymer type of structure.

The polyelectrolyte used in this study was Quatrisoft LM, a commercial hydrophobically modified cationic cellulose derivative which is weakly charged. Quatrisoft LM is a chloride salt of an N,N-dimethyl-N-dodecyl derivative of hydroxyethyl cellulose and has a molecular weight of approximately 100,000. The charges are located on the hydrophobic side chains of the molecules and the chain substitution has been determined as 2.0×10^{-4} moles of hydrophobic chain per gram of monomer, equivalent to approximately 5.4 side chains per 100 sugar residues. The hydrophobic modification is achieved by grafting a cationic surfactant onto the hydrophilic polymer backbone. Due to the hydrophobic and charged nature of the polymer interactions with oppositely charged surfactants may occur through both hydrophobic and electrostatic interactions. These interactions are strong and lead to the formation of mixed micelles.

1.3.3 Copolymers.

A copolymer is a polymer chain which consists of two (or more) different monomer units. A copolymer may be described as "random" when there is no correlation at all between the distribution of the different blocks or a "block" when all of the monomers of the same type are grouped together. Consequently, any random copolymer is essentially a mixture of many different chains.

Block copolymers (termed AB or ABA copolymers where A and B are different blocks) are probably the most studied and the most interesting of all types of copolymer because of their dual character. This type of copolymer displays a rich variety of structures both in solution and at the interface including the tendency to self-associate[10]. In many ways the behaviour of block copolymers is similar to

that found for surfactant molecules. If under any particular solvent conditions one block (say block A) has a high affinity for the solvent and the other block (block B) has a poor affinity with the solvent there will be a strong tendency for the B blocks to associate with each other. This may even cause the formation of intermolecular aggregates.

1.3.4 Polymer Microgels.

A microgel is classed as an intermediate between a branched and a macroscopically cross-linked system. The overall dimensions of microgels are comparable to high molecular weight linear polymers and microgels have a porous 'sponge-like' structure.

The microgel used in this study, poly(N-isopropylacrylamide), Poly(NIPAM) is a water soluble polymer which forms monodispersed colloidal microgels by emulsion polymerisation and extensive crosslinking[11]. An important property of poly(NIPAM) is that it has a lower critical solution temperature of 32 °C in water[12]. Thus, poly(NIPAM) solution and gel properties can be "switched" by changing temperature, surfactant concentration and, in some cases, the electric field strength. Much of the literature involves potential applications which use either linear poly(NIPAM) or crosslinked macroscopic gels[13,14]. Comparison of microgel and macrogel results reveals that the properties of linear polymer solutions, macrogels and microgels are similar. Presumably this is because the specific interaction of the isopropyl groups on the poly(NIPAM) with water dominates the behaviour.

1.4 Polymer Surfactant Interactions.

The original work on the interaction of water soluble polymers with surfactants was based on poly(vinyl alcohol) (PVA) and poly (vinyl pyrilidone) (PVP) which both have polar side groups. It was suggested that the polymer-surfactant complex formed resulted from surfactant ions binding onto the polymer chain.

With decreasing hydrophobic character of the polymer the adsorption of the surfactant ions also decreased. It was therefore concluded that the binding mechanism was due to the hydrophobic interaction between the polymer and the surfactant. The later, and somewhat more extensive work, concentrated on the PEO/SDS system which differs from the early studies since PEO has no polar side groups. It therefore may be concluded that the binding mechanism may be very different for this type of polymer. More recently still there appears to be a whole wealth of literature concentrating on these polymer/surfactant interactions using complicated polyelectrolytes and bio-molecules.

***Figure 1.1*; Schematic Representation of a Polymer-Surfactant Interaction.**

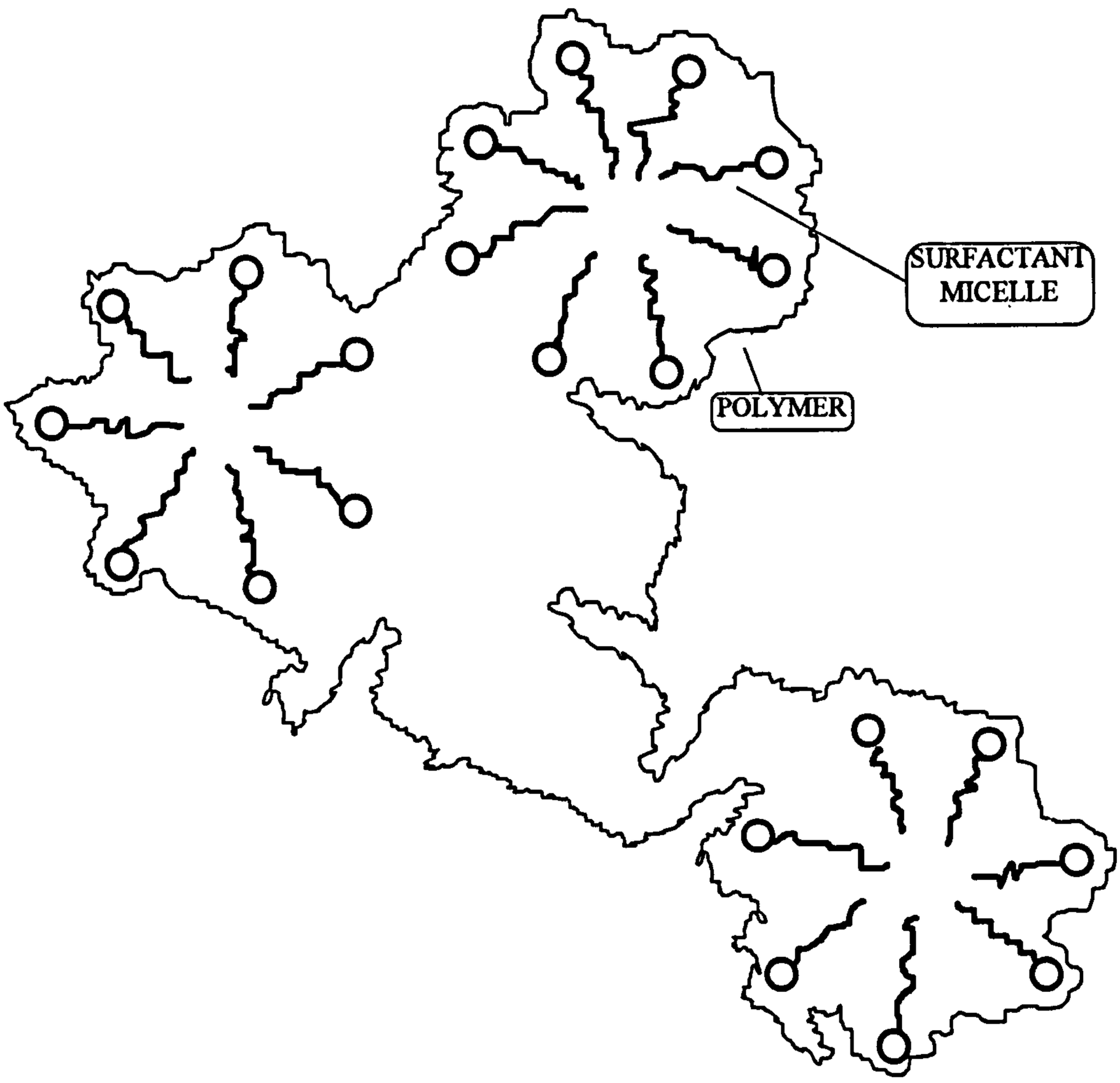

1.4.1 Poly(ethylene oxide) / SDS

Probably the best documented polymer/surfactant interaction is that of poly(ethylene oxide) PEO and SDS. The literature dates back from the early sixties and has been at a steady and constant rate ever since. It is well documented that PEO interacts with SDS at surfactant concentrations above a critical aggregation concentration (CAC) to form well-defined micelles with aggregation number of approximately 80[15-18]. Cabane[15] has suggested that the structure of these mixed micelles may be represented as the polymer loosely wrapping around the surface aggregate, the "pearl necklace model", **Figure 1.1**. It is suggested that the SDS/PEO/water interface retains a certain stoichiometric concentration, and when the composition of the solution departs from this stoichometry the mixed micelles resist this change resulting in an excess of either polymer or surfactant in solution. More recent papers[19] have suggested that there may be some interaction between SDS and PEO molecules even at surfactant concentrations as low as 4×10^{-4} mol dm^{-3}.

Jones[16] in 1967 performed an extensive study of PEO/SDS aggregates by measurements of conductance, surface tension and viscosity. This investigation differs from many later studies in that all measurements were performed in the absence of any added salt, which affects parameters such as the CMC quite significantly. Specific conductance measurements were performed as a function of SDS concentration for a fixed concentrations of PEO. The specific conductance initially increases linearly as in the absence of polymer but at a certain SDS concentration (*for example* 6.1×10^{-3} M for a 0.09 % w/w PEO solution) deviates from a straight line and follows a curve which ultimately approaches a second straight line (at 18×10^{-3} M for a 0.09 % w/w PEO solution) - again the same as that for pure SDS. Similarly, the surface tension measurements showed very similar results when plotted as a function of SDS concentration. As before, both transitions were clearly seen with the surface tension going through a short plateau after the first transition and then falling to a final value, which is also very close to that of pure SDS. The surface tension at

which the first plateau occurred was found to be weakly dependent upon the initial polymer concentration with a plateau being reached for a polymer concentration of approximately 0.5 % w/w. At very high surfactant concentrations, above 1.0 % w/w, surface ageing was observed. When the position of the first transition point was plotted against polymer concentration for two different molecular weights of the polymer it was found that all of the points lay on the same straight line. Therefore, it may be said that the position of this first transition point is independent of molecular weight. From the relative viscosity measurements performed by Jones the second transition point was clearly seen. The slope before this transition was similar to that of pure SDS but beyond this transition was significantly altered. The first transition point was not visible using this technique.

Jones concluded that there was a formation of a complex or that the polymer formed nucleated micelles between PEO and SDS. There were two transition points which separated three distinct regions of behaviour.

- *Below the first transition* - No interaction between PEO and SDS.

- *Between the first and the second transition* - At the first transition SDS ions bind to the polymer. This transition occurs abruptly similar to the critical micelle concentration of a surfactant. The effect of PEO is analogous to the effect of salt on the CMC of a surfactant. The presence of the polymer alters the structure of the water significantly so that it is more favourable for the surfactant ions to bind to the polymer than to exist discretely in solution. As all of the available sites are filled up, the concentration of unbound SDS builds up and this is shown by a further decrease in surface tension. As saturation is reached the second transition occurs.

- *Above the second transition* - It is now likely that two species are possible; ordinary micelles and polymer/surfactant complexes which may differ from those below the second transition. However, since the values of surface tension and specific conductance are the same as in the absence of PEO above the normal CMC of SDS, this may suggest that indeed normal micelles are formed.

Figure 1.2 shows the "phase diagram" of PEO and SDS as proposed by Cabane[15]. In this figure, region I contains only unassociated polymer and surfactant molecules, region II polymer-surfactant aggregates in equilibrium with excess polymer molecules and region III contains polymer-surfactant aggregates in equilibrium with excess surfactant molecules.

Several, direct studies probing the PEO/SDS complex have been performed using techniques such as small-angle neutron scattering[20] and nitroxide spin probes[21] to give information on the structure of the PEO/SDS complex and the size of the polymer bound micelles. The possible structures postulated can again be visualised as consisting of a polymer molecule wrapped around surfactant micelles, with the polymer segments partially penetrating the polar head groups of the micelles. A single polymer molecule can associate with not one but a number of surfactant micelles which implies that the surfactant molecules are binding to the polymer molecule as clusters rather than individual surfactant molecules. It is suggested that the micelles are of the order 20 Å in diameter and that the polymer is associated with the interface between the hydrocarbon and water. Hydrodynamic measurements on the PEO/SDS complex using viscometry, conductometry and ultracentrifugation have shown that the saturated complex has properties which resemble those of a polyelectrolyte of similar charge density[22]. Similarly, Brown *et al*[23] noted a pronounced polyelectrolyte effect compared to free polymer.

Figure 1.2

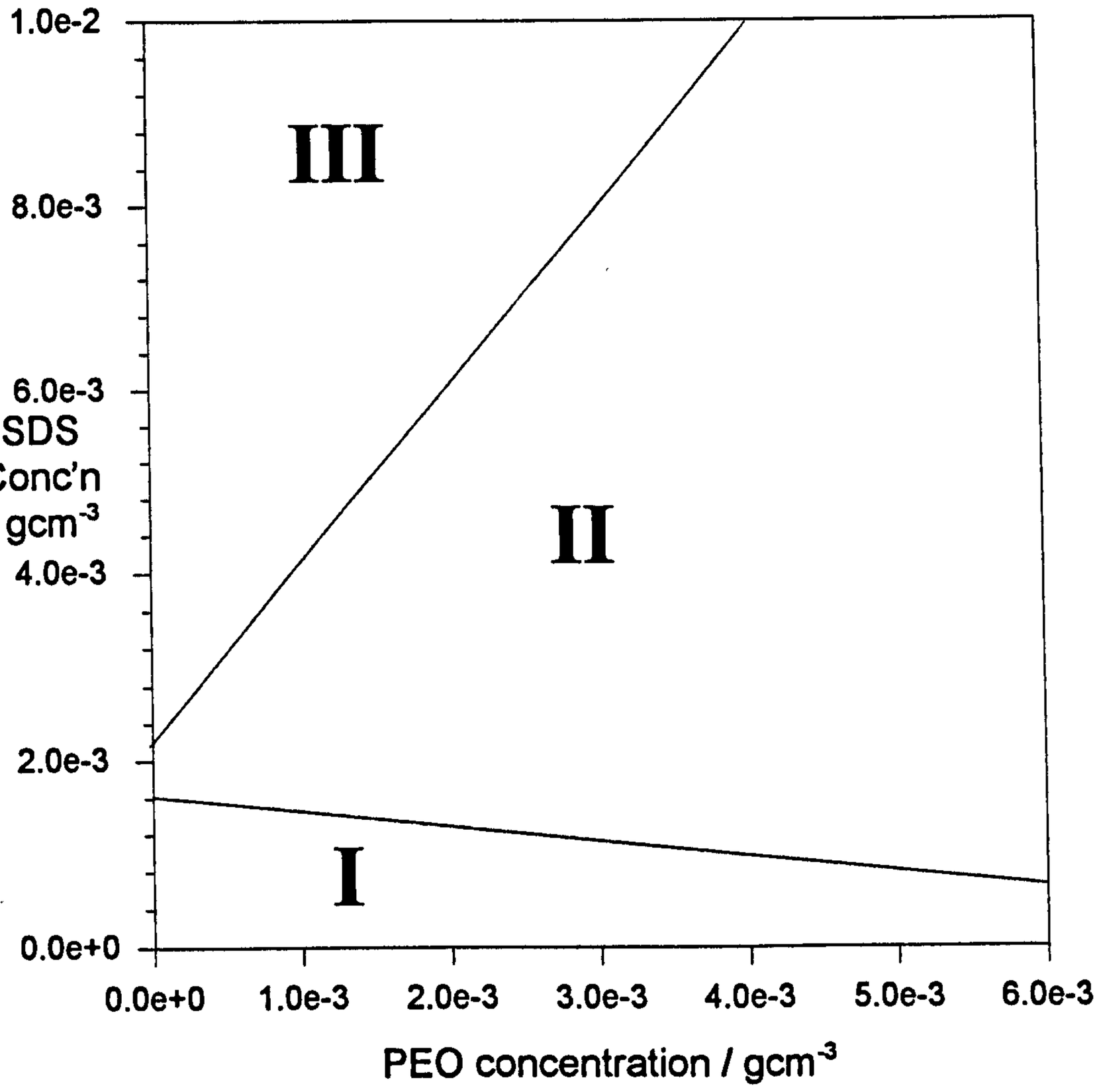

Chari[24] *et al* performed SANS experiments on the PEO/SDS complex and found that although the PEO coil is stretched (compared to a coil in a good solvent) the coils are not fully stretched. It was proposed that the polymer resembled a swollen cage, rather than a necklace around the SDS micelles. Since the addition of salt to a PEO/SDS solution near saturation with surfactant caused a compression of the swollen cage it was argued that the swelling of the polymer coil was due to long-range electrostatic repulsions between attached SDS micelles. Fluorescence measurements on the PEO/SDS complex[25,26] have indicated that the aggregation number of SDS is low around concentrations at which interaction with PEO first occurs, but increases with surfactant

concentration to a maximum of around 80; this is similar to that of free SDS micelles at concentrations around 1.0 % w/w.

1.4.2 Polyelectrolytes/SDS

Ya Tret'yakova *et al*[26] have reported on the interactions between SDS and positively charged poly(4)vinylpyridine. In that paper the binding isotherms were investigated using a surfactant-selective electrode as a function of the degree of quaternisation of the polymer. It was found that the SDS introduced to the system is almost completely bound by the polyelectrolyte until this becomes saturated with surfactant molecules and the binding reaches saturation. Increasing the degree of quaternisation tended to decrease the binding capacity and it was suggested that although the polymer and surfactant were oppositely charged, the method of binding was to the hydrophobic segments rather than the charged segments

SANS investigations on the bio-polymer gelatin[27] in the presence of SDS, have shown structural changes associated with the individual components and their interactions with each other. In particular, contrast variation was used to highlight the various components in the mixture. In that work the changes caused by the addition of salt and effects of the variation in pH were investigated. The addition of gelatin to SDS resulted in a significant reduction in the CMC of the SDS and the structure of the gelatin was reported to have become more compact. As the SDS concentration is increased there is a greater change in the gelatin structure as more micelles become bound to the bio-polymer.

In solution the side chains of hydrophobically-modified water-soluble polymers such as Quatrisoft LM associate in microdomains at low concentrations. Thus, "micelles" are formed which have the capacity to solubilise individual surfactant molecules. This is different to the homopolymer case where interactions only occur above a well defined concentration, and the interaction is with micelles rather than individual surfactant molecules. *For example*, Quatrisoft LM

associates with SDS at concentrations as low as 10^{-5} M and this binding is closely analogous to the binding of a surfactant to a micellar solution of a second surfactant. At these surfactant concentrations phase separation will be observed and is accompanied with a rise in viscosity. The system exhibits a high affinity binding isotherm *i.e.* all SDS is bound until charge neutralisation has been reached at which point free SDS will build up. Aqueous mixtures of SDS with Quatrisoft LM have been investigated using various techniques[28]. Steady state fluorescence measurements showed that hydrophobic microdomains were formed in aqueous solutions of the polymer at very low concentrations. On adding SDS, liquid-liquid phase separation occurred around the regime of charge neutralisation, followed by redissolution upon the addition of further SDS. Viscosity measurements confirmed this. These results were interpreted in terms of a binding isotherm of surfactant to polymer, analogous to isotherms observed for surfactants binding to proteins or to micelles of other surfactants. It was proposed that the first stages of the binding involved the binding of individual surfactant molecules to the mixed micelles, and the latter stages (when the free surfactant concentration approaches the normal CMC) involved strong co-operative binding related to the self-association of the surfactant.

1.4.3 Poly(NIPAM)/SDS.

An important property of poly(NIPAM) solutions and gels is that they can bind ionic surfactants. Early work on the interaction of poly(NIPAM) homopolymer with SDS[29] showed that a 1% w/w solution of SDS increased the intrinsic viscosity and the cloud point of poly(NIPAM) homopolymer. More recently, Kokufuta[30] *et al* reported the effects of SDS on the swelling of macroscopic poly(NIPAM) gels. It was found that the SDS bound to the poly(NIPAM) gels and increased the phase transition temperature of the gel to a maximum of around 90°C. This is analogous to the poly(NIPAM) homopolymer case where the cloud point is raised from 31 °C to a similar temperature[31]. Interestingly, although cationic surfactants do bind to poly(NIPAM) microgel latices, the induced swelling of the microgels is very limited. The concentration of SDS at which the

surfactant first interacts with the linear poly(NIPAM) homopolymer has been reported to be 7.9 x 10^{-4} M[32] and 6.9 x 10^{-4} M[33], although Tam *et al*[34] observed that no swelling of a microgel was induced even at 1 x 10^{-3} M. In that paper, however, it was reported that at low temperatures the size of the poly(NIPAM) microgel measured by dynamic light scattering, increased with SDS concentration; swelling from 400 nm in a 0.0082 M SDS solution (approximately CMC of pure SDS) to 570 nm in the presence of 0.2 M SDS. Moreover, the mobility of the poly(NIPAM) microgel was found to become more negative as the SDS concentration was increased, *i.e.* the binding of SDS increased the surface charge density of the microgel. Since, the SDS binds with the poly(NIPAM) gel particles there will be an increase in the concentration of sulphate charge groups on the particles and hence the swelling may be due to electrostatic or osmotic effects. At very high surfactant concentrations, these electrostatic effects dominate and prevent the collapse of the poly(NIPAM) microgel.

It was concluded by Tam *et al*[34] that there are many parallels between poly(NIPAM) microgel behaviour and linear poly(NIPAM) homopolymer behaviour. However, to date there does not appear to be any information on the structure of the polymer/bound SDS complex, or the bound micelle size and number.

1.5 Adsorption to a Solid Substrate.

For adsorption from solution onto a surface to take place there must be a net decrease in the Gibbs free energy of the system. The Gibbs free energy arises from a combination of enthalpic and entropic factors. Upon adsorption the spatial structure of a polymer is likely to change resulting in a considerable loss of conformational entropy compared with the bulk. However, small species, such as solvent molecules or ions, must be displaced when the polymer adsorbs and this will give a positive entropic contribution. Another important parameter when considering adsorption is the solvation energy - the change in energy when a

polymer segment is transferred from the melt to the pure solvent. When the solvent quality is poor, adsorption of the polymer is favoured. The final conformation of the polymer at the surface is determined by a balance of these entropic and enthalpic contributions to the free energy. The enthalpic factors will prefer the polymer to lie flat on the surface maximising the number of segment-surface contacts. This arrangement, however, is not entropically favoured since many possible conformations are inaccessible. The structure of the adsorbed layer is also highly dependent upon polymer concentration. At very low coverages, where there are many surface sites available, the energy of adsorption dominates and the polymer will adopt a flat configuration. As the polymer concentration is increased there is competition for surface sites and the entropic factors become more important. Eventually, when the surface becomes saturated the conformation of the layer is only weakly dependent upon the solution concentration.

The configuration of a flexible linear polymer adsorbed at a solid surface may be regarded as consisting of three types of entities: *trains, loops* and *tails*. Train segments lie in direct contact with the surface whereas loops and tails extend into the bulk phase. A loop is a string of segments between any two segments bound to the surface and tails protrude into the bulk. The overall adsorption process of a polyelectrolyte, in contrast to an uncharged polymer, is also dependent upon the distribution of charged groups. The net charge and its distribution affects the molecular conformation, both in solution and when adsorbed onto the surface. The charges arise from either the ionisation of an ionisable group or by ions binding to the polyelectrolyte molecule. It is possible that upon adsorption, the PEO/SDS complex behaves as a polyelectrolyte.

1.5.1 Adsorption of PEO

The adsorption of PEO onto both silica and polystyrene latex has been studied extensively by a number of authors. On both of these substrates the adsorption isotherm is of the high affinity type and the adsorbed amount shows a log

dependence with the log of the polymer molecular weight[35,36]. The experimental dependence compares favourably with the theoretical predictions of Scheutjens-Fleer in a θ solvent[37]. Furthermore, different end groups of the polymer substantially affect the adsorption behaviour of the polymer[38]

The hydrodynamic thickness of PEO physically adsorbed onto polystyrene latex (or silica) shows a log dependence with the log of molecular weight [36,39]. For PEO, the hydrodynamic thickness increases with molecular weight at a greater rate than the radius of gyration. The hydrodynamic thickness of PEO is low at low coverage followed by a steep increase as the adsorbed amount exceeds a certain threshold.

Nuclear magnetic resonance experiments on PEO adsorbed onto polystyrene latex[40] have given values of the bound fraction in the range 0.05 to 0.1. In contrast thickness measurements using ellipsometry[41] have shown that PEO forms very thin compact layers.

Small-angle neutron scattering measurements of physically adsorbed PEO on polystyrene latex have been used to determine the second moment of the layer[42]. It was found that this value was three times less than the corresponding values of hydrodynamic thickness although qualitatively the same trends with molecular weight were shown. Volume fraction profiles for 5×10^4 M. Wt PEO showed a simple exponential decay with a segment density at the interface of around 0.6 and a layer extending to around 5 nm. On the other hand, terminally attached PEO onto polystyrene latex showed a distinct maximum in the volume fraction profile[43].

1.5.2 Adsorption of Quatrisoft LM.

The Quatrisoft LM used in this thesis belongs to a class of hydrophobically modified polyelectrolytes which has a high affinity to adsorb on oppositely charged surfaces. Thus, the industrial applications are wide-ranging. The

adsorption of Quatrisoft LM onto negatively charged surfaces (mica and silica) has been studied using a surface force apparatus and *in situ* null ellipsometry[44]. Using the surface force apparatus, it was found that the measurable repulsive force extended to a separation of about 60 nm. Under large applied pressures, the layer could be compressed down to 8.5 nm, but could not be squeezed out. The adsorbed amount of Quatrisoft LM on several silica wafers was determined by ellipsometry as 1.6 ± 0.2 mg m^{-2}. The adsorption was not affected by rinsing which indicates the irreversibility of the adsorption of this group of polymers. The RMS layer thickness measured by ellipsometry was less than that by the surface force apparatus at 7 ± 1 nm.

1.5.3. Mixed Adsorption.

Although adsorption from mixed component systems has been studied extensively[45-48] most of this work has been directed at systems in which both components can adsorb. Changes in adsorption may occur either because of competitive adsorption, or for reasons associated with the polymer/surfactant interactions, making data interpretation more complex. In general, it is the complexation that appears dominant. For example, Ma and Li[45] reported that on the surface of ferric oxide, the adsorption of SDS was almost unaltered by the presence of PVP. The adsorption of PVP however was observed to increase markedly due to the presence of SDS at low concentrations (less than the CMC), followed by a dramatic decrease in adsorption at high SDS concentrations. It was suggested that this was due to complex formation between SDS and PVP, with surface complexes at low SDS concentrations and solution complexes at high SDS concentrations. Similarly, Esumi and Matsui[46] investigated the adsorption of PVP and poly(dimethyldiallylammonium chloride) (PDC) on silica as a function of PVP concentration in the presence of PDC. In this study it was reported that the adsorption of PDC decreases with increasing PVP concentration, especially at high concentrations of PDC.

Esumi *et al*[47] investigated the adsorption of the polyelectrolyte poly(styrene sulphonate) (PSS) and SDS from their single solutions and from mixed solutions onto positively charged alumina. Adsorbed amounts were determined. Since both PSS and SDS are negatively charged in aqueous solution, both had a high affinity for the positive alumina surface. The effect of the addition of SDS on the adsorption of PSS was investigated, initially maintaining a fixed concentration of PSS. The SDS adsorption reached a plateau at approximately the CMC of SDS, but this was significantly different to that in the absence of PSS. On the other hand, the adsorbed amount of PSS decreased linearly until at approximately 5 mMol of SDS it became almost zero. This suggested that the SDS had replaced the PSS with an increased SDS concentration. When the SDS concentration was maintained at a constant value of 5 $x10^{-3}$ M and the adsorbed amounts measured as a function of PSS concentration, the adsorbed amount of PSS increased whilst that of SDS remained approximately constant with increasing PSS concentration. The adsorbed amount of PSS corresponded to that which would be attached to a bilayer of SDS. These results indicated that the adsorption of PSS and SDS occurred through an electrostatic attraction between their anionic groups and positively charged sites on alumina. Moreover, it was likely that there was further hydrophobic attraction between the hydrophobic chains on PSS and the hydrocarbon chains of SDS adsorbed on the alumina.

Most recently, Shubin[48] has investigated the effect of SDS on the structure of adsorbed layers of the commercial polyelectrolyte Quatrisoft LM 200 on mica. This system differs from the others mentioned above in that only the polymer, not SDS, adsorbs onto the substrate. A dramatic decrease in the adsorbed amount around the CMC was reported, so that at an SDS concentration slightly above the CMC, the polymer was almost completely desorbed. Shubin also measured the thickness of the adsorbed layer by ellipsometry, finding that levels of SDS around the CMC led to extended though sparse polymer layers. It seems likely that this effect is due to the formation of micelles along the polymer chain, which repel each other, causing the chain to adopt a more extended configuration.

The effect of SDS on pre-adsorbed PEO on porous silica has been investigated by Somasundaran and Maltesh[49]. In that paper the effect of pre-adsorbed PEO on porous silica on the subsequent adsorption of SDS was examined. Even though SDS does not normally adsorb onto silica, in the presence of PEO it was removed from solution in significant amounts. The amount of SDS removed from solution was independent of the molecular weight of the PEO. Furthermore, the amount of SDS adsorbed from mixed solutions was less than that from pre-adsorbed PEO. However, no mention in that paper was made of the effect of SDS on any adsorbed PEO layer or whether or not the PEO desorbed.

References.

1. Goddard E. D.; in Goddard E. D. and Ananthapadmanabahan K. P. (Eds.) *Interactions of Surfactants with Polymers and Proteins*, CRC press, Boca Raton **1993**

2. Hayakawa K., Kwak J. C. T.; *in Cationic Surfactants - Physical Chemistry*, Rubingh D. N., Holland P. M. Eds. Dekker, New York **1991**

3. Shubin V., Petrov P., Lindman B.; *Colloid and Polymer Science* 1994 272 1590

4. Goodwin J. W., Hearn J., Ho C. C., Ottewill R. H.; *Colloid and Polymer Science* 1974 252 464

5. Mukerjee P., Mysels K. J.; C in *Critical Micelle Concentrations of Aqueous Surfactant Systems*. Nat. Stand. Ref. Data System **1971**, Superintendent of Documents US Government Printing Office, Washington DC 20402 USA

6. Heath T.; *University of Bristol PhD. Thesis* **1989**

7. Hey M. J., Illett S. M., Mortimer M., Oats S. G.; *J. Chem. Soc. Faraday Trans.* **1990** 86 2673

8. Bailey F. J. Jr., Karera J. L., Imhol L. G.; *J. Polym. Sci* **1958** 32 517

9. Woodley D. M., Dam C., Lam H., Le Cave M., Deverand K., Selser J. C.; *Macromolecules* **1992** 25 5283

10. Ameil C., Sikka M., Schneider J. W. Tsao Y-H, Tirrell M., Mays J. W.; *Macromolecules* **1995** 28 3125

11. Pelton R. H., Chilbante P.; *Colloids and Surfaces* **1986** 20 247

12. Heskin M., Guillet J. E.; *J. Macromolecular Sci. Chem*. **1968** A2(8) 1441

13. Scheild H. G.; *Prog. Polym. Sci*. **1992** 17 163

14. Pelton R. H., Pelton H. M.; Morfesis A., Rowell R. L.; *Langmuir* **1989** 5 816

15. Cabane B.; *J. Phys. Chem.* **1977** 81 1639

16. Jones M.; *J. Coll. Int. Sci* **1967** 23 36

17. Nagaragan B.; *Colloids and Surfaces* **1895** 13 1

18. Shirakama K.; *Colloid and Polymer Science* **1974** 252 978

19. Ramachandran R., Kennedy G. J.; *Colloids and Surfaces* **1991** 54 261

20. Cabane B.; *J. Physique* **1982** 43 1529

21. Kang Y. S., Kevan L.; *J. Phys. Chem.* **1994** 98 7624

22. Francois J., Dayantis J., Sabbodin J.; *Eur. Polym. Journal* **1985** 25 165

23. Brown W., Fundin J., Miguel M. da G.; *Macromolecules* **1992** 25 7192

24. Chari K., Antalet B., Lin, M. Y., Sintra S. K.; *J. Chem. Phys* **1994** 100(7)

25. Vansatam J., Brown W., Fundin J., Almgren M., Lindblad C.; *ACS Symposium Series* **1993** 532 194

26. Ya Tret'yayova , Bilavav A. V., Barabanov V. P.; *Polymer Science* **1992** 34(5) 425

27. Heenan R.K., White S.J., Cosgrove T., Zarbakhsh A., Howe A., Blake A.M ; *Prog. Colloid Polym. Sci* **1994** 97

28. Guillmet F., Piculell L.; *J. Phys Chem* **1995** 99(2) 9201

29. Elaisaaf J.; *J. Appl. Polym. Sci.* **1978** 22 873

30. Kokufuta E., Zhang Y., Tanaka T., Mamada A.; *Macromolecules* **1993** 26 1053

31. Heskin M., Guillet J.; *J Macromolecular Sci - Chem.* **1968** A2(8) 1441

32. Schild H. G., Tirrell D. A.; *Polym. Prepr. (Am. Chem. Soc., Div. Polym. Chem.)* **1989** 30(2) 350

33. Wu X. Y., Pelton R. H., Tam K. C., Woods D. R., Hamielic A. E., *J. Polym. Sci., Part A Polym. Chem.* **1993** 31 957

34. Tam K. C., Ragaram S., Pelton R. H.; *Langmuir* **1994** 10 418

35. Stuart M. A. C, Cosgrove T., Vincent B; *Adv. Coll. Int. Sci* **1986** 24(2-3) 143

36. van der Beek G. P.; *PhD Thesis, Agricultural University of Wageningen.*

37. Scheutjens J. M. H. M., Fleer G. J.; J. *Phys. Chem.* **1980 84** 178

38. Santore M. M., Kelly M. S., Mubarekyan E., Rebar V. A.; *ACS Symposium Series* **1995** 615 183

39. Stuart M. A. C., Waajen F. H. W. H., Cosgrove T., Vincent B.; *Macro-molecules* **1984** 17(9) 1825

40. van der Beek G. P., Stuart M. A. C., Cosgrove T.; *Langmuir* **1991** 7(2) 327

41. Malmsten M., Linse P., Cosgrove T.; *Macromolecules* **1992** 25 (9) 2474

42. Cosgrove T., Heath T. G., Ryan K., Crowley T. L; *Macromolecules* **1987** 20(11) 2879

43. Cosgrove T., Ryan K., *Langmuir* **1990** 6(1) 136

44. Shubin V., *Langmuir* **1994** 10(4) 1093

45. Ma C., Li C.; *J. Coll. Int. Sci.* **1989** 132(2) 485

46. Esumi K., Matsui H.; *Colloids and Surfaces* **1993** 80 273

47. Esumi K., Masuda A., Otsuka H.; *Langmuir* **1993** 9 284

48. Shubin V.; *Langmuir* **1994** 10 1093

49. Somasundaran P., Maltesh C.; *J. Coll. Int. Sci.* **1992** 153(1) 298

Chapter 2

Polymer And Surfactant Theory

This chapter deals with the theoretical aspects of polymer and surfactant solution theory and the theories of adsorption. Initially the solution theory will be dealt with and then later in the chapter the adsorption aspects.

2.1 Polymers in Solution

2.1.1 Dilute Polymer Solutions

2.1.1.1 Conformation. - the configuration of a soluble polymer may be described in terms of a hierarchy of chain structure.

Primary Conformation - mainly describes the chemical structure and the tacticity of the polymer chain. Simply, the tacticity defines where any side groups in the polymer chain lie. These may be classed as,

- ISOTACTIC — All the side groups lie on the same side.
- SYNDIOTACTIC — Side groups lie on alternate side of the molecules.
- ATACTIC — The side groups are formed randomly.

Secondary Conformation - relates to the rotation of the polymer structure. *For example*, a polymer containing a flexible oxygen linkage in its backbone is able to rotate to a higher degree than a simple C-C bond. The number of secondary configurations a polymer may attain is related to the dihedral angle between adjacent atoms in the chain. The number of configurations (Ω) is given by,

$$\Omega = 3^m$$

[2.1]

where m is the number of monomer units and Ω is related to the entropy such that,

$$S = k_B \ln \Omega$$

[2.2]

Tertiary Configuration - defines the specific structure of the secondary structure. These tertiary structures are typically random or helical; *i.e.* defining either random or helical order.

Quaternary Structure - exists only when there is more than one chain involved and is the structure of the sub-units involved.

2.1.2 Models for Polymer Chains in Solution.

2.1.2.1 Lattice Model.

Figure 2.1 **Schematic representation of a lattice model for polymer chains.**

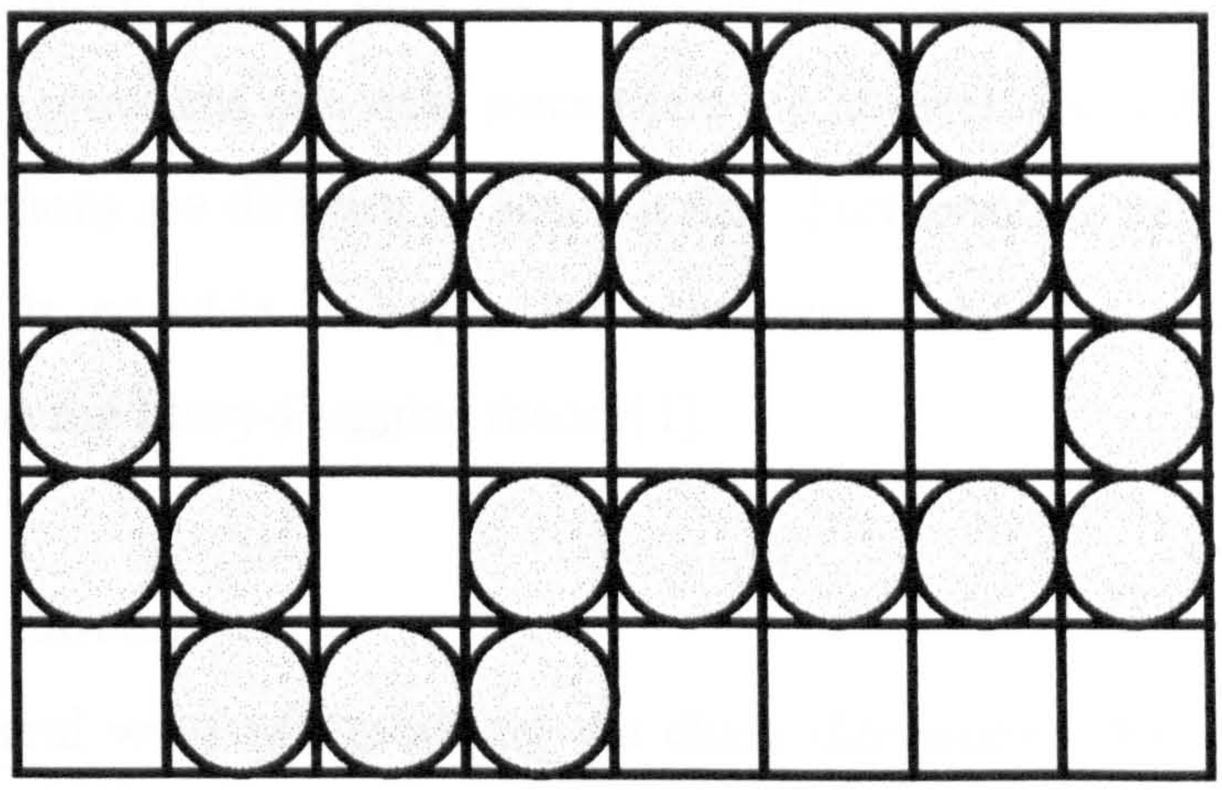

In these models the solvent is considered to exist as a three dimensional lattice, the sites of which may be occupied by either a polymer segment or a solvent molecule. When a site becomes occupied it is excluded to other solvent molecules or polymer segments, *i.e.* an *excluded volume effect*. The energy or enthalpy can be calculated for a segment-segment interaction, a segment-solvent

interaction or a solvent-solvent interaction. The major weakness with this model is that contravening geometry assumes that solvent molecules have the same volume as a polymer segment which results in not only size constraints, but also angular constraints.

2.1.2.2 Continuum Models.

Figure 2.2 **Schematic representation of a continuum model for polymer chains**

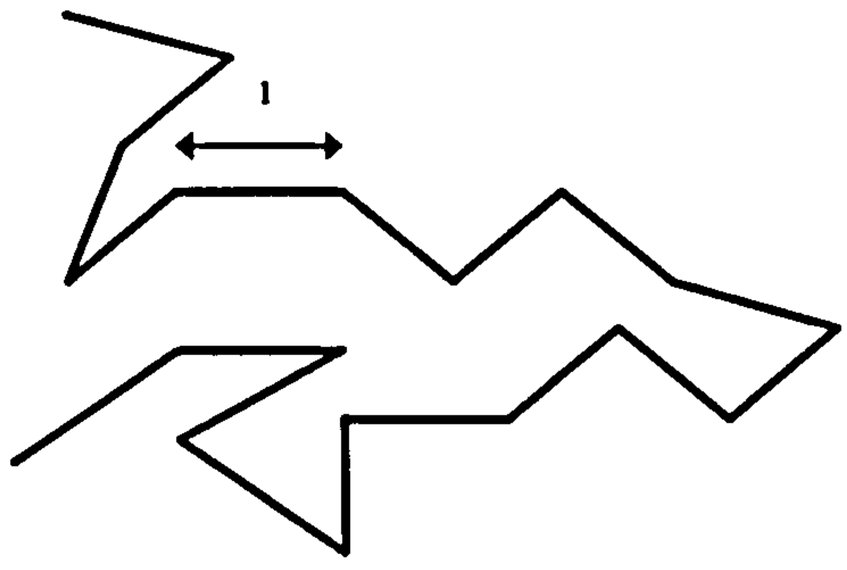

These models consider the polymer chain as consisting of N bonds, each of length l and is more general than the lattice model since there are no geometric constraints, but problems can arise since there are no excluded volume effects and solvent interactions are difficult to account for. Furthermore, using bond lengths and angles it is possible to apply the continuum model to traditional lattice theories such as the Flory-Huggins theory[1].

2.1.3 Chain Dimensions.

There are several ways of describing the chain dimensions, *for example*, small-angle neutron scattering measurements may yield the radius of gyration of a polymer chain, whilst photon correlation spectroscopy reveals the hydrodynamic dimensions.

The Root-Mean-Square Dimensions (RMS) of a Polymer Chain - To obtain the RMS dimensions the average of all possible conformations of the polymer chain is required; *i.e.* $\langle r^2 \rangle^{1/2}$. (where r is the end-to-end distance).

The Radius of Gyration (R_g) - If the centre of mass for any conformation is defined, there is a finite probability of finding a part of the polymer chain at a certain distance from the centre of mass. In general, the radius of gyration is defined as,

$$R_g^2 = \frac{\sum_{i=1}^{N} m_i r_i^2}{\sum_{i=1}^{N} m_i} \qquad [2.3]$$

For a freely jointed chain,

$$\langle r^2 \rangle^{1/2} = N^{1/2} l \qquad [2.4]$$

and the radius of gyration is given by,

$$R_g = \frac{N^{1/2} l}{\sqrt{6}} \qquad [2.5]$$

However, for a polymer chain with fixed bond angles, θ,

$$R_g^{\,0} = \frac{N^{1/2} l}{\sqrt{6}} \left(\frac{1 - \cos\theta}{1 + \cos\theta} \right)^{1/2} \sigma \qquad [2.6]$$

where $R_g^{\,0}$ is the unperturbed value of the radius of gyration, *i.e.* there are no solvent or excluded volume effects. It is $R_g^{\,0}$ that is obtained by theoretical calculations whilst R_g is obtained from experimental studies. σ is a steric factor which has a value of unity for freely rotating chains. For very rigid chains such as poly(vinylnaphthalene), σ may be as high as 3.2. To take into account solvent

and excluded volume effects and relate R_g with R_g^o a further parameter is required such that

$$R_g^2 = \alpha R_g^{o2} \qquad [2.7]$$

α is an expansion factor which can be measured experimentally. The effects which determine α are.

- **Excluded Volume Effect** - for example a self avoiding chain is bigger than a chain of random dimensions resulting in a larger value of α.

- **Solvent Effects** - There are three types of interaction such that,

E_{pp}	The energy of polymer-polymer interactions.
E_{ps}	The energy of polymer-solvent interactions.
E_{ss}	The energy of solvent-solvent interactions.

The χ parameter (or Flory parameter) links E_{pp}, E_{ps} and E_{ss}. If pure polymer and solvent are mixed the change in energy can be described systematically.

Figure 2.3 **Schematic representation of the mixing of polymer segments.**

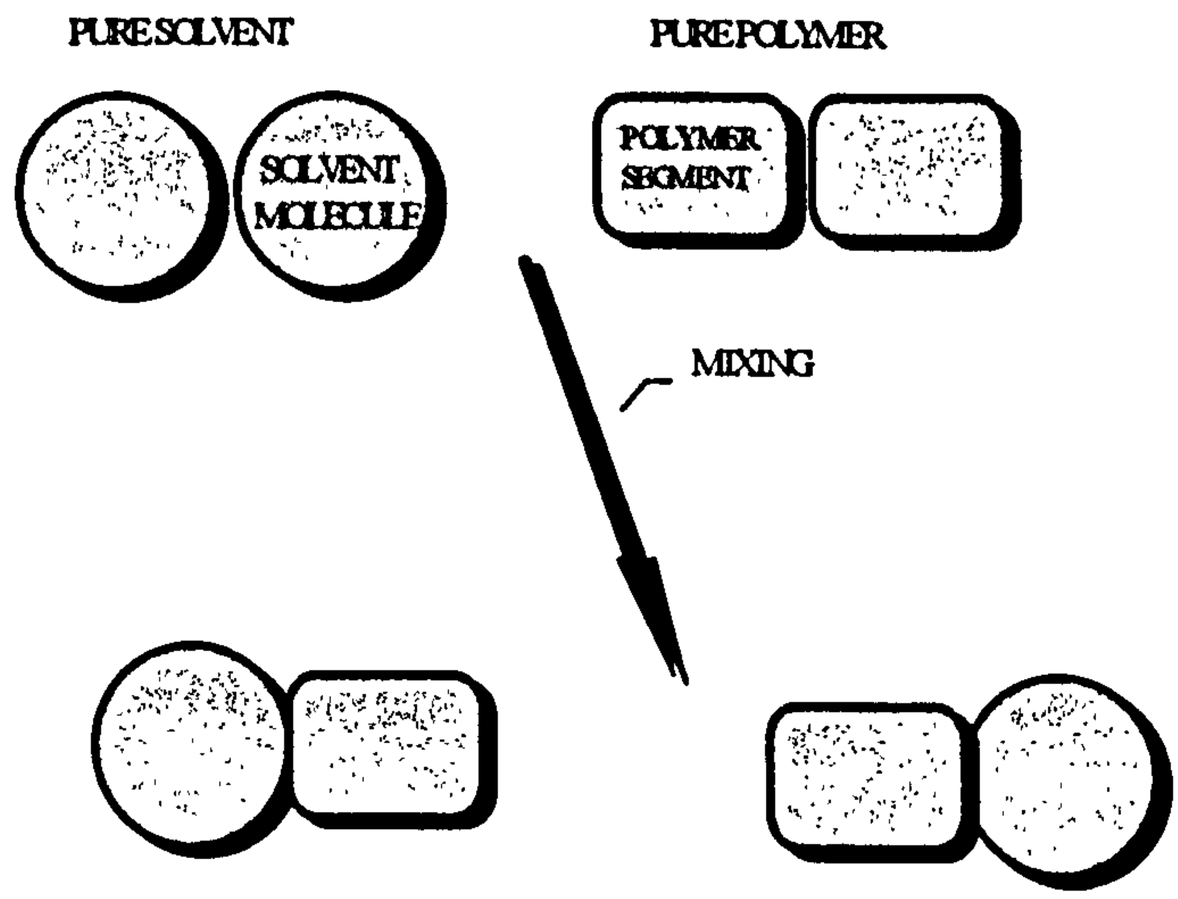

The change in energy is given by,

$$\Delta E = E_{ps} - \tfrac{1}{2}\left(E_{pp} - E_{ss}\right) \qquad [2.8]$$

and the *Flory parameter* (χ) is related to this energy by,

$$\chi = \frac{Z\Delta E}{k_B T} \qquad [2.9]$$

where Z is the co-ordination of the lattice used, *i.e.* Z = 4 for a tetrahedral lattice and Z = 6 for a cubic lattice. There are two special values of χ,

- $\chi = 0$ **athermal solvent** and $\alpha > 1$. The net energy of mixing is zero or in other words, E_{ps} is simply the mean of E_{pp} and E_{ss}, *i.e.* $\Delta E = 0$
- $\chi = \frac{1}{2}$ **theta solvent** $\alpha = 1$. A theta solvent is a special case when the solvent effect is equal and opposite to the excluded volume effect. The net result is that the polymer adopts random coil dimensions

The radius of gyration may be related to the number of bonds by,

$$R_g \propto N^{\nu} \qquad [2.10]$$

where ν is a scaling exponent which varies with solvent type *For example*, in a theta solvent $\nu = 0.5$. Since a chain in such conditions behaves essentially as if there is no solvent, its trajectory can be described by the diffusion equation for a purely random walk. On the other hand, for a good solvent, ν takes on a value of 0.6. In general ν may be described as $\nu = 3/(d+2)$, where d is the dimensionality of the volume V.

The Hydrodynamic Radius (R_h) - The hydrodynamic radius is related to how much solvent a polymer chain has associated with it. This associated solvent defines R_h which is related to viscosity such that,

$$[\eta] = \frac{\Phi z R_h^{\ 3}}{M_z} \qquad [2.11]$$

where $[\eta]$ is the measured intrinsic viscosity, $\Phi = 3 \times 10^{22}$ if R_h is in nm and M_z is the z-average molecular weight for the particular polymer in question.

Figure 2.4 **Schematic Representation of the hydrodynamic radius of a polymer chain.**

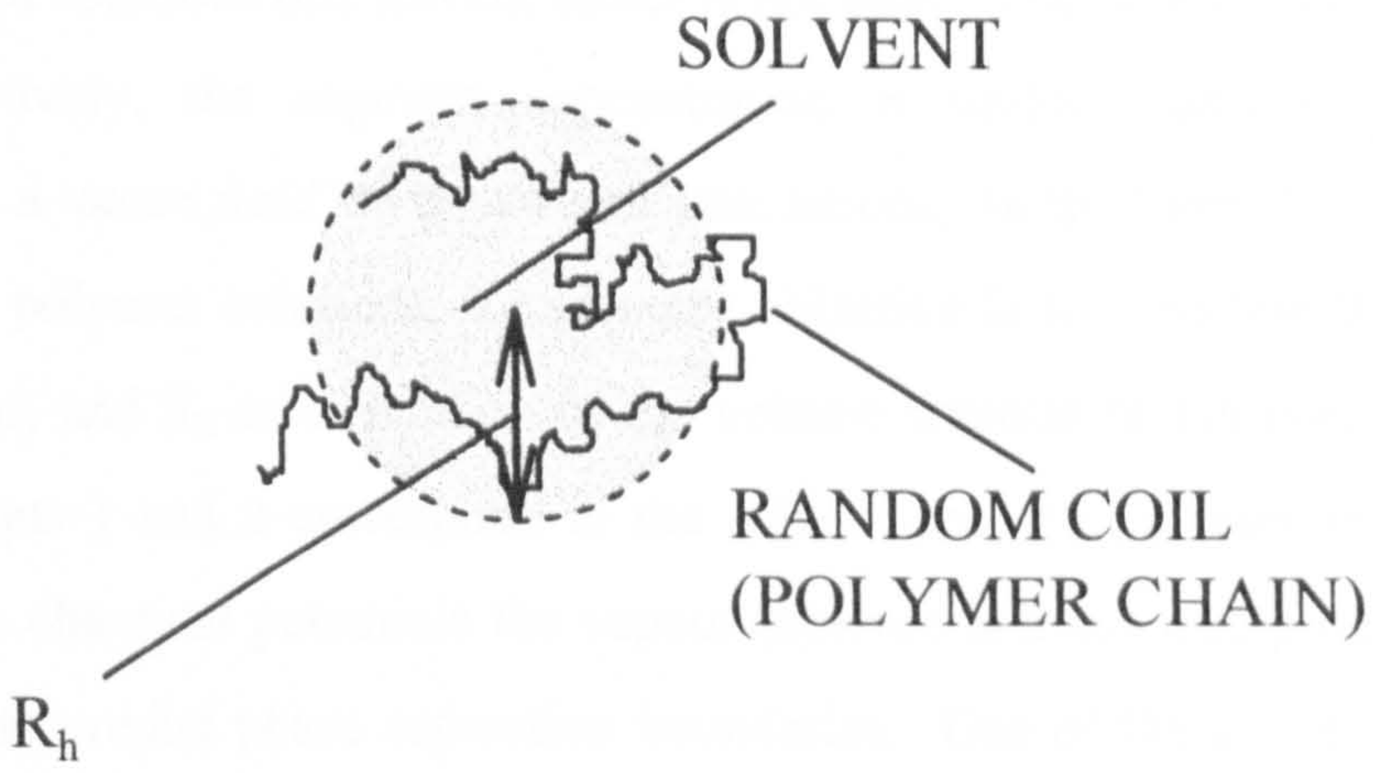

2.1.4 Semi-Dilute Polymer Solutions.

When considering more concentrated polymer solutions it is useful to use the volume fraction, ϕ, which may take values from zero to unity. ϕ^* is the volume fraction at which the polymer coils just begin to touch. ϕ^* is dependent on molecular weight and beyond this region the polymer solution is classed as being concentrated. As R_g increases, the volume fraction at which the chains just begin to touch decreases, (*i.e.* $\phi^* \propto 1/R_g^3$). Beyond the dilute region, the polymer coils may ether overlap or collapse.

2.1.4.1 Flory-Huggins Theory.

The *Flory-Huggins theory* describes the mixing of a polymer with a solvent. This theory is based on a lattice model and employs the following assumptions,

- The lattice is full.
- The solvent size and segment size are identical.
- Random mixing occurs
- The mean field approximation is valid.
- Pairwise energy interactions

The Flory-Huggins theory, predicts that in a good solvent, a dilute polymer segment will prefer to interact with the solvent rather than with itself. In concentrated solutions this solvent effect is not seen. The mean field condition is that, effectively, the segment concentration is uniform and each segment contributes a '*mean field*' to the overall interactions. In the Flory-Huggins theory for neutral polymer solutions, the primary objective is to calculate the chemical potentials μ_1 and μ_2 as a function of the volume fraction of the polymer (where the subscripts 1 and 2 correspond to the solvent and the polymer respectively). From these chemical potentials the vapour pressure and osmotic pressure can be calculated to predict phase separation boundaries. One of the major triumphs of the Flory-Huggins theory is the ability to predict phase separation of a polymer in a poor solvent.

The chemical potentials can be described as,

$$\mu_1 - \mu_1^{\varnothing} = \left(\frac{\partial \Delta F_{mix}}{\partial n_1} \right)_{n_2} \qquad [2.12]$$

and similarly,

$$\mu_2 - \mu_2^{\varnothing} = \left(\frac{\partial \Delta F_{mix}}{\partial n_2}\right)_{n_1}$$

[2.13]

The required expression (the *Flory-Huggins equation*) relates ΔF_{mix} as a function of ϕ.

$$\Delta F_{mix} = \Delta U_{mix} - T\Delta S_{mix} = k_B T[n_1 \ln\phi_1 + n_2 \ln\phi_2 + n_1\phi_2\chi]$$

[2.14]

where n_1 and n_2 are the numbers of solvent molecules and polymer molecules respectively. The volume fraction may be represented as

$$\phi_1 = \frac{n_1}{n_1 + n_2 x}$$

[2.15]

where x is chain length of the polymer. From equation 2.9, when there is no heat of mixing (*i.e.* $\Delta E=0$) then $\chi = 0$. Generally, χ is positive and dependent upon temperature (equation 2.9) such that as the temperature is increased solution conditions generally get better.

***Figure 2.5;* Effect of Temperature on χ**

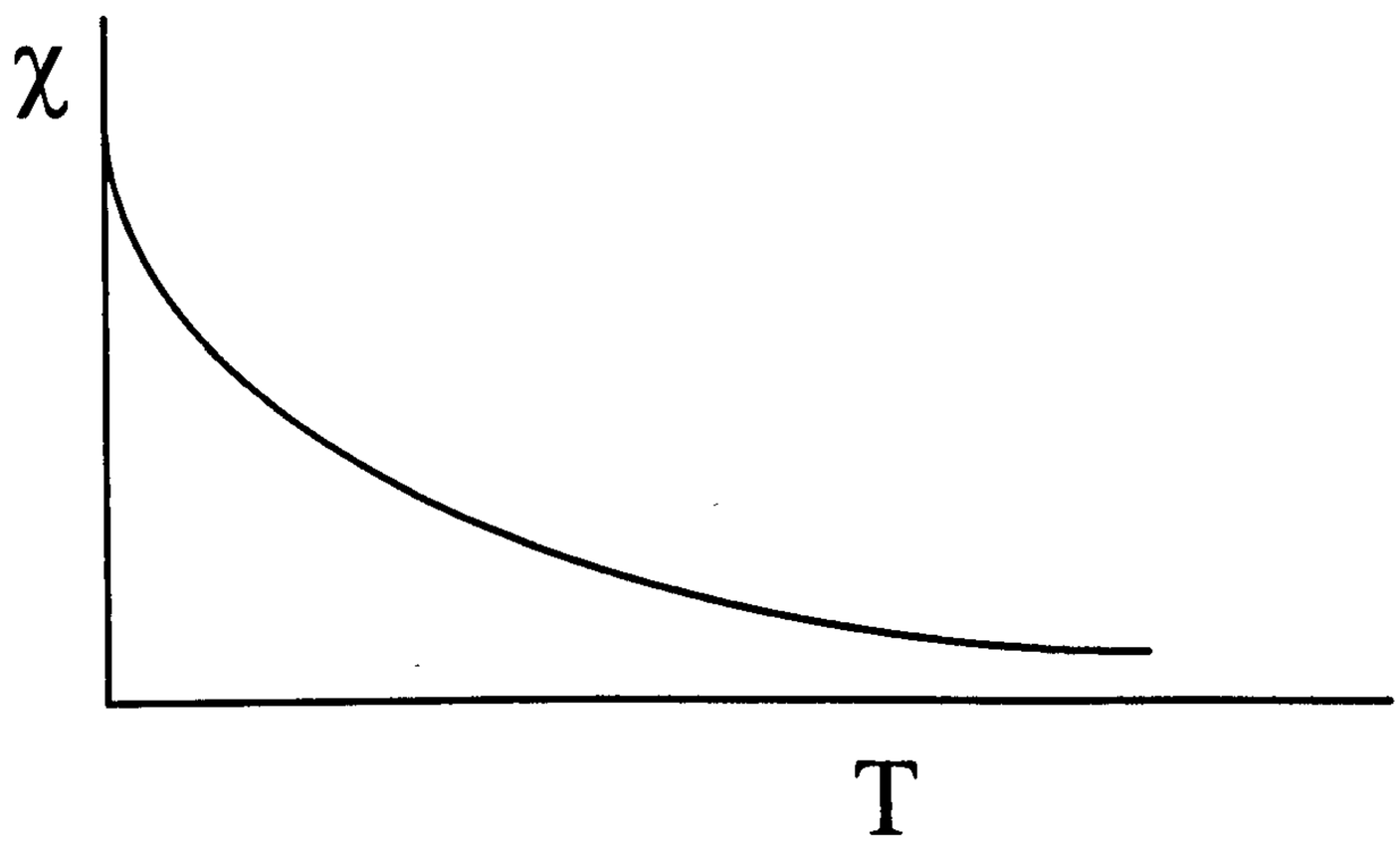

The above Flory-Huggins model is a simple approach which ignores any free volume effects. Incorporating these, equation 2.15 may be represented as,

$$\chi = \frac{Z\Delta E}{k_B T} + \alpha T \qquad [2.16]$$

The result is phase separation upon heating or cooling.

$$\mu_1 - \mu_1^{\varnothing} = \left(\frac{\delta \Delta F_{mix}}{\delta n_1}\right)_{n_2} = -k_B T\left[\phi_2 + (½ - \chi)\phi_2^2 + \ldots\ldots\ldots\right]$$
$$= -RT\left[x_2 + (½ - \chi)x_2^2 + \ldots\ldots\right] \qquad [2.17]$$

where x_2 is the mole fraction of polymer. The first term in this polynomial expression describes the ideal behaviour whilst subsequent terms describe the non-ideal behaviour. When $\chi = ½$ the non-ideal terms disappear and only the first term (or ideal term) remains *i.e.* a θ solvent is one which behaves ideally.

***Figure 2.6*; Effect of Temperature on χ; Incorporating Free Volume Effects**

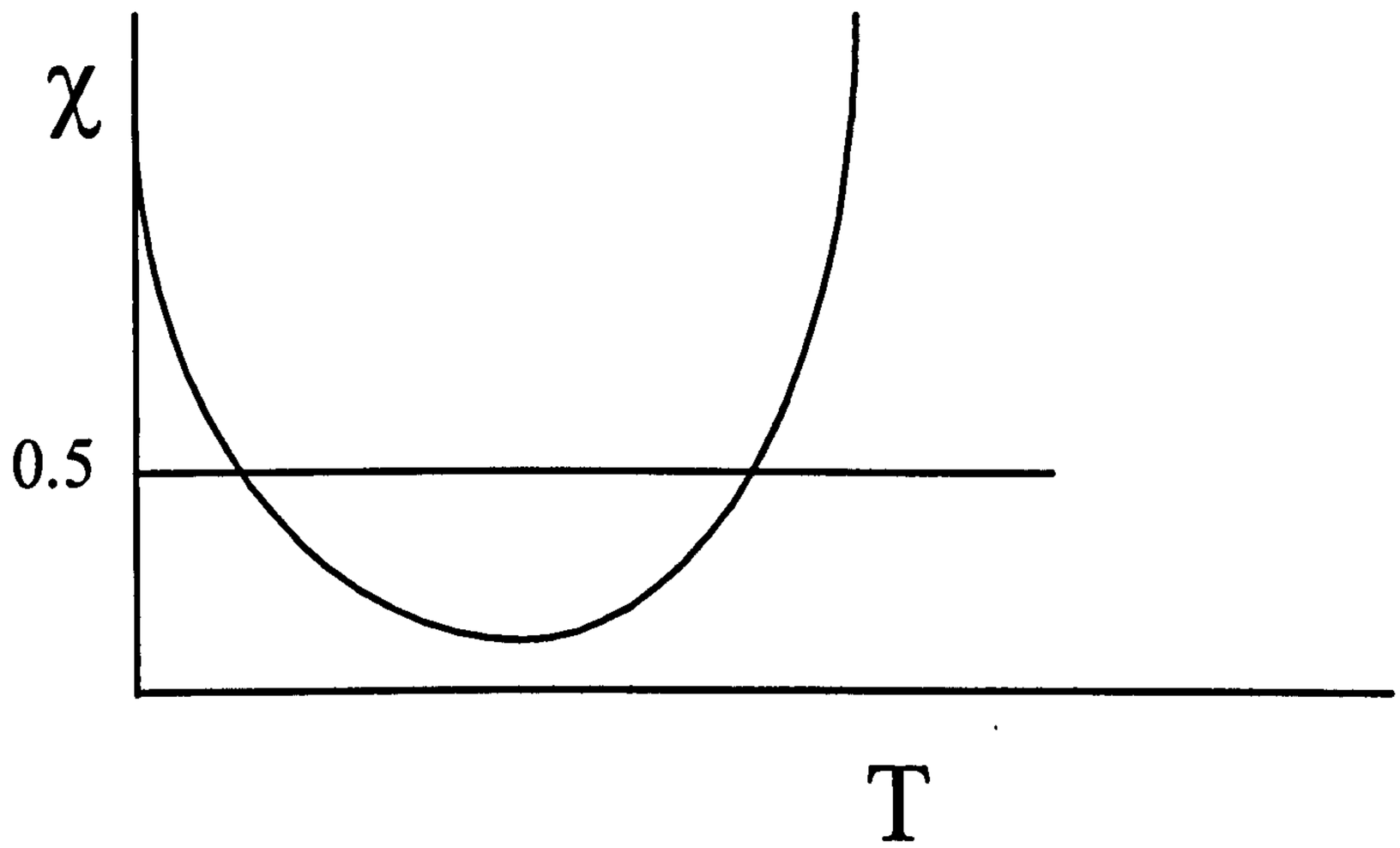

2.1.4.2 De Gennes Scaling Theory.

Another approach to examine concentrated polymer solutions is via *De Gennes scaling theory* which is based on a continuum approach. In this model, polymer segments are arranged in groups known as 'blobs'. It is these blobs which are considered rather than the individual polymer segments. *For example,* the solid line in **Figure 2.7** shows a polymer of N=40 segments, where each segment is of length a.

***Figure 2.7;* Scaling for a polymer where N=40.**

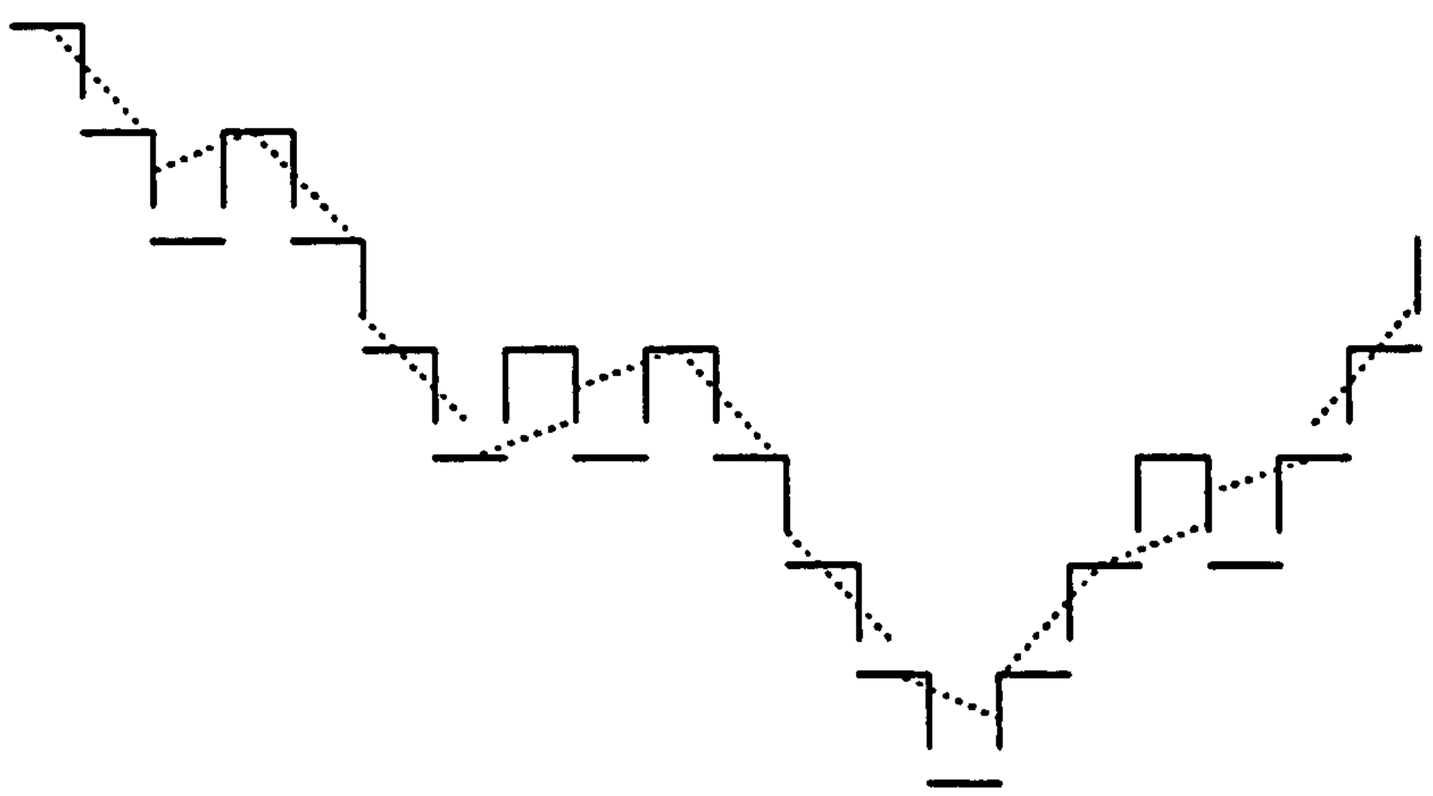

The problem may be simplified by grouping the segments together in small groups rather than individually hence

$$N \Rightarrow \frac{N}{\lambda} \qquad [2.18]$$

and

$$a \Rightarrow a^{\nu} \qquad [2.19]$$

where, λ is the number of segments in a blob and ν is some scaling exponent. For a polymer undergoing a random walk (θ solvent), $\nu = ½$ and for a polymer in a good solvent which undergoes a self-avoiding walk (good solvent), $\nu = ⅗$. The

newly defined polymer (**Figure 2.7**, dotted line) follows the same path as the previously defined polymer, but contains less information. However, whilst both the old and the new polymer still have the same characteristics some dimensional corrections may be required.

Using scaling theory R_g can be obtained by considering the polymer chain as a series of blobs of diameter ξ with λ monomers per blob. If it is taken that inside the blob the polymer undergoes a self-avoiding walk and outside the 'blob' the chain undergoes a random walk, then,

Inside the blob

$$\xi \approx \lambda^{3/5} \qquad [2.20]$$

Outside the blob

$$R_g^2 \approx \left(\frac{N}{\lambda}\right)\xi^2 \qquad [2.21]$$

and therefore

$$R_g^2 \approx N\lambda^{1/5} \qquad [2.22]$$

3.1.5 Gels.

Gels arise when the polymer concentration becomes so high that physical entanglements or chemical bonding between chains occurs. At low concentrations, a gel will be viscous but in more concentrated systems a gel solution will be viscoelastic.

3.1.6 Polyelectrolytes

A simple polyelectrolyte may be defined as a homopolymer where each monomer unit contains an ionisable group. When a polyelectrolyte is dissolved in water, it acquires a degree of electrical charge. If l_e is the distance between elementary

charges on the chain, then the linear charge density will equal e/l_e. As a direct result of these charges a strong electrostatic repulsion builds up, the strength and range of which depends on l_e and the concentration of counter-ions in solution.

In solution the chains become rigid since the internal repulsions are minimal for a straight charge. The polymer chain can be described through the worm-like chain model which replaces the bare persistence length (q_o) of the equivalent uncharged polymer with the total persistence length,

$$q_t = q_o + q_e \qquad [2.20]$$

where q_e accounts for the electrostatic effect. q_t is dependent upon salt concentration, being small at high ionic strength and large at low ionic strengths. For large values of q_t, the general expression for the mean-square end-to-end distance may be written as,

$$\langle R^2 \rangle = L^2\left(1 - \frac{L}{3q_t}\right) \qquad [2.21]$$

where L is the contour length of the chain (L=lN). Therefore, for high values of q_t, equation 2.21 approaches the limit for a rigid rod, $\langle R^2 \rangle = L^2$

2.2 Surfactants in Solution

2.2.1 Classification of Surfactants.

Surfactants tend to be classified according to their head group type; typically

- **Anionic** - Negatively charged head group, such as the alkyl sulphates and the alkyl benzene sulphonates.

- **Cationic** - Positively charged head group, such as the alkyl ammonium bromides.

- **Zwittterionic-** These surfactants contain both negative and positive head groups. Many naturally occurring surfactants fit into this category such as lecithin.

- **Non-Ionic** - These surfactants do not contain a charged group at all. These have only been in use since the 1960's but have wide ranging applications in personal products due to their reduced basicity.

2.2.2 Interfacial Properties at the Air/Water Interface.

Surfactants readily adsorb at most interfaces such as the air-water, oil-water or a solid-liquid interface. The *Gibbs adsorption equation* relates the concentration of material in the interfacial region to the concentration in solution, and to the surface tension at the air-liquid interface. Consider a 2 component system containing a solvent and a surfactant separated by an arbitrary mathematical interface, (usually taken as the air-water interface). These may be defined as having a chemical potential μ and a surface concentration Γ so that the surface tension may be given as

$$\delta\gamma = -\Gamma_1 d\mu_1 - \Gamma_2 d\mu_2 \qquad [2.22]$$

where the subscripts 1 and 2 correspond to the solvent and surfactant respectively. The magnitudes of Γ_i may be either positive or negative depending on the position of the interface between the solvent and the surfactant. If the interface is taken to be in a position such that Γ_1 is zero, then equation 2.22 simplifies to

$$\delta\gamma = -\Gamma_2 d\mu_2 \qquad [2.23]$$

Further, the chemical potential of the surfactant can be related to its concentration (c_2) by,

$$\mu_2 = \mu_2^{\varnothing} + RT\ln c_2$$

[2.24]

Such that,

$$\Gamma_2^{(1)} = -\frac{d\gamma}{RTd\ln c_2}$$

[2.25]

This equation is known as the *Gibbs Adsorption Isotherm*. Therefore, by measuring the surface tension at the air-water interface as a function of surfactant concentration one can calculate the number of moles adsorbed per unit area by taking the gradient at various points on this graph.

2.2.3 The Formation of Micelles.

At a critical solution concentration surfactant molecules will aggregate to form larger entities, known as micelles. These are typically approximately spherical in shape and in aqueous solution form with the hydrocarbon tail group of the surfactant pointing inwards and the surfactant head group pointing outwards. This aggregation occurs at a well-defined concentration, known as the *critical micelle concentration* and the process is known as *self-assembly*. The micelle is a dynamic colloidal entity and does not form a rigid structure. There are several models and techniques for examining micellisation,

- **Light Scattering -** Above the critical micelle concentration (CMC), the amount of light scattered at 90 ° increased. This is indicative of an increase in molar mass. The CMC can accurately be determined in this manner.

- **Solubility -** If the solubility of micelle forming surfactants is measured as a function of temperature, there exists a specific temperature at which the solubility increases dramatically. This arises because unassociated surfactant only has a limited solubility, whereas micelles

are highly soluble. This is known as the *Krafft Temperature* and is the temperature at which micelles can first form.

- **Hartley Micelle** - Hartley proposed the first model for micellisation. The model assumed that the micelles were spherical, consisted of 50-100 monomer units and that micellisation occurred over a narrow concentration region. A number of counter ions is bound to the micelles and these control the conductance and surface charge. The interior of the micelle is composed of hydrocarbon chains and therefore is capable of solubilising species insoluble in water, such as fats and oils. This is a very important property in processes such as detergency.

2.3 Polymers at Interfaces.

Polymers at interfaces have many important industrial applications as wide ranging and diverse as the pharmaceutical industry and waste water treatment. In general, polymers in the interfacial region may be used as dispersants and flocculants, as surface coatings such as lubricants and adhesives, for drag reduction and composite materials.

2.3.1 The Process of Adsorption.

There are three processes which lead to polymer adsorption and these are shown schematically in **figure 2.8**.

- **Diffusion** - The initial process can be through purely Brownian motion or can be enhanced by flow. During this stage the polymer retains its solution conformation.

- **Contact** - The point at which the polymer makes contact with the interface.

- **Relaxation-** If the polymer-interface interactions are favourable, the polymer will relax onto the surface.

Figure 2.8; **The processes which lead to polymer adsorption**

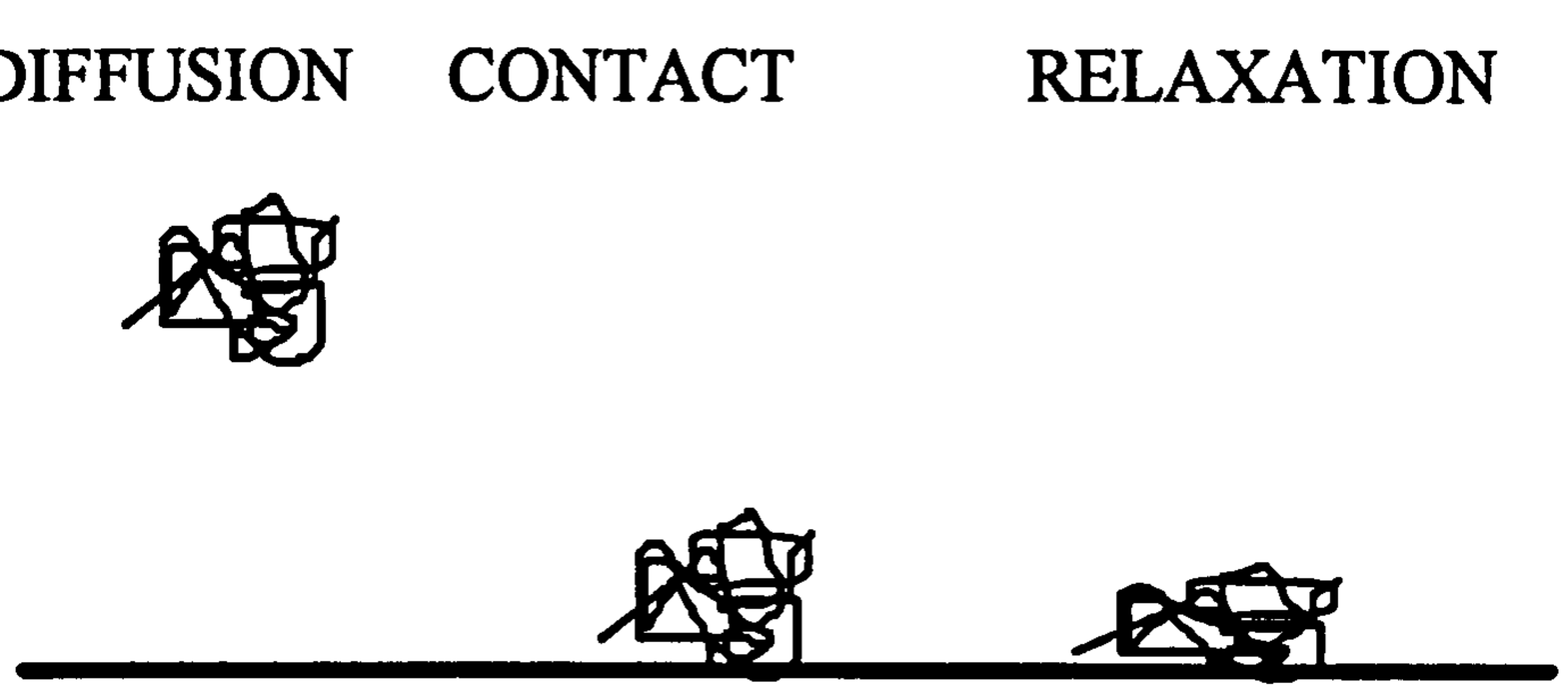

The generally accepted model of the structure of the polymer on the surface consists of loops, trains and tails, **figure 2.9**. Trains are polymer segments in direct contact with the interface, whilst loops and tails protrude into the bulk solution.

Figure 2.9; **The structure of an adsorbed polymer layer.**

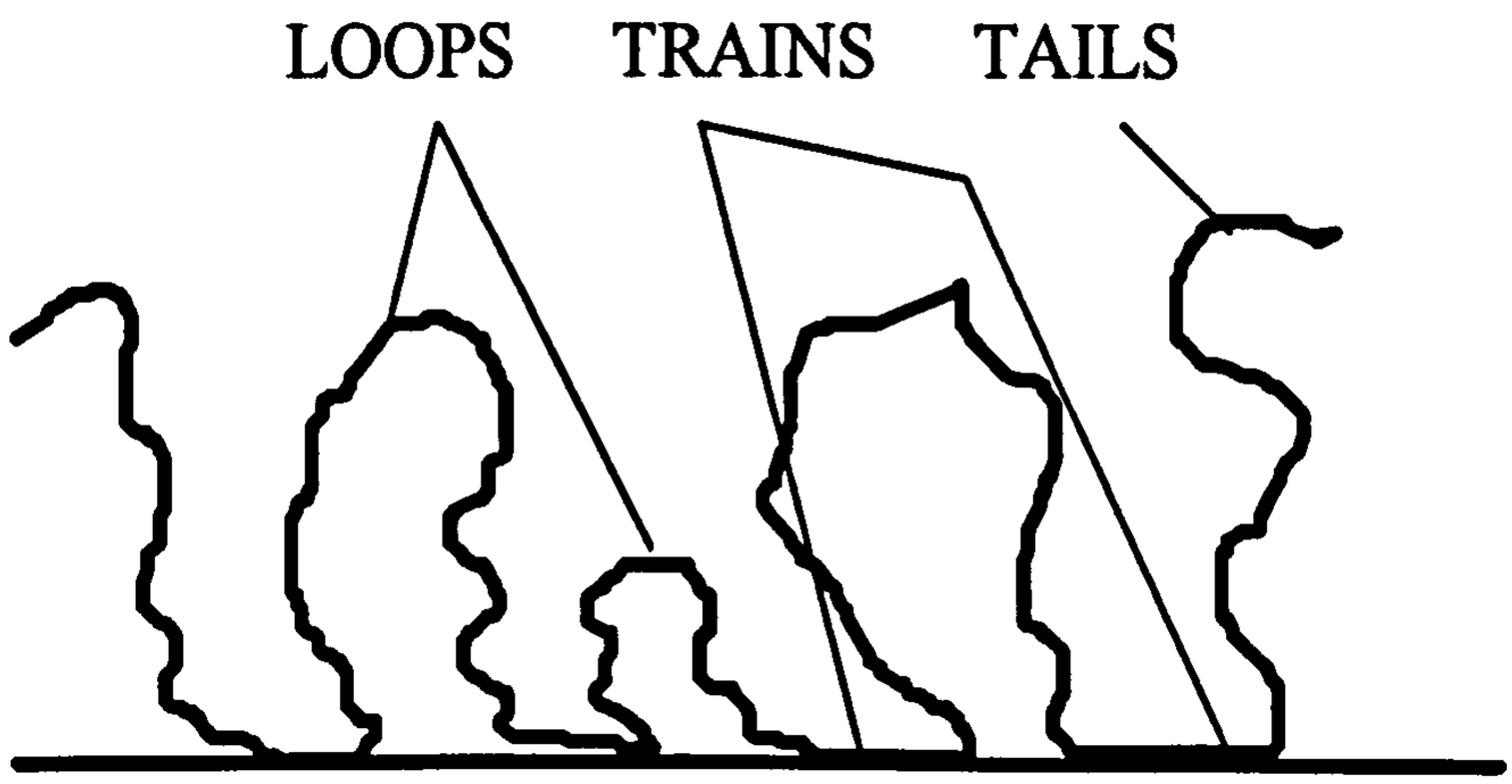

2.3.2 Adsorption Isotherms.

An adsorption isotherm measures the amount of polymer at the interface as a function of the equilibrium polymer concentration in the bulk: **figure 2.10**. The normal units of adsorbed amount, Γ, are mgm^{-2} and Γ may be given by

$$\Gamma = \frac{\Delta C V}{A}$$

[2.26]

where ΔC is the change in concentration of the adsorbed species and V is the total solution volume. A is the available surface area for adsorption. In general, ΔC is very small and therefore inaccuracies are inevitable in its measurement.

Figure 2.10; **An adsorption isotherm for a polymer adsorbed onto a surface.**

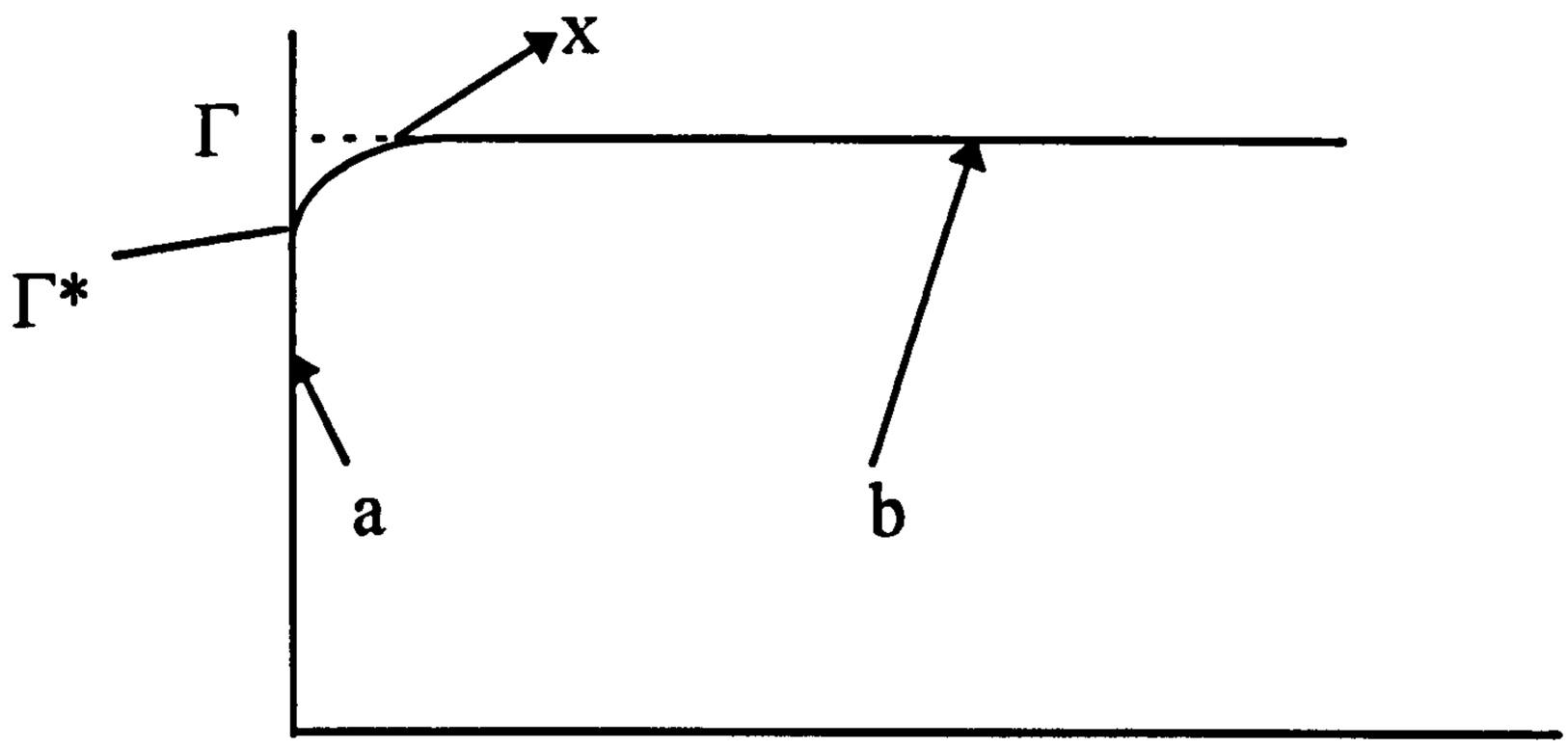

There are two main regions of an adsorption isotherm; the rising part and the pseudo plateau region. For a high affinity isotherm, initially every chain in the system finds its way to the surface and so all of the polymer is adsorbed. This results in a rapid rise in Γ with polymer concentration (region **a** in **figure 2.10**). At position **x** on **figure 2.10** saturation is being reached, the polymer packing becomes tighter until a final plateau in the adsorbed amount is reached (region b in **figure 2.10**). At this position all of the available surface sites are filled. Γ^* is the point at which the adsorbed polymer chains begin to touch and lateral interactions occur. The energy of adsorption is given by

$$\Delta F_{ads} = \Delta U_{ads} - T\Delta S_{ads}$$

[2.27]

In order for adsorption to take place ΔF_{ads} must be negative. Unlike mixing, which is entropy driven, the main driving force for adsorption is ΔU_{ads}. Consider the change in entropy upon adsorption; *i.e.* going from three to two dimensions.

$$\Delta S_{ads} = k_B \ln \Omega^{2D} - k_B \ln \Omega^{3D} \qquad [2.28]$$

Therefore from equation 2.1,

$$\Omega^{3D} = 3^m \qquad [2.29]$$

and

$$\Omega^{2D} = 2^m \qquad [2.30]$$

and so,

$$\Delta S_{ads} = m k_B \ln(⅔) \qquad [2.31]$$

where m is the number of monomer units. The enthalpy of adsorption, ΔU_{ads} is equal to the energy of each contact multiplied by the number of contacts. For adsorption to occur this must equal approximately $-0.4 k_B T$ per monomer. , ΔU_{ads} is related to χ_s, the Flory-Surface parameter by,

$$\Delta U_{ads} = m \chi_s k_B T \qquad [2.32]$$

χ_s may be given by

$$\chi_s = \frac{E_1^a - E_2^a}{k_B T} \qquad [2.33]$$

where E_1^a is the adsorption energy of a solvent molecule and E_2^a is the adsorption energy of a polymer segment. If χ_s is positive, then adsorption will occur. Even for positive values of χ_s, there is a critical value of χ_s below which adsorption will

not occur. This is due the loss of entropy in moving from three dimensions to two dimensions,

$$\chi_s^{critial} = -\ln(1-\lambda_1)$$

[2.34]

where λ_1 is a lattice parameter such that $\lambda_1 z$ is the number of neighbours a site has in each of the adjacent layers. For a tetrahedral or hexagonal lattice $\chi_s^{critial}$ takes a value of approximately 0.29.

2.3.3 Volume Fraction Profiles.

A volume fraction profile describes the volume fraction of adsorbed polymer segments (ϕ) as a function of distance normal to the interface - by convention described by the z-plane. An important parameter when describing volume fraction profiles is the bound fraction, denoted by p. The *bound fraction* is equal to the fraction of total segments in direct contact with the interface and may take any value from $1/N$ to unity. A typical volume fraction profile for an adsorbed uncharged homopolymer is shown schematically in **figure 2.11,**

Figure 2.11; **Schematic Representation of a Typical Volume Fraction Profile**

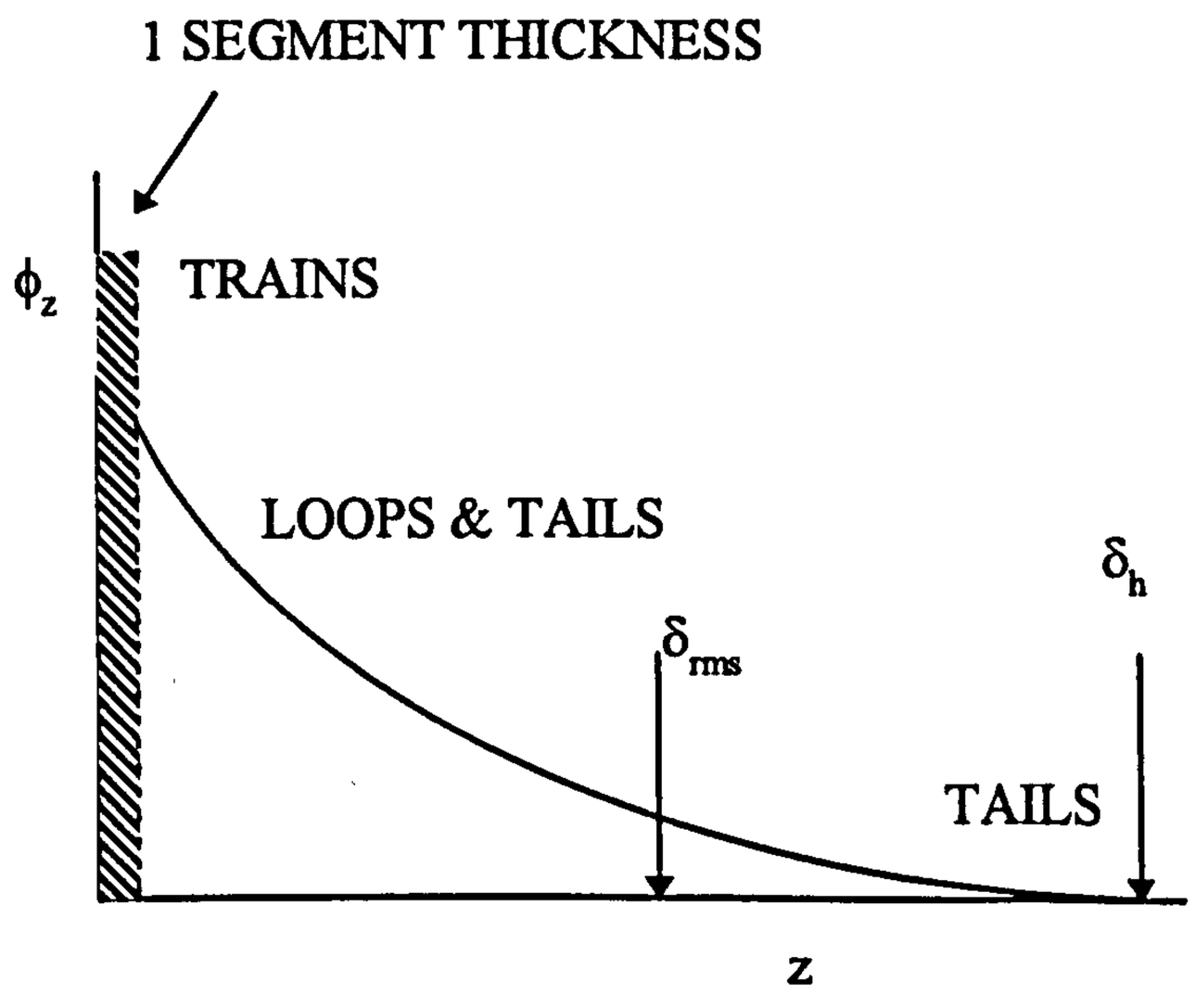

The total area under this curve is equal to the adsorbed amount and may be obtained by integration,

$$\Gamma = \rho \int_0^\infty \phi_z dz \qquad [2.35]$$

where ϕ_z is the volume fraction of segments at any position z from the interface.

2.3.4 Variation of Measured/Theoretical Parameters.

Most commercial polymers formed by free radical polymerisation tend to be polydisperse. This polydispersity is measured by comparing the weight average molecular weight and the number average molecular weight. **Figure 2.12** shows the effect of polydispersity on the adsorption isotherm for two polymer samples of the same molecular weight but differing polydispersity,

Figure 2.12; **Comparison of adsorption isotherms of monodisperse and polydisperse polymers.**

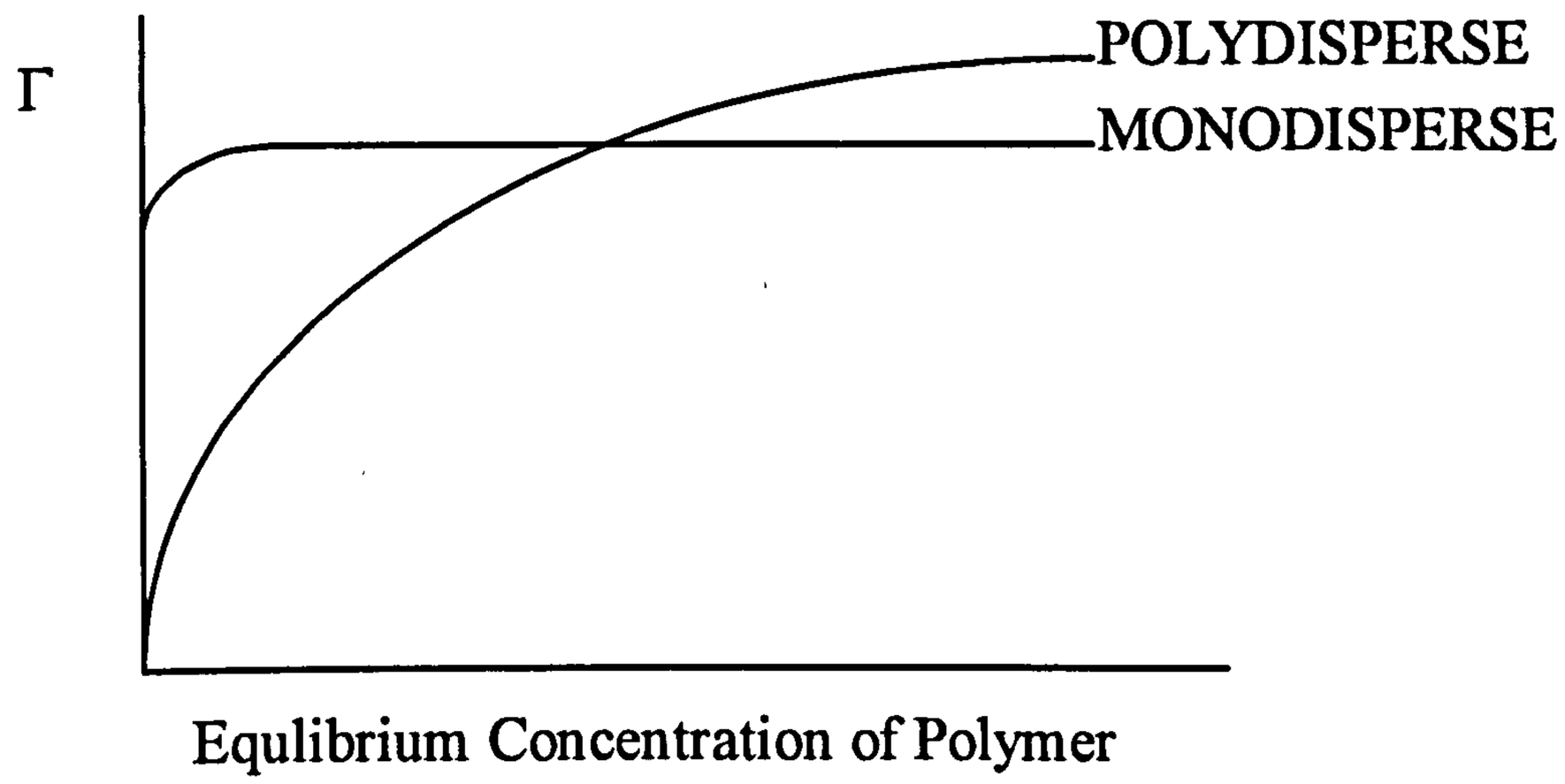

At low coverages, all sizes of molecules can adsorb. However as the surface becomes crowded smaller molecules are squeezed out allowing larger polymer molecules to adsorb minimising entropy factors. Therefore, since larger polymer chains are adsorbed, the adsorbed amount subsequently increases. Another factor to be considered is the time which the system takes to reach equilibrium. For

monodisperse samples the steady state may takes minutes or hours to reach equilibrium owing to rearrangements on the substrate surface. On the other hand, a polydisperse system may take days to reach equilibrium due to rearrangements of adsorbed chains and the desorption of smaller polymer chains.

2.3.5 Polyelectrolyte Adsorption

In polyelectrolyte adsorption, electrostatics play a very important role. The electrostatic interaction is dependent upon charge density (of both the surface and the polymer) and the ionic strength. The adsorbed amount is highly dependent upon these two variables. At low ionic strength, a highly charged polyelectrolyte will adsorb only to a small degree. Increasing the ionic strength will usually increase the adsorbed amount. On the other hand, weakly charged polyelectrolytes tend to give higher adsorbed amounts at low ionic strengths (compared to highly charged polyelectrolytes). At higher ionic strengths, weakly charged polyelectrolytes have been shown to show both increased and decreased adsorbed amounts.

2.3.6 Models of Adsorption.

There are several theoretical models of adsorption and a few of these will be briefly covered in this next section. These models include

- **Exact Enumeration** - This a lattice model for attached single chains. In this model all possible conformations of the polymer chain are counted. *For example*, if the lattice is taken as being a cubic lattice, for one polymer segment there are 5 possible conformations; (the sixth conformation is excluded by the surface.) If m is the number of contacts with the surface then, for example, for a 16 bond chain (17 atoms) m may take values of 1 to 17. The number of walks with m contacts with the surface is given by c(m) and for a 16 bond chain this is equal to 4.393 if m=1 and 2 if m=17. Thus, c(m) can be used to

calculate the average number of contacts with the surface, equation 2.36

$$\langle m \rangle = \frac{\sum_m c(m) m \exp(m\chi_s)}{\sum_m c(m)}$$

[2.36]

$\frac{c(m)}{\sum_m c(m)}$ is the probability that a walk has m visits to the surface.

The bound fraction, p, for a conformation of r segments, m of which are adsorbed can be obtained by weighting each conformation by a Boltzmann factor, $\exp\left(-\Delta U_{ads}/k_B T\right)$ - where ΔU_{ads} is given by equation 2.32. If N_m is the number of conformations with m adsorbed segments then,

$$p = \frac{1}{r} \frac{\sum_m m N_m e^{m\chi_s}}{\sum_m N_m e^{m\chi_s}}$$

[2.37]

Results using this method[1] have shown that a critical value of χ_s exists such that as r tends to infinity p tends to zero if $\chi_s < \chi_s^{critical}$

- **Monte Carlo** - this model is a lattice model which generates a self-avoiding walk by a random number method for a single chain[3]. This procedure is repeated many times in order to obtain a weighted representative set of conformations. The volume fractions in each layer are calculated for each chain and averaged. The effect of coverage or multiple chains are accounted for by using the periodic boundary condition, which generates replicas of the first chain in adjacent cells in the lattice. An advantage of this method is that it is easy to adapt for

specific cases, such as copolymers although it is not practicable using the Monte Carlo method to account directly for the equilibrium between the adsorbed and solution phase.

- **Scheutjens-Fleer** - the Scheutjens-Fleer theory is an extension of the Flory-Huggins lattice theory for polymer solutions[3,4]. The addition of an interface requires evaluating the probabilities of all possible conformations of adsorbed chains in equilibrium with the bulk solution. In this model, chains with similar conformations are grouped together in degenerate sets. From these subsets it is then possible to maximise the partition function for the system by varying the number of chains in each set. The enthalpy for any given set is calculated using the number of solution and surface nearest neighbour contacts.

Consider if there are M lattice layers each of which has L sites. In order to determine ΔH_{ads}, ΔU and S are required. From equation 2.14 we know, that we can obtain approximate values for ΔU and ΔS in solution. However, for a surface,

$$\frac{\Delta U_{ads}}{k_B TL} = \phi^s(1)\chi_s + \sum_{i=1}^{M}\phi^s(i)\langle\lambda\rangle\chi_s \qquad [2.38]$$

where $\phi^s(1)$ is the volume fraction of adsorbed species in the surface layer and $\phi^s(i)$ is the volume fraction of adsorbed species in layer i. $\langle\lambda\rangle$ is the fraction of neighbouring solvent molecules. The entropy is more difficult to obtain.

Like the Flory-Huggins model, the Scheutjens-Fleer model is achieved through a mean-field approximation applied to each layer in the lattice parallel to the interface. In order to obtain the correct equilibrium between adsorbed and free polymer chains the number of layers chosen

must extend well into the bulk solution. Similar non interacting monomers are grouped together with a weighting factor, G(i). This weighting factor is defined as the probability that a segment in layer i with respect to the bulk assuming that all of the monomers are non interacting. Then,

$$G(i) = \exp(\chi_s) \qquad \text{if } i=1$$

$$G(i) = 0 \qquad \text{if } i < 1$$

$$G(i) = 1 \qquad \text{if } i > 1$$

Unfortunately, the Scheutjens-Fleer model does not provide a simple solution and a series of simultaneous equations is obtained. These equations can be solved numerically.

Scaling Theory

The de Gennes scaling theory may be also be applied to polymers at interfaces[5,6]. The application of scaling theory is restricted to the cases of weak adsorption, where $\chi_s << 1$ and for athermal solvents, where $\chi_s < ½$. Both the real and excluded volumes are assumed to be equal. A single parameter κ is utilised to account for interactions between the surface and the polymer chains. κ is related to χ_S:

$$\kappa = \frac{k_B T \chi_s}{A} \qquad [2.39]$$

where A is the area of the surface site. Using this treatment, there are three distinct regimes of adsorbed polymer segments normal to the interface,

- *The proximal regime*; The region of the adsorbed layer where segments are in contact with the surface.

- *The central regime;* The polymer is present as loops or tails which form a fluctuating network of chain segments.

- *The distal regime*; here only long loops and tails contribute, the segmental concentration falls in an exponential profile to that of the bulk solution. (This is the basis for using an exponential volume fraction profile for modelling the small-angle neutron scattering data reported in Chapter 8)

An important note about this scaling theory when applied to physically adsorbed polymer is that the tails of the conformation are ignored. The derived parameters are dominated by the largest loops in the adsorbed layer. Hence, scaling treatments may underestimate the hydrodynamic thickness for physisorbed polymers.

In the case of physically adsorbed polymer a self-similar structure in the central regime is predicted. for the volume fraction $\phi(z)$. The volume fraction profile is predicted to scale as below

$$\phi(z) \approx z^{-4/3} \qquad [2.40]$$

where z is the distance normal to the interface. This $z^{-4/3}$ parameter is related to the fluctuations in the adsorbed layer terms discussed in Chapter 8.

2.4 Surfactant Adsorption.

Surfactants are often used as adsorbates at the solid-liquid interface in order to change the surface charge and/or the hydrophilic/hydrophobic nature of the surface. On a hydrophobic surface the hydrocarbon of the chain of the surfactant can readily displace water from the surface and so adsorption tends to begin with the hydrocarbon chain lying horizontally on the surface in order to make maximum contact. As the surfactant concentration increases so does the density of adsorbed chains and therefore, the hydrocarbon chains begin to interact laterally. This makes adsorption even more favourable. If the surface charge is low and is opposite to that of the surfactant, then the chains tend to remain horizontal to the surface until the solution concentration approaches the CMC. At this point, the chains can stand perpendicular to the surface in order to accommodate a higher packing density. Hemimicelles may even be formed at interfaces with a high surface charge (and hence a large attraction between the surface and surfactant). Moreover, this usually occurs at surfactant concentrations way below the solution CMC.

However, on a hydrophilic surface, the surfactant cannot so easily displace water from the interface. On surfaces with a low charge density little or no adsorption occurs and that which does occur arises through electrostatic interactions. The surfactant adsorbs head-group first (although this is to a certain extent dependent upon the particular surface). On the other hand, if the surface charge is very high, a large number of surfactant molecules may be attracted to the interface. If they are sufficient in number the surfactant molecules encourage other surfactant molecules into the spaces between then interacting laterally by van der Waals forces. This may result in bilayer (or even multilayer) adsorption. The result is a stepped adsorption isotherm. In extreme cases it is even possible, near to the CMC, to change the effective sign on the surface.

Figure 2.13; **Adsorption isotherm of a Surfactant.**

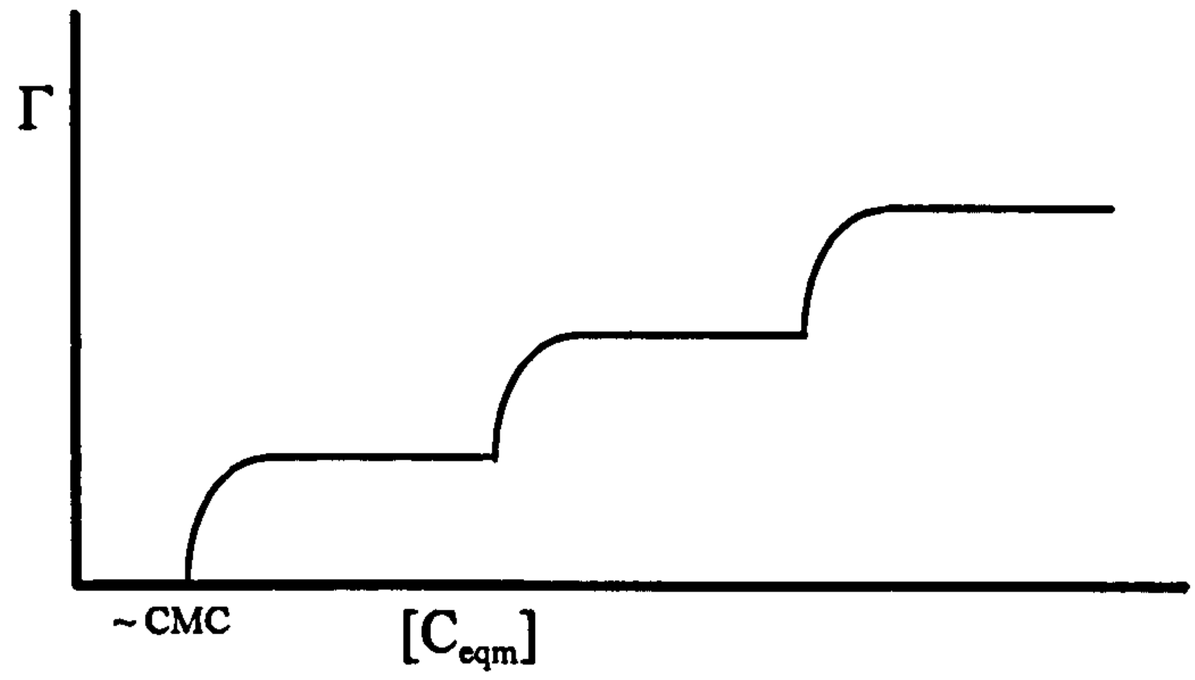

In principle, adsorption from solution to the surface of a solid can be described in terms of the Gibbs Adsorption Models discussed in section 2.2.2. In practice however, problems tend to arise due to surface inhomogeneity and the difficulty associated with defining and measuring the surface tension of solids. The most common method of describing surfactant adsorption is the *Langmuir Adsorption Model* which was first applied to the adsorption of gas molecules at solid surfaces. The isotherm is obtained by considering the process in terms of a simple surface-solute equilibrium,

$$K = \frac{[SX]}{[S][X]} \qquad [2.41]$$

where [S] corresponds to the concentration of empty surface sites, [X] corresponds to the concentration of solute molecules and [SX] corresponds to the concentration of surface sites occupied by solute molecules. If the concentration of surface sites remains constant them the total concentration of surface sites (N_T) can be defined,

$$N_T = [S] + [SX] \qquad [2.42]$$

Combining equations 2.41 and 2.42 leads to the Langmuir Adsorption Isotherm, equation 2.43,

$$[SX] = \frac{N_T K[X]}{(1 + K[X])}$$

[2.43]

This relationship contains relatively few parameters and therefore is easily applied to experimental adsorption data. However, the model is based on the assumption that all adsorption site energies are the same and that the adsorption energy is independent of surface coverage. This situation is rarely obtained in practice and as a consequence of this, this model proves less than satisfactory. To some extent, this problem is alleviated by the *Freundlich Adsorption Isotherm* which is based on the assumption that that there is an exponential distribution of surface sites with respect to adsorption energy. In equation 2.44, K^* is a constant related to the heat of adsorption and n is a constant related to the distribution of surface site energies.

$$[SX] = K^*[X]^{1/n}$$

[2.44]

References.

1. Barber M. N., Guttman A. J., Middlemiss K. M., Torrie G. M., Whittington S. G.; *J. Phys A* **1978** 11 1833
2. Wall F. T., Erpenbeck J. J.; *J. Chem. Phys.* **1959** 30 634
3. Scheutjens J. M. H. M., Fleer, G. J.; *J. Phys. Chem.* **1979** 83 1621
4. Scheutjens J. M. H. M., Fleer, G. J.; *J. Phys. Chem.* **1980** 84 178
5. de Gennes, P.G.; Scaling Concepts in Polymer Physics, Cornell University, Ithica, New York, **1979**
6. de Gennes, P.G.; Adv. Colloid and Int. Sci. **1987** 27 189

Chapter 3

Nuclear Magnetic Resonance (NMR) Spectroscopy.

Magnetic resonance experiments owe their existence to the property that certain nuclei possess magnetic moments which interact with applied magnetic fields. Many NMR techniques have been developed over the last 25 years based on either continuous wave (CW) or pulsed NMR techniques, although continuous wave techniques are now rarely used. Pulsed techniques are more efficient and with Fourier Transform analysis can yield more information in a considerably shorter time compared to continuous wave methods. A most important feature of the NMR technique in general is the fact that it is non-invasive and non-destructive. This, coupled with the fact that the measured properties have a molecular significance make NMR a powerful tool. In this study pulsed NMR techniques are used to measure the spin-spin (T_2) relaxation times of the bulk solvent and the self-diffusion coefficient of polymers or surfactants.

The early work on pulsed NMR suggested by Bloch *et al*[1], put into practice by Hahn[2], made use of short bursts of radio frequency power at a discrete frequency. The observation of the nuclear spin system is made after the power is turned off - this is the essence of the pulsed NMR method. Pulsed NMR has been particularly useful in the study of macromolecular systems providing insight into the dynamic properties of polymer chains.

3.1. Properties of the Nucleus.

All nuclei with an odd atomic number possess the property of spin (I), and this spin gives rise to an intrinsic angular momentum associated with the nucleus. A nucleus with an angular momentum quantum number I may take up 2I+1 different allowed orientations to the reference axis. The value of spin for the hydrogen nucleus, the most common nucleus for NMR, is ½. Nuclei with an even number of nucleons are spinless. The value of angular momentum is given by,

$$\bar{I} = \frac{I(I+1)}{2\pi}h \qquad [3.1]$$

and when defined in the z direction can be written as so that,

$$\bar{I}_z = \frac{m_z h}{2\pi} \qquad [3.2]$$

Where h is Planck's constant and $\bar{I}$ is a vector quantity. m_z is the spin quantum number and defined as,

$$m_z = I,(I+1)(I+2).....-I \qquad [3.3]$$

As mentioned above, hydrogen has a spin of ½ and therefore has two degenerate quantum states where m_z = ½ or -½. In the absence of an external magnetic field the spin states are degenerate, but this degeneracy is lifted when a field is applied. A magnetic moment, $\bar{\mu}$, is produced by a spinning charge (such as a nucleus) and is directly proportional to the magnitude of the spin angular momentum vector $\bar{I}$. The proportionality constant is the magnetogyric ratio, γ, which characterises any particular nucleus.

$$\overline{\mu} = \frac{\gamma h \left|\overline{I}\right|}{2\pi}$$

[3.4]

3.2. Application of an External Magnetic Field.

When a proton is placed in a magnetic field it is possible for it to orientate in $2I+1$ directions, each one at a particular angle, θ, to the field direction. If the magnetic field is B_o and the nucleus has a magnetic moment, $\overline{\mu}$, then the energy of the spin states can be written as,

$$E = -\overline{\mu}B_0$$

[3.5]

The energy separation between the levels is constant and dependant upon the field such that,

$$\Delta E = \frac{h\gamma B_o}{2\pi} = h\omega_o$$

[3.6]

where ω_0 is the frequency in rad s^{-1} and γ is known as the magnetogyric ratio. The magnetogyric ratio is the proportionality constant which relates the observation frequency for a particular nucleus and the applied field. Hence,

$$\omega_o = \gamma B_o$$

[3.7]

The lower energy state (where $m_i = ½$) is usually labelled as the α state and the upper energy state as the β state. The α state is opposed to the direction of B_o whilst the β state is aligned in the same direction. These two energy states are differently populated and since the frequency of nuclear magnetic resonance absorbance is low, the energy difference between the two states is quite small. The ratio of the populations can be given by the Boltzman distribution.

$$\frac{N_\beta}{N_\alpha} = \exp\left(-\frac{\Delta E}{k_B T}\right)$$

[3.8]

where N_α and N_β are the numbers of nuclei residing in the upper and lower states respectively. k_B is the Boltzman constant and T is the absolute temperature. The difference in population between the two states results in a bulk magnetisation, M, of the sample; which is in effect the sum of the magnetisations of the individual spins.

M is aligned to the static field and remains there unless the system is disturbed in some way. (By convention, the direction in which the field is applied becomes the z axis of the system.) When the induced magnetisation is somehow perturbed from the applied field, a torque develops on M_z by B_o. This causes M_z to precess about B_o with a frequency of γB_o rad s^{-1} (from equation 3.7) or $\gamma B_o/2\pi$ Hz. This is known as the Larmor precession frequency, ω_o.

The Larmor precession frequency of magnetic moments in a magnetic field B_o, can be regarded as being equal to the frequency of the energy separating the two spin states of the hydrogen nuclei. If a pulse of radio frequency (r.f.) radiation is introduced at the same frequency as this Larmor precession, energy is adsorbed from the r.f. field.

$$\omega_{rf} = \omega_o$$

[3.9]

The magnetic vector of the r.f. field, B_1, rotates in the xy plane (perpendicular to B_o) - indicated in **figure 3.1**. Moreover, on adsorption of energy from B_1 the magnetic moment tips to a different angle, θ, with the precession frequency remaining the same.

Figure 3.1: **The precession of a magnetic moment $\bar{\mu}$ about a fixed magnetic field, B_0.**

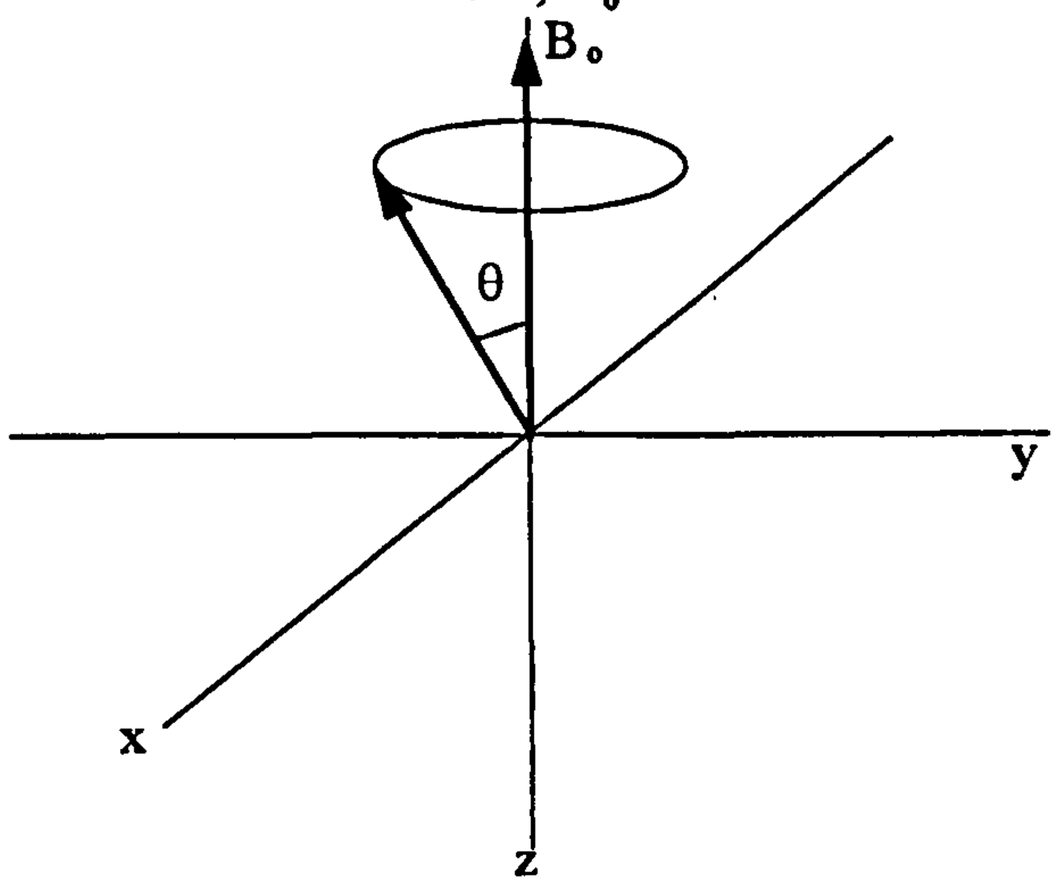

However, in an actual nuclear magnetic resonance experiment, a collection of nuclei are studied rather than a single nuclear spin. In such a system of identical spins the magnetic moments will all precess at the Larmor frequency, ω_o

Figure 3.2: **The precession of an ensemble of identical magnetic moments of nuclei with I = ½. The net macroscopic magnetisation is orientated along the z axis.**

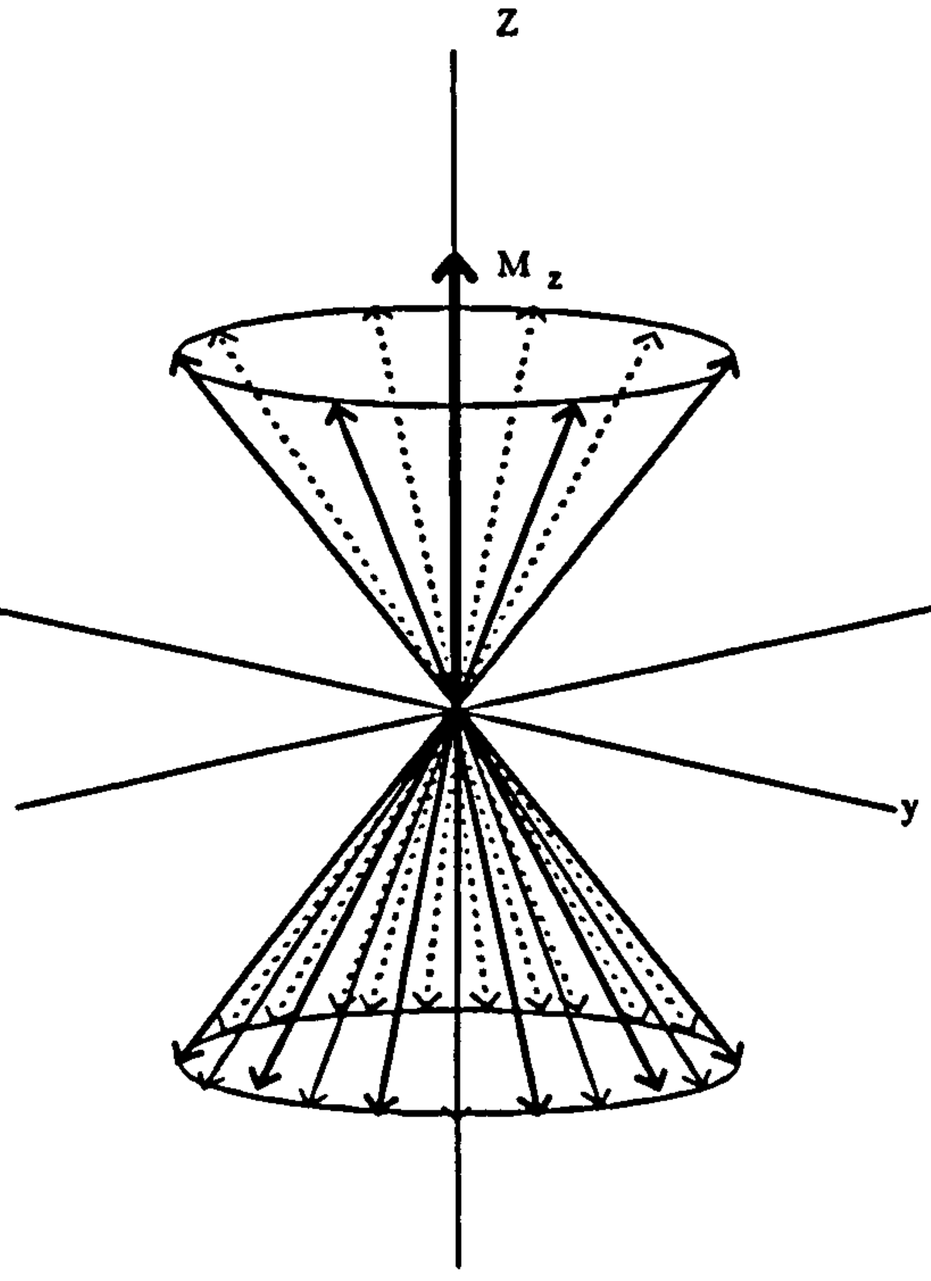

Figure 3.2 depicts the precession of moments of nuclei with I = ½. The actual magnetic moments are distributed equally around all parts of the precsessional cone since the field is perfectly homogeneous. This equal distribution results in no phase coherence in the xy plane. The xy component of the magnetisation is effectively zero, but since the Boltzman distribution slightly favours the lower energy state, at equilibrium there are slightly more nuclei aligned in the direction of B_o than opposed to it. Consequently, there is a macroscopic magnetisation which is aligned along the z axis.

3.3. The Bloch Equations.

Bloch *et al* [1,5] proposed a series of phenomenological equations to describe the motion of the macroscopic magnetisation in the presence of an applied magnetic field. The net magnetisation may be considered as the sum of the individual dipole moments and so,

$$\frac{dM}{dt} = \gamma M \hat{} B \qquad [3.10]$$

where B is the magnetic field which consists of the sum of both the static applied field (B_o) in the z direction and the magnetic vector of the r.f. field (B_1) in the xy plane. M is the vector sum of all of the individual magnetic moments. Since the field due to the r.f. radiation rotates about z with an angular frequency ω, the components of B can be resolved as:

$$B_x = B_1 \cos\omega t \qquad [3.11]$$

$$B_y = B_1 \sin\omega t \qquad [3.12]$$

$$B_z = B_0 \qquad [3.13]$$

Combining equations 3.10 - 3.13 a set of differential equations describing the time dependence of the components of M are obtained;

$$\frac{dM_x}{dt} = \gamma\left(M_y B_o + M_z B_1 \sin\omega t\right)$$

[3.14]

$$\frac{dM_y}{dt} = \gamma\left(M_z B_1 \cos\omega t - M_x B_o\right)$$

[3.15]

$$\frac{dM_z}{dt} = \gamma\left(M_x B_1 \sin\omega t + M_y B_1 \cos\omega t\right)$$

[3.16]

Since the application of an r.f. field disturbs the Boltzman distribution between the α and β states, relaxation back to the Boltzman equilibrium state will occur. Inclusion of relaxation processes in equations 3.14 - 5.16 results in,

$$\frac{dM_x}{dt} = \gamma\left(M_y B_o + M_z B_1 \sin\omega t\right) - \frac{M_x}{T_2}$$

[3.17]

$$\frac{dM_y}{dt} = \gamma\left(M_z B_1 \cos\omega y - M_x B_o\right)\frac{M_y}{T_2}$$

[3.18]

$$\frac{dM_z}{dt} = \gamma\left(M_x B_1 \sin\omega t + M_y B_1 \cos\omega t\right) - M_z - \frac{M_o}{T_1}$$

[3.19]

The longitudinal relaxation time T_1 and the transverse relaxation time T_2 are assumed to be single exponential functions and M_o is the equilibrium value of the magnetisation in the z direction. Thus M_z and M_y decay back to their equilibrium value of zero. All of these phenomenological equations are collectively known as the Bloch equations. T_1 and T_2 will be discussed further in sections 3.5 - 3.12

3.4. The Rotating Frame of Reference.

When considering pulsed nuclear magnetic resonance methods, it is useful to refer the motion of, *for example* the magnetic vectors, in a frame of reference which rotates about B_o in the same direction as the nuclear moments precess. In this "rotating frame of reference" the xy axes rotate about the z axis with an angular frequency ω_o and thus any interactions with a frequency ω_o in the xy plane appear to be static. The magnetisation M (within the rotating frame) is considered in terms of its individual components,

$$M = M_x\bar{i} + M_y\bar{j} + M_z\bar{k} \qquad [3.20]$$

Where $\bar{i}$, $\bar{j}$ and $\bar{k}$ are unit vectors whose rotation (but not length) can be changed by their time derivatives. The rotation can be described mathematically in terms of vector cross-products. If the angular frequency of rotation about the unit vector is given by ω, then in such a rotating co-ordinate system ω is common to all the unit vectors, Thus,

$$\left(\frac{dM}{dt}\right)_{fixed} = \frac{dM}{dt} + \omega\left(M_x\bar{i} + M_y\bar{j} + M_z\bar{k}\right)$$

$$= \left(\frac{\partial M}{\partial t}\right)_{rot} + \omega M \qquad [3.21]$$

The total derivative $(dM/dt)_{fixed}$ represents the overall motion of M in the fixed frame of reference. The partial derivative $(\partial M/\partial t)_{rot}$ represents the time dependence of M in the rotating frame. From equation 3.10,

$$\left(\frac{dM}{dt}\right)_{fixed} = \gamma MB \qquad [3.22]$$

and from equation 3.21,

$$\left(\frac{\partial M}{\partial t}\right)_{rot} = \gamma MB - \omega M \qquad [3.23]$$

Rearranging equation 3.23 and using vector cross product rules

$$\left(\frac{\partial M}{\partial t}\right)_{rot} = \gamma MB + \gamma M\frac{\omega}{\gamma}$$

$$= \gamma M\left(B + \frac{\omega}{\gamma}\right) \qquad [3.24]$$

The term ω/γ can be regarded as a contribution to the field arising from the effect of rotation since it has the dimensions of a magnetic field. We may therefore write an equation for the motion of M in the rotating frame in terms of the effective magnetic field B_{eff},

$$\left(\frac{dM}{dt}\right)_{rot} = \gamma MB_{eff} \qquad [3.25]$$

where B_{eff} may be given by,

$$B_{eff} = B + \frac{\omega}{\gamma} \qquad [3.26]$$

Hence the equations used in the fixed frame of reference remain valid in the rotating frame provided B_{eff} is substituted for B_o. Thus in the rotating frame the magnetisation precesses about B_{eff} instead of B_o with a frequency - γB_{eff}. It is convenient to choose a frame which rotates at the frequency of the applied r.f. field B_1, since in such a frame B_1 is stationary. When the only field present is the static B_o field the effective field can be given by equation 3.26 and when the frame rotates at the Larmor frequency B_{eff} is zero and consequently,

$$\frac{dM}{dt} = 0$$

[3.27]

This illustrates that when the frame rotates at the Larmor frequency the magnetisation vector M is stationary with respect to that frame.

3.5 The Origin of Relaxation.

Whenever a physical system is perturbed from its equilibrium condition and the external influence is removed, it will relax to its original equilibrium condition. Relaxation does not occur instantaneously. The rate at which relaxation occurs can be characterised by a characteristic time, T such that if T is short then the relaxation is fast; conversely if T is long then the relaxation is slow.

For a system of protons, such as the hydrogen nucleus, (where I =½) a small excess of spins will exist in the lower α state at equilibrium. This distribution can be disturbed by either changing M_z (which also changes the energy of the system) or by changing M_{xy} (which involves no energy change). If M_{xy} is made non-zero by the introduction of a rotating field, B_1, applied perpendicular to B_o then the effective field B_{eff} can be given by

$$B_{eff} = B_o + \frac{\omega}{\gamma} + B_1$$

[3.28]

Under resonant conditions the field due to rotation will exactly cancel B_o and the magnetisation interacts only with the B_1 field in the xy plane. B_1 rotates with the same frequency as the frame and is arbitrarily assigned along the rotating axis x'. Therefore, in the rotating frame M precessess about the x' axis; or in other words, the field is trying to turn M into the x' direction.

If a pulse of magnitude B_1 is applied for a time, t_p, then the magnetisation M will tip through an angle ϕ dependant upon t_p such that

$$\phi = \gamma B_1 t_p$$

[3.29]

If the pulse is applied along the x' axis for such a time that $\phi=\pi/2$ radians (90°) then a detector placed along y' will observe a maximum signal. If B_1 is switched off, M_{xy} returns to zero by a first order process with a relaxation time T_2 known as the transverse or spin-spin relaxation time.

$$M_{xy(t)} = M_{xy(O)} \exp\left(\frac{-t}{T_2}\right)$$

[3.30]

This relaxation occurs because the precessional frequencies of all the spins are not the same because of field inhomogeneity or different phases which change randomly during an $\alpha \rightarrow \beta$ transition, but cover a range, some being faster and some slower than the nominal frequency. Thus the precessional cone created by B_1 is blurred out and the spins spiral back to their equilibrium position. However, if a 180° pulse is applied along the x' axis then no signal will be observed along the y' axis since all the magnetisation now lies in the z' direction. The system relaxes to its equilibrium value by the spins undergoing transitions from the upper to the lower level. This involves a loss of energy by the system and hence requires a finite time. This relaxation process which affects only the longitudinal magnetisation is known as longitudinal relaxation and is given the symbol T_1. This process may obey first order kinetics and following the 180° pulse, M_z can be given by

$$M_{z(t)} = M_{z(O)}\left(1-2\exp\left(\frac{-t}{T_1}\right)\right)$$

[3.31]

3.6 Relaxation Mechanisms

There are many different processes under which energy can exchange between the lattice resulting in relaxation. Examples of phenomena which give rise to relaxation in polymer systems include-

- **Dipole-Dipole Interactions** - arise from the interaction of the magnetic fields of nearby nuclear dipoles and is by far the most important in the study of polymers.
- **Quadrupole Interactions** - arises since the distribution of charge in the nucleus is not spherical but ellipsoidal resulting in a net torque exerted on the nucleus.
- **Chemical Shift Anisotropy** - arise from nuclei with different electron clouds shielding the nucleus to varying extents and producing a B_{eff}.
- **Spin-Rotation Relaxation.** - arise from molecules which contain freely rotating small groups. These groups will generate a magnetic field which may couple with the nuclear spin.
- **Scalar Interactions** - If two nuclear spins couple indirectly, for example, via electrons, a magnetic field may be produced by one at the other. If this induced magnetic field fluctuates a relaxation mechanism may be produced.

3.7.Free induction decay

When a 90° pulse is applied along the x' axis in the rotating frame the resultant magnetisation lies entirely along the y' axis. As a consequence of this pulse, a "free induction decay" (FID) can be detected in coils fixed along either the x or the y axes. The magnitude of this pulse is representative of the M_{xy} component of the magnetisation. When the r.f. pulse is applied at exactly the Larmor frequency the subsequent decay is purely exponential and directly measures the decrease in M_{xy}. Conversely, if the frequency of the r.f. pulse is slightly different to the Larmor frequency interference occurs between the reference signal and M_x (or M_y). The resultant interference pattern is known as a Free Induction Decay (FID).

FID's are particularly useful in determining the magnitude and other characteristics of the magnetisation M. The FID following a sequence of two or more pulses is used in the measurement of relaxation times.

3.8 The Measurement of T_1 by the Inverse Recovery Method.

The most common pulse sequence employed to measure T_1 relaxation times is the $180°_x - \tau - 90°_x$ sequence. This is known as the inverse recovery method since the first $180°_x$ pulse inverts the magnetisation along the z' axis. Longitudinal relaxation occurs causing M_z. to go from a value of $-M_0$ through zero to its equilibrium value of M_0. At a time τ after the $180°_x$ pulse has been applied a 90° pulse is applied along the x' axis. The result is that M is rotated to the y' axis. A FID is produced whose height is proportional to the magnitude of M; hence the value of M_z. at time τ. If the system is allowed to return to equilibrium by waiting at least 5 times T_1 and this pulse sequence is repeated for a different value of τ, the decay rate of M_z can be determined as a function of τ by plotting,

$$\ln(A_\infty - A_\tau) = \ln 2A_\infty - \frac{\tau}{T_1} \qquad [3.32]$$

where A_τ is the initial amplitude of the FID following the 90° pulse at a time τ and A_∞ is the limiting value of A_τ for very long intervals between the 180° and 90° pulses (*i.e.* A_0). If $\ln(A_\infty - A_\tau)$ is plotted against τ, T_1 can be determined from the slope.

3.9 Measurement of T_2 by the Spin-Echo Technique.

The spin-echo technique was first proposed by Hahn[2] and consists of a 90°-τ–180° sequence and the observation at a time 2τ of a free induction "echo". The magnetisation vector is tipped through 90° by an r.f. pulse along the x' axis. Since the total magnetisation can be regarded as the vector sum of the individual macroscopic magnetisations, those magnetisations arising from nuclei in different parts of the sample will each experience slightly different values of the applied field - due to field inhomogenities. Therefore a range of precessional frequencies arise which are centred around the rotating frame. Consequently, the individual

magnetic moments appear to "fan-out" as some nuclei precess faster and some slower than the rotating frame.

At a time, τ, after the 90° pulse, a 180° pulse is then applied along the x' axis. The effect of this pulse is to rotate the magnetic moments by 180°, although the magnitude of the precession velocity is not affected. The faster nuclei will now rejoin the y-axis at a faster rate (although they have further to travel), whilst the slower nuclei (which have less far to go) drift back towards this value more slowly. At a further time, 2τ, all the magnetic moments will have come into phase with each other along the y axis; hence the term "echo". The echo amplitude is dependant upon T_2 and therefore T_2 can be determined by a plot of peak echo amplitude as a function of τ. As with the inversion recovery method for T_1 measurements, it is necessary to perform separate pulse sequence for each value of τ. To ensure that equilibrium has been re-established it is also necessary to wait for at least $5T_1$ between experiments. The major limitation with this technique arises due to the effects of molecular diffusion which causes nuclei to move from one part of the inhomogenenous field to another. The echo amplitude is therefore significantly reduced. Carr and Purcell[6] showed a simple modification to Hahn's original technique which can drastically reduce the effect of diffusion on T_2.

3.10 The Carr-Purcell Sequence.

The method proposed by Carr and Purcell may be described as a $180°_x - \tau - 180°_x - 2\tau - 180°_x - 2\tau$.... sequence (or more commonly the Carr-Purcell sequence). All of these pulses are applied along the positive x' axis (as in the spin-echo technique). The 180° pulses at 5τ, 7τ, *etc.* cause echoes at 6τ, 8τ, *etc.* alternately negative and positive in phase. The advantages to this method are two fold. Firstly, there is a considerable saving in time since many echoes may be obtained in a single sequence. Secondly, the effect of diffusion is virtually eliminated by making τ short. However problems may arise for long values of T_2 when many 180° pulses

are required. Imperfections in the length of the pulses cause incomplete rephasing and resultant errors.

3.11. The CPMG Sequence

The solution to this problem was proposed by Meiboom and Gill[7] by shifting the phase of successive 180° pulses by 90°. The same pulse sequence is used as in the Carr-Purcell technique except the 180° pulses are applied along the positive y' axis. The net result is that every pair of 180° pulses show no pulse length error. However, whilst the CPMG sequence can largely overcome problems arising from diffusion and field drift can seriously affect the results obtained

3.12 The Application of NMR to Solvent Relaxation Measurements.

The relaxation behaviour of the solvent molecules observed can be understood by means of a rapid exchange between solvent molecules constrained at an interface (bound) with a short relaxation time, T_{2b} and free solvent molecules in the bulk with a longer time, T_{2f}[8]. Although there are solvent molecules with different relaxation times in the system, a single exponential magnetisation is observed. The dynamically averaged relaxation rate between the two different environments can be given by,

$$\frac{1}{T_{2obs}} = \frac{1-P_b}{T_{2f}} + \frac{P_b}{T_{2b}} \qquad [3.33]$$

Where T_{2obs} is the observed relaxation time and P_b is the fraction of protons in the bound environment, or the fraction time each proton spends in this environment. Thus, the shorter the overall relaxation time the more solvent molecules are bound at the surface. Consequently relaxation time measurements are a method of probing how many solvent molecules are at the surface under particular conditions. It is convenient to discuss the results in terms of the relaxation rate R_2

which is defined as $1/T_2$ or the specific relaxation rate R_{2sp} which describes the relaxation rate with respect to pure water and removes many instrument variables.

$$R_{2sp} = \frac{R_2}{R_2^0} - 1 \qquad [3.34]$$

where $R_2^0 = 1/T_2$ of a standard, usually water.

3.13 Pulsed-Gradient Methods

The pulsed gradient spin echo sequence used to measure diffusion was developed from the spin-echo sequence of Hahn[2] for the measurement of T_2 relaxation times. The attenuation of detected echoes due to molecular diffusion in an inhomogenous field was recognised as a possible method of measuring molecular diffusion. The accuracy and success of this method depends upon the control and quantification of the inhomogeneity used. The application of a linear field gradient across a sample, spatially labels spins according to their position.

$$\omega^{(z)} = \gamma\left[B_o + \overline{G}_z \Delta \overline{z}\right] \qquad [3.35]$$

Where G_z is the magnetic field gradient across the sample and Δz is the position of the nuclear spin from the centre of the sample tube. This equation shows that spins experiencing a high field within the sample will precess more quickly, whilst spins in a low field position will precess more slowly.

Therefore, by applying a linear field gradient, the 'inhomogeneity' may be defined, labelling the nuclei with respect to their position via their precessional frequency. One commonly used sequence to measure diffusion effects was proposed by Stejskal and Tanner[9]. This sequence is based upon a modified CPMG sequence with two field gradient pulses of width δ, which are applied for equal durations during the time Δ ,**figure 3.3**,

Figure 3.3: **The Stejskal and Tanner Sequence for Measuring Diffusion Coefficients.**

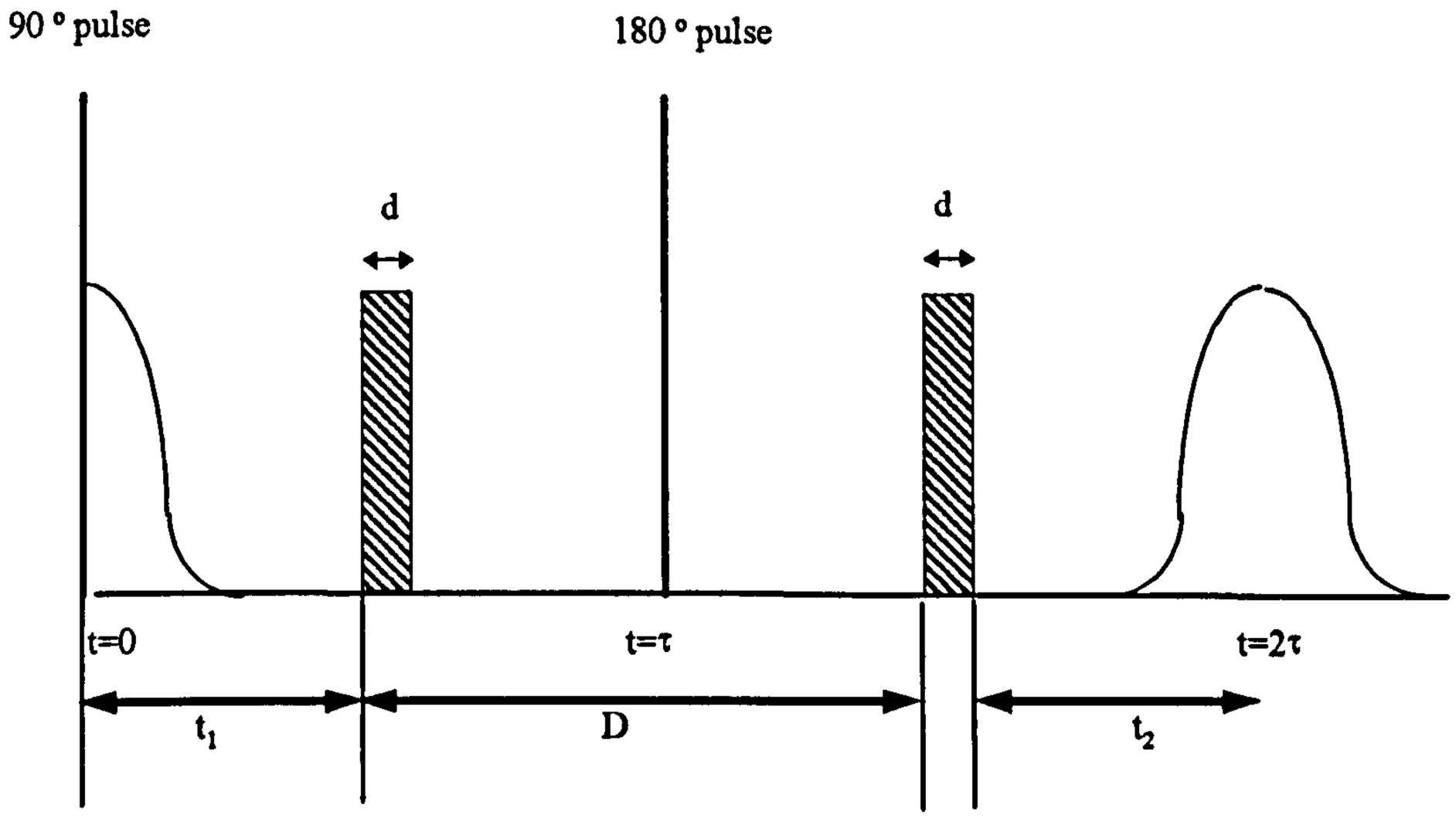

3.13.1 Derivation.

Stejskal and Tanner[9] derived the effect of a time dependent magnetic field gradient on a spin-echo experiment in the presence of diffusion. An approach initially developed by Torrey[10] and extended by Abragem[11]. The following equation defines the spin system when one 90° pulse is followed by one 180° pulse.

$$\frac{\partial \Psi}{\partial t} = -i\gamma(r.G)\Psi + D\nabla^2\Psi \qquad [3.36]$$

where

$$M_x + iM_y = \Psi \exp\left[-(i\omega_o + \frac{1}{T_2})t\right] \qquad [3.37]$$

∇ is the differential operator and M_z+iM_y represents the behaviour of the components of M in the plane perpendicular to the applied magnetic field H_o. The gradient G(t) which is assumed to be uniform is defined by,

$$H_z = H_o + (r.G)$$

[3.38]

The function Ψ, which is independent of T_2 describes the variation of magnetisation in a co-ordinate system rotating with angular velocity $\omega_o=\gamma H_o$ about the z-axis and in the same sense as M precesses. D is the self-diffusion coefficient.

In the absence of the diffusion term, between the 90° pulse (at t=0) and the 180° pulse (at t=r), Ψ can be given by,

$$\Psi = A\exp(-i\gamma r.F)$$

[3.39]

where,

$$F(t) = \int_0^t G(t')dt'$$

[3.40]

The boundary condition is imposed where Ψ=A immediately following the 90° pulse. The effect of the 180° pulse is to set back the phase of Ψ by twice the amount by which it has advanced. Therefore, following the 180° pulse,

$$\Psi = A\exp[-i\gamma r.(F-2f)+i\varphi]$$

[3.41]

where, f=F(r). φ is the phase angle and depends upon the phase of the 180° pulse relative to that of the 90° pulse. The echo is expected at t=τ such that F(r')=2f since Ψ=A for all values of r as it did immediately following the 90° pulse. The behaviour of Ψ from the 90° pulse to echo and beyond may be represented as,

$$\Psi = A\exp\{-i\gamma r.[F+(\xi-1)]\}$$

[3.42]

and,

$$\xi = +1 \qquad \text{for } 0 < t < r$$

$$\xi = -1 \qquad \text{for } t > r$$

If we now consider the diffusion term in equation 3.36 and if A is a function only of t, then,

$$\frac{dA}{dt} = -\gamma^2 D\left[F + (\xi - 1)f\right]^2 A \qquad [3.43]$$

Integrating between $t = 0$ and $t = \tau'$

$$\ln\left[\frac{A(\tau')}{A(0)}\right] = -\gamma^2 D\left[\int_0^{\tau'} F^2 dt - 4f.\int_{\tau}^{\tau'} F dt + 4F^2(\tau' - \tau)\right] \qquad [3.44]$$

Since, $\Psi = A(0)$ immediately after the 90° pulse and $\Psi = A(\tau')$ at the peak of the echo, then $\frac{A(\tau')}{A(0)}$.

The nuclei are subjected to a steady gradient g_o which is due to field inhomogenieties and a second gradient g, which can be turned on for a time δ between the 90° and 180° pulses and again between the 180° pulse and the echo. If the first gradient pulse occurs at a time t_1 and the second at a time $t_1+\Delta$, for this choice of G(t) the echo occurs at $t = 2\tau$. The effect on the echo amplitude is given by,

$$\ln\left[\frac{A(2\tau)}{A(0)}\right] = -\gamma^2 D\left\{\begin{array}{l} \frac{2}{3}\tau^3 g_o^2 + \delta^2(\Delta - \frac{1}{3}\delta)g^2 - \\ \delta\left[\left(t_1^2 + t_2^2\right) + \delta(t_1 + t_2 + \frac{2}{3}\delta^2 - 2\tau^2\right] g.g_o \end{array}\right\} \qquad [3.45]$$

where,

$$t_2 = 2\tau - (t_1 + \Delta + \delta)$$

[3.46]

and is the time between the end of the second gradient pulse and the peak of the echo. When g vanishes only the term in g^2 remains and the result is,

$$\ln\left[\frac{A(2\tau)}{A(0)}\right] = -\gamma^2 D(\Delta - \frac{1}{3}\delta)g^2$$

[3.47]

If δ is allowed to approach zero (or at least until $\frac{1}{3}\delta <<< \Delta$, the result is even simpler.

$$\ln\left[\frac{A(2\tau)}{A(0)}\right] = -\gamma^2 D\delta^2 \Delta g^2$$

[3.48]

3.13.2 Effect of Pulse Sequence on Nuclear Spins.

The effect of this sequence on the nuclear spins in a sample and the manner in which it allows the measurement of molecular diffusion may be considered by visualising the effect of the experiment on three spins in a sample tube as depicted in **Figure 3.4**

Figure 3.4; **Effect of the Diffusion Experiment on Nuclear Spins.**

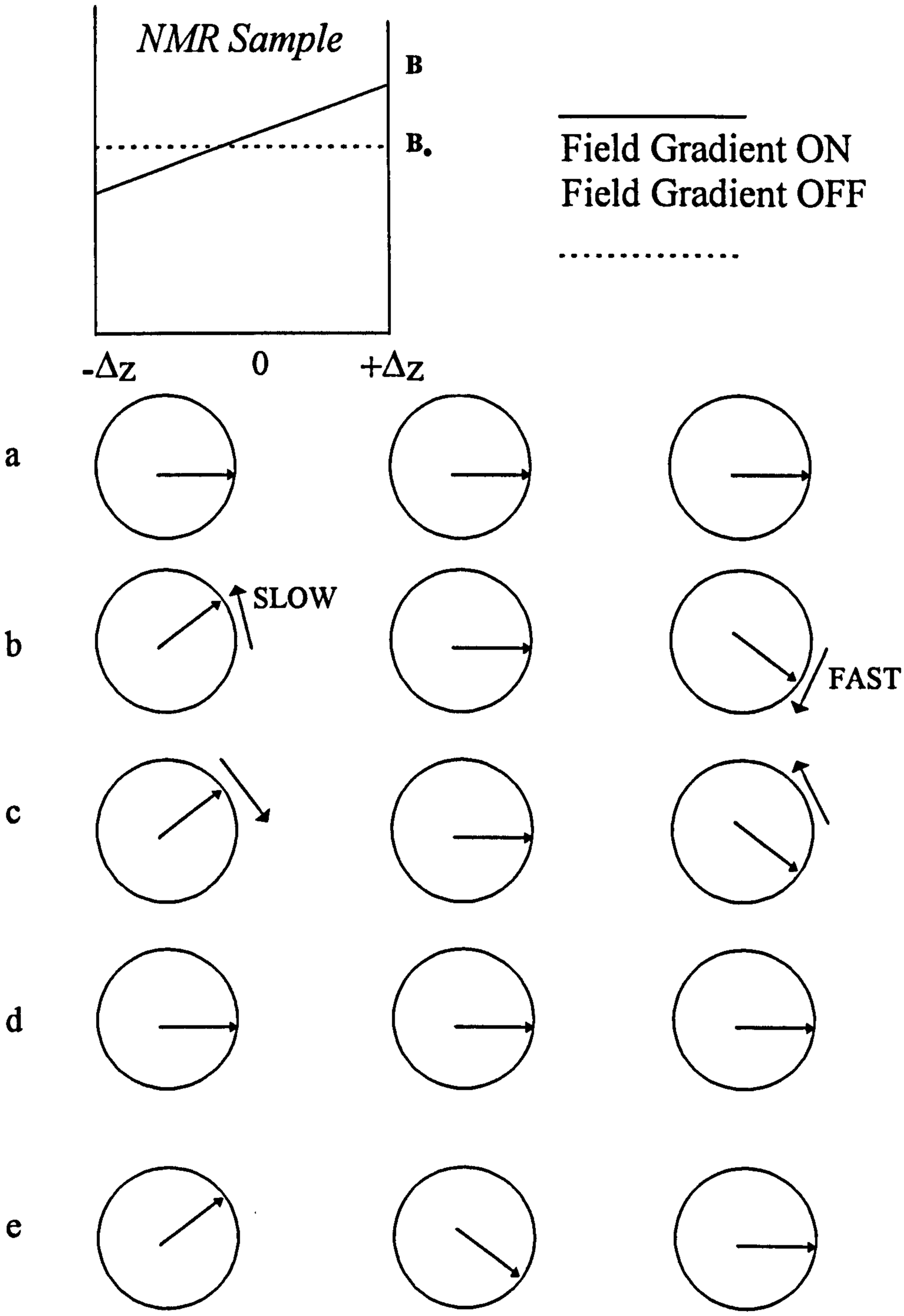

i. the 90° pulse leaves all three spins precessing in the xy plane at the Larmor frequency and stationary in the rotating frame (figure 3.4 a)

ii. Figure 3.4b. The field gradient is turned on for a time δ and those spins experiencing a stronger field will precess more quickly, whilst those in a weaker field more slowly. (On the diagram, the right hand nuclear spin in the sample tube will precess faster than the left hand spin or the central spin.) The effect of the field gradient pulse has been to artificially bring about the same dephasing of the spins that field inhomgenieties bring to any CPMG experiment. The important factor is that the induced inhomogeneity is known and may be applied again at will.

iii. At another set time interval after the 90° pulse a 180° pulse is applied. The effect of this pulse is to invert the magnetisations and thus reverse the directions of the spins as shown in figure 3.4.c.

iv. Figure 3.4.d. After another time interval a second field gradient pulse is applied for the same period δ. Applying the same field gradient pulse as after the 90° pulse has the same effect as applying a field gradient of opposite sign. If there has been no diffusion, then the spin vectors will be in phase and an echo occurs. Therefore t_1 seconds after the second field gradient pulse and 2Δ after the initial 90° pulse, the spins should be completely refocused the yield an echo of maximum amplitude.

v. In figure 3.4.e, the diffusion within the sample of three spins may be visualised as an exchange of position by two spins in the tube. This exchange will lead to a loss of phase coherence and an attenuated echo.

The degree of attenuation in a real sample gives a measure of diffusion within that sample.

3.13.3 LED Sequence.

Gibbs and Johnson[12] have recently developed a longitudinal eddy current delay pulse sequence (LED sequence) which is particularly useful in studying colloidal systems. In this sequence an additional r.f. pulse pair is added which has the effect of storing the simulated echo in the z-direction until the eddy currents over the sample volume have decayed. The LED experiment is normally less influenced by spin relaxation processes, since relaxation is primarily longitudinal during this experiment. Colloidal systems in solution usually have components of re-orientation at a rate of the order of the Larmor frequency. Therefore, T_1 is significantly larger than T_2 and much less dependant upon molecular weight for polydisperse colloidal systems.

3.13.1 Restricted Diffusion.

In systems such as emulsions and micelles, restricted diffusion may arise. In these situations there is an impenetrable boundary so the diffusion is no longer free. D_s is equal to the bulk value when the distance travelled during Δ is less than the boundary size. However, when the distance travelled is comparable with the boundary size, the species interacts with the wall. In PGSE-NMR, this can lead to a maxima in the attenuation plot where spin coherence is regained not through the gradients but because there is coherence in the positions.

References.

1. Bloch F.; *Phys. Rev.* **1946** *70* 460
2. Hahn E. L.; *Phys Rev.* **1950** 80 580.
3. Cosgrove T., Griffiths P. C.; *Adv. Coll. Int. Sci* **1992** *42* 175
4. Blum F.; *Colloids and Surfaces* **1990** *45* 361
5. Bloch F., Hansen W. W., Packard M.; *Phys. Rev.* **1946** *70* 474
6. Carr Y. H., Purcell E. M.; *Phys. Rev.* **1954** 94 630
7. Meiboom S, Gill D.; *Rev. Sci. Instrum.* **1958** 29 688
8. van der Beek G. P., Cohen Stuart M. A., Cosgrove T.; *Langmuir* **1991** 7 327
9. Stejskal E. O., Tanner J. E., J.; *Chem. Phys.* **1965** 42 288
10. Torrey H. C.; *Phys. Rev.* **1956** 104 566
11. Abragem A.; *The Principles of Nuclear Magnetism,* Oxford University Press, London **1961**

PAGE

MISSING

IN

ORIGINAL

Chapter 4

Small-Angle Neutron Scattering

Neutrons offer several advantages over light and x-rays for studying condensed matter with dimensions in the range 10 to 1000 Å. In contrast to x-rays, where the scattering length varies with atomic number, for neutrons it tends to vary irregularly. Secondly, and perhaps more importantly, the scattering length of any given molecule may be altered by employing different isotopes in many cases without substantially changing any intermolecular interactions. Most notable is the technique of deuterium substitution, *i.e.* the substitution of deuterium for hydrogen. There is a large difference in the scattering lengths of hydrogen and deuterium and this property forms the basis of contrast variation experiments.

4.1 The Neutron

Neutrons have no charge yet possess a magnetic moment and a mass virtually equal to that of a proton. The wavelength of a neutron is dependent upon its velocity.

$$mv = \frac{h}{\lambda} \qquad [4.1]$$

where m is the mass, v is the velocity, h is Planck's constant and λ is the wavelength. Neutrons and electromagnetic radiation share many wave-like properties. *For example*, both may be polarised, exhibit birefringence and optical activity. The refractive index of neutrons is only very slightly less than unity which allows neutrons to be totally externally reflected and provides the basis of the technique of neutron reflection. However, in contrast to electromagnetic radiation, neutrons interact with the nucleus rather than the electrons surrounding

the nucleus. Neutrons are scattered by short range repulsive interactions at the nucleus and this interaction may be elastic, inelastic or quasi-elastic:

- **Elastic Scattering** - There is no energy change of the neutron upon collision with the bulk material.

- **Inelastic Scattering** - There is a finite energy change during the scattering event. Energy can be either gained or lost.

- **Quasi-elastic Scattering** - Occurs when the change in energy tends to be small and the spectrum obtained contains no discrete peaks. This type of scattering is used to provide information on translational and rotational diffusion in liquids and solids.

Since, for the purposes of structure and conformation investigations, the elastic scattering gives sufficient information, this discussion will only concentrate on elastic scattering.

4.2. The Scattering Vector

The principle of the neutron scattering experiment from a bulk material is to bring a beam of radiation (wavelength λ) onto the sample and measure the intensity of the scattered neutrons as a function of scattering vector Q. The scattering vector is the resultant between the vector for the incident radiation ($\underline{k}_o$) and the vector describing the scattered radiation ($\underline{k}_s$). If the scattering is elastic in nature then the magnitude of $\underline{k}_o$ and $\underline{k}_s$ will be the same and equal to $2\pi/\lambda$, pointing in the direction of travel of the neutrons. **Figure 4.1** shows schematically the typical scattering from a particle.

Figure 4.1: **Schematic Representation of the Scattering from a Particle**

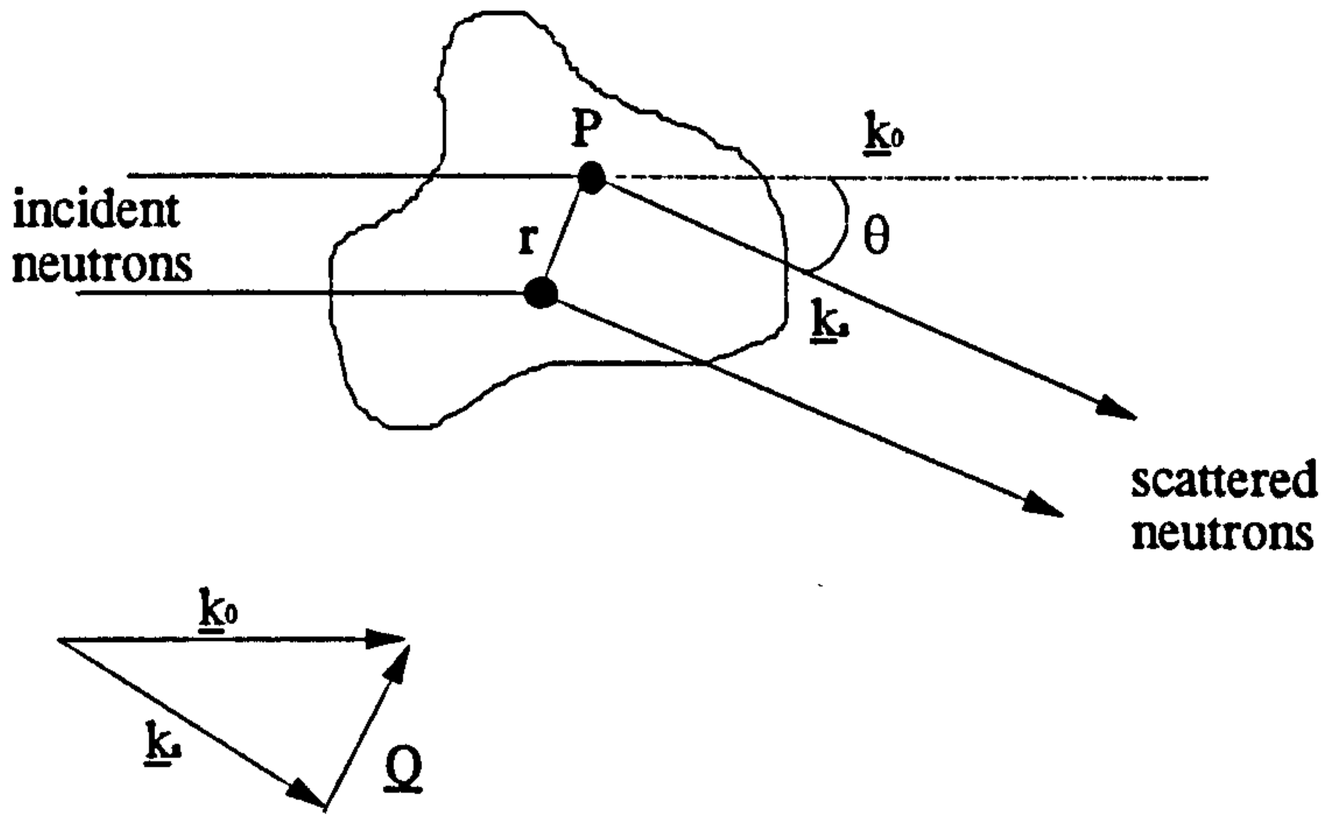

$$|\underline{k}_o| = |\underline{k}_s| = 2\frac{\pi}{\lambda}$$

(*i.e* elastic) [4.2]

$$Q = \underline{k}_0 - \underline{k}_s = 2\underline{k}_s \sin\left(\frac{\theta}{2}\right)$$

[4.3]

Therefore,

$$Q = \frac{4\pi}{\lambda}\sin\left(\frac{\theta}{2}\right)$$

[4.4]

4.3. Neutron Scattering Length Density

The scattering length density is denoted by the symbol ρ and has units of reciprocal length squared:

$$\rho = \frac{b_i}{V}$$

[4.5]

where b_i is the scattering length of nucleus type i,(dependent upon molecular composition) and V is the molar volume. The efficiency of the scattering process

depends on the scattering length. The scattering length density of molecule n, ρ_n, can be obtained by summing over all the scattering lengths in a molecular volume. Thus,

$$\rho_n = \frac{\rho_m}{m}\sum_i n_i b_i \qquad [4.6]$$

where, n_i is the number of atoms of type i per molecule, ρ_m is the physical density and m is the molar mass. The scattering length is uniquely dependent on the isotope which produces the scattering and tends to vary randomly across the periodic table. *For example*, the hydrogen nucleus has an approximate value of b of -0.374×10^{-6} Å, whilst for the deuterium nucleus the value is 0.667×10^{-6} Å[1]. The negative value for the hydrogen nucleus is due to a 180° phase shift between waves scattered by hydrogen and deuterium.

If the scattering length density for each type of molecule in the system can be calculated, it is possible through a judicious choice of solvent (or indeed mixed solvent) to arrange for the scattering length density of the solvent to match a particular component. This is usually achieved by isotopic substitution. There is the very large difference in scattering length between hydrogen and deuterium which makes contrast matching such a valuable tool in neutron scattering. *For example*, it is possible to determine the thickness of an adsorbed polymer layer by arranging for the solvent to have the same scattering length density as the core particles. In this case the particle is said to be '***contrast matched***' to the solvent. The scattering is now dominated by the adsorbed layer and its thickness, amongst other parameters, can now be determined.

4.4 Neutron Instrumentation and Data Reduction.

There are two main methods of producing neutrons in significant controlled amounts; one is to use a nuclear reactor and the other is via a pulsed or spallation source. The Institut Max von Laue - Paul Langevin (ILL) in Grenoble, France is the most powerful reactor source in the world today. Neutrons are released

during the fission of Uranium-235 nuclei. A spallation source such as the ISIS facility at the Rutherford Appleton Laboratory, Didcot, UK, uses a particle accelerator to raise protons to very high energies. These protons are directed at a heavy metal target, typically Uranium, and due to their very high energy, can blast the nuclei in the target apart thus producing neutrons.

The basic components of a small-angle neutron scattering instrument are very similar to those for x-ray or light scattering: a collimated beam of neutrons passes through the sample and ultimately onto a detector. The primary flight path (that before the sample) contains various devices to collimate the incident neutron beam, to select the wavelength of desired neutrons and to measure the neutron flux. Both the primary and secondary flight paths are evacuated and the whole instrument is surrounded by neutron adsorbent shielding for safety reasons and to reduce radiation level backgrounds. The detector is a two-dimensional area detector which may be visualised as a chequers board.

The absolute values of the scattered intensities can be calculated from the scattering and the transmission of a standard sample as a background. The transmission is the ratio of the number of neutrons entering the sample to the number leaving it. By dividing by a standard sample, often water, many instrument variables can be omitted.

$$I_{corr} = \frac{I_s / M_s(1-T_w)}{4d\pi T_s \, I_w / M_w} \qquad [4.7]$$

where I_{corr} is the corrected intensity, I_s is the intensity from the sample, M_s is the sample monitor count, T_w is the transmission of water, T_s is the transmission of the sample, I_w is the intensity due to the standard sample, M_w is the standard monitor count and d is the sample thickness.

4.5 Scattering from Dilute Dispersions of Spherical Particles.

The scattering amplitude from spherical particles is dependent upon two terms: a contrast factor and a geometric interference factor. The interference term is a function of the scattering vector (Q) and is directly related to the shape, size and structure of the scattering entity. The contrast factor ($\Delta\rho$) is dependent upon the nuclear composition. The intensity of the scattering is the amplitude squared. An instrument constant (A) which takes into account parameters such as the detector efficiency is also required to find the absolute scattering intensity.

$$I(Q) = AN_p V_p^2 (\Delta\rho)^2 P(Q) \qquad [4.8]$$

where the geometric interference factor (or form factor) is denoted by P(Q) and is in general given by

$$P(Q) = \left(\frac{1}{V_p} \int_V \exp(iQr) dr \right)^2 \qquad [4.9]$$

where r is the particle radius and V_p is the volume of the particle. At intermediate values of Q, the slope of a plot of log P(Q) versus log Q varies with the particle shape. *For example*, needles give a Q^{-1} dependence, disks Q^{-2}. For a dispersion of N_p non-interacting spherical particles of radius r and volume V_p the form factor is given by,

$$P(Q) = \left[3 \frac{(\sin(Qr) - Qr\cos(Qr))}{(Qr)^3} \right]^2 \qquad [4.10]$$

This appears as a series of maxima and minima in intensity and the number of these increase as the value of r increases. The figure below shows models of the curves obtained for monodispersed spheres with radii of 25 nm and 100 nm. In reality, only the first few maxima are seen, even for the most monodispersed samples.

Figure 4.2: **Log I(Q) Against Q for Spherical Particles Calculated Using Equation 4.10 for 25 nm and 100 nm Spheres.**

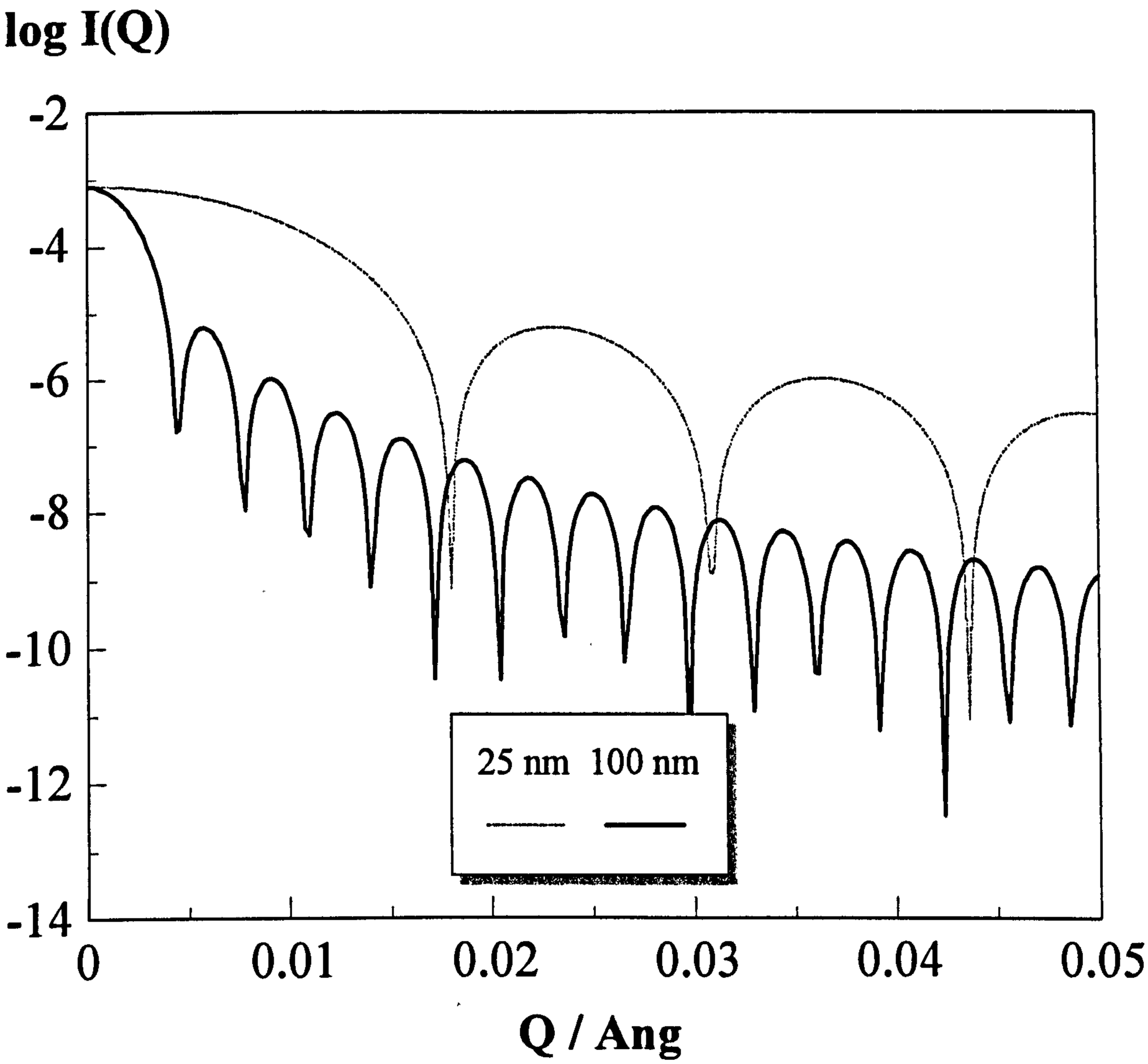

4.5.1 Polydispersity Effects

This model for the form factor of a sphere makes no allowance for any polydispersity effects. To allow for these a log-normal distribution summed over all values of r is taken. A log normal distribution is simply the logarithm of a normal distribution and therefore, the form factor of the scattering from a spherical particle with polydispersity can be represented as

$$P(Q) = \int \left[3 \frac{(\sin(Qr) - Qr\cos(Qr))}{(Qr)^3} \right]^2 p(r)dr$$

[4.11]

where p(r) is the log normal probability of there being a particle with radius r.

$$p(r) = \exp\left[-r\frac{\ln 2}{2} \Big/ (2\pi)^{1/2} \right]$$

[4.12]

Polydispersity effects have the effect of 'smearing' the maxima and minima in the P(Q) decay and consequently only a monotonic decay is observed.

4.5.2 Guinier Analysis.

For a spherical particle with a radius of gyration R_g, using an expansion of equation 4.10, the R_g may be approximated to give the expression below[2], provided that the value of $QR_g << 1$,

$$I(Q) = I(0)\exp\left(\frac{-Q^2R_G^2}{3}\right)$$

[4.13]

where I(0) is the scattering at zero Q. The very low Q range is described as the Guinier region and a linear plot may be obtained from ln I(Q) versus Q^2, known as a *Guinier plot*.

$$\ln I(Q) = \ln I(0) - R_G^2\frac{Q^2}{3}$$

[4.14]

Therefore, the radius of gyration of the particle or polymer may be obtained from the gradient of a Guinier plot.

4.5.3 Porod's Law.

At high Q, where the shortest distance scales are probed, a measure of the surface area per unit volume may be obtained, provided that the particle has a well defined, smooth interface[3]. This is known as Porod's law and in this region the scattering goes as Q^{-4}.

$$I(Q) = AN_p(\rho_p - \rho_m)^2 2\pi A_s Q^{-4} \qquad [4.16]$$

where A_s provides a measure of the surface area per unit volume and ρ_m and ρ_p are the scattering length densities of the medium and the particle respectively.

4.5.4 Concentrated Dispersions

In a dilute dispersion in which the interparticle interactions are minimal, the arrangement of the particles will be as random as Brownian motion allows. As the number of particles increases, the total volume of space occupied by the particles will also increase. Consequently, the probability of interaction between the particles increases and the forces between the particles become important in determining the overall properties of the dispersion. This effect is further increased if the particles are charged. Therefore, for interacting systems of charged micelles, such as the sodium dodecyl sulphate used in this study, the scattering must also include interparticle interference effects. This requires an additional factor known as S(Q). The neutron scattering intensity can now be described in terms of an structure factor S(Q), a form factor P(Q) and the scattering length density term.

$$I(Q) = AN_p V_p^2 (\Delta\rho)^2 P(Q)S(Q) \qquad [4.16]$$

The structure factor is calculated for a given micellar charge and ionic screening using the mean spherical approximation given by Hayter and Penfold[4] This method is based on an electrostatic repulsive potential (V_R) of the form:

$$V_R = \frac{4\pi\varepsilon_r\varepsilon_0 R^2\psi_s^2 \exp[-\kappa(r-2R)]}{r}$$

[4.17]

where, ε_r is the relative permittivity of the medium, ε_0 is the permittivity of a vacuum, κ is the reciprocal Debye Huckel length and ψ_S is the surface electrostatic potential. The spherical micelles are taken as having a hard core and the structure factor is calculated by solving the Ornstein-Zernike equation[5] in the mean field spherical approximation[6]. This model is dependent upon such parameters as size, volume fraction and surface charge: The Hayter-Penfold model was used to calculate the structure factor for the SDS micelles.

4.6 Particles with Adsorbed Layers

For the case of particles with an adsorbed polymer layer the scenario becomes more complex with the total scattering pattern from a dilute dispersion with an adsorbed polymer layer taking the form

$$I(Q) = I_{ll}(Q) + I_{pp}(Q) + 2I_{pl}(Q) + \tilde{I} + B_{inc}$$

[4.18]

where I(Q) is the total scattering intensity, $I_{ll}(Q)$ is the scattering intensity arising from the average structure of the polymer layer, $I_{pp}(Q)$ the scattering intensity of the particle and $I_{pl}(Q)$ is a particle-layer interference term. These terms are often referred to as partial structure factors. The scattering from the particle, $I_{pp}(Q)$ is given in equation 4.11. The $I_{ll}(Q)$ term is,

$$I_{ll}(Q) = \frac{8\pi^2 r_o^2 \phi_p (\rho_l - \rho_s)^2}{Q^2 V_p} \left| \int_0^t \phi_z e^{iQz} dz \right|^2$$

[4.19]

where V_p is the particle volume, $\phi(z)$ is the volume fraction of polymer at a distance z from the interface and t is the maximum extent of the adsorbed layer. ρ_l

is the scattering length density of the layer. Finally, the interference term $I_{pl}(Q)$ can be given by,

$$I_{pl}(Q) = \frac{6\pi\phi_p(\rho_p - \rho_s)(\rho_l - \rho_s)}{Q^4 r_o}\left[\int_0^\infty \phi(z)\cos(Qz)dz - Qr_o\int_0^\infty \phi(z)\sin(Qz)dz\right] \quad [4.20]$$

Further, there are two more factors that may contribute to the observed scattering,

- B_{inc} (the incoherent background)
- $\tilde{I}$ (the scattering arising from fluctuations in the adsorbed layer).

4.7 Fluctuations in the Adsorbed Layer.

The fluctuations in the adsorbed layer term, $\tilde{I}$, arises because of non-uniformity in the adsorbed layer, or in other words they are due to local variations in the average concentration of the adsorbed layer. The contribution of these fluctuations to the scattering has been considered by many authors including Crowley[7] and Auvray and de Gennes[8]. Auroy and Auvray[9-11], from their studies of high density layers, proposed that there was a non-negligible contribution from spatial fluctuations in the adsorbed layer in addition to the background arising from incoherent scattering events. The magnitude of these fluctuations is strongly dependent upon the structure of an adsorbed layer. The early work of Cosgrove *et al*[12] shows that in cases where the radius of gyration of the physically adsorbed polymer is less than that of the particle the fluctuation term is negligible. However, on the other hand, for systems where there is a very high polymer density at the interface (*e.g.*, a grafted polymer brush) or large polymers on small particles (under conditions where the particle scattering length density is matched to that of the solvent), a significant background can be observed[10,11].

According to Auvray and Auroy, the fluctuations in a grafted layer (polymer brush) take on a Lorentzian dependence such that,

$$\tilde{I} = \frac{1}{(1+\xi^2 Q^2)} \qquad [4.21]$$

where ξ is a characteristic correlation length.

Auvray and Cotton[13] have suggested that the fluctuations in a physisorbed adsorbed layer go as $Q^{-4/3}$ such that the total scattering is given by

$$I = \frac{C}{Q^2} + A\tilde{I} + B_{inc}$$

$$= \frac{C}{Q^2} + \frac{A}{Q^{4/3}} + B_{inc} \qquad [4.22]$$

Therefore,

$$Q^{4/3} I = \frac{C}{Q^{2/3}} + A + Q^{4/3} B_{inc}. \qquad [4.23]$$

where A and C are constants. C is related to the average volume fraction and is independent of the profile shape at $\theta = 0$. From this expression it follows that a plot of $Q^{4/3}I$ against $Q^{4/3}$ will yield the incoherent background (B_{inc}) from the slope and a measure of the fluctuation term from the intercept on the y-axis.

Recently, concentration fluctuations have been observed in the scattering from physisorbed polymer layers when the polymer molecular weight is very large[14]. Under these conditions it was shown that the fluctuation scattering was more like a large polymer in solution than that of an adsorbed polymer.

4.8 The Incoherent Background.

The incoherent scattering, B_{inc}, arises when the phase of the neutron is randomised during a scattering event. Considering the fluctuation term as $A\tilde{I}$ and the background term as B_{inc}, then the coherent aspect of the scattering length density may be given by $\rho = \frac{\sum b_i}{V}$ where $\sum b_i$ contains both coherent and incoherent scattering length terms. B_{inc} is independent of Q

The following diagram (**figure 4.3**) represents a coherent scattering event,

***Figure 4.3*: A Schematic Diagram of a Coherent Scattering Event.**

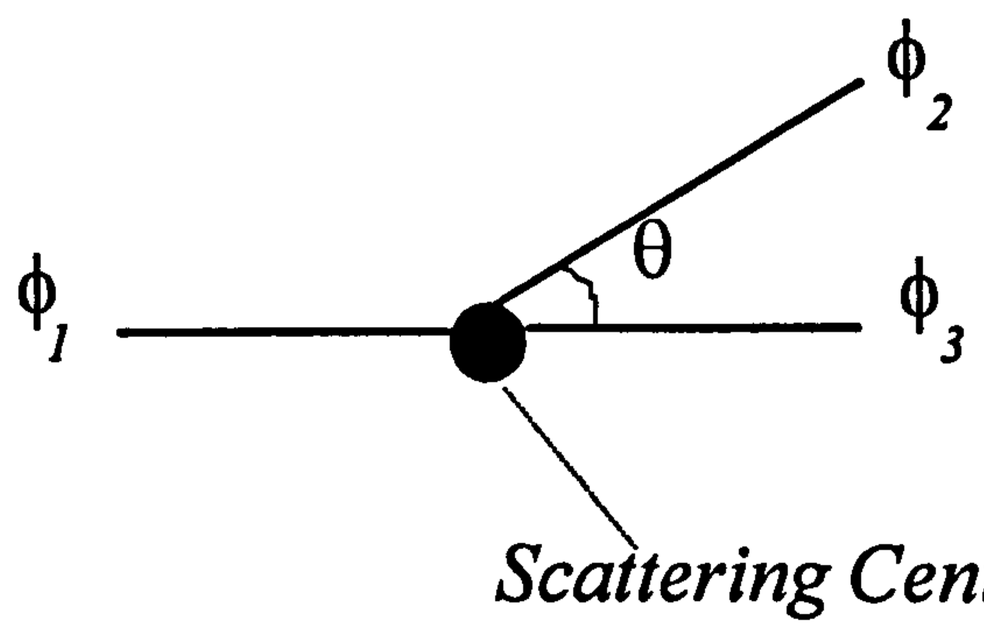

ϕ_1 and ϕ_2 are related to a characteristic distance which gives rise to the coherent scattering. Incoherent scattering arises when ϕ_3 is independent of ϕ_1. This scattering is independent of Q and at a random angle. If the coherent scattering tends to zero at large values of Q, then all of the scattering at high values of Q arises incoherently.

4.9 Data Analysis

4.9.1 At Zero Contrast for the Particle.

The simplest form of analysis of scattering data involves the analysis at contrast match for the particle when $\rho_p = \rho_s$. Under these conditions only the scattering

from the layer, the incoherent scattering and the fluctuation term are seen. Therefore the general equation for the scattered intensity simplifies to:

$$I(Q) = \frac{8N\pi r_o^2 \Delta\rho_s^2}{Q^2 V_p}\left|\int_0^s \phi(z)\exp(iQz)dz\right|^2 + \tilde{I} + B_{inc}$$

[4.24]

If the limit is taken when Q is small and expanding the $I_{II}(Q)$ term as a power series using a Guinier type analysis, the total scattering from the adsorbed polymer layer at zero contrast for the particle may be written:

$$I_{II} = \frac{6\pi\phi_p(\rho_1 - \rho_s)^2}{Q^2 r_o}\theta\left[1 - \sigma^2 Q^2\right]$$

[4.25]

This Guinier approximation allows experimental parameters like the adsorbed amount and the second moment of mass distribution of the adsorbed polymer layer to be determined

- **The Adsorbed Amount** - The adsorbed amount is represented by θ, where θ is:

$$\theta = \int \phi(z)dz$$

[4.26]

ϕ is the volume fraction. θ has units of length, so in order to calculate the absolute adsorbed amount, Γ, θ needs to be multiplied by the density of the polymer.

- **Second Moment** - σ is the second moment of the layer and is equal to,

$$\sigma^2 = \langle z^2 \rangle - \langle z \rangle^2$$

[4.27]

where z is the distance from the surface. Hence, the second moment is the difference between the rms. value of z and the average value of z. The second moment gives information on the shape of the volume fraction profile of the adsorbed polymer layer and is model independent.

Figure 4.4 **Schematic Diagram of an Adsorbed Polymer chain and the Corresponding Volume Fraction Profile.**

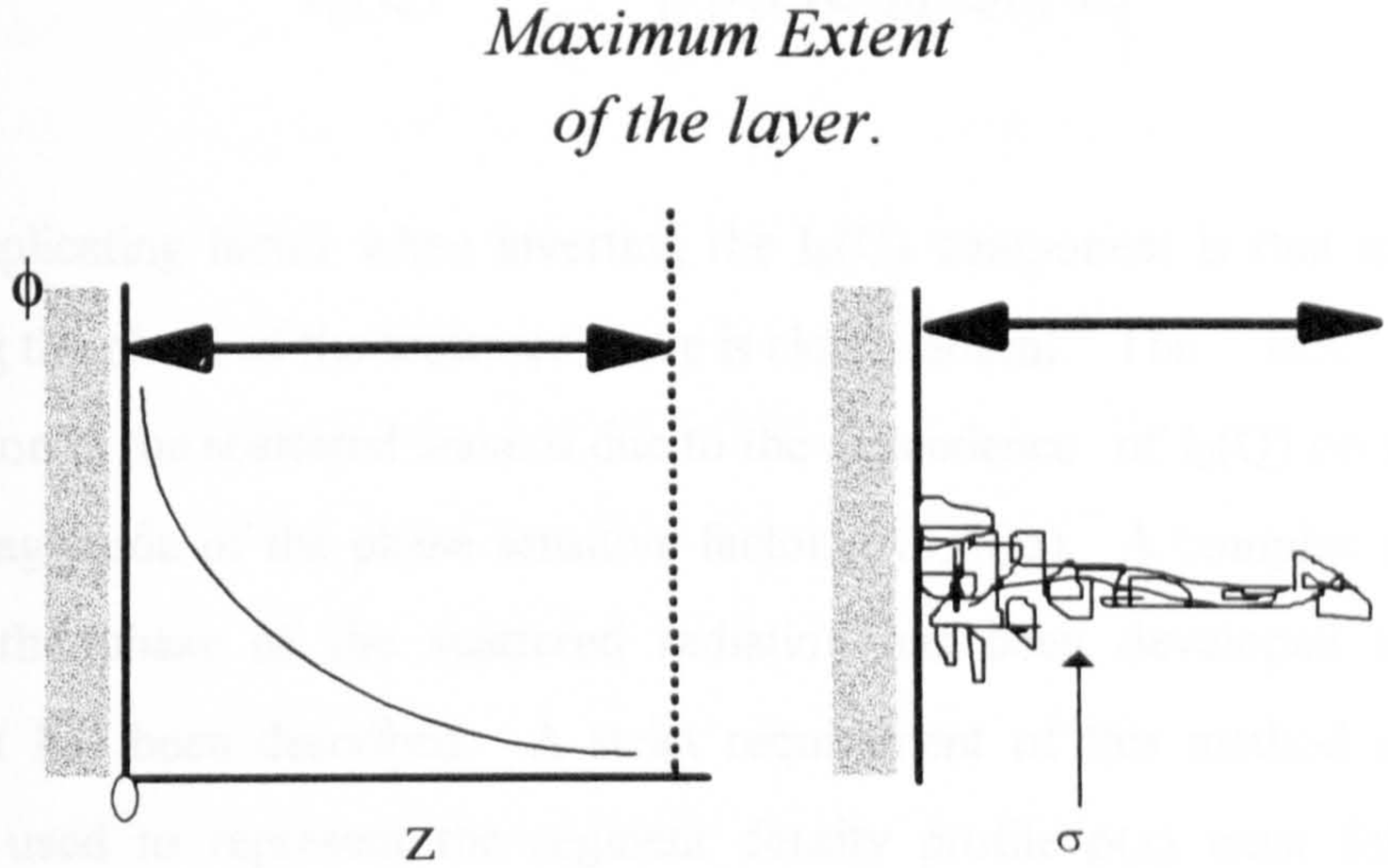

Consider the average value of z,

$$\langle z \rangle = \frac{\int (\phi(z).z)dz}{\int \phi(z)dz} \qquad [4.28]$$

where $\phi(z)$is the probability that there is a segment in layer z and $\langle z^2 \rangle^{1/2}$ is the rms. value of z . Further, using the Guinier approximation, $[1-\sigma^2Q^2]$ can be written $e^{-\sigma^2Q^2}$ so that a plot of $\ln Q^2 I$ against Q^2 will give a straight line of slope σ^2.

Once the incoherent background and the fluctuations have been subtracted the I_{layer} term is solely visible and can then be fitted. There are two main approaches to fitting the data in order to obtain the full volume fraction profile

Direct Inversion Method - A method has been developed by Crowley[7] which allows the inversion of the $I_{II}(Q)$ component to obtain the segment density profile $\rho(z)$, if the data collected stretches over a wide enough Q range. When considering the scattering from the layer term (Equation 4.21) without the incoherent scattering and fluctuation terms:

$$I_{II}(Q)=\frac{8\pi^2 r_o^2}{Q^2}\left|\int_0^s \rho(z)\exp(iQz)\,dz\right|^2 \qquad [4.29]$$

The complicating factor when inverting the $I_{II}(Q)$ component is that information regarding the phase of the scattered wave is clearly absent. The lack of this information in the scattered wave is due to the dependence of $I_{II}(Q)$ on the square of the magnitude of the phase sensitive factor, exp.(iQz). A complex analysis to retrieve the phase of the scattered radiation has been developed and a full treatment has been described. A strict requirement of this method is that the function used to represent the segment density profile $\rho(z)$ must fulfil certain conditions; *i.e.* $\rho(z)=0$ for $z<0$. When the system under study consists of a hard impenetrable surface, this is a realistic assumption.

A serious complication of the inversion method is related to the uniqueness of the function $\rho(z)$ used in this analysis. For many simple forms of the segment density profile the solution can be easily shown to be unique. Simple profiles with single maxima and monotonically decreasing profiles offer unique solutions. Fortunately many of the mathematical functions used to represent $\rho(z)$ adsorbed and terminally attached homopolymers fall into this category.

The first step in this process is the subtraction of the incoherent scattering and fluctuation term to give solely the layer term. Before the inversion is carried out the data are transformed to yield scattering profiles in the form $Q^2I(Q)$ versus Q, rather than I(Q) versus Q. The requirement that the data extends over a wide Q

range is achieved via extrapolating the $I_{II}(Q)$ component, both to high and low Q values. This extrapolation may be achieved in two parts. In the low Q range the Guinier approximation is used, Equation 4.23. If the layer component of the scattering is not zero at high Q, then in the measured experimental range it can be extrapolated further. An interpolation routine may then be used to yield a function over evenly spaced Q intervals prior to inversion.

Indirect Fitting Method - With the indirect fitting method, a trial profile $\rho(z)^{trial}$ may be used to calculate the scattering over the whole experimental Q range. The first step of this indirect method again involves the subtraction of the incoherent background. Equation 4.27 can then be used to calculate the simulated scattering over the experimental Q range from this trial profile. A simple least squares fitting procedure then minimises the difference between the simulated and experimental data set. An iterative procedure allows the simulated scattering to approach the experimental scattering by adjusting several variables in the set parameters such as the intensity of scattering at zero Q and all of the parameters defining the trial profile. The incoherent background may also be treated as a variable in this model.

4.9.2 Data analysis when all components are visible.

Under conditions where neither the polymer nor the particle are contrast matched to the solvent and the scattering from all the components is observed. When the fluctuation term and incoherent scattering have been subtracted, the scattering formalism takes the form,

$$I(Q) = I_{ll}(Q) + I_{pp}(Q) + 2I_{pl}(Q) \qquad [4.30]$$

The I_{ll} term has already been obtained for the contrast match situation and a simple ratio of the scattering length densities will allow I_{ll} to be calculated in the new solvent. To obtain the interparticle interference term we must also subtract $I_{pp}(Q)$, or in other words the scattering from the bare particle.

Therefore, the total scattering contributions may be described as:

$$I(Q) = I_{pp}(Q)^{x} + I_{ll}(Q)^{zero}\frac{(\Delta\rho^{x})^{2}}{(\Delta\rho^{zero})^{2}} + 2I_{pl}Q \qquad [4.31]$$

where $\Delta\rho^{x}$ is the difference in scattering length density between the polymer and solvent away from contrast and $\Delta\rho^{zero}$ is the difference in scattering length density between the polymer and solvent under conditions of contrast match for the particle. $I_{pp}(Q)^{x}$ is the particle scattering in the absence of polymer away from contrast match conditions for the particle. $I_{ll}(Q)^{zero}$ is the scattering from the layer when the particle is invisible.

The interparticle interference term, once isolated, allows the analysis to proceed using equation 4.21. This method has the advantage that, the layer scattering under conditions where the particle is contrast matched also contains the fluctuation term. Therefore when this scattering is scaled for the difference in scattering length density the fluctuation term also scales and can therefore be subtracted from the total scattering at the same time as the layer scattering.

References.

1. *Neutron News* **1992** 3 (3) 29

2. Guinier A., Fournet G.; *Small Angle Scattering of X-rays. John Wiley, New York* **1955**

3. Porod G.; *Kolloid Z.* **1951** 124 83 (1951)

4. Hayter J. B, Penfold J; *Molecular Physics* **1981** 42(1) 109

5. Ornstein L. S., Zernike F.; *Proc. Sect. Sci. K. Ned Akad. Wed* **1914** 17 793

6. Lebowiz J. L., Percus J. K., *Phys. Rev* **1966** 144 251

7. Crowley T. L.; *D. Phil. Thesis University of Oxford* **1984**

8. Auvray L., de Gennes P. G.; *Europhys. Lett.* 2 647

9. Auvray L., Auroy P.; eds Linder P. and Zemb Th.; *Neutron, X-Ray and Light Scattering Elsevier Science Publishers: Holland* **1991.**

10. Auroy P., Mir Y., Auvray L.; *Phys. Rev. Lett.* **1993** 69 93

11. Auroy P., Auvray L., Leger L.; *Phys. Rev. Lett.* **1991** 66 719

    Auroy P., Auvray L.; J. *Phys. II France* **1993** 3 227

12. Cosgrove T., Heath T. G., Ryan K.; *Langmuir* **1994**, 10(10) 3500

13. Auvray L., Cotton J. P., *Macromolecules* **1987 20** 202

14. Cosgrove T., Griffiths P.C. - *In preparation.*

Chapter 5

Experimental

This chapter deals with the experimental aspects of this work; the first part with the sources, synthesis and characterisation of the materials used and the latter part describes the instrumentation and techniques utilised to perform the measurements reported in this thesis.

5.1 Materials

5.1.1 Substrates.

- **Silica** - the substrate used in this study for the photon correlation spectroscopy (PCS) measurements was the commercial silica Snowtex ZL, which has an average particle diameter of 90 ± 5 nm by transmission electron microscopy and 104 ± 1 nm by PCS. For the nuclear magnetic resonance (NMR) measurements and some of the small-angle neutron scattering measurements, the commercial silica Snowtex 50 was used. This is identical to Snowtex ZL except it has a diameter of only 20-30 nm[1]. **Figure 5.1** shows the TEM micrograph for this silica dispersion. These silica dispersions have an isoelectric point at approximately pH 4 and under the conditions used in this study a pH of approximately 7 was used. Before use, these silica dispersions were extensively dialysed against double distilled "milli-pore" water to remove any impurities.

Figure 5.1; **TEM micrograph of Snowtex 50.**

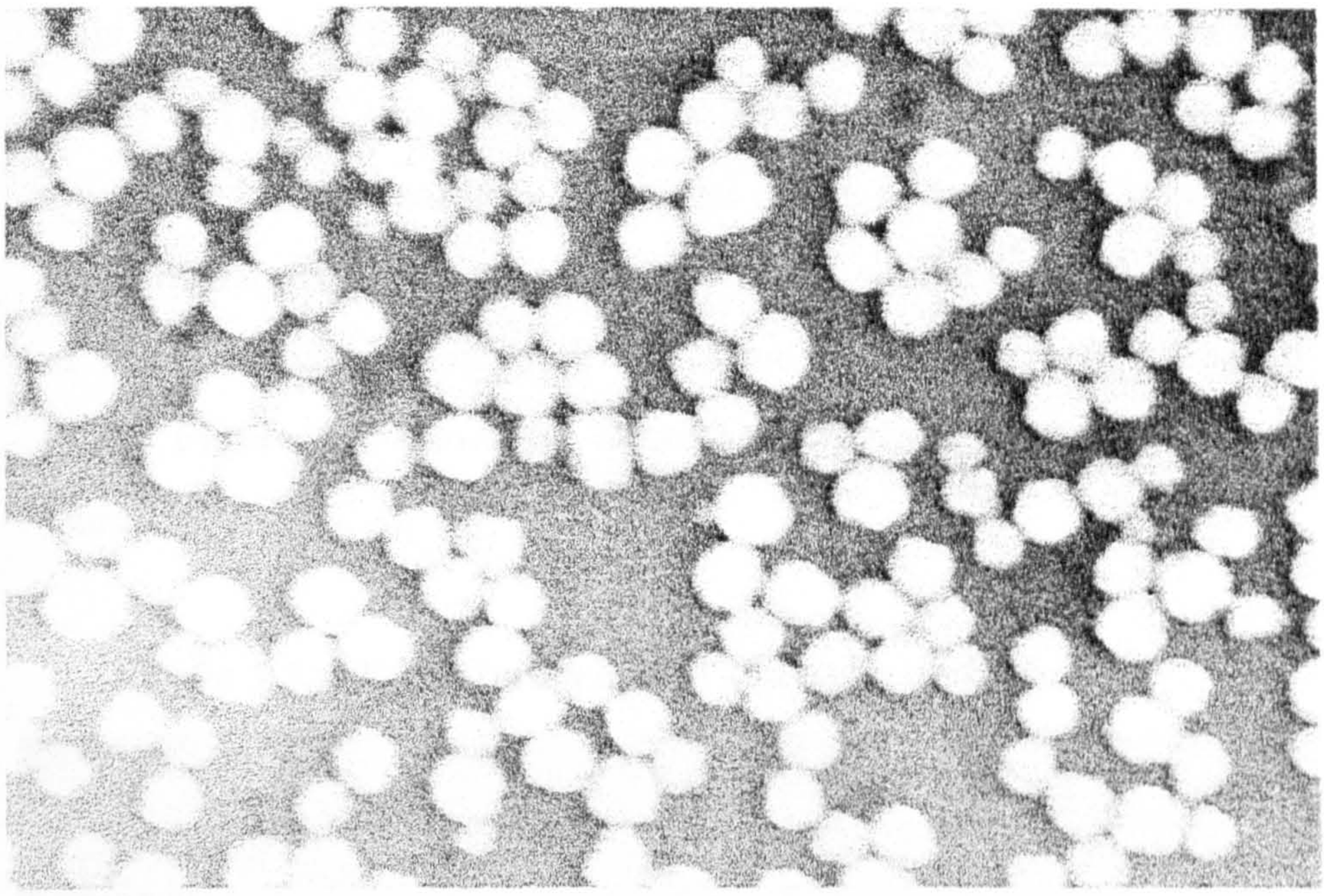

- **Polystyrene Latex** -Three difference polystyrene latex samples were used in this study. The substrate used in the SANS study on the poly(ethylene oxide) (PEO)/sodium dodecyl sulphate (SDS)/polystyrene latex (PSL) system was a deuterated polystyrene latex. This was prepared 'in-house' using a surfactant free emulsion polymerisation[a] according to the method of Goodwin *et al*[2]. The latex had an average particle radius of 75 ± 3 nm (TEM) and 78 ± 3 nm (PCS). Before use the latex was dialysed against D_2O to remove any residual monomer and initiator. 20 % w/w hydrogenous-styrene was added in order to ensure that the contrast match point of the latex with the solvent could be obtained. Prior to use, the hydrogenous styrene and deuterated styrene were distilled in order to remove any inhibitor present. The latex was prepared in H_2O and re-dispersed in D_2O after centrifugation. The concentration of H_2O remaining in the sample was estimated at 5 % w/w from high resolution NMR spectra. The corresponding PCS measurements for this system were performed

[a] Dr. T. Obey, University of Bristol, UK

using a hydrogenous polystyrene latex prepared in the same manner[a]. This PSL had an average radius of 55 ± 4 nm (TEM) and 59 ±5 nm (PCS). The polystyrene latex used in the SANS experiments on Quatrisoft LM was partially deuterated (20 % hydrogenous styrene and 80 % deuterated styrene) and prepared by a similar method. The size of this latex was estimated at 84 ± 4 nm by TEM and 97 ± 4 nm by PCS. **Figure 5.2** shows the electron micrograph of this polystyrene latex.

Figure 5.2; **TEM micrograph of Polystyrene Latex.**

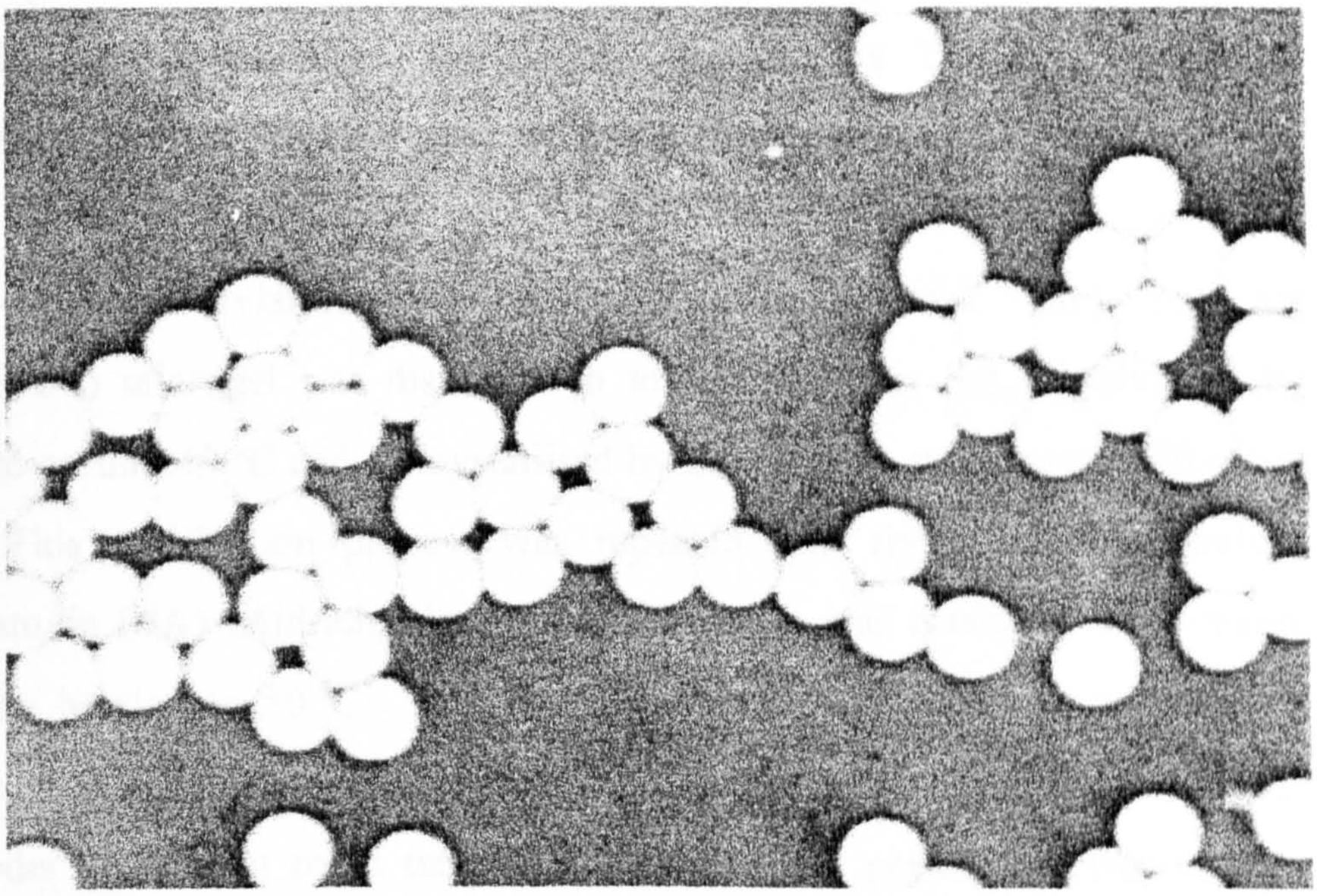

5.1.2 Polymers

The polymer PEO was of molecular weight 114,000 (M_w/M_n = 1.1) and was obtained from Polymer Laboratories Limited, UK. Since this polymer was of analytical grade it was used as received. The commercial polyelectrolyte Quatrisoft LM was obtained from Union Carbide and in order to purify it, was extensively dialysed against "Milli-Pore" water and freeze dried before use. The

[a] Miss S. R. Calpin-Davies; University of Bristol, UK

quaternised polystyrene-poly(vinyl pyridine), (PS-PVP^+) was prepared by N. Wright[a] and this preparation is explained fully elsewhere[3].

5.1.3 Surfactant.

The principle surfactant used in this study, sodium dodecyl sulphate, SDS, was obtained from BDH chemicals (purity > 99 %). The deuterated SDS was obtained from MSD isotopes (isotopic purity > 98 %). Both of these were used as received.

5.1.4 Poly(NIPAM)

The poly(NIPAM) microgel was kindly supplied by Dr. R. Pelton[b] and Dr. Y. Deng[c] and was prepared using the following procedure.

The N-isopropylacrylamide, (NIPAM) (Eastman Kodak Co.) for the poly(NIPAM) microgel was dissolved in toluene (Fischer Sci., Analytical) by heating to around 40 °C and re-crystallised by the addition of n-hexane (BDH) at 0 °C. This purification process was repeated four times. N-N'methylene bisacrylamide (BA) (Aldrich, electrophoresis grade) was dissolved in methanol (BDH) by heating to 50 °C. Any insoluble impurities were then removed by filtration at 50 °C and re-crystallised at 0 °C. Both the NIPAM and the BA were dried under vacuum at room temperature. Potassium persulphate was used as received and Milli Q water was used throughout the preparation

The poly(NIPAM) latex was prepared by suspension polymerisation in a 1L batch reactor equipped with a mechanical stirring paddle. The polymerisation was performed at 65 °C under nitrogen for 4 hours. This poly(NIPAM) latex was first cleaned via dialysis against Milli Q water until the conductivity of the wash water was below 10 μScm^{-1} and then was centrifuged at 20,000 r.p.m for 2 hours. A

---

[a] N. Wright; Ph.D. Thesis, University of Bristol 1997.
[b] Mc. Master Institute of Pulp & Paper Technology, Hamilton, Canada
[c] Georgia Institute of Pulp and Paper Technology, Georgia, USA

portion of the latex was dispersed in D_2O and centrifuged at 20,000 r.p.m for 3 hours. This purification process was also repeated 4 times in order to obtain a stable poly(NIPAM) microgel latex in D_2O.

5.2 Adsorption Isotherms.

The conventional adsorption isotherms for PEO and Quatrisoft LM were determined using traditional gravimetric methods The excess adsorbed amount of polymer, Γ, is determined by measuring the change in bulk polymer solution from its initial value (C_{init}) to the equilibrium concentration (C_{eqm}) on exposure to a known surface area A of absorbent. The adsorbed amount in mass per unit area is given by;

$$\Gamma = \frac{C_{init} - C_{eqm}}{A} \qquad [5.1]$$

The variation of Γ with C_{eqm} gives the adsorption isotherm. In these techniques free polymer is separated from the adsorbed polymer by centrifugation (14,000 r.p.m. for 30 minutes). For the PEO, the concentration of polymer remaining in the supernatant was detected colourimetrically by complexation with tannic acid using UV/visible spectroscopy[3]. A stock solution containing 0.025 g of tannic acid in 50 ml of 2 M sodium chloride was prepared. 5 ml of PEO stock solution (concentration 2 - 20 ppm) was added to 1.25 ml of the stock tannic acid/sodium chloride solution and shaken. The absorbance of the solution was measured in a Uvikon 940 spectrophotometer at 25 °C at a wavelength of 400 nm with 'milli-pore' water as the reference. The absorbance was measured as a function of time until a clear maximum was observed (after approximately 30 minutes). A plot of maximum optical density against PEO concentration was found to be linear in the range 0 - 20 ppm PEO (**figure 5.3**.)

Figure 5.3; **Calibration Data for PEO using the Tannic Acid Method.**

Figure 5.3

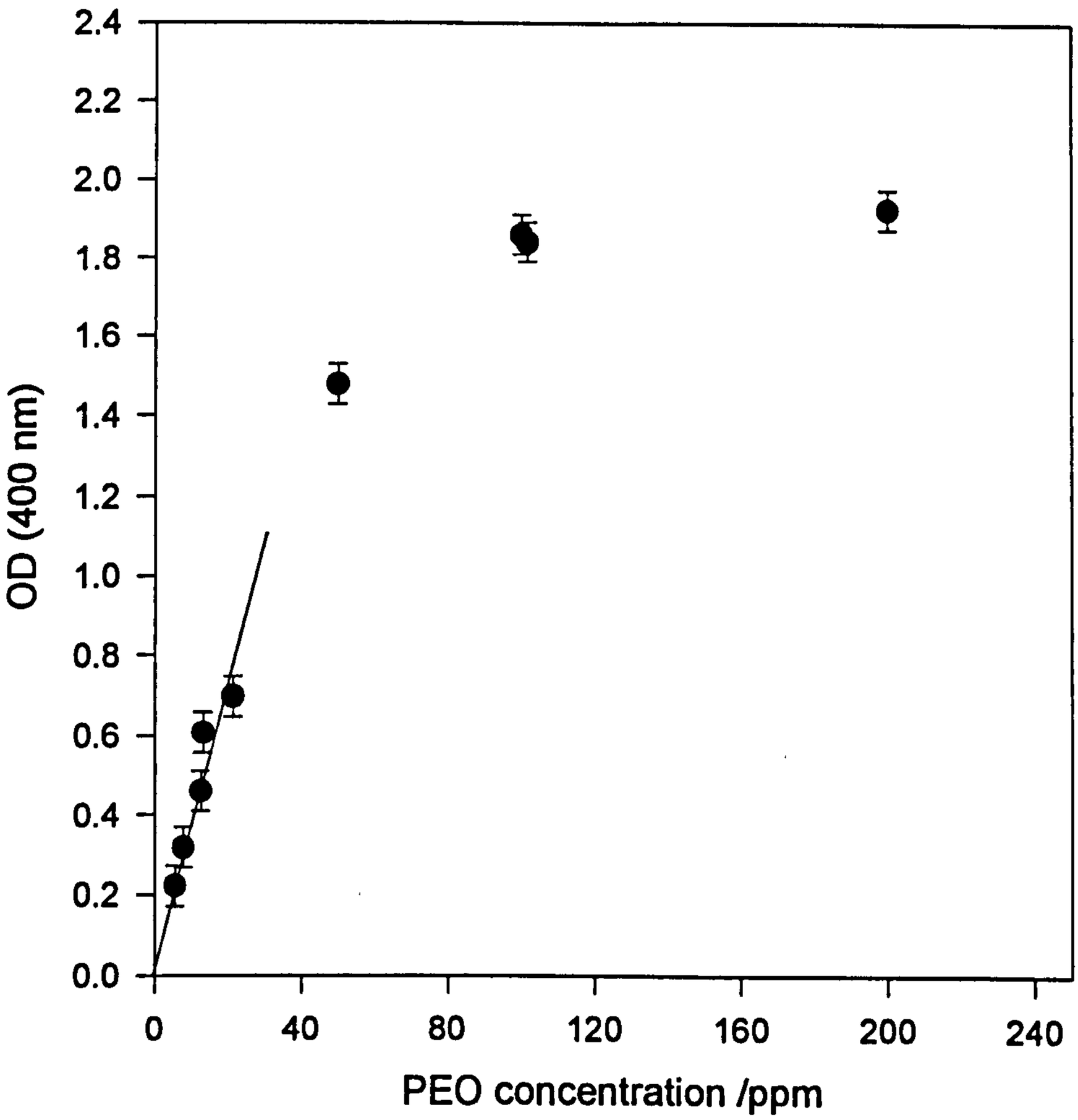

SDS alone does not adsorb in the UV/visible region, nor does it complex with tannic acid. However, the addition of SDS causes the nature of the PEO/tannic acid complex to be affected. The result is a loss of linearity of the calibration plot. Without knowing the exact concentration of SDS in the supernatant (as is likely in an adsorption experiment) one cannot accurately calibrate the PEO concentration with the tannic acid method, or indeed any other traditional gravimetric or spectroscopic method[5]. It may, however, be possible to measure

these isotherms using NMR methods. **Table 5.1** shows the effect of SDS on the optical density of PEO solutions.

Table 5.1: **Calibration Data for PEO and SDS Using the Tannic Acid Method**

PEO Concentration (ppm)	SDS Concentration (ppm)	OD (400 nm)
15	2000	0.4824
13	0	0.608
9	2000	0.3420
4	2000	0.4270
0	2000	0.0857

The adsorption isotherms on the polyelectrolyte used in this study, Quatrisoft LM were measured in a similar manner to the PEO adsorption isotherms. The amount of Quatrisoft LM remaining in the supernatant was determined by treating the supernatant with a mixture of phenol and concentrated sulphuric acid[6]. 2 ml of Quatrisoft LM solution containing between 0 and 300 ppm of polymer was added to 0.05 ml of 80 % phenol solution. 5 ml of concentrated sulphuric acid was added, the tubes shaken and allowed to stand for 10 minutes. A characteristic orange/red colour developed which was measured by the Uvikon 940 spectrophotometer at 480 nm. As in the PEO/tannic acid case, the absorbance was linear with respect to polymer concentration. Unfortunately, SDS also interfered with this calibration. **Figure 5.4** shows the calibration plot for Quatrisoft LM.

Figure 5.4; **Calibration Data for Quatrisoft LM.**

Figure 5.4

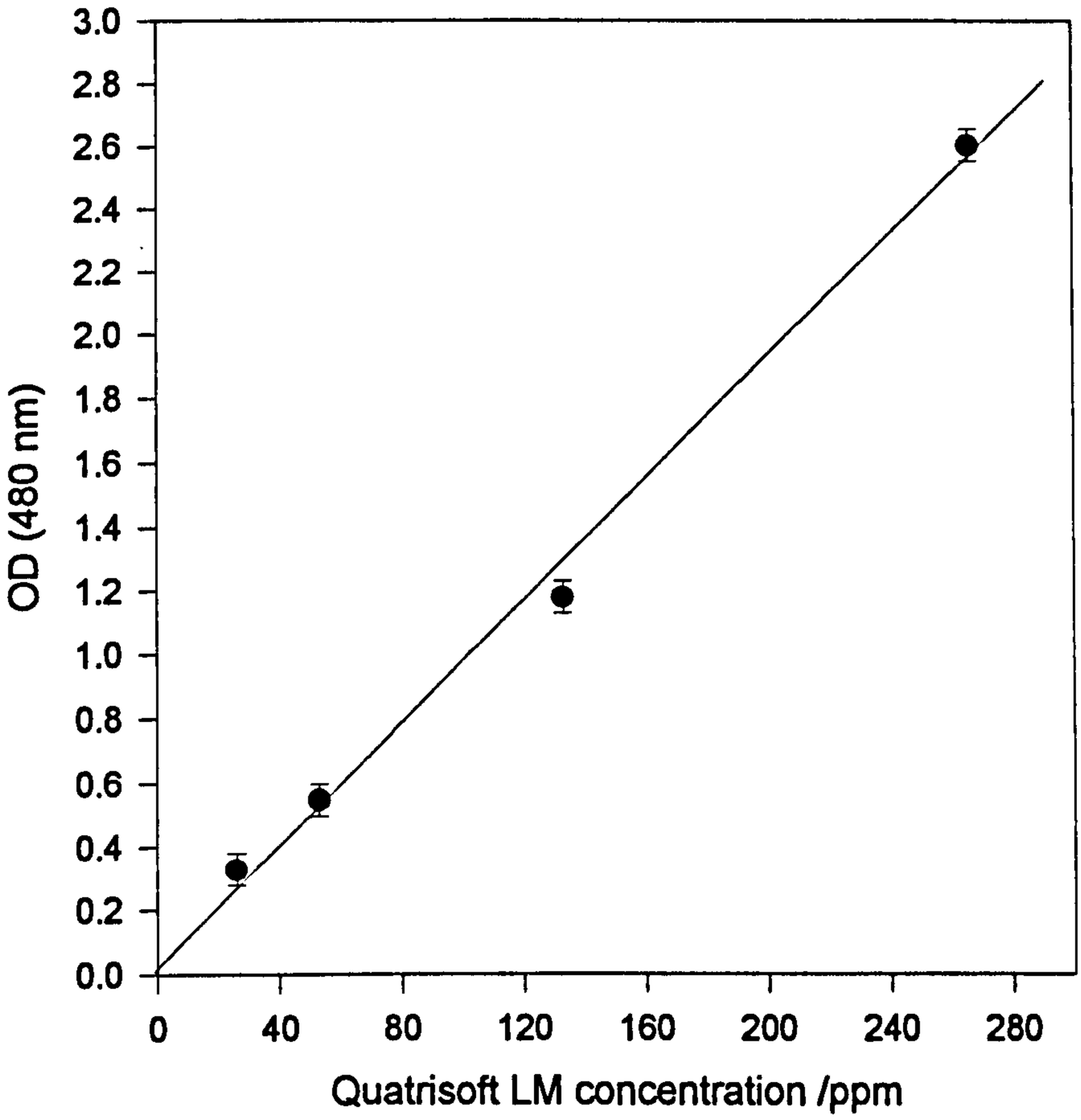

5.3 Photon Correlation Spectroscopy

The hydrodynamic thickness of the adsorbed layers was determined by photon correlation spectroscopy (PCS). The main components of the spectrometer are shown in **figure 5.5**. A 1.6 W Argon laser operating at 514 .5 nm was employed. All measurements, unless stated otherwise were performed at 25 °C and each data point is the average of 10 experimental runs, each run having 10 averages over 20 seconds. The photomultiplier was mounted on a turntable which could be rotated through 180° and was connected to a Malvern real-time multibit correlator K7027. The correlator had a capacity of 128 data channels and a sample time (τ) range of

0-32767 μs. The rejection factor for a data series was 0.005 (or 0.5 %) to eliminate dust and the experimental duration 20 s. The sample time was adjusted to give a smooth exponential correlation function which decayed over a maximum number of corellator channels.

***Figure 5.5*; Schematic Diagram of the PCS Equipment Used in this Study.**

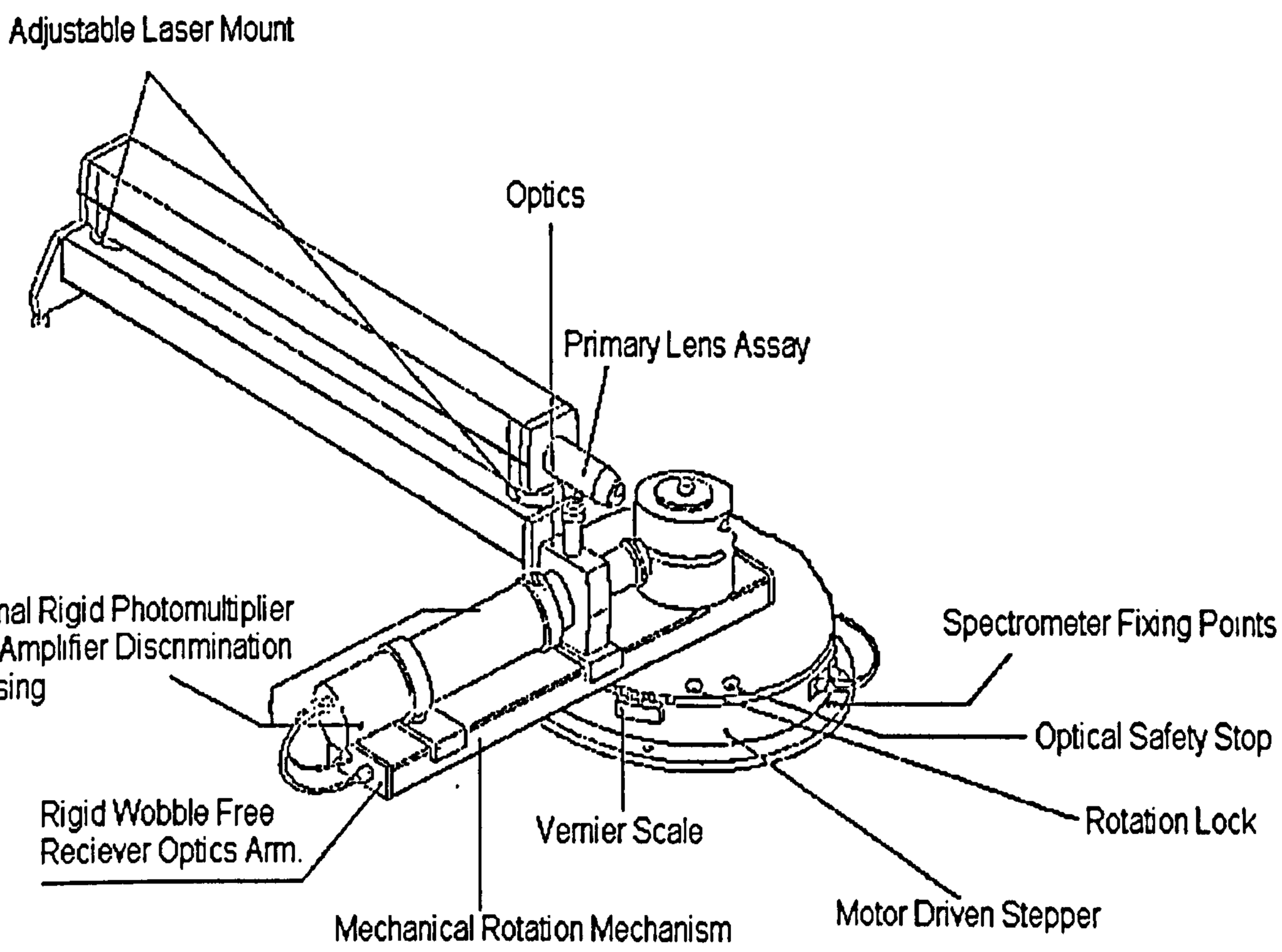

All of the measurements presented in this thesis were performed at a measuring angle of 90° and each size quoted is the average of several results.

The basis of PCS relies on the fact that the particle is moving due to the Brownian motion of the diffusing particles and hence there is a Doppler Shift of the scattered light. The scattered light therefore has a different frequency from the incident light. Since in a sample there are many particles moving at different

speeds then the scattered fields from each particle suffer different Doppler shift. The laser linewidth is consequently broadened and is typically Lorentzian in shape. This width ($\Delta\omega$) is dependant upon the diffusion coefficient D, thus;

$$\Delta\omega = DQ^2 \qquad [5.2]$$

where

$$Q = \frac{4\pi}{\lambda}\sin\left(\frac{\theta}{2}\right) \qquad [5.3]$$

Upon Fourier transform, for monodispersed spheres, the Lorentzian broadening becomes an exponential decay whose time constant is $2DQ^2$. This value of D can be inserted into the Stokes-Einstein equation to obtain a particle radius.

$$D = \frac{kT}{6\pi\eta a} \qquad [5.4]$$

where a is the particle radius, T is the absolute temperature, k is Boltzmann's constant and η is the solution viscosity. For the case of adsorbed polymer layers the hydrodynamic thickness can be extracted from a knowledge of the particle radius with and without polymer layer.

In practice, a correlation function, essentially a memory function, is used to study the fluctuating electric fields which are incident on the photomultiplier tube. The intensity correlation has an exponential form whose time constant is also related to a diffusion coefficient.

5.3.1 Correlation Functions, Choice of Sample Time (τ)

Consider the fluctuating light intensity as a function of time, I(t). Irrespective of the value of t chosen the intensity cannot change infinitely quickly to a new value. Therefore the intensity of the light at a time (t+τ) is, to a certain extent, dependant upon the intensity at time t For very long values of τ, the intensity I(t) and I(t+τ) will be independent of each other. At very short delays the dependence is greatest. The auto correlation function G' is the mean value over many starting points of t for the product I(t)I(t+τ) expressed as a function of τ. Therefore at τ=0 $\langle I(t)I(t+\tau)\rangle$ is the mean square of the intensity $\langle I^2\rangle$ and at large values of τ where I(t+τ) is not dependent upon I(t) the average can be factorised and $G(\infty) = \langle I \rangle^2$. If this auto correlation function is normalised it will decay from 2 to 1. It is this normalised auto correlation function that we measure via the intensity of the fluctuating light.

5.4 Nuclear Magnetic Resonance Spectroscopy

The main contribution to the diffusion measurements were performed on a 300 MHz Bruker NMR spectrometer* fitted with a field gradient unit. The spin echoes were Fourier transformed and then the peak height measured. The self diffusion coefficients were extracted by fitting the spin echoes to equation 5.2 which is based on Fick's Law and assumes Brownian motion.

$$\ln\frac{A_\delta}{A_0} = \left(-\gamma^2 G^2 \delta^2 \left(\Delta - \frac{\delta}{3}\right) D_s\right) \qquad [5.2]$$

where γ is the magnetogyric ratio, A_δ is the integrated intensity for a given field gradient pulse of length δ, A_0 is the integrated intensity in the absence of a field gradient pulse and D_s is the self-diffusion coefficient. G is the field gradient strength. The value of Δ, the time between field gradient pulses, was maintained at 50 ms and δ varied from 0 to 25 ms. The peaks were plotted as a function of δ and their intensities measured. **Figure 5.6** shows a typical stack plot of intensities

* By kind permission of Unilever, Port Sunlight Laboratory.

for water as a function of δ. The diffusion coefficients are extracted from the slope of a plot of ln (attenuation) against β; where attenuation is A_δ/A_0 and $\beta=\gamma^2G^2\delta^2(\Delta-\delta/3)$. A full series of stack plots and attenuation data are given in appendix A..

***Figure 5.6*; Stack Plot of Intensity as a Function of Field Gradient Pulse Length for 0.4 % w/w SDS and 0.5 % w/w PEO in D_2O.**

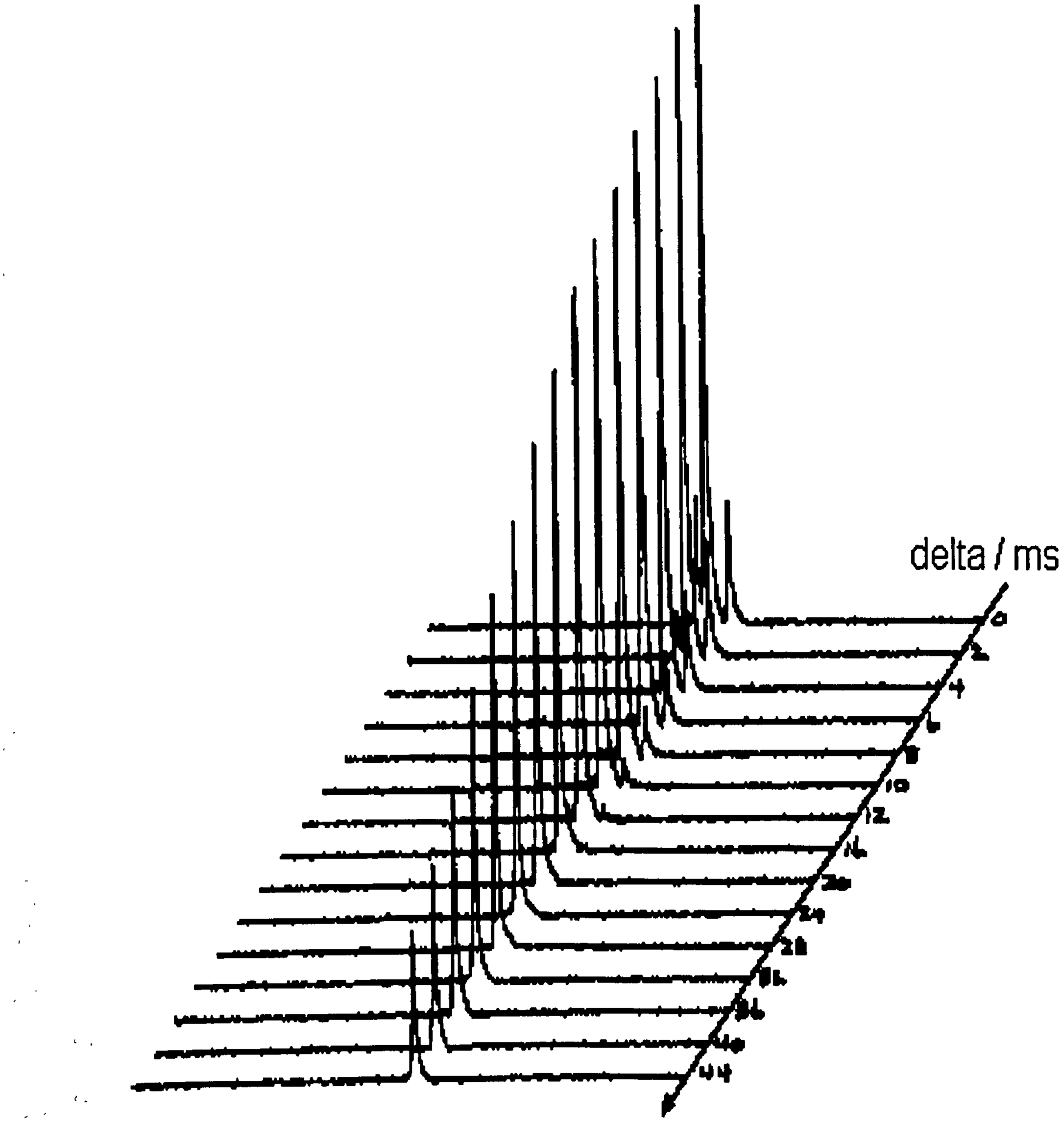

Figure 5.7 shows a typical plot of ln attenuation against β. Unfortunately, G is unknown and therefore D, is obtained by comparing the slope from the

experimental run with that of water which has a known diffusion coefficient at any particular temperature[7].

Figure 5.7; **Plot of ln Attenuation Against β for 1.0 % w/w SDS.**

Figure 5.6

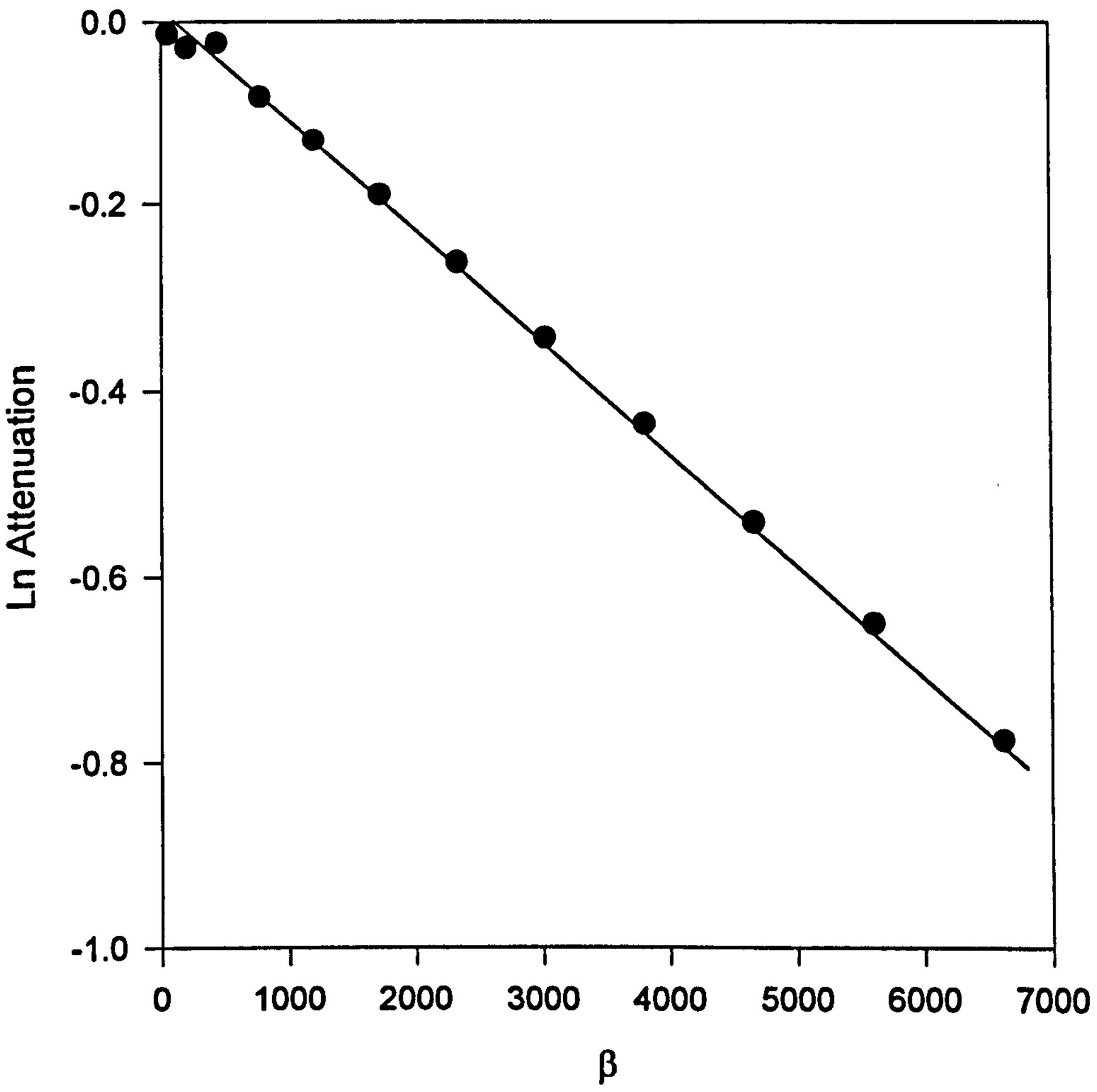

The relaxation measurements were carried out using a JEOL FX-200 Spectrometer upgraded with a SMIS (Surrey Medical Imaging Systems) console which replaces the computational and rf parts of the JEOL system. The SMIS console consists of a PC with several extra compatible boards which allow the connection and control of the rf circuitry of an existing spectrometer. The standard Carr-Purcell-Meiboom-Gill (CPMG) sequence was employed[7] and the

spin-spin relaxation times extracted by a non-linear least squares analysis of equation 5.3;

$$M_y(\tau) = M_y(0)\exp(-\tau/T_2) \qquad [5.3]$$

where $M_y(\tau)$ is the instantaneous signal intensity between even pairs of 180° pulses separated by a time τ.

5.5 Small Angle Neutron Scattering.

The small-angle neutron scattering (SANS) experiments were performed using two instruments, the LOQ instrument at the ISIS facility, Rutherford Appleton Laboratory, Didcot, UK and the D17 instrument at the Institut Laue Langevin (ILL), Grenoble, France. The experiment involving PEO, SDS and PSL was performed at the ILL facility whilst all others reported in this thesis were performed at the ISIS facility. **Figure 5.8** shows the layout of the D17 instrument at the ILL facility[9].

In all cases samples were measured in 2 mm path-length Quartz Helma cells at 25 °C. The effective Q range of the LOQ instrument was 0.006 Å to 0.25 $Å^{-1}$ whilst the wavelength of the D17 instrument could be adjusted to achieve a Q range minimum of 0.0008 $Å^{-1}$ to a maximum of 25 $Å^{-1}$. Typically, SANS samples were run for 4-6 hours each.

We used two neutron wavelengths, 8.5 Å and 17 Å which gave Q values from 0.003092 $Å^{-1}$ to 0.2429 $Å^{-1}$.

In order to study the effects of changes in the system on any individual component it is necessary to render at least one of the components in the system invisible to the neutrons. This is achieved by contrast variation of H-water/D-water mixtures or by substituting deuterated SDS for hydrogenous SDS.

Table 5.2 gives the scattering length densities of the individual components examined in this thesis.

Table 5.2: **Scattering Length Densities of the Individual Components Examined in this Thesis.**

Material	$\rho/10^{-6}$Å^{-2}
H_2O	-0.56
D_2O	6.39
poly(NIPAM)	0.59
H-SDS	0.39
D-SDS	6.73
Poly(ethylene oxide)	0.69

Once obtained, the ISIS data was reduced using the Collette program at the ISIS facility by which the transmission of the sample was accounted for and the scattering from the cell and solvent subtracted. The absolute values of the scattering intensities for the data from the ILL were calculated from the scattering and the transmission of water as a background. All of the scattering data was fitted using a non-linear least-squares fitting program.

Figure 5.8; **Schematic Layout of the D17 Instrument at the ILL Facility.**

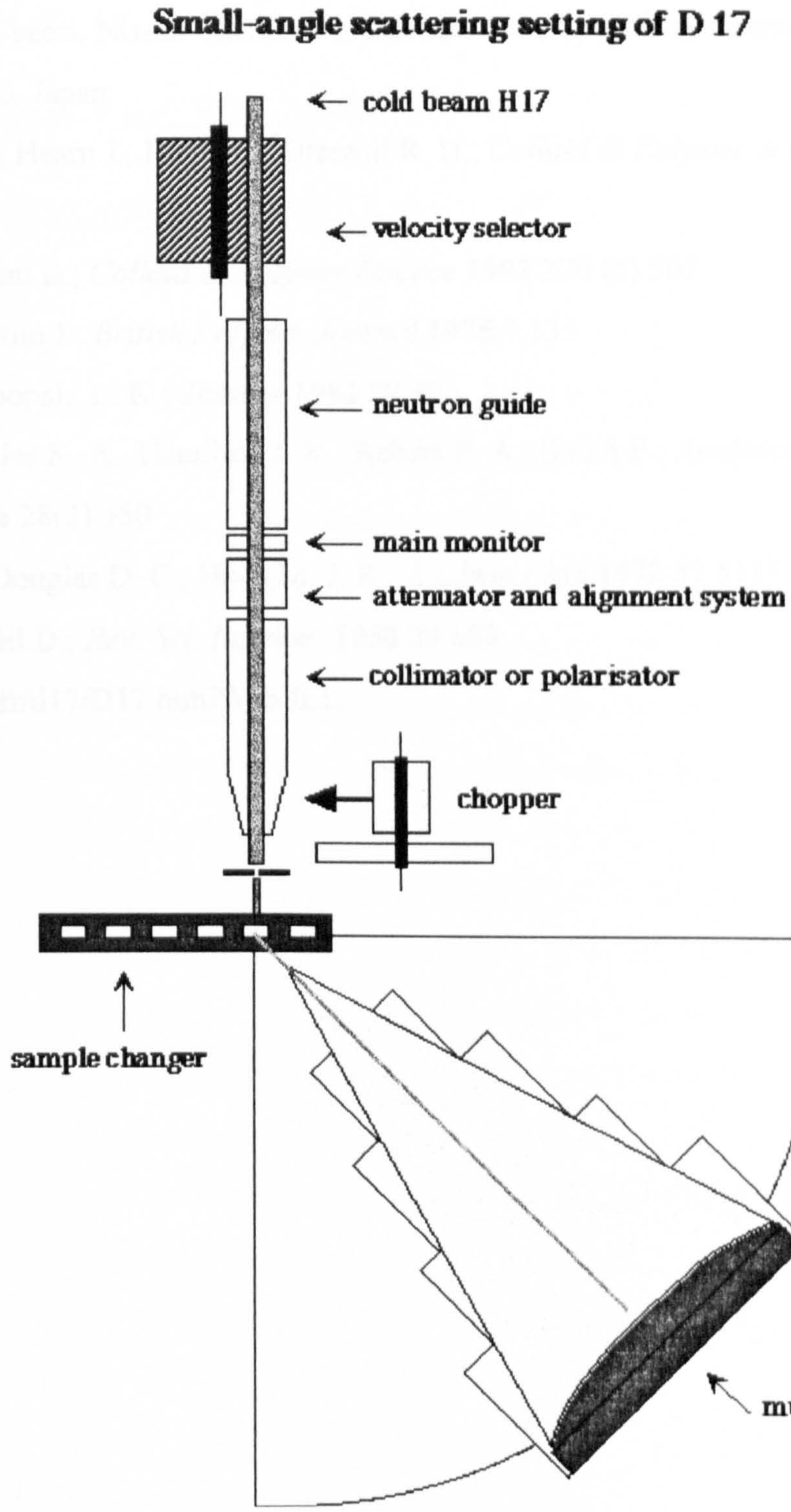

References.

1. Snowtex Data Sheets; Nissan Chemical Indsustries Ltd., Specitality Chemicals Division. Tokyo, Japan.
2. Goodwin J. W., Hearn J., Ho C. C., Ottewill R. H.; *Colloid & Polymer Science* **1974** 252 464
3. Biggs S., Vincent B.; *Colloid & Polymer Science* **1992** 270 (5) 505
4. Attia Y. A., Rubio J.; *British Polymer Journal* **1975** 7 135
5. Nuysink, J., Koopal, L. K.; *Talanta* **1982** 29 495
6. Dubois M., Gilles K. A., Hamilton J. K., Rebers P. A., Smith F.; *Analytical Chemistry* **1956** 28(3) 350
7. Gillen K. T. , Douglas D. C., Hoch M. J. R.; *J. Chem Phys* **1972** 57 5117
8. Meiboom S., Gil D.; *Rev. Sci. Instrum.* **1958** 29 688
9. http://www.ill.fr/d17/D17.htmlWeb ILL

Chapter 6.

Adsorption and Hydrodynamic Thickness Results on PEO and SDS.

In this chapter, the results obtained on the substrate/PEO/SDS system using adsorption isotherm measurements and photon correlation spectroscopy (PCS) measurements are presented. It contains both the results on silica and polystyrene latex. Unless stated elsewhere, the temperature is at 25 °C and all other conditions are ambient. It was also chosen for simplicity to keep the pH and ionic strength ambient. The results are presented in such a manner as to lead the reader through simple systems containing only one or two components, onto those more complex systems involving polymer, surfactant and substrate. Unless stated otherwise the order of addition of the components was to equilibrate the polymer and surfactant mixture before the addition of particles. Initially, the adsorption isotherm results are presented since these plateau adsorbed amounts form the basis of many of the later experiments. The error bars presented in this chapter indicate a typical maximum error on a standard sample using this technique. Towards the end of this chapter, the results are discussed and interpreted in terms of the interactions between the polymer and the surfactant. Unless stated elsewhere, the lines on the figures in this chapter are to guide the eye and are not the result of data fitting.

6.1. Adsorption Isotherms.

The conventional adsorption isotherms for PEO on silica and polystyrene latex were determined using traditional gravimetric methods[1]. **Figure 6.1** and **Figure 6.2** show the adsorption isotherms for PEO on silica and on polystyrene

latex respectively. **Figure 6.1** depicts the adsorption isotherm in the absence of surfactant (○) and with an added SDS concentration of 30 ppm (●).

Figure 6.1

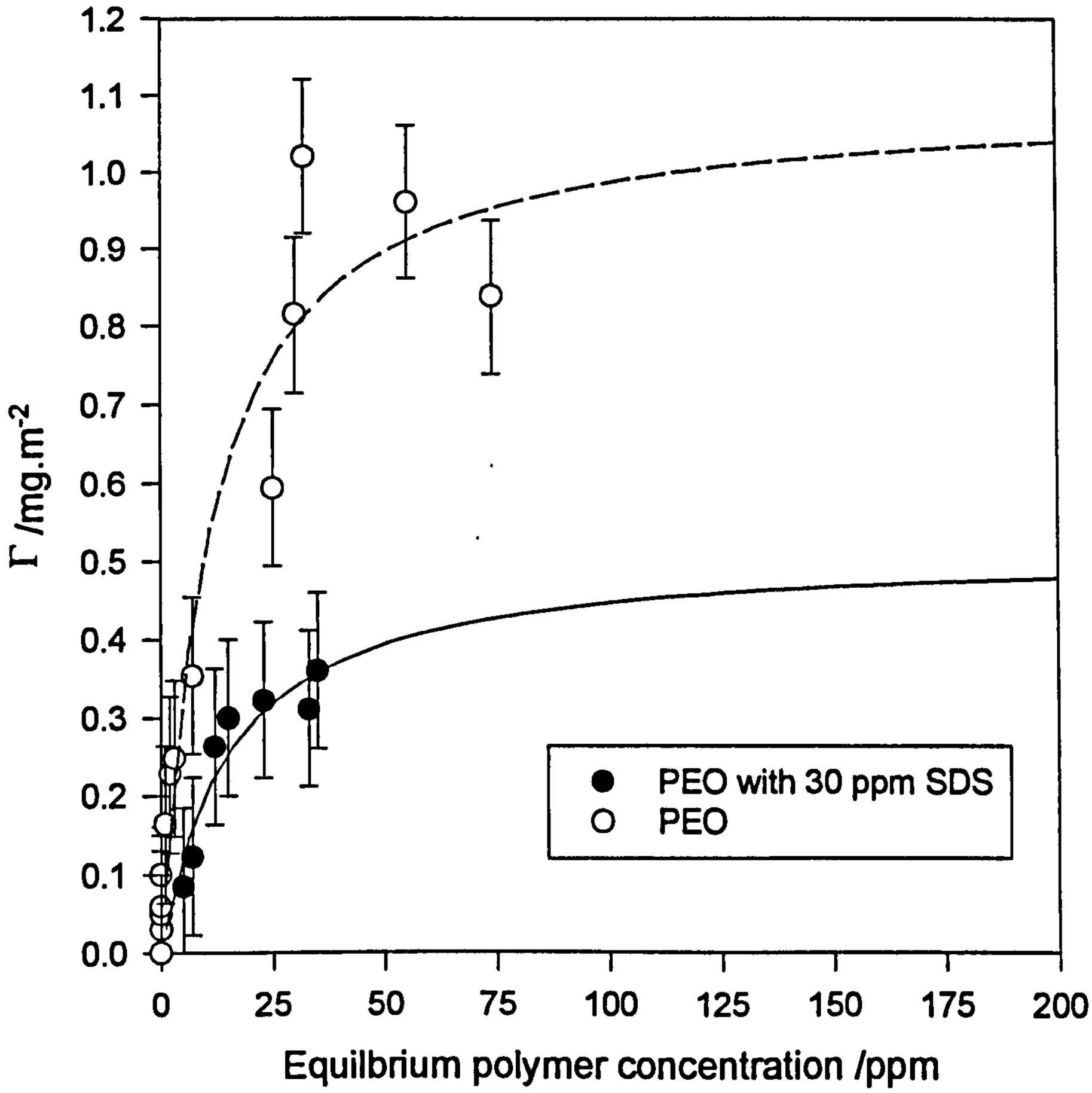

For this case, in the absence of any surfactant, the adsorption isotherm is, as expected, of the high affinity type and yields a plateau measured adsorbed amount of 0.9 ± 0.1 mgm^{-2}. The value of monolayer adsorbed amount from fitting to a Langmuir isotherm was 1.1 ± 0.1 mg m^{-2}. The adsorption isotherm of PEO on polystyrene latex is very similar to that on silica (**Figure 6.2**).

Figure 6.2

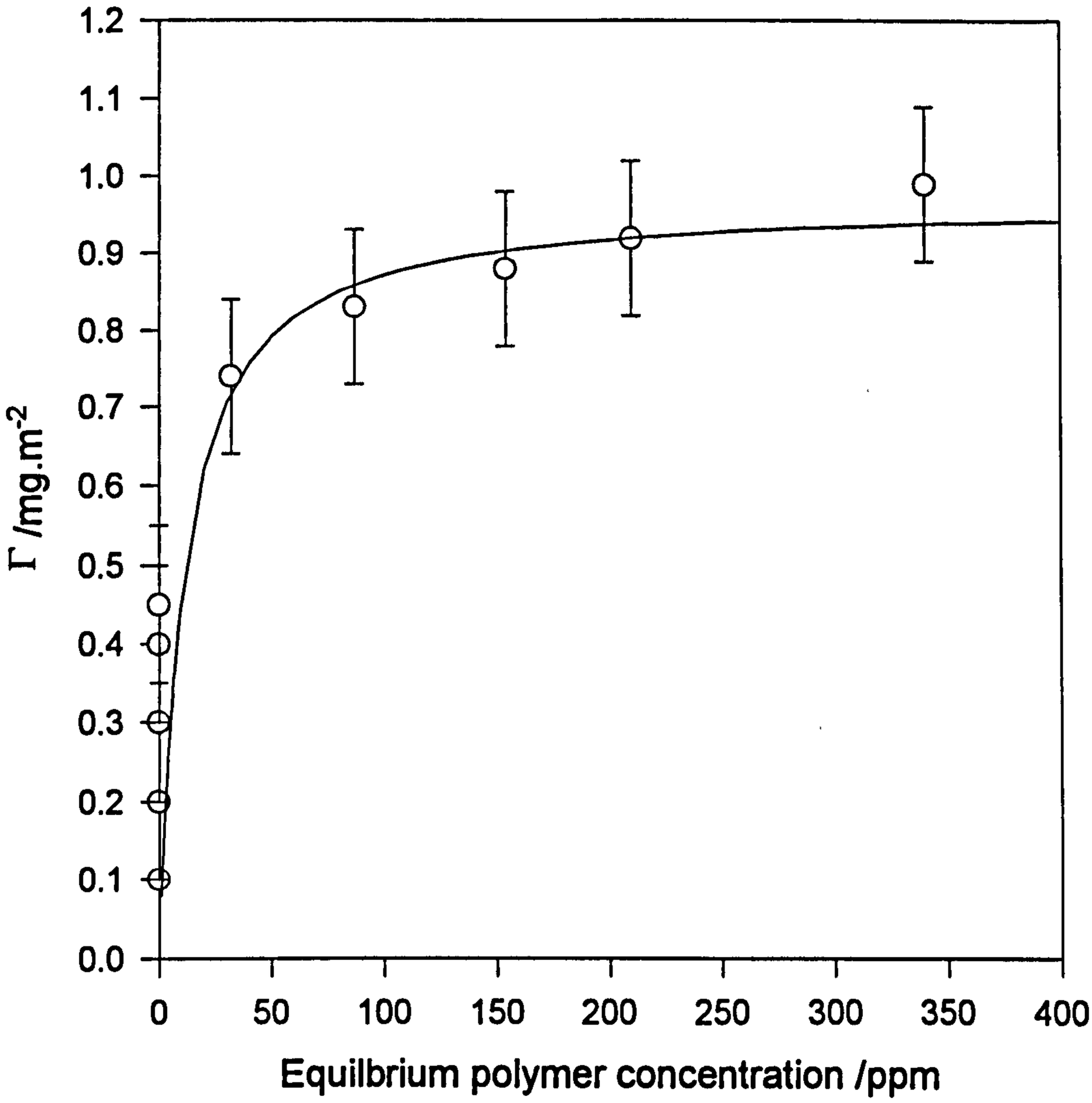

Again it is of the high affinity type and yields a plateau measured adsorbed amount of $0.9 \pm 0.1\ mgm^{-2}$. In this case, the value from fitting the data was $0.96 \pm 0.1 mgm^{-2}$. These values of adsorbed amount correspond well with those in the literature[2,3]. The amount of polymer required to yield these plateau adsorbed amounts and corresponding equilibrium concentrations were used for all of the subsequent photon correlation spectroscopy experiments. Unfortunately, using conventional methods, (such as the tannic acid method used in this study), it was not possible to obtain reproducible PEO adsorption isotherms in the presence of more surfactant than 30 ppm. This was most probably due to the formation of

tannic acid/PEO/SDS aggregates in solution. This indicates an interaction between PEO and SDS (using this technique) at even lower concentrations than previously reported[4]. The maximum measured adsorbed amount was approximately $0.35 \pm 0.1\ mgm^{-2}$, whilst the value yielded from data fitting was $0.51 \pm 0.1\ mgm^{-2}$.

Although the adsorption isotherms were difficult to obtain, there was clear indication from figure 6.1 that on the addition of even small quantities of surfactant (< 50 ppm) appreciably less PEO adsorption took place. However, because of the uncertainty of measuring the absolute PEO concentration due to the problems outlined above, the only isotherm that could be accurately plotted was the one with 30 ppm added SDS.

6.2. Background PCS Experiments.

Initially, experiments were performed in order to determine the optimum working conditions of the correlator for any particular sample. These included adjusting the sample time (τ) in order to obtain a smooth exponential correlation function which decayed over a maximum number of correlator channels. **Figure 6.3** shows a typical decay profile from which the data are calculated. Diffusion coefficients are determined from the slope of a log-log plot of these data.

Figure 6.3

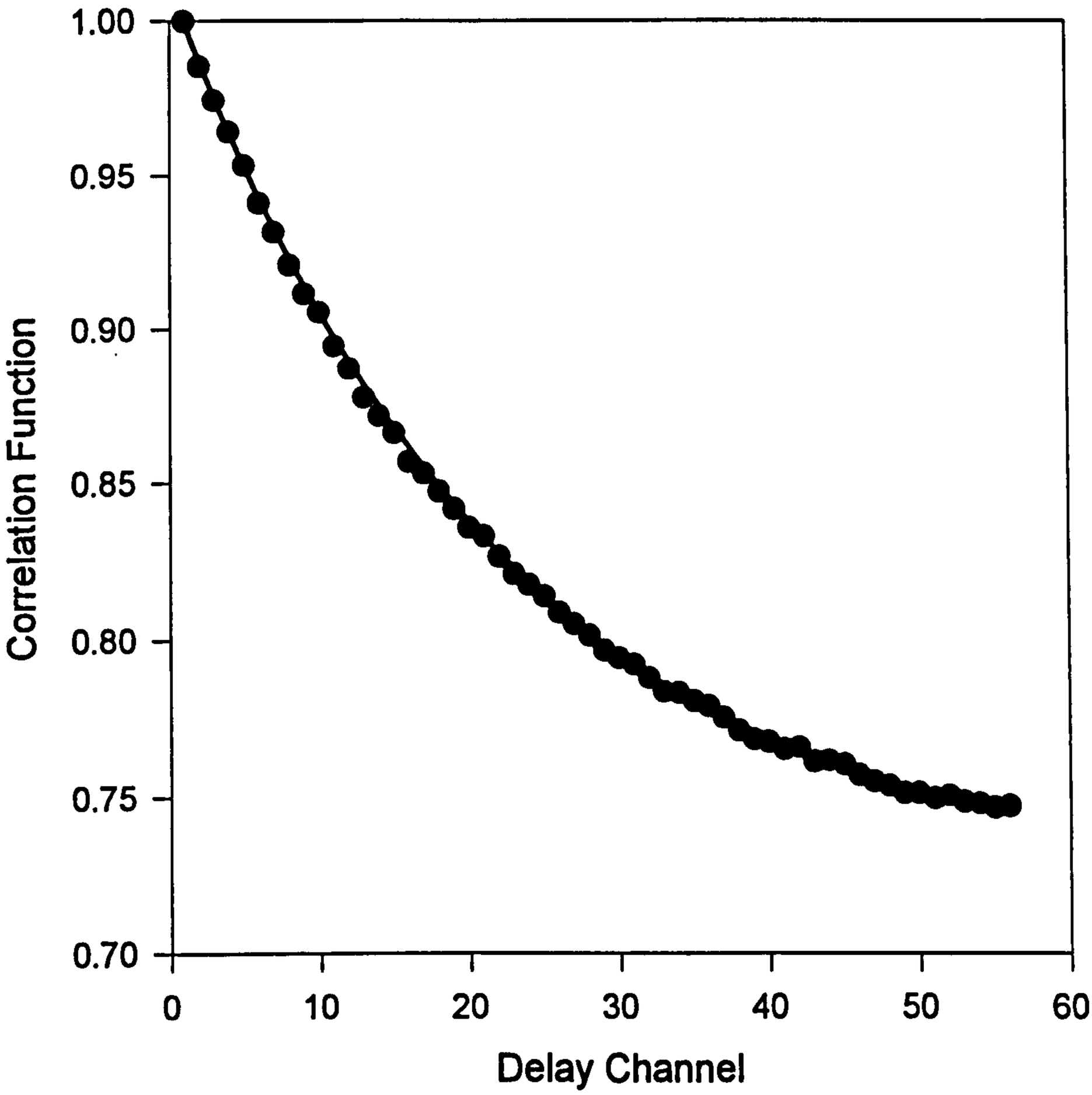

Furthermore, since particle-particle interactions may affect the measured diffusion coefficient, experiments were performed at varying particle concentrations in order to determine the concentration at which the system approached 'infinite' dilution and inter-particle interactions were eliminated.

Figure 6.4

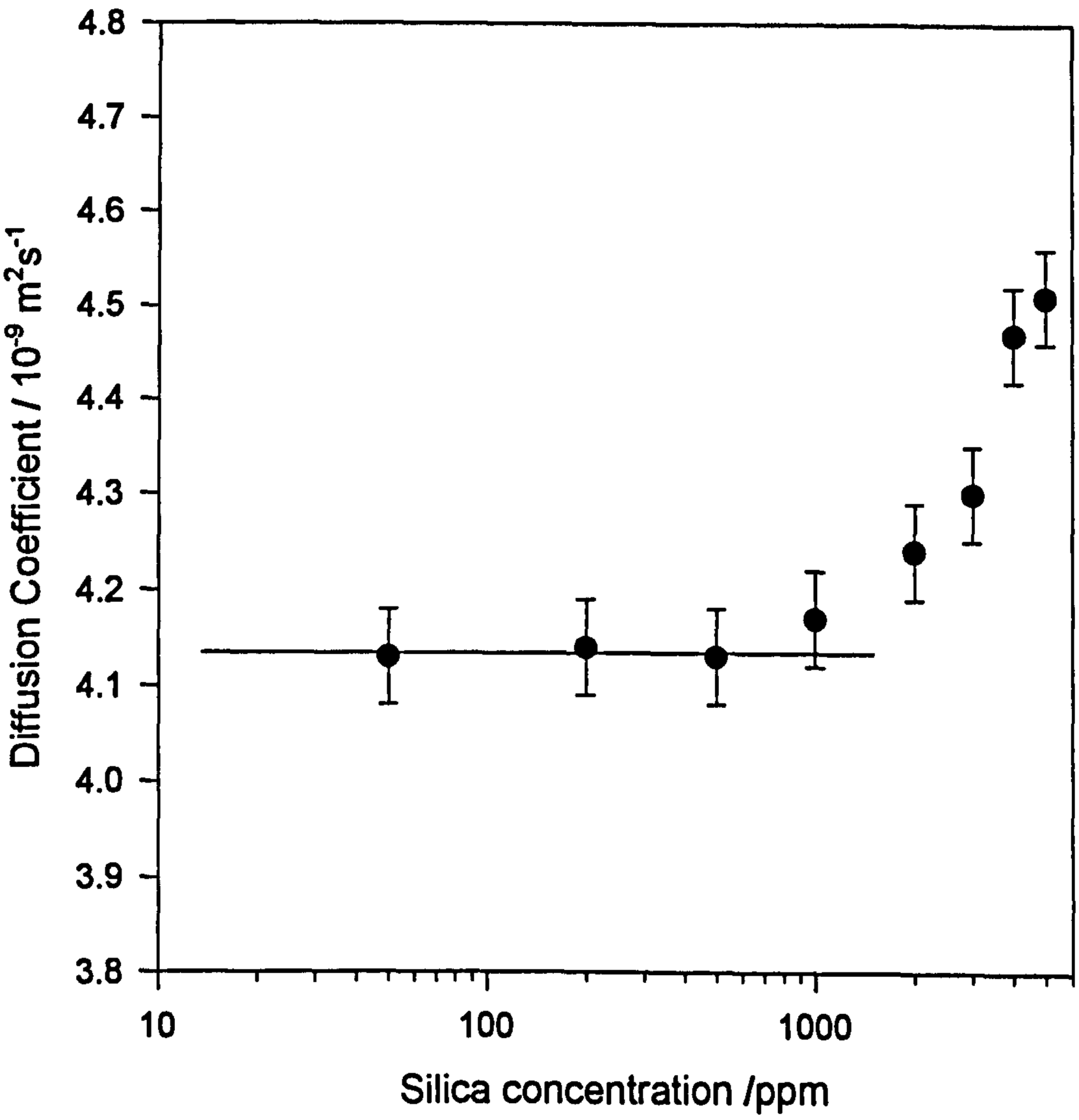

Figure 6.4 depicts the diffusion coefficient of a silica dispersion as a function of log concentration at 25 °C. As the particle concentration is increased there is an increase in the observed diffusion coefficient of the sample. The limit was chosen at silica concentrations less than 500 ppm

Figure 6.5

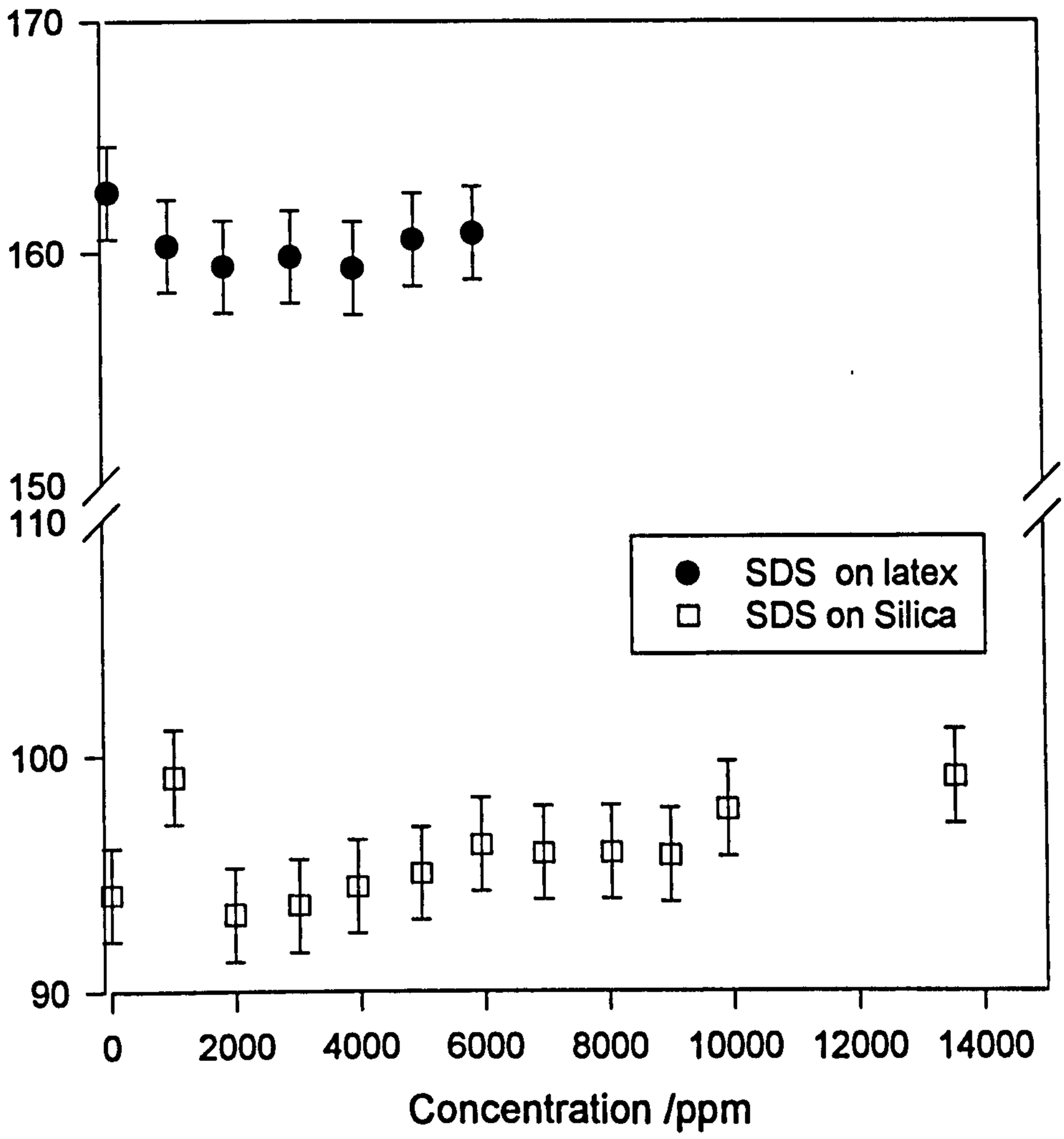

As background experiments the hydrodynamic diameters of the individual components onto both substrates were investigated. The hydrodynamic diameter of SDS adsorbed onto polystyrene latex and onto silica as a function of SDS concentration is shown in **figure 6.5**. The diameter of the bare silica particle was 94 ± 1.00 nm and the bare polystyrene latex particle was 163 ± 1.00 nm. Both of these experiments may show a slight dip in the diameter at around the normal CMC of SDS (2300 ppm SDS) although this is still within the experimental error for these results. At very high surfactant concentrations, above 10,000 ppm, the hydrodynamic diameter appears to rise rapidly. However, this is almost certainly

an increased viscosity effect, rather that any change in any adsorbed surfactant layer. The data for polystyrene latex in the presence of SDS showed similar trends to that on silica.

For PSL in the presence of SDS, one would have perhaps expected to see an increase in hydrodynamic diameter at SDS concentrations above the CMC since SDS adsorbs onto PSL at these concentrations. Brown and Zhao[5] performed an extensive study of the adsorption of SDS on polystyrene latex using PCS measurements and reported that the adsorption of SDS proceeded by a two step mechanism; an initial hydrophobically driven adsorption of single surfactant molecules followed at increased SDS concentrations by a co-operative adsorption at SDS concentrations close to the CMC. The PCS measurements reported in that paper show significant effects on the hydrodynamic diameter by the addition of SDS (up to 20 nm). These changes were attributed to the alkyl groups of the surfactant associating with the polystyrene chains of the latex. Changes in the conformation of the polymer chains at the interface were involved; steric interaction and repulsive forces which lead to an extension of the polystyrene chains and the observed increase in hydrodynamic size. SDS has not been reported to adsorb significantly onto silica particles having similar charge densities to polystyrene latex[6]. This tends to suggest that hydrophobic forces are the driving force primarily involved in the adsorption process of SDS from aqueous solution.

The huge increase in diameter reported by Brown and Zhao[5] was not observed in our PSL/SDS system. The small reduction in hydrodynamic diameter observed at SDS concentrations below the CMC may be due to a small number of alkyl chains of the surfactant lying flat on the surface. Therefore, since the particles are now effectively more hydrophobic, there may be fewer water molecules associated with the particle, hence the apparent reduction in hydrodynamic diameter.

The hydrodynamic thickness (δh) as a function of adsorbed amount for 200,000 molecular weight PEO on silica was investigated and the results are presented in **figure 6.6**. The values of adsorbed amount were extracted from the data in **figure 6.1.**

Figure 6.6

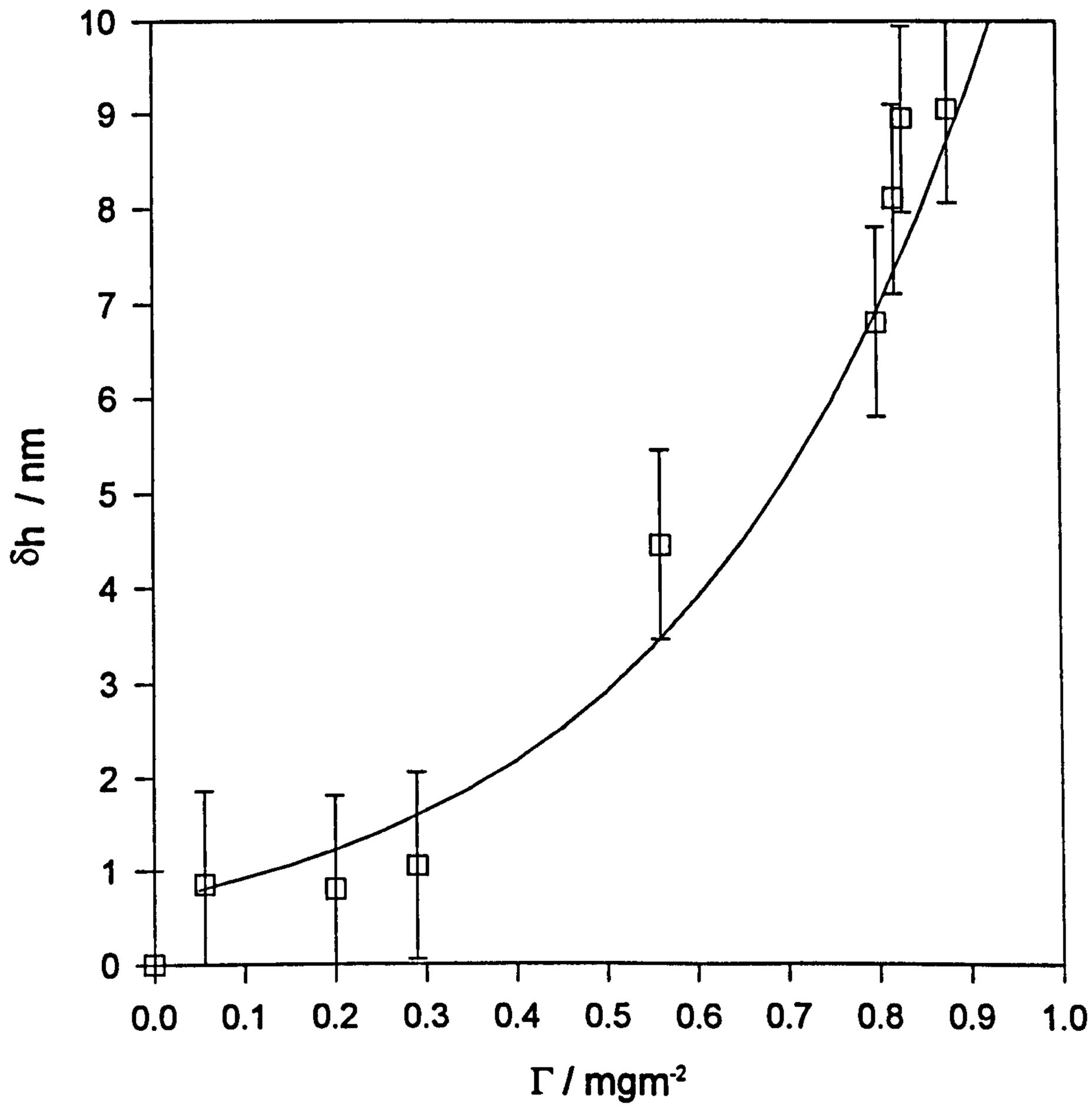

As expected, there was a very low thickness at low coverage, followed by a steep increase in the hydrodynamic thickness (δh) as the adsorbed amount approached full coverage. The hydrodynamic thickness (δh) is the difference in the particle radius with and without the polymer layer determined by hydrodynamic

techniques. The maximum thickness obtained for this molecular weight PEO on silica corresponds well with literature values[7,8]. Similar data have been reported for PEO adsorbed on a PSL substrate[9]. An important point to note from this observation is that the tail segments contribute more to the hydrodynamic thickness than the train segments. As a result, any variations in hydrodynamic thickness observed are more likely to arise from interactions at the periphery of the molecule than directly at the surface. This is especially true beyond the knee of the adsorption isotherm.

6.3 Hydrodynamic Thickness Measurements on PEO, SDS and Silica

Figure 6.7 shows the effect on the hydrodynamic thickness of an aqueous dispersion of silica and PEO by the addition of SDS. The concentration of both the silica and the polymer remained fixed, whilst the surfactant concentration was varied up to 10,000 ppm.

It can be observed from **figure 6.7** that the hydrodynamic thickness of the adsorbed PEO layer is highly dependent upon the SDS concentration. Complete, or near complete desorption, appeared to occur around the 2300 ppm of pure SDS whilst the hydrodynamic thickness in the absence of any surfactant compared well with that observed in **figure 6.6**. At very high concentrations of SDS the hydrodynamic thickness approached the measured value in the absence of surfactant. The increase in viscosity of the solution on addition of this quantity of SDS is of the order 5 % and neither this nor scattering from PEO-SDS complexes, (which cannot be detected using our apparatus) can account for the observed effects. It is not clear (using this technique) whether at high surfactant concentrations there remains an adsorbed layer and if so, whether this adsorbed layer consists purely of PEO molecules or a mixed SDS/PEO layer.

Figure 6.7

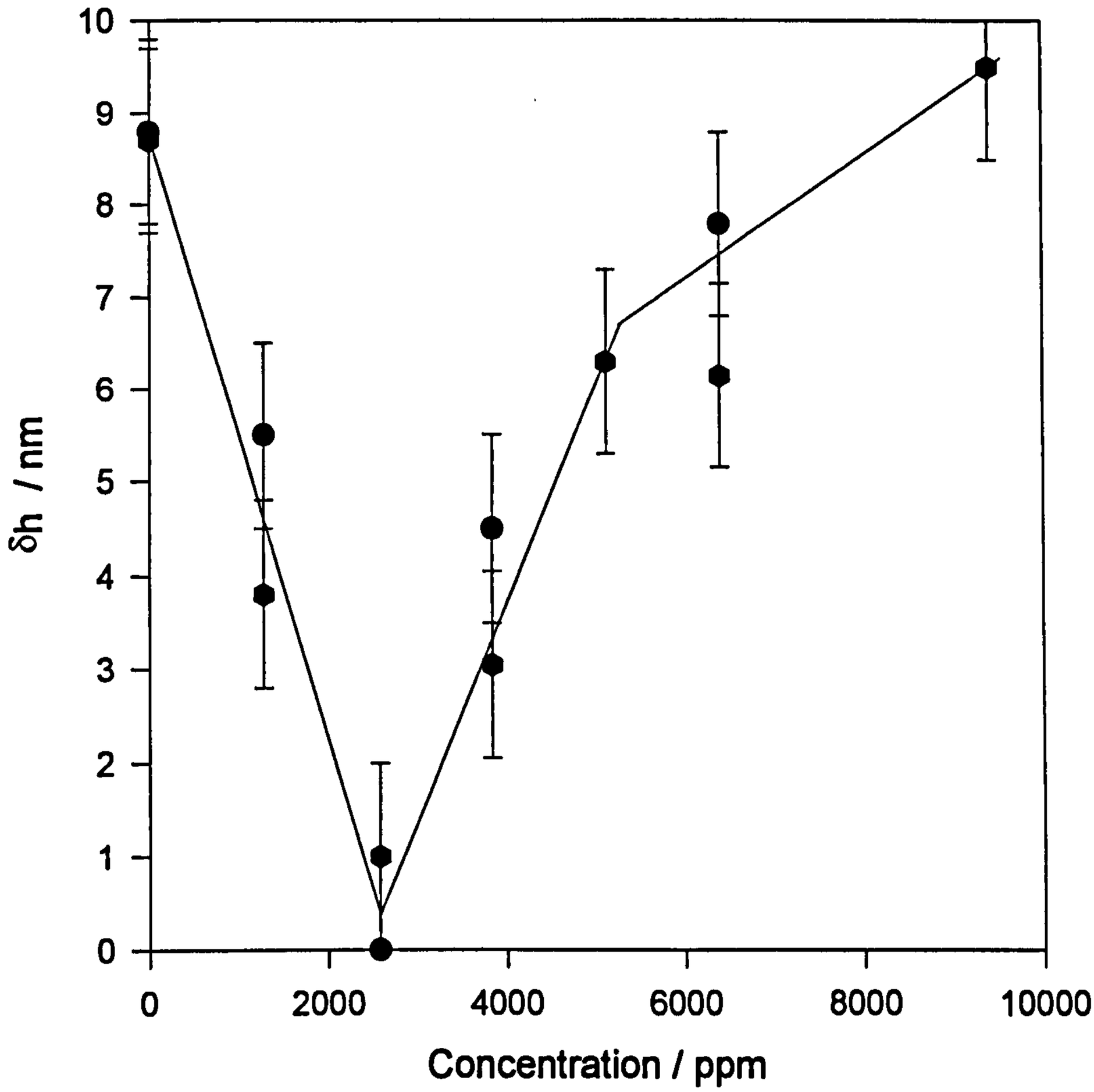

A measure of the kinetics of this system is presented in **figure 6.8**. In this case, the concentration of the polymer, surfactant and substrate were all maintained at a constant value and the hydrodynamic radius measured as a function of time. In the absence of added surfactant,(⊙) the hydrodynamic thickness reached its final value almost immediately and showed very little change with time, whilst a system containing only 1000 ppm of surfactant (□) required approximately 15 minutes to reach equilibrium. At the highest surfactant concentration used (11,200 ppm) the final hydrodynamic thickness was only achieved after

approximately 10 hours (Δ) and for this reason all samples were left to equilibrate for at least 24 hours before use.

Figure 6.8

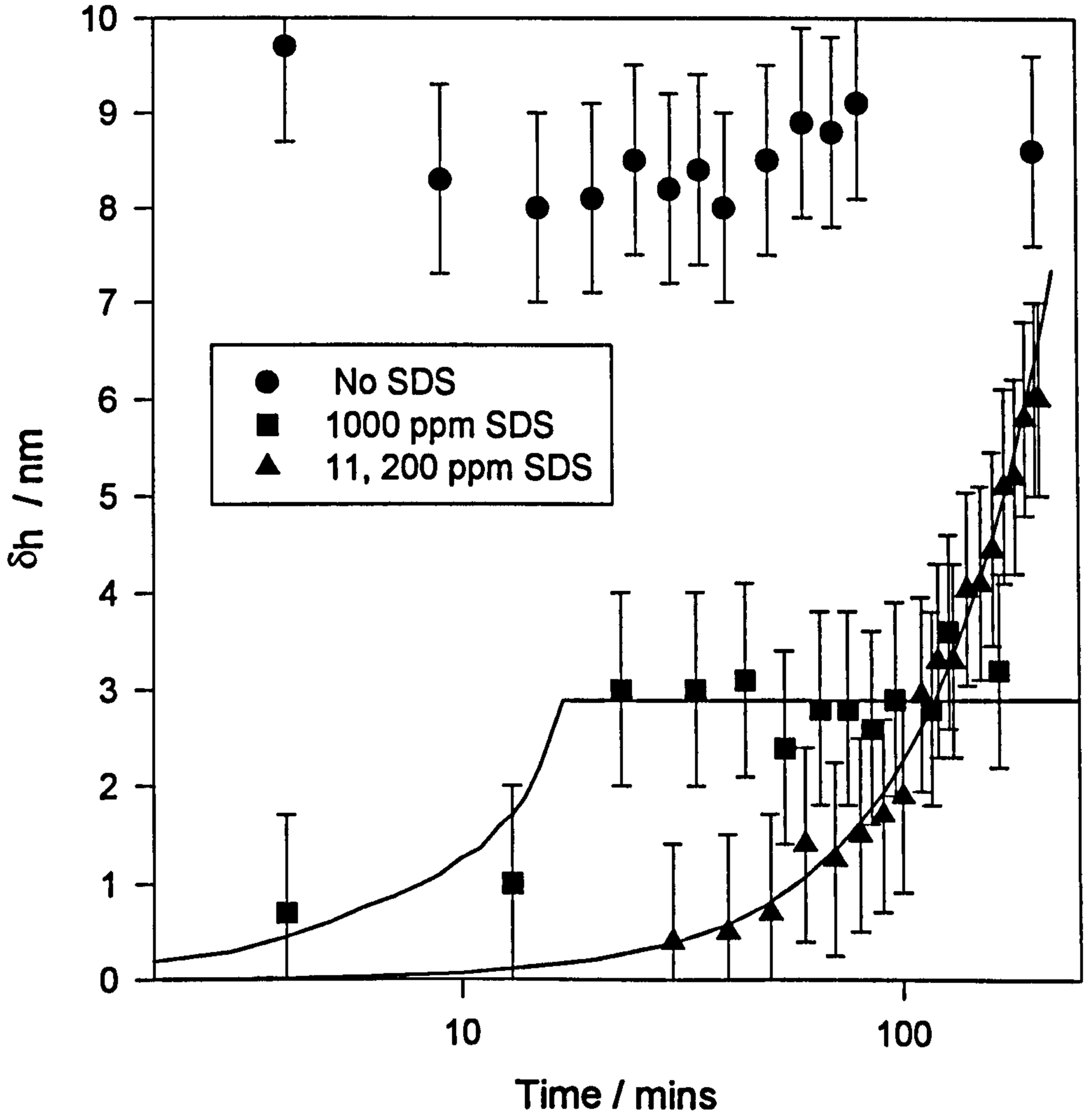

Next, the effect of temperature on the adsorbed layer was investigated. These results are depicted in **figure 6.9**. In all of these samples, the concentrations of each of the components remained fixed. For the case of SDS in the absence of polymer (○), no change in the hydrodynamic thickness was observed across the whole temperature range studied. However, for both the PEO in the absence of SDS (□) and for PEO with 2,000 ppm added SDS (Δ) a decrease in the apparent hydrodynamic radius was observed with increasing temperature. This can be

related to the decreased solvency of PEO at increased temperature. The net result is that the loops and tails of the adsorbed polymer do not have such an affinity for the solvent and to a certain extent the polymer collapses back onto the surface.

Figure 6.9

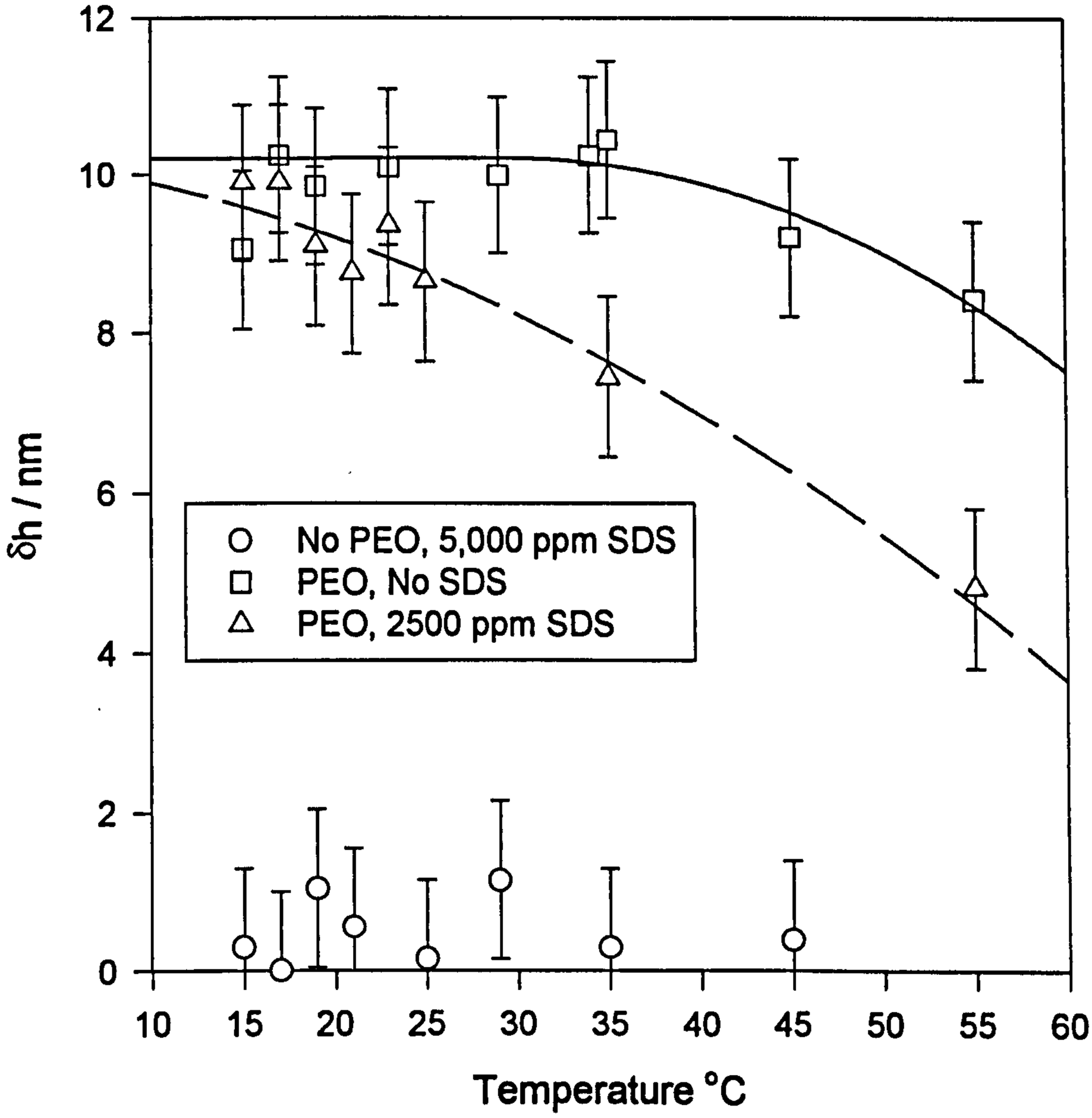

An interesting point to note is that increasing the SDS concentration will increase the overall ionic strength of the system. Generally, on increasing the ionic strength of the system the hydrodynamic thickness of an adsorbed PEO layer increases[10] In the system reported in this thesis, below the normal CMC of SDS a reduction in the hydrodynamic thickness of the adsorbed layer is reported with increasing ionic strength.

Figure 6.10

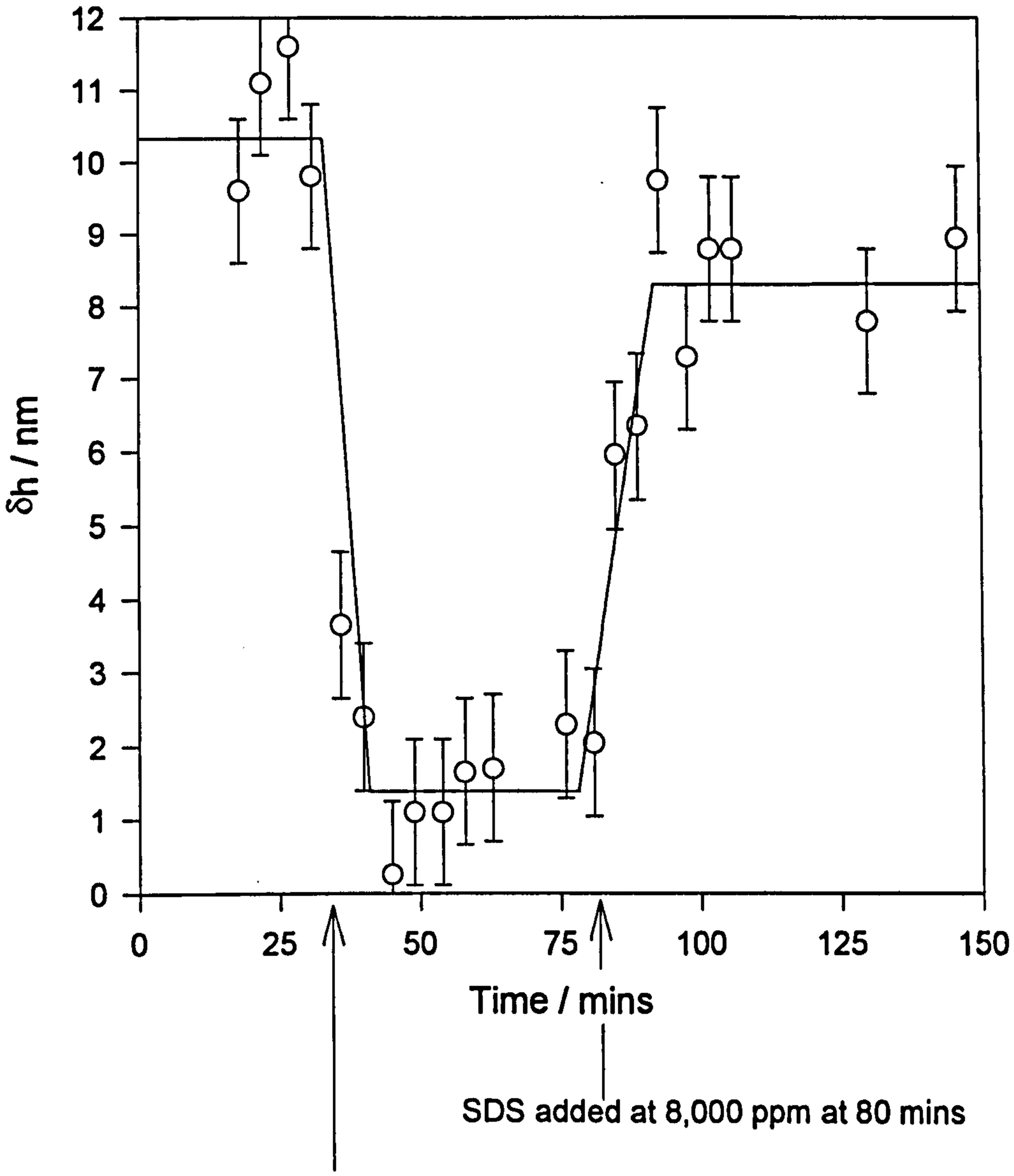

In order to check the somewhat surprising re-adsorption in the presence of excess SDS reported in **figure 6.7**, the experiment was repeated by using sequential addition of surfactant and these results are presented in **figure 6.10**.

Initially a substantial layer was formed and this was left to equilibrate for 30 minutes. The sample was then mixed with solid SDS to give a 2700 ppm SDS solution. Almost immediately the adsorbed layer thickness was strongly

depressed, either by a reduction in the adsorbed amount or by a collapse of the layer. After a further hour, excess SDS was added to increase the surfactant concentration to 8000 ppm. Over the next 30 minutes, an effective increase in the adsorbed layer was observed which confirmed the previous result in **figure 6.7** was at equilibrium.

One possible explanation for the minimum in **figure 6.7** was that a surface active impurity in the surfactant could displace the polymer below the CMC, but is taken into the micelles above the CMC, so that re-adsorption of the polymer could occur.

***Table 6.1*: Effect of Various Alcohols on the Hydrodynamic Thickness of Adsorbed PEO Layers**

Alcohol	Solubility	Thickness without polymer / (nm)	Thickness with polymer / (nm)
Methanol	Totally miscible in all proportions	-----	9.0 ± 1
Ethanol	Totally miscible in all proportions	0	8.5 ± 1
Butanol	soluble	0	8.0 ± 1
Pentanol	insoluble	-----	8.2 ± 1
Hexanol	slightly soluble	-----	8.7 ± 1
Dodecanol	insoluble	0	8.7 ± 1

The only such impurity that could reasonably be proposed for this system is dodecanol. SDS will readily hydrolyse into dodecanol and dodecanol is extremely hydrophobic and surface active. In order to clarify this situation a

series of PCS measurements were performed on various alcohols. Since dodecanol itself is insoluble in aqueous solution a series of alcohols; soluble insoluble and slightly soluble were used to cover all possibilities. At higher alcohol concentrations than 20 µl per 10 ml the silica dispersions flocculated. The table below summarises the hydrodynamic thickness' recorded when 5 µl of alcohol are added to the polymer solution prior to the addition of silica. 5 µl corresponds roughly to twice the amount of dodecanol likely to be found in a 10,000 ppm SDS solution. This quantity would give sufficient coverage, if adsorbed, (100 $Å^2$/molecule) to a polymer coated dispersion in the absence of SDS. As can be seen in **table 6.1**, none of the alcohols had any discernible effect on the PEO layer thickness. It may therefore be concluded that it is in fact the SDS causing the observed effects and not any contamination from dodecanol.

6.4 Measurements on PEO, SDS and Polystyrene Latex

Initially, all of the PCS measurements concentrated on the silica/PEO/SDS system and the full investigation reported in the previous section was performed. It was therefore thought unnecessary to repeat the vast majority of these measurements for PSL, especially since similar trends were observed for both systems. **Figure 6.11** shows the hydrodynamic thickness of aqueous dispersions of polystyrene latex, SDS and PEO. In this case, the substrate is PSL which allows both the SDS and PEO to adsorb making complexation at the interface even more favourable. As before, the concentration of the PSL and the polymer remained fixed, whilst the surfactant concentration was varied from 0 - 10,000 ppm. The hydrodynamic thickness was again observed to go through a minimum at a surfactant concentration close to the usual CMC of SDS and then rise back to its original value at high surfactant concentrations.

Figure 6.11

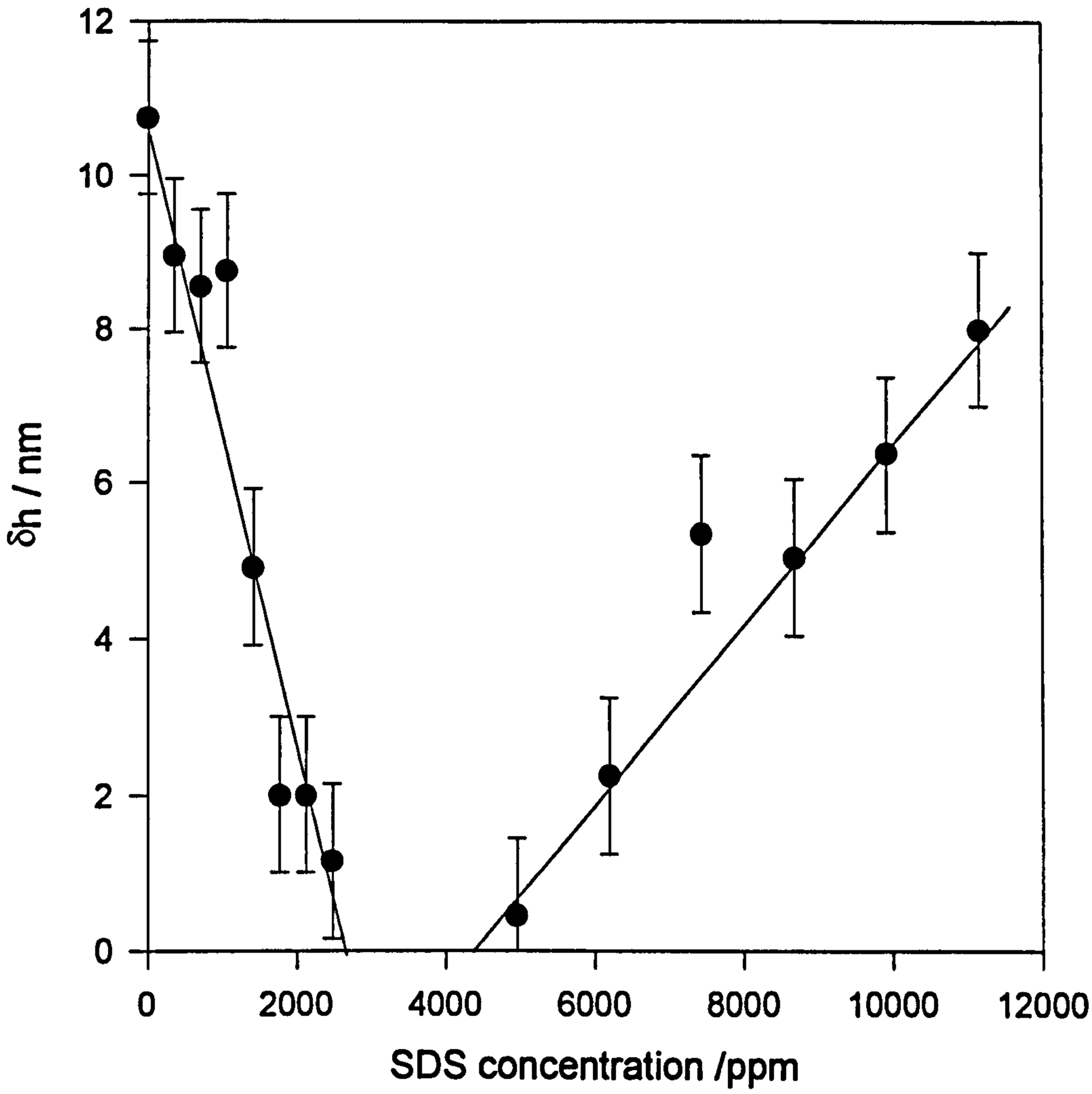

A preliminary investigation was performed into the effect of SDS on a grafted PEO layer[a]. This data is shown in **figure 6.12**. Unfortunately, it is difficult to synthesise a monodispersed grafted layer of high molecular weight PEO and because of this the grafted PEO (g-PEO) was only of molecular weight approximately 2000. (It must be noted here that in solution PEO and SDS do not interact at PEO molecular weights less than 4000). Nevertheless, due to the nature of a grafted layer, the g-PEO produced highly extended chains of length

[a] Kindly supplied by Dr. J. Eastman, University of Bristol.

estimated at approximately 5 - 6 nm. In the absence of any added surfactant the diameter of the g-PEO polystyrene latex was 178 ± 1.00 nm.

Figure 6.12

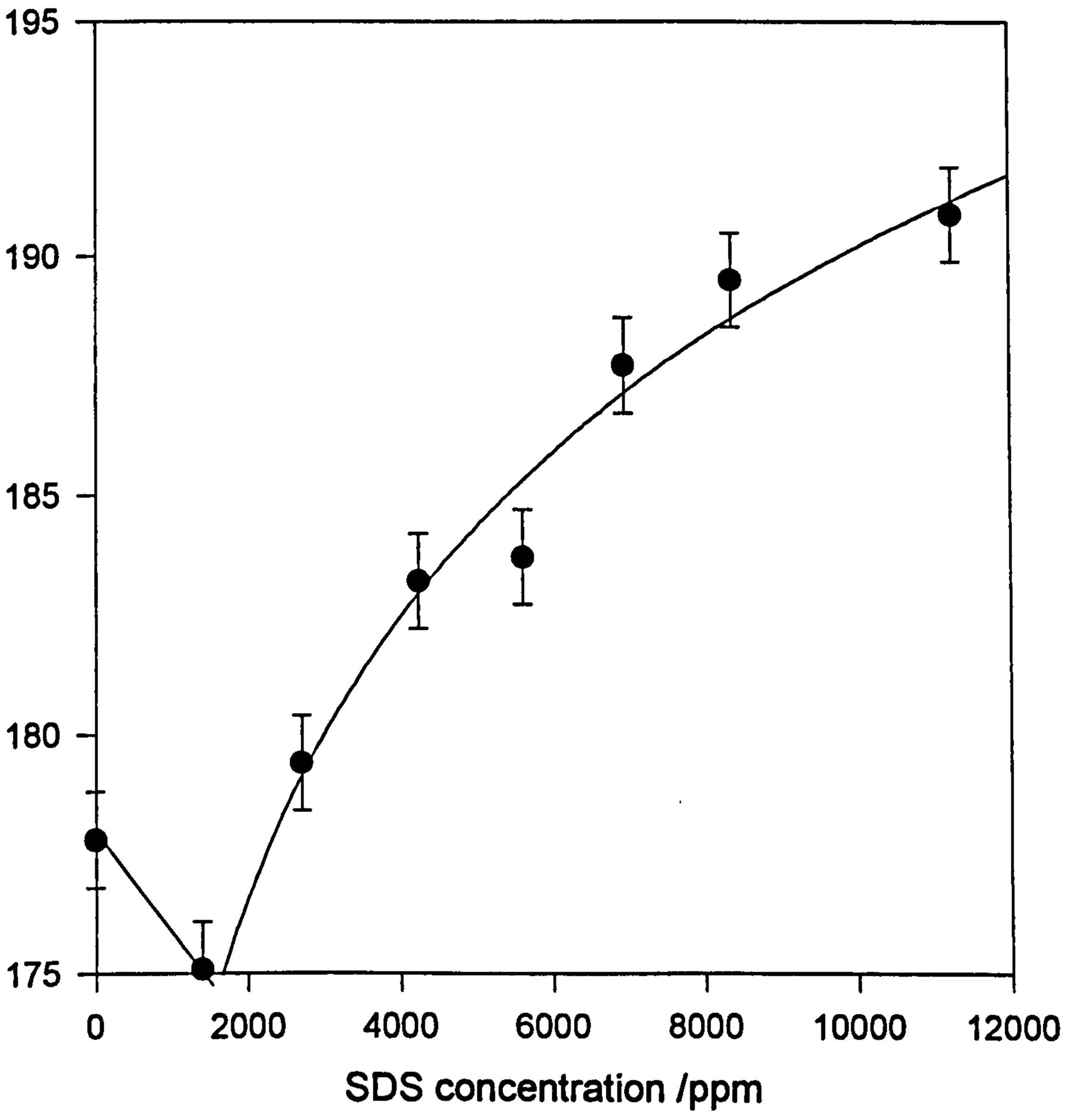

On addition of small amounts of SDS (less than the CMC of SDS) this had reduced to 175 ± 1.00 nm, a reduction in the hydrodynamic thickness of 1.35 ± 1.00 nm. Although not quite on the scale of the adsorbed system this reduction in δh shows that SDS also has some marked effect on a g-PEO layer. At SDS concentrations beyond the normal CMC, the more surprising observation was recorded. The diameter of the g-PEO and polystyrene latex showed a marked increase (compared with the grafted layer thickness) as the SDS concentration

was raised, such that at the maximum SDS concentration measured the diameter had risen to 190.9 ± 1.0 nm, an increase in δh of 6.5 ± 1.0 nm.

6.5 Interpretation and Discussion of Results.

It is evident from the data presented in the earlier sections of this chapter that the adsorption of PEO from aqueous solutions is markedly affected by the presence of SDS. Below the normal CMC of SDS (2300 ppm) a progressive desorption (or thinning) of the PEO layer was indicated by a rapid decrease in the hydrodynamic thickness. This can be attributed to complexing of the adsorbed PEO with SDS monomers making it increasingly negatively charged; the same sign as the charge in the silica or polystyrene latex particle. A similar effect was observed for a grafted PEO layer, although this was less pronounced (possibly due to the smaller molecular weight of the polymer). At higher concentrations of the surfactant, a surprising increase in the layer thickness was seen, which was reversible. The hydrodynamic thickness of this layer did not indicate *per se* that the adsorbed amount reaches that which was found in the absence of surfactant, but could indicate a very dilute but extended layer comprised of the polymer decorated with micelles. These results are not dissimilar to those of Shubin[11] for SDS/cationic polyelectrolyte adsorbed on mica. Shubin's data showed that increasing surfactant induced a steady desorption of material from the interface above a concentration of 5 ppm SDS. The reduction in adsorption correlates well with our data up to 2000 ppm. Between 50 ppm and 600 ppm, however, the adsorbed layer in that system became substantially more extended. It seems likely that this effect was due to micelles along the polymer chain, which repel each other, causing a more extended configuration. In the system in this study, the increase in adsorbed layer thickness occurred at a higher concentration, but this may simply be a reflection of the higher CMC for PEO/SDS.

Unfortunately, neither of the techniques reported in this chapter can give direct information on the structure of the adsorbed layer or on the location and size of the SDS molecules. Therefore in order to progress further with the understanding of this system, a technique is required which has greater molecular recognition. In the following two chapters these systems are examined using nuclear magnetic resonance (NMR) spectroscopy measurements and small-angle neutron scattering (SANS) investigations. NMR measurements can give information on the bound fraction of the adsorbed polymer layer and the size of SDS micelles. On the other hand, using SANS one can obtain the full surface volume fraction profile of the adsorbed polymer and detailed information on the size and structure of the SDS molecules. These three chapters will combine to give detailed information on this model polymer, surfactant, substrate system.

References.

1. Nuysink, J., Koopal, L. K.; *Talanta* **1982**, 29, 495
2. Cohen Stuart, M. A., Waajen, F. H. W. H., Cosgrove, T., Vincent B., Crowley T. L.; *Macromolecules* **1984** 17 1825
3. Cosgrove T., Griffiths P. C., Lloyd P. M.; *Langmuir* **1995** 11(5) 1457
4. Ramachandran R., Kennedy G. J.; *Colloids & Surfaces* **1991** 54 261
5. Brown W., Zhao J.; *Macromolecules* **1993** 26 2711
6. Gao Y., Yue C., Lu S., Gu W., Gu T.; *J. Coll. Int. Sci* **1984** 100 (2) 581
7. van der Beek G., *et al*; *J. Physique (Paris)* **1988** 49 1449
8. Killmann E., Wild Th., Gütling N., Maier H., *Colloids & Surfaces* **1986** 18 241
9. Shar J. A., *Ph.D. Thesis, University of Bristol* **1997**
10. Cosgrove T, Crowley T. L., Ryan K., Webster J. R. P.; *Colloids and Surfaces* **1990** 51 255
11. Shubin, V.; *Langmuir* **1992**, 10, 1093

Chapter 7.

NMR Results on PEO and SDS.

In order to investigate the multiple interactions between all of the various components of interest in this study, a technique is required which can discriminate between them. Nuclear magnetic resonance (NMR) spectroscopy is ideal in this respect since it is 'molecularly specific' and can reveal information on the dynamics of a system such as PEO, SDS and particles which can ultimately be related to the structure of the system. This chapter discusses the self-diffusion and solvent relaxation measurements performed on these systems.

7.1. Solvent Relaxation Measurements.

7.1.1. Individual Components.

For background information, the single and binary systems were first examined. The ^1H spin lattice relaxation time of the solvent, T_1 was determined by detecting the amplitude of the free induction decay signal after a 90° pulse in a 180°-τ-90° pulse sequence. A suitable range of values of τ, the spacing between the two pulses, was used. The re-establishment of M_z magnetisation after the 180° pulse to the equilibrium value M_z^0 satisfies equation 7.1,

$$M_z(\tau) = M_Z^0\left(1 - 2\exp\left(-\tau/T_1\right)\right) \qquad [7.1]$$

The ^1H spin-spin relaxation times of the solvent were determined from the amplitudes of the spin-echoes produced by a CPMG sequence[1]. The value of T_2

was obtained by fitting the magnetisation decay to equation 7.2 where $M_y(0)$ is the transverse magnetisation immediately following the 90° pulse.

$$M_t(t) = M_y(0)\exp\left(-t/T_2\right) \qquad [7.2]$$

Figure 7.1 shows both the longitudinal (R_{1sp}) and transverse (R_{2sp}) relaxation rates of aqueous dispersions of the silica Snowtex 50 as a function of solids concentration. All of the T_1 measurements were performed at 40°C due to instrumental limitations.

Figure 7.1

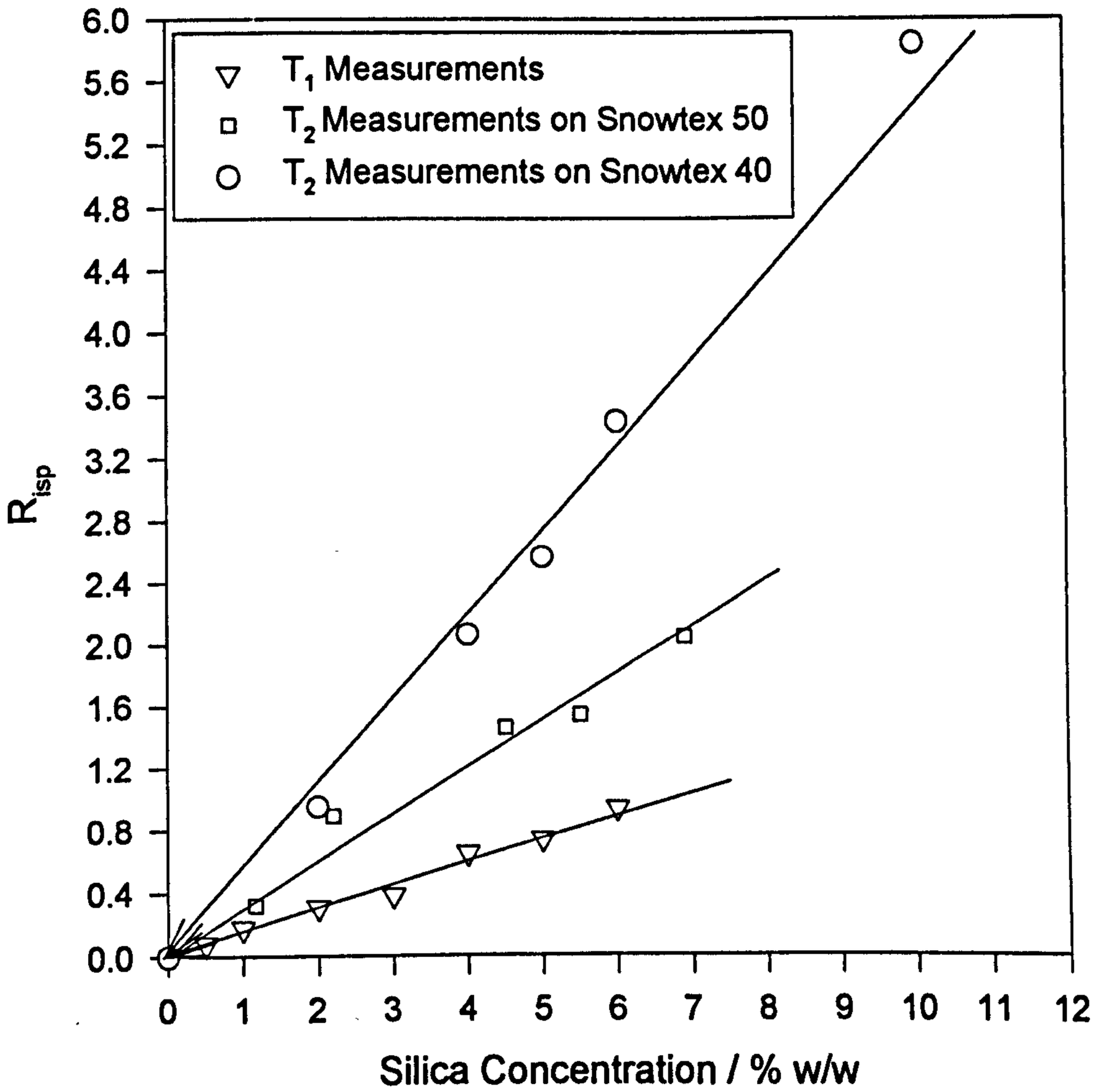

The relaxation rate is the reciprocal of the relaxation time and these values have been normalised against H_20 for all of these measurements, to give the specific relaxation rate according to equation 7.3,

$$R_{isp} = \frac{R_i}{R_i^0} - 1 \qquad [7.3]$$

where R_i is the relaxation rate and R_{isp} is the specific relaxation rate with respect to the relaxation rate of the standard, R_i^o. As expected, within the range examined, there is a linear relationship between the available surface area and the relaxation rate. This only occurs if there is fast exchange occurring between water molecules in the bound state and highly mobile free water molecules. The slope of this line is proportional to $R_{2sp}{}^b$ - the averaged specific relaxation rate of protons near the surface, equation 7.4

$$R_{isp} = P_b R_{isp}^b \qquad [7.4]$$

The fraction of these protons P_b is proportional to the amount of silica per solvent volume. For water bound to silica, the transverse relaxation rate is higher than the longitudinal one due to low frequency molecular motions at the interface. Also shown in **Figure 7.1** is the transverse relaxation rate for Snowtex 40 which is identical in composition to Snowtex 50, but with a much smaller radius (and hence increased surface area). This is reflected in the much greater specific relaxation rate for a given solids concentration. Cosgrove *et al*[2] measured the specific relaxation rate of a series of different sized silica particles as a function of silica concentration and in all cases with increasing surface area per volume, the amount of bound water increased accordingly. A linear relationship was obtained between relaxation rate enhancement and surface area confirming this idea. This was tested for the Snowtex 40 and Snowtex 50 dispersions. This is shown in **Figure 7.2** which clearly demonstrates the linear relationship between surface area and enhancement.

Figure 7.2

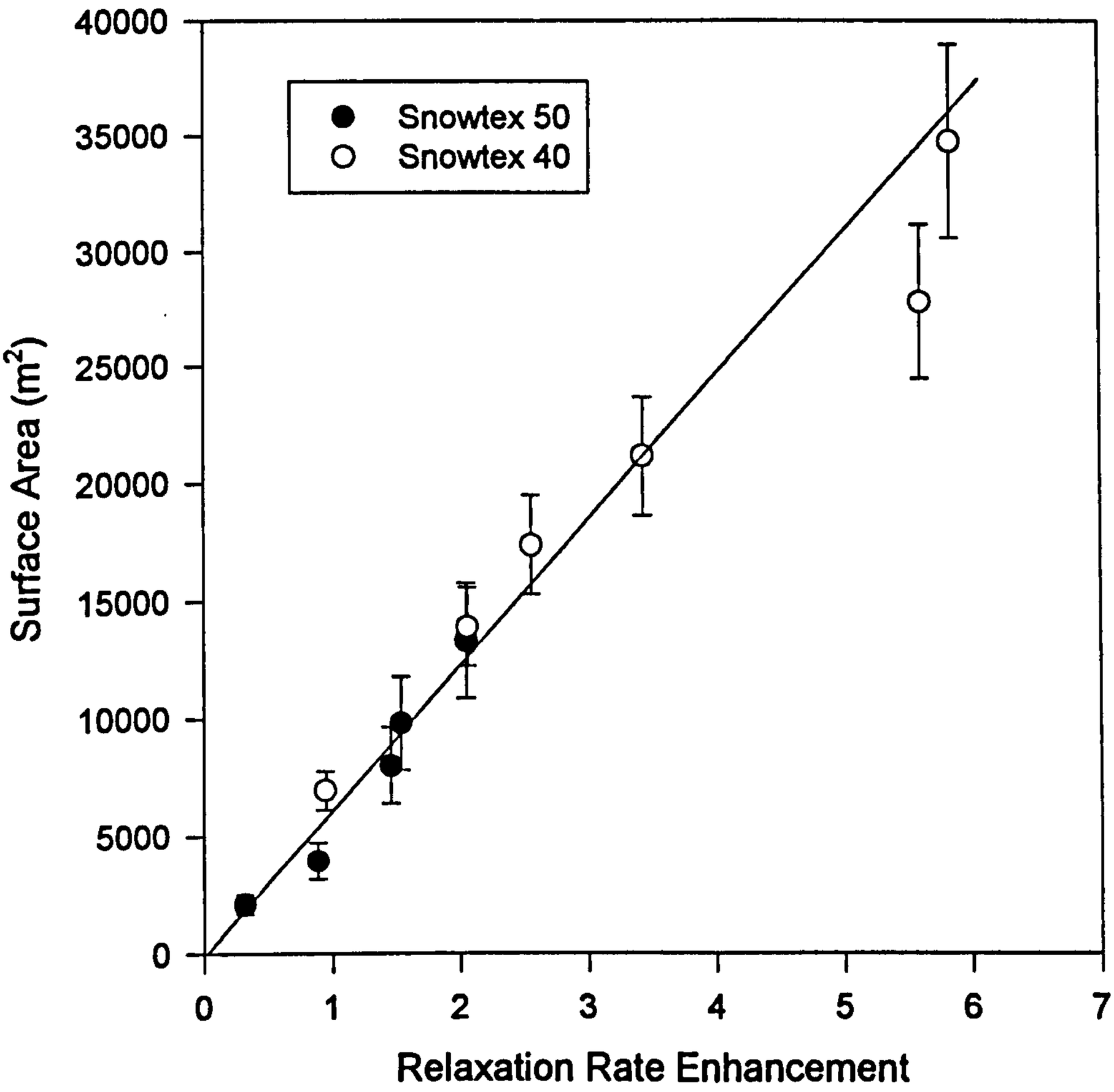

Polystyrene latex shows only a very small enhancement with concentration due to its hydrophobic nature[3] and therefore was not used for these measurements. All of the subsequent experiments were performed using Snowtex 40 due to the increased enhancement over Snowtex 50.

Shown in **Figure 7.3** is the specific longitudinal and transverse relaxation rates for the surfactant SDS as a function of concentration. As can be observed, across the whole concentration range under investigation, there is very little enhancement in the relaxation rate, compared with the silica case; *for example,* a

4.0 % w/w Snowtex 40 dispersion gives an enhancement of 2.10 compared with a measured enhancement 0.256 for a 3.93 % w/w SDS solution (*Note*, this data point is not shown on the figure). Both sets of results may suggest some form of increase with concentration beyond the CMC of SDS (0.23 % w/w) but since this is within the experimental error of these measurements it is impossible to determine at this stage whether this is indeed a true effect. Since, these effects are relatively small, they are negligible in systems which have very short relaxation times compared to water, such as the silica case reported in **Figure 7.1**

Figure 7.3

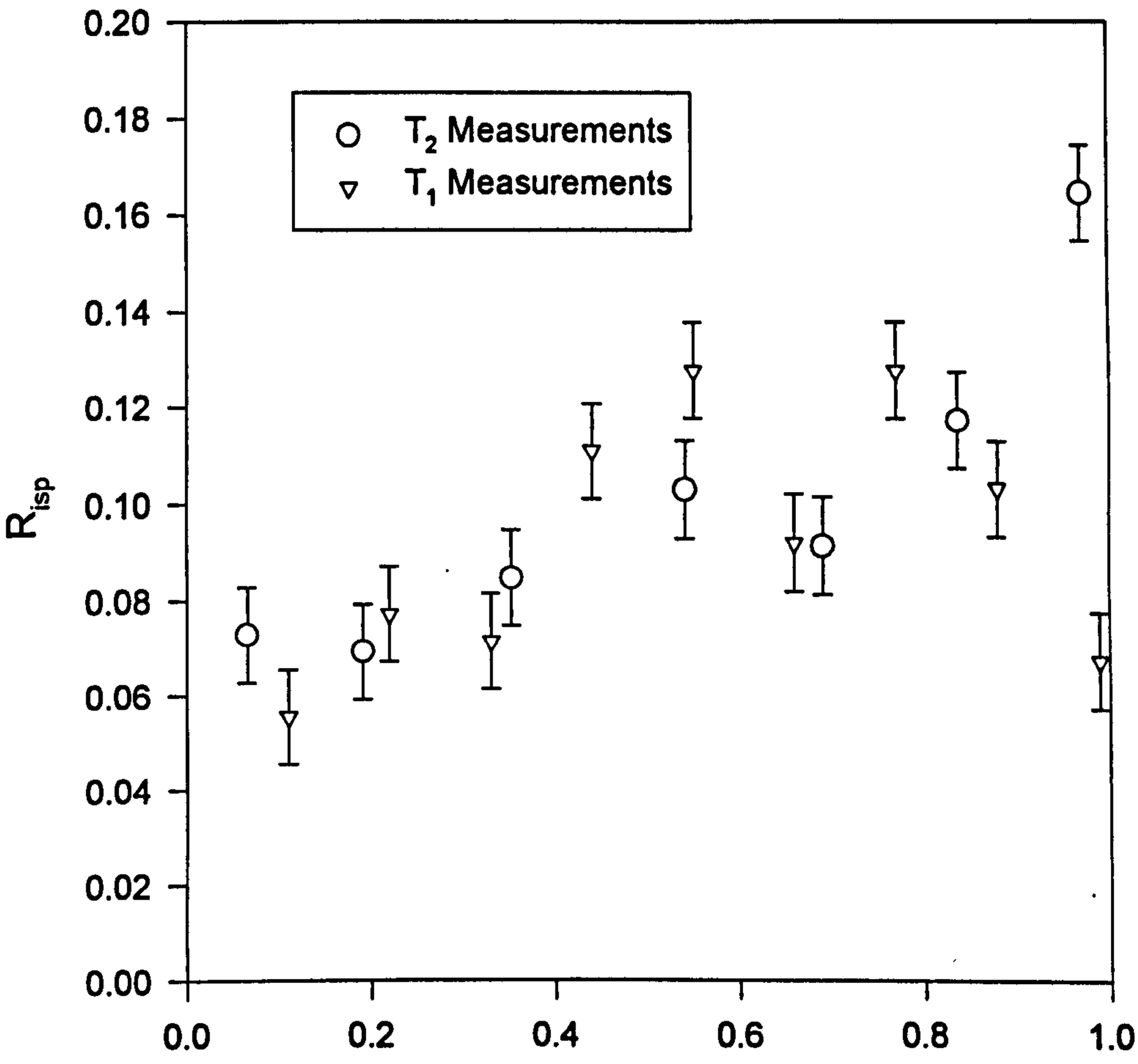

7.1.2 Binary Mixtures.

Figure 7.4

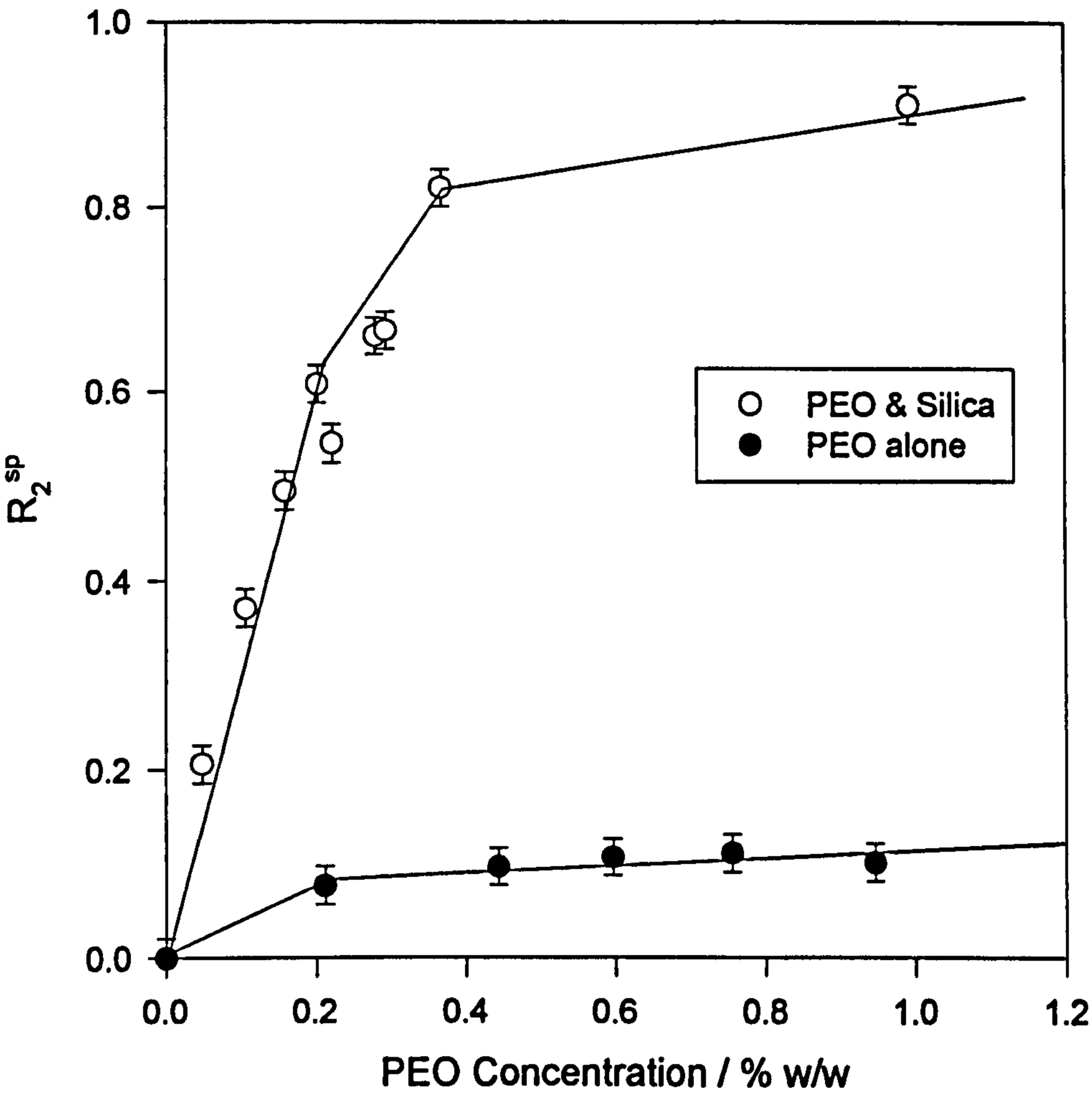

Figure 7.4 shows the transverse specific relaxation rates of 114,000 M. Wt. PEO as a function of polymer concentration in the presence and absence of Snowtex 40 silica. It can be observed that the values of R_{2sp} in the absence of silica show an increase, albeit relatively small, with concentration. This increase was not observed in earlier studies[4], but is most likely either a result of the higher molecular weight polymer, or the increased resolution of the instrument used in this study. Also shown in **figure 7.4** is the corresponding data for adsorbed PEO. Since relaxation rates are additive, the enhancement from bare silica has been subtracted from these data in order to investigate the effect of adsorption directly.

Evidently, from **figure 7.4**, an enhancement is produced which is in excess of that for PEO in solution, suggesting that the mobility of the water has either been substantially constrained or that its residence time in the bound environment has increased. The filled circles (PEO in the absence of silica) indicate this effect is not due to free polymer. These effects are in good agreement with previous studies[2,4].

Cosgrove *et al*[2] added different molecular weight PEO samples to silica dispersions and found that the enhancement was independent of molecular weight. Therefore, it was suggested that since the observed enhancement is not proportional to molecular weight, not all of the polymer segments contribute equally to the relaxation rate enhancement. It was shown by van der Beek *et al*[4] that this enhancement was proportional to the adsorbed amount in trains (Γ_{trains}) according to equation 7.5

$$\Gamma_{trains} = k^{-1} R_2'^{sp} \qquad [7.5]$$

where $R_2'^{sp}$ is the specific relaxation rate normalised against silica rather than water and k is a proportionality constant. Furthermore, the bound fraction <p> may be calculated,

$$\langle p \rangle = \frac{\Gamma_{trains}}{\Gamma_{total}} \qquad [7.6]$$

Therefore, a plot of $R_2'^{sp}$ against the total adsorbed amount (**Figure 7.5**) at low coverage's will yield a straight line with slope of k^{-1}. Taking the first 4 points from **figure 7.5**, k was obtained as 0.145 $mg^{-1}m^2$ and this value was inserted into equations 7.5 and 7.6 to obtain values of <p> as a function of adsorbed amount.

Figure 7.5

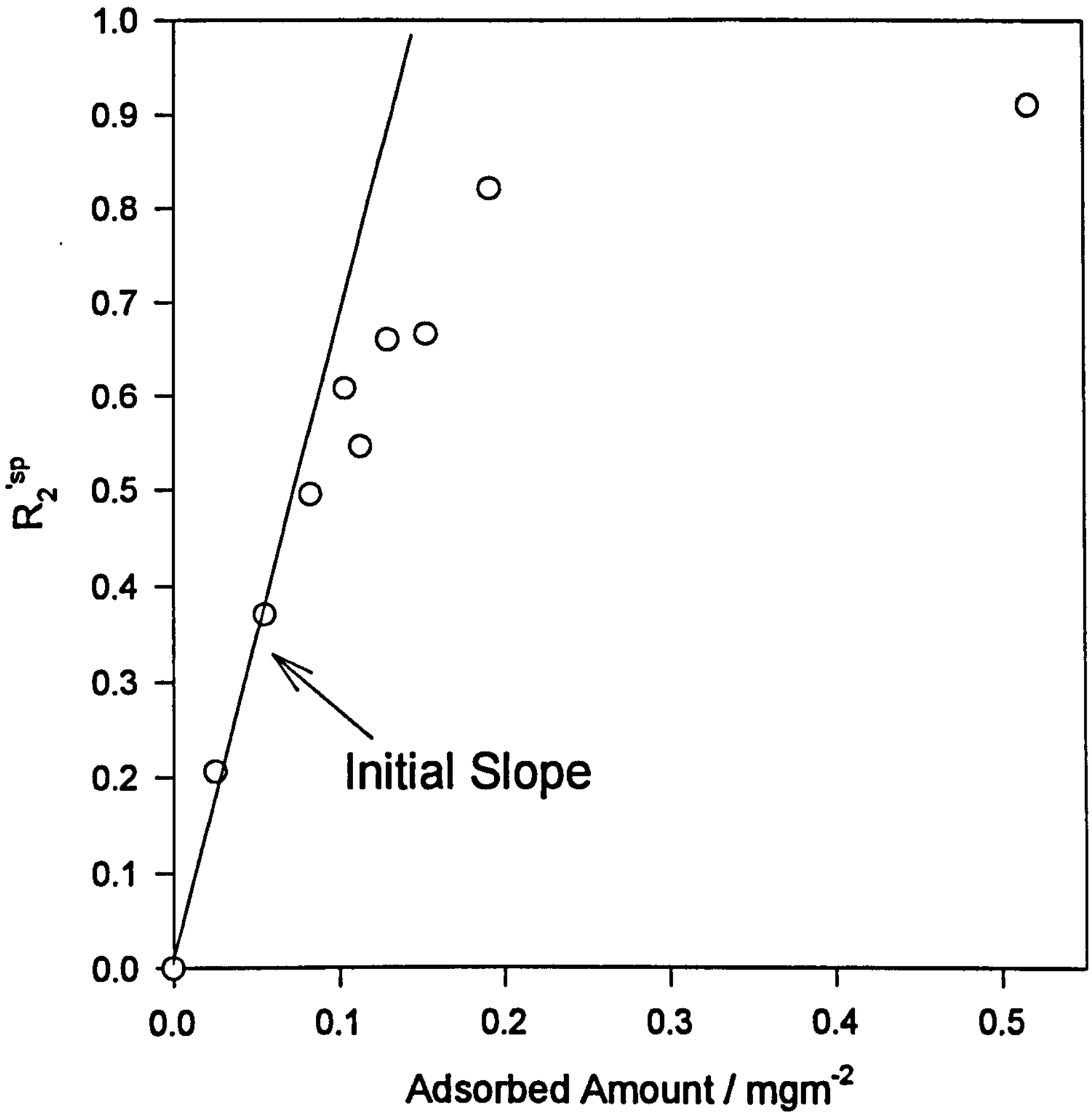

This is shown in **figure 7.6** (the line in this figure is simply to guide the eye and has not been fitted) This figure shows that at low coverage's the bound fraction approaches unity, whilst at higher coverage's where longer loops and tails are formed the bound fraction is reduced until at full coverage it is only about 0.15. These data agree very well with those obtained previously by van der Beek *et al*[4] and Lloyd[5] on similar systems.

Figure 7.6

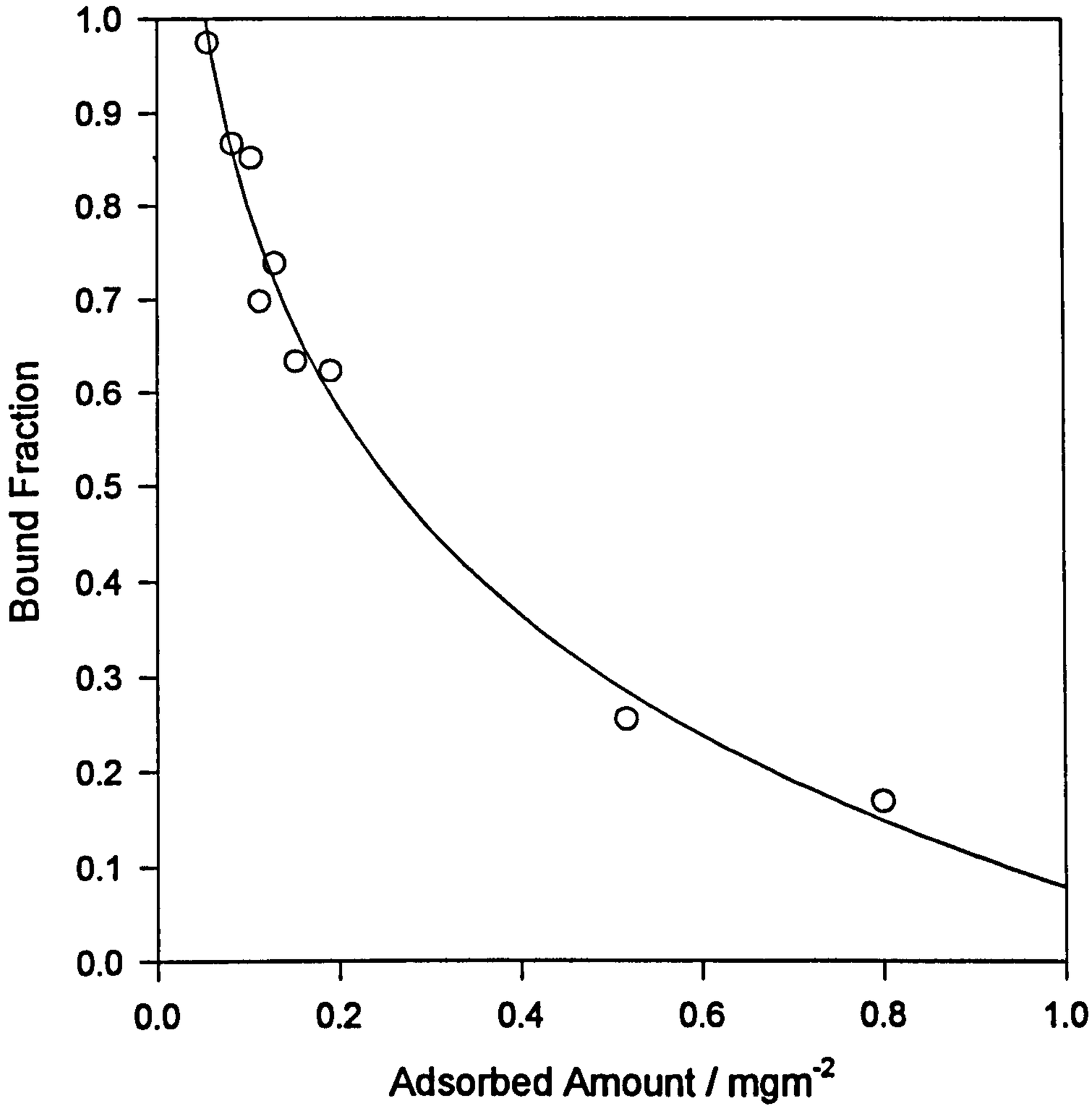

Figure 7.7 shows the specific relaxation rates of the solvent in the presence of silica and SDS. The specific relaxation rate of the silica has been subtracted. SDS does not adsorb onto silica and therefore no enhancement in the relaxation rate is observed in excess of that for the bulk SDS. This demonstrates beautifully the additive effect of relaxation rates in non interacting systems.

Figure 7.7

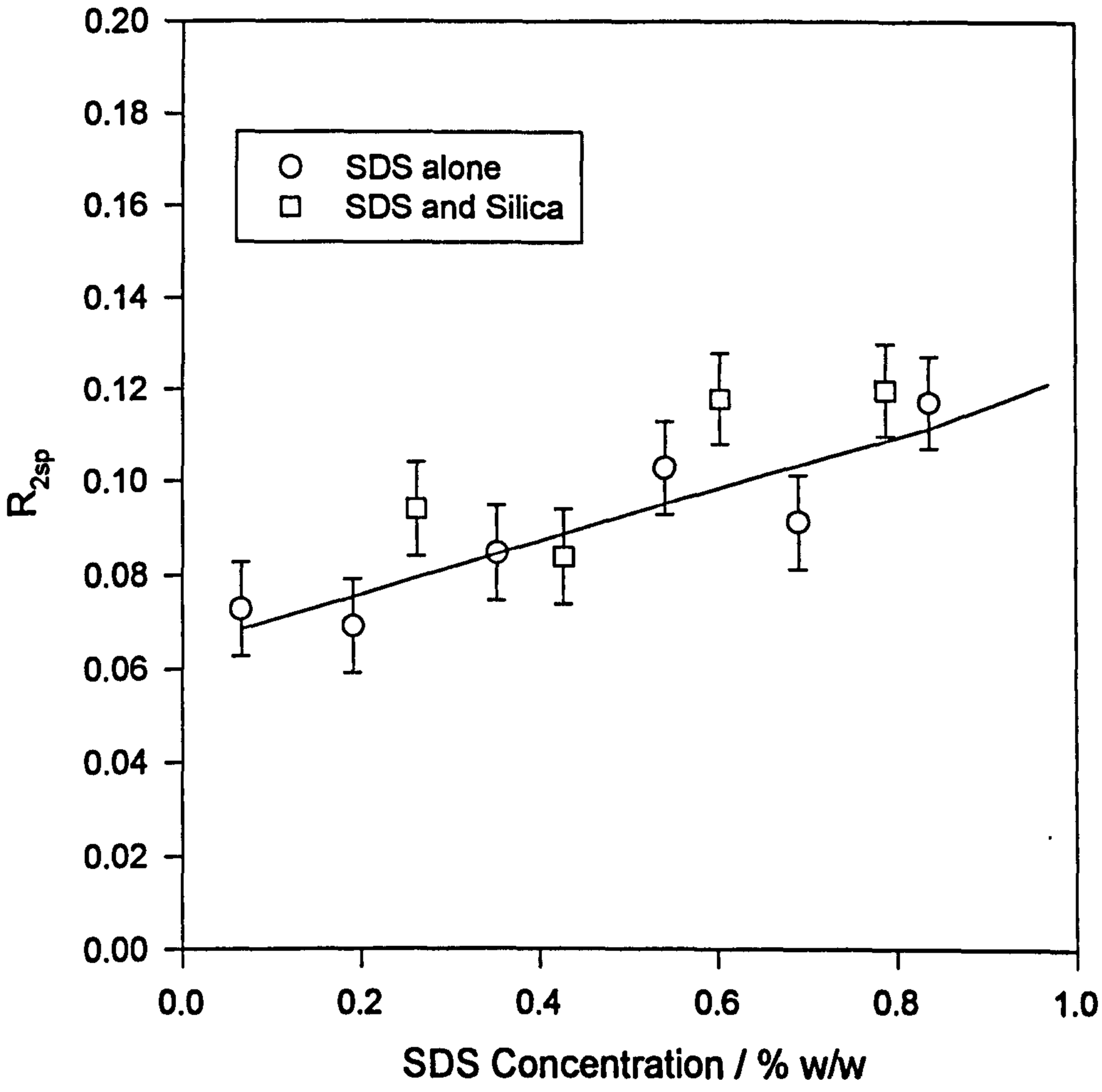

Figure 7.8 shows the effect of mixtures of PEO and SDS on the solvent relaxation rate. For all of these data the PEO concentration is maintained at 0.5 % w/w and the SDS concentration varied in the range 0 - 1.0 % w/w. Evidently from this figure, there is very little enhancement in the relaxation rate on mixing SDS and PEO. This shows that the interaction between the two species incorporates only a small amount of bound water or water that has only a very short residence time in the bound state.

Figure 7.8

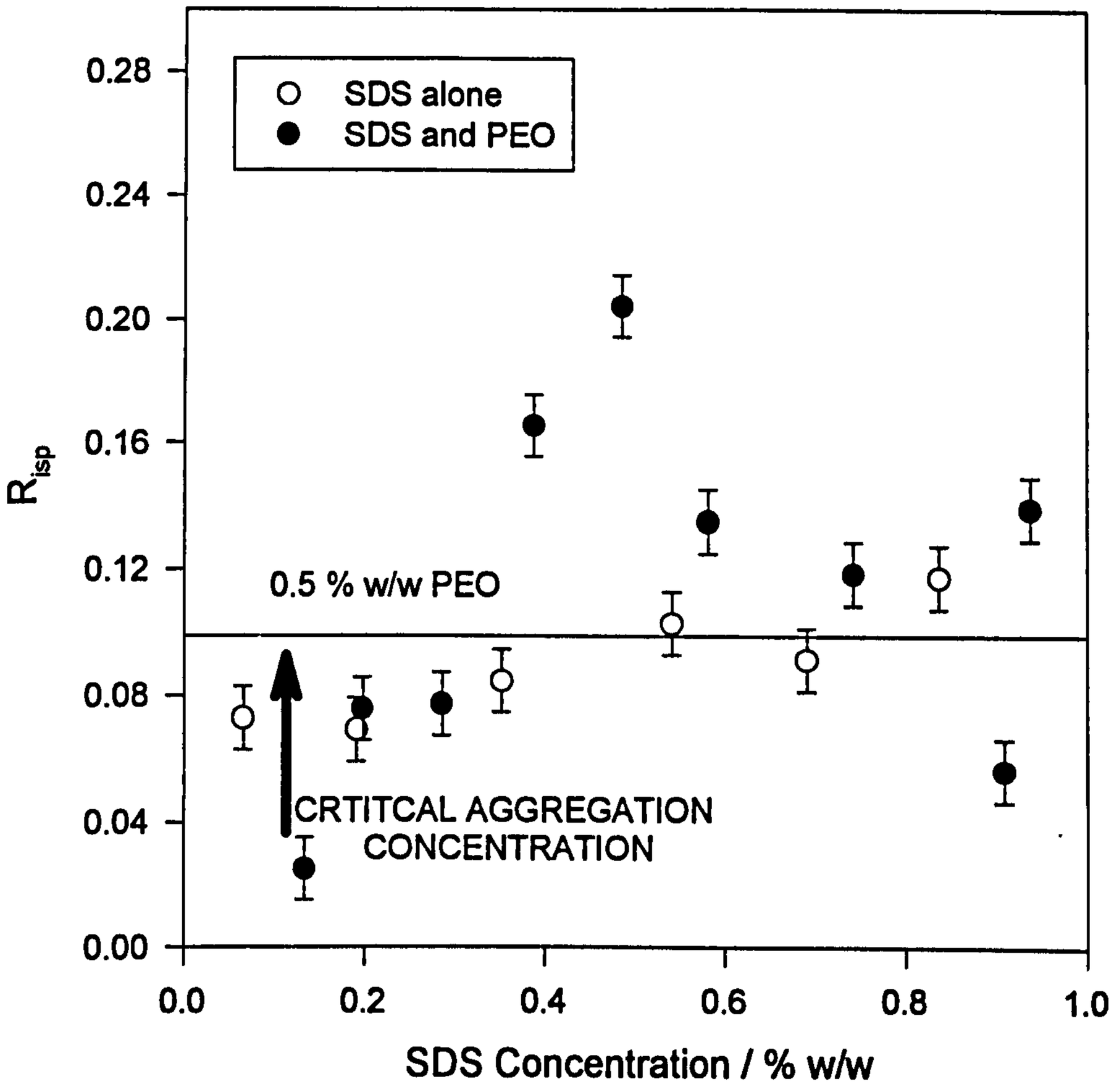

7.1.3 Mixtures of all three Components.

Figure 7.9 shows the effect of SDS on an adsorbed PEO layer. In this instance the silica concentration is maintained at 5.0 % w/w and the PEO concentration maintained at 0.5 % w/w. This corresponds to an adsorbed amount of 0.6 mg m^{-2} which is not quite at full coverage (full coverage ≈ 0.8 mgm^{-2}). However, this concentration of polymer was chosen so that the surface was saturated with trains and there would be no free polymer in the bulk. The SDS concentration was varied from 0 - 1.0 % w/w. Also shown on this plot is the data for SDS in the presence of silica and all of this data is shown normalised against silica.

Figure 7.9

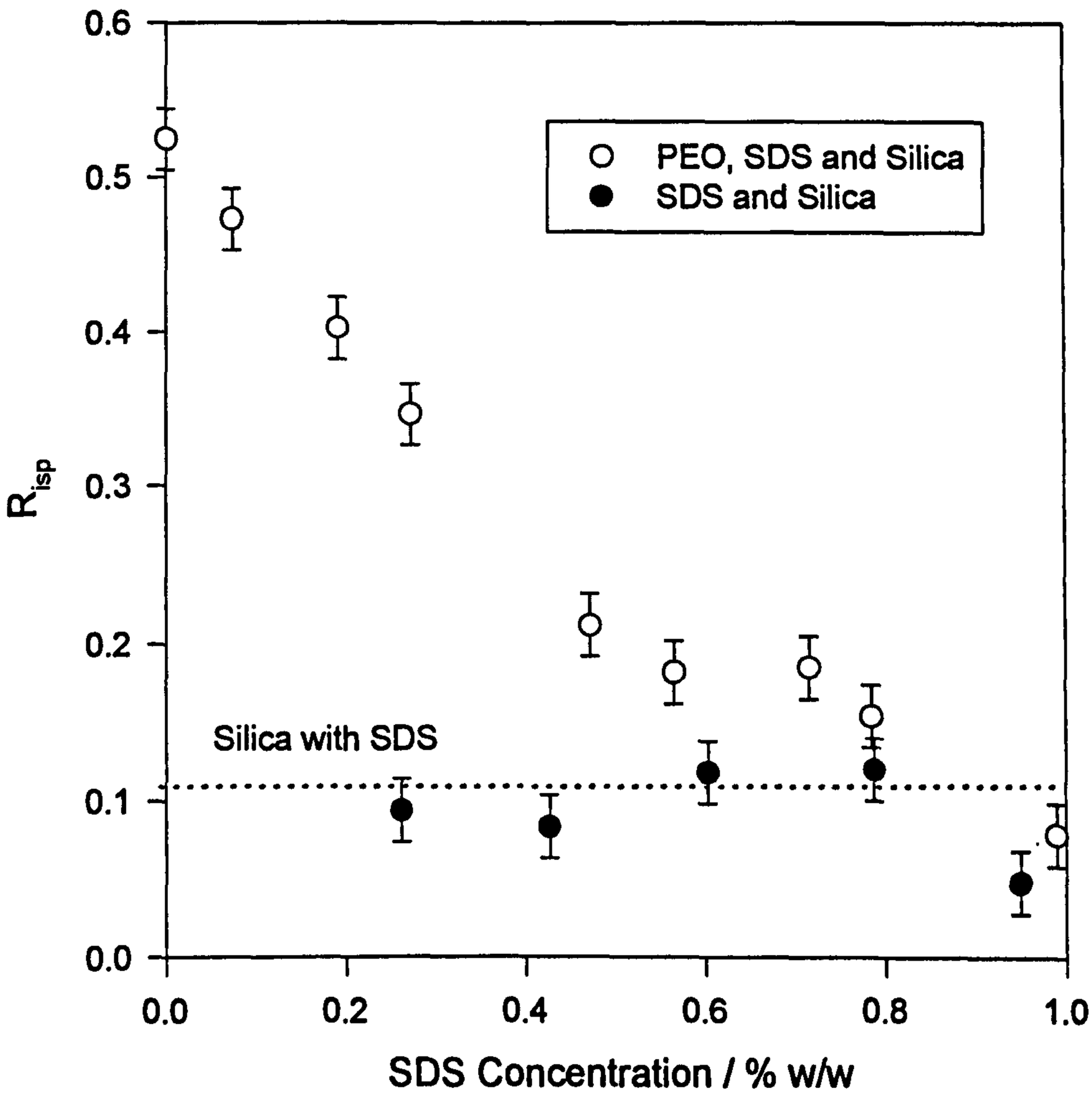

In the absence of any SDS, the specific relaxation rate normalised against silica is 0.5250. Upon addition of SDS, this value shows a sequential decrease, until at the highest SDS concentration measured (1.0 % w/w) it is at approximately the same value as in the absence of polymer. These data indicate that the structure of the bound water (or the residence time of the bound water) in the adsorbed PEO layer is significantly affected by the addition of SDS. Since the enhancement is showing a sequential decrease it is reasonable to suggest that the adsorbed layer structure is changing significantly, quite possibly desorbing with increasing SDS concentration. At surfactant concentrations above 0.4 % w/w the value of enhancement has become almost constant. This ties in well with the minimum

observed in the dynamic light scattering measurements reported in chapter 6, but does not explain the apparent increase in the hydrodynamic thickness at high surfactant concentrations. These results do however show that any remaining adsorbed layer at high surfactant concentrations is very different in structure to that in the absence of SDS and has only a negligible number of segments adsorbed as trains.

7.2 Self-Diffusion Measurements

7.2.1 Pure SDS Solutions.

In **figure 7.10** the measured self-diffusion coefficient (D_{meas}) of SDS is plotted as a function of concentration. The solvent in all instances was D_2O and these self-diffusion coefficients were calculated according to equation 7.7 using a value of the self-diffusion coefficient of water of 2.23×10^{-9} m^2s^{-1}.

$$\frac{S_{sample}}{S_{water}} = \frac{D_{meas}}{D_{water}} \qquad [7.7]$$

where S corresponds to the slope of a ln attenuation plot (**Figure 5.7**, chapter 5).

The CMC of SDS is approximately 0.23 % w/w in aqueous solution and as may be observed, below this concentration, the measured value of self-diffusion coefficient remains approximately constant at a value of 4.56×10^{-10} m^2s^{-1}; this is due to free monomers. This compares well with literature values[6]. Unfortunately, due to instrumental sensitivity it was not possible to obtain data for concentrations less than 0.1 % w/w. Beyond the CMC, the effective value of D_{meas}, begins to fall as micelles are formed. Depending on the concentration (C), the surfactant solution may consist entirely of discrete surfactant molecules (often described as monomers or unimers) [if C is below the CMC], or may consist of surfactant micelles with surfactant molecules [if C is above the CMC]. The

measured self-diffusion coefficient is therefore a weighted average of the micellar and monomeric environments.

Figure 7.10

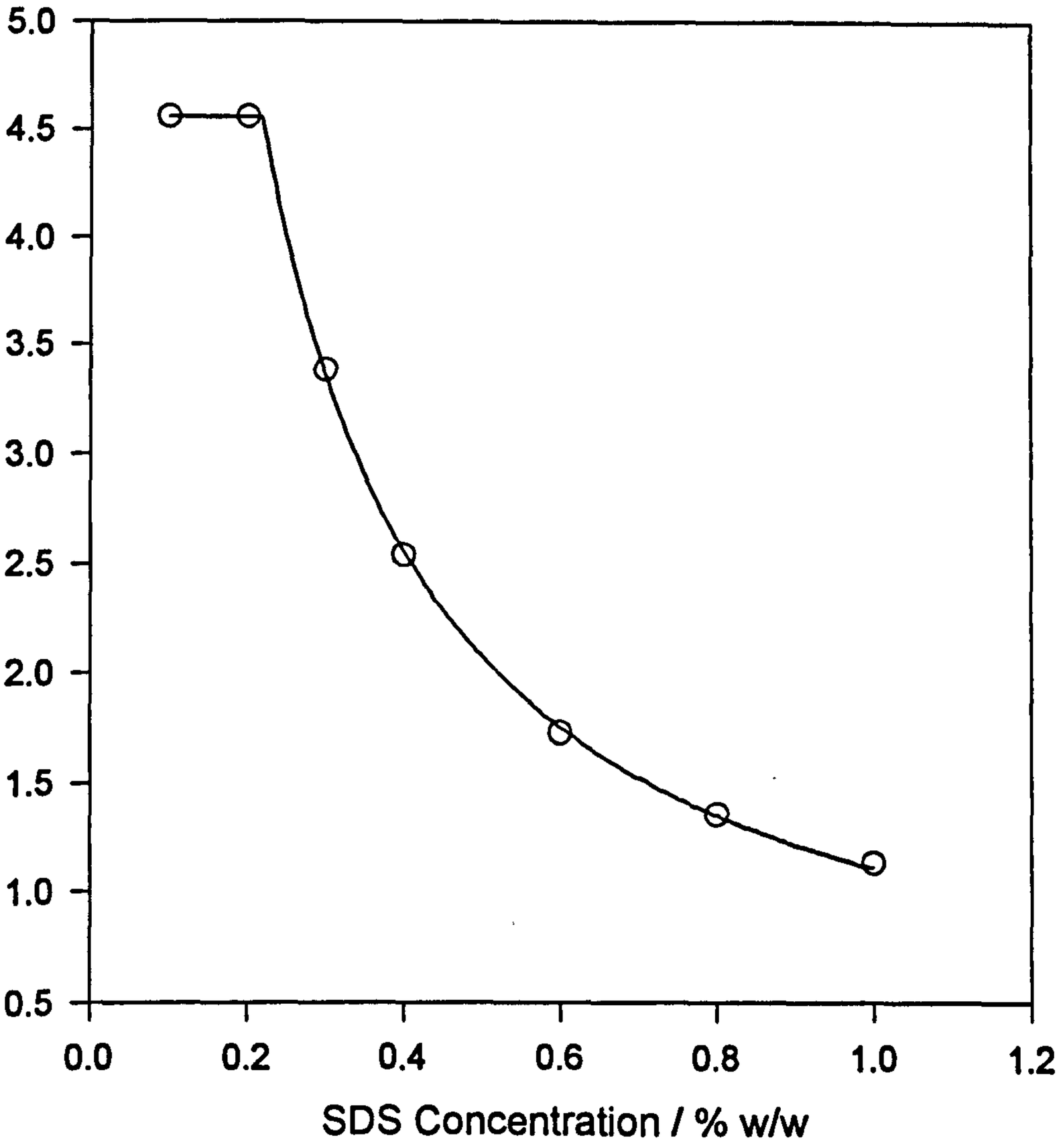

I

n this study, the self-diffusion coefficient of the micelle will be represented as $D_{micelle}$ and the self-diffusion coefficient of the molecular SDS as D_{free}. Below the CMC where there are no micelles present D_{meas} will equal D_{free}. On the other hand, above the CMC, D_{meas} will decrease since the surfactant monomers spend a fraction of the experimental time in the more slowly diffusing micellar environment. Thus, below the CMC, D_{meas} is constant whilst above the CMC, D_{meas} decreases with increasing concentration. D_{meas} may be represented by the two state model given in equation 7.8

$$D_{meas} = \left[\frac{C_{CMC}}{C} D_{free}\right] + \left[\frac{(C - C_{CMC})}{C} D_{micelles}\right] \quad [7.8]$$

where C_{CMC} is the normal critical micelle concentration of SDS and C is the total concentration of SDS. Taking a value of D_{free} of 4.56×10^{-10} m^2s^{-1} and C_{CMC} of 0.23 % w/w, $D_{micelle}$ was calculated for each data point and the equivalent hydrodynamic diameters of the micelle obtained from the Stokes-Einstein equation (equation 7.9)

$$D_{micelle} = \frac{kT}{6\pi\eta a} \quad [7.9]$$

where k is the Boltzmann's constant, T is the absolute temperature, η is the solution viscosity and a is the micellar radius. An important point to note is that, within the concentration range under investigation (0 - 1.0 % w/w SDS) the viscosity does not change significantly from that of water[7] It should also be noted that the calculated radii are hydrodynamic, (the same as those calculated using PCS) whilst those calculated from SANS data (chapter 8) are based on a summation over all atoms dependent upon the size and shape of the aggregates. Values of the radii of SDS in the literature very quite substantially depending upon the technique used; *for example* SANS measurements quote 24 ± 1 Å[8] and light scattering 16 ± 1 Å[9].

The values of $D_{micelle}$ obtained varied quite considerably across the concentration range under investigation and as a result at high SDS concentrations, the calculated radii from equation 7.9 were much too large (*for example* using this approach 1.0 % w/w SDS yielded a hydrodynamic radius of 158 Å). However, the calculated radii at lower SDS concentrations were more reasonable (*for example* 0.3 % w/w SDS yielded a hydrodynamic radius of 21 Å). The data obtained in **figure 7.10** is in excellent agreement with the literature[6] and it is

therefore likely that at high SDS concentrations, obstruction effects are significant and equation 7.8 may not be a true representation.

Although, the two state model in equation 7.8 is the most common for investigating surfactant self-diffusion, it makes no allowance made for interparticle interference effects. In some cases these may be significant so technically the two-state model is only applicable at concentrations not too far above the CMC where the number of micelles are few and do not interact with one another. *For example*, Hammorström *et al* [6] investigated the interaction of non-ionic water-soluble polysaccharides with surfactants by chemical shift and NMR self-diffusion measurements. It was taken that when $D_{micelle} << D_{free}$ (*i.e.* just above the CMC) equation 7.8 would become

$$C_{bound} = \frac{C(D_{free} - D_{meas})}{D_{free}} \qquad [7.10]$$

where C_{bound} is the concentration of SDS bound as micelles (or $C\text{-}C_{CMC}$). D_{free} was obtained by extrapolating D_{meas} to zero concentration. This approach has also been used successfully by several other authors to determine micellar self-diffusion coefficients[10-13].

For SDS, there are two phenomena which may lead to the measured value of the self-diffusion coefficient (D_{meas}) being different to D_{act}, the actual self-diffusion coefficient;

- **Obstruction effects** - *for example*, due to monomers, micelles or the solvent
- **Electrostatic effects** - *for example*, due to the ionic strength or the Debye Screening Length of the micelle.

The Maxwell-Fricke mixture relation[14] has been applied to dilute suspensions of impermeable spheres in a continuous medium and is the most commonly

applied model to account for obstruction effects due to surfactant monomers, or the solvent, in these type of systems. The self-diffusion coefficient of the solvent in the solution (of polymer or surfactant) D relative to the solvent pure D_o is given by

$$\left(1-p_{comp}\right)\frac{D}{D_o}=\left(1-p\right)\left(1+\frac{p}{2}\right) \qquad [7.11]$$

where p_{comp} is the volume fraction of the polymer (or surfactant) and p is the volume fraction of polymer and tightly bound solvent. If the solvent binding effects are taken to be negligible then p_{comp}= p and the equation simplifies to

$$D=D_o\left(1+\frac{p}{2}\right) \qquad [7.12]$$

However, this model has not proved to be a good approximation for polymer solutions such as polystyrene and poly(ethylene oxide) and makes no allowance for the effects of larger molecules (such as micelles) on the solvent.

Griffiths and Cosgrove[15] used solvent self-diffusion to characterise adsorbed polymer layers and found that a more satisfactory model to account for obstruction effects could be given by Mackie and Meares[16]. They used a lattice model to calculate the obstruction effects in a cation exchange resin. A cubic lattice was used and in the model the volume fraction (ϕ) was substituted for the number of occupied lattice sites such that

$$\frac{D_{meas}}{D_o}=\frac{\left(1-\phi\right)^2}{\left(1+\phi\right)^2} \qquad [7.13]$$

These two models have been applied to the data in **Figure 7.10**, but neither model could account adequately for the observed reduction in self-diffusion coefficient.

Therefore, in order to obtain qualitative information from the self-diffuison coefficients, the data must be extrapolated to low SDS concentrations.

7.2.2 SDS and PEO in solution.

7.2.2.1 Self-diffusion of SDS

Shown in **figure 7.11** are the self-diffusion coefficients for SDS in the presence of 0.5 % w/w PEO of molecular weight 114,000. Also shown for comparison is the data for SDS alone (from **figure 7.10**). All of the solutions were prepared and allowed to equilibrate for 24 hours prior to measurement.

Figure 7.11

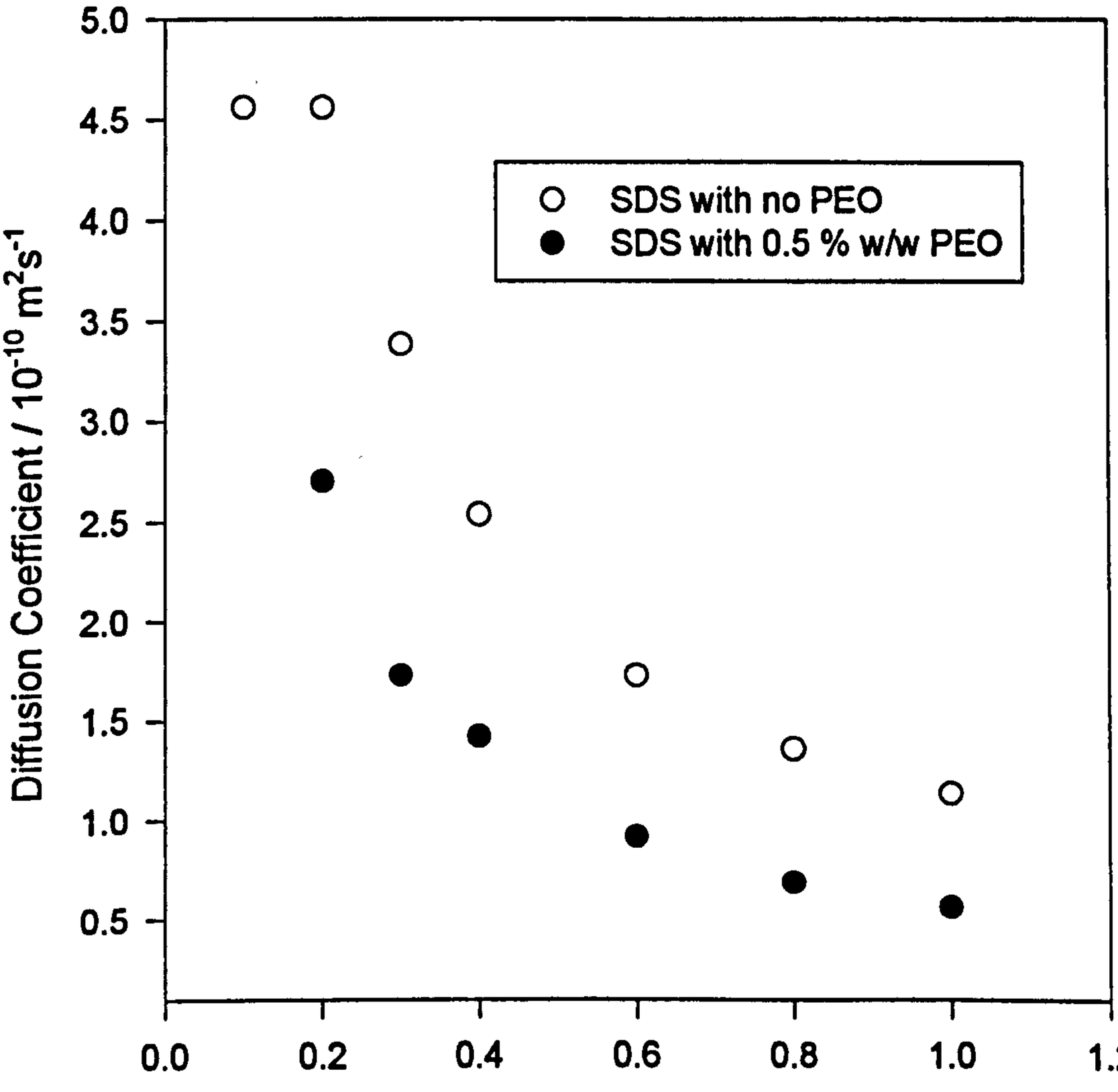

The general trend shows that the addition of polymer to SDS results in an overall reduction in the value of D_{meas} for SDS compared to that in the absence of

polymer. As before, with increasing SDS concentration the measured SDS self-diffusion coefficient decreases. This trend is in good agreement with other experimental data on similar systems[10,12]. However, unlike the data in the absence of PEO, there is no distinct break in the curve at the CMC.

Under conditions where polymer is present, the SDS may exist in three possible forms.

- As discrete monomer units within the bulk solution.
- Bound to the PEO as aggregates.
- As micelles within the bulk solution

Literature on the PEO/SDS interaction[17] reports that the concentration at which PEO and SDS begin to interact to form polymer bound aggregates (C_1) is approximately 0.09 % w/w at this polymer concentration. Furthermore, over the range of SDS concentrations considered there are no free micelles in solution. Below C_1 all SDS molecules exist as discrete monomer units. Between C_1 and saturation of the polymer (the concentration range under investigation in this study) the surfactant will exist as discrete monomers or as polymer-bound aggregates. At concentrations where the polymer is saturated with surfactant, SDS may exist in all three states. On the time-scale of a self-diffusion experiment all of these states will be in fast exchange with one another

Measurements performed on the PEO/SDS complex[7] have shown that the viscosity exhibits a peak at a certain SDS concentration followed by a decrease before finally exhibiting a steep rise. The latter steep rise is observed even in the absence of polymer and is attributed to a change in the shape of the SDS micelles. The peak in the viscosity curve has been attributed to the point at which all of the polymer molecules are saturated with SDS and hence the coil attains its largest size due to intermicellar repulsion. **Figure 7.12** shows viscosity data for 0.5 % w/w PEO of molecular weight 160,000 as a function of molecular weight (extracted from reference Chari *et al* [7]). Evidently, only at the very highest

surfactant concentrations used in this thesis does the viscosity change significantly with SDS concentration, although the presence of the polymer affects the viscosity of all of the samples.

Figure 7.12

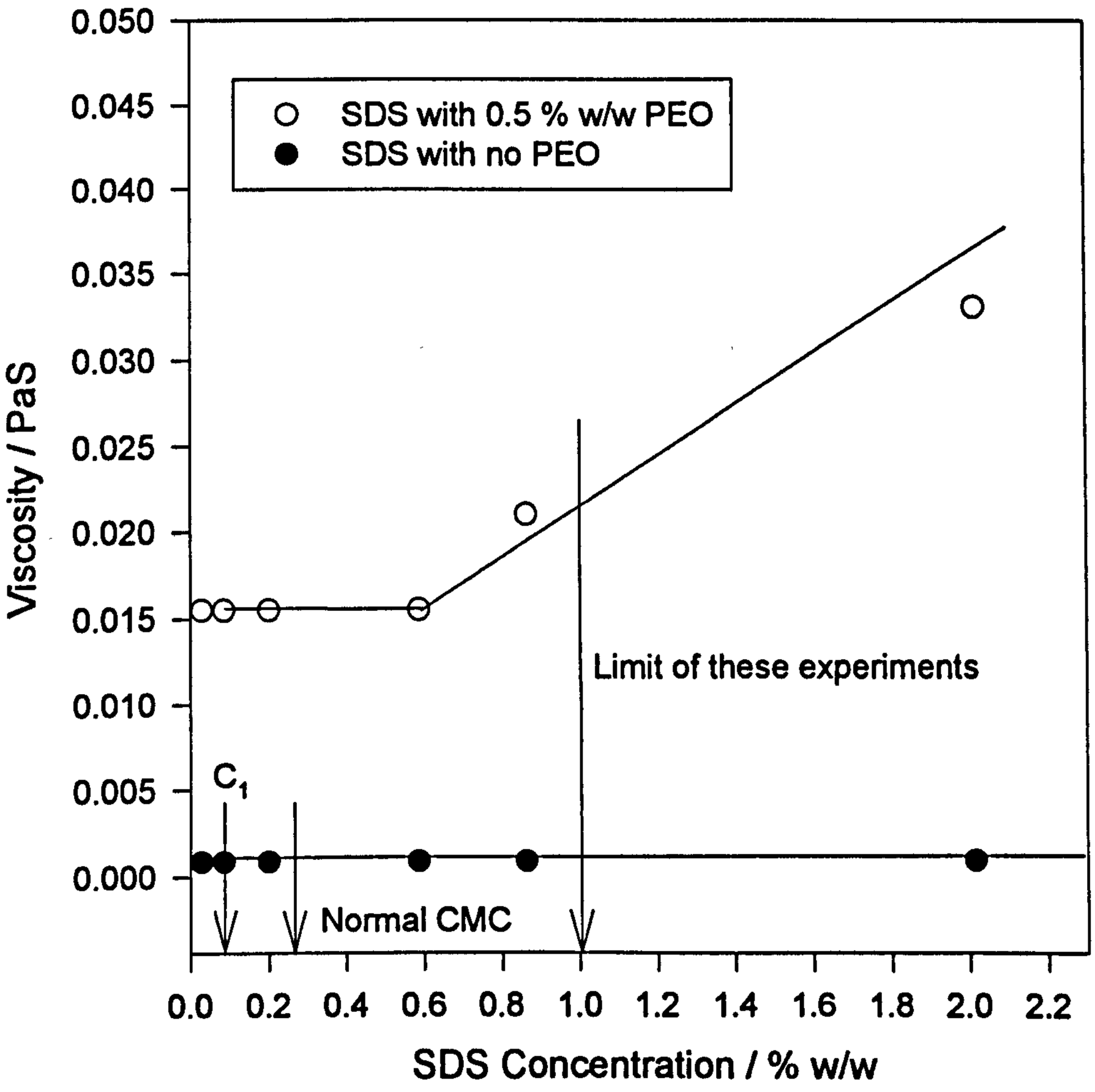

$D_{micelle}$ for each data point was calculated according to equation 7.8. The value of D_{free} was taken from the value in the absence of polymer, scaled for the change in viscosity according to equation 7.14

$$\frac{D_{(Nopolymer)}}{D_{(withpolymer)}} = \frac{\eta_{(withpolymer)}}{\eta_{(Nopolymer)}} \qquad [7.14]$$

This yielded a value of D_{free} in the presence of polymer of 2.68 x 10^{-10} m^2s^{-1}, which was inserted into equation 7.8 in order to estimate viscosity corrected values of $D_{micelle}$ which could be compared with those in the absence of polymer. Using these values and a value of C_1 of 0.09 % w/w SDS, the value of the self-diffusion coefficient of SDS at 0.1 % w/w was calculated. This is shown on **figure 7.11**.

As in the case in the absence of polymer the calculated values of $D_{micelle}$ varied with concentration (**Table 7.1**), suggesting that obviously obstruction effects are important here too.

Table 7.1; **Calculated Values for D_{bound} as a function of SDS Concentration in the Presence of 0.5 % w/w PEO.**

C / % w/w	D_{meas} / 10^{10} m^2s^{-1}	D_{free} / 10^{10} m^2s^{-1}	D_{bound} / 10^{10} m^2s^{-1}
1	0.568	2.68	0.359121
0.8	0.69	2.68	0.437746
0.6	0.92	2.68	0.609412
0.4	1.42	2.68	1.054194
0.3	1.73	2.68	1.322857
0.2	2.71	2.68	2.73454

7.2.2.2 Self-diffusion of PEO

The measured values of self-diffusion coefficient from the polymer in the mixture are given in **Figure 7.13**. These are approximately an order of magnitude smaller than those obtained from the SDS peak. A typical spectrum showing the SDS and PEO peaks is given in Chapter 5, **figure 5.6**.

Figure 7.13

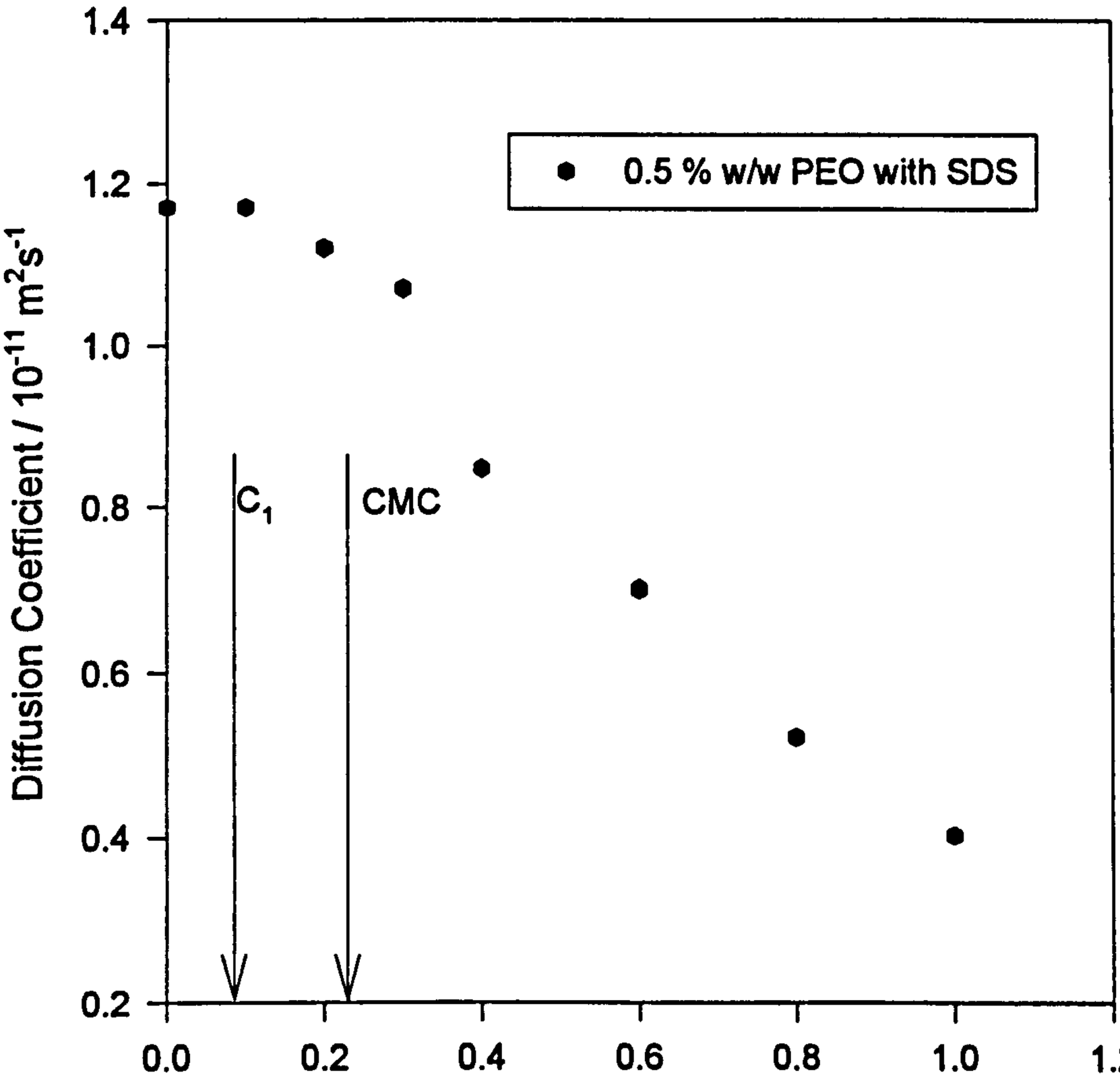

From this figure, it is evident that below the concentration where PEO and SDS begin to interact (the first two data points on **figure 7.13**), the measured value of self-diffusion coefficient for the polymer remains constant. Inserting these values into the Stokes-Einstein, below C_1 the value of D_{meas} corresponds to a hydrodynamic radius of 164 Å which compares well with values obtained for the radius of gyration by SANS measurements (Chapter 8) of 165 Å and calculated values of 185 Å. On addition of SDS above C_1, the measured self-diffusion coefficient decreases with SDS concentration and consequently hydrodynamic radius increases. At the maximum SDS concentration used in this study the hydrodynamic radius has reached 327 Å - indicative of strong binding. Assuming that the aggregates are spherical, this increase in corresponds to a change in

volume for each PEO chain from 1.84×10^{-23} m^3 to 1.46×10^{-22} m^3 - an 8 fold increase.

Brown *et al*[18] investigated the PEO/SDS complex using static and dynamic light scattering techniques. From the dynamic light scattering measurements they were able to determine the mutual diffusion coefficients of these species. Measurements of the diffusion coefficient of the complex were made at several PEO/SDS ratios as a function of PEO concentration. At low PEO/SDS ratios (below PEO:SDS 1:5) a linear relationship with concentration was observed. On the other hand at high PEO/SDS ratios a non-linear increase in diffusion coefficient with polymer concentration was noted. However since these measurements were performed in the presence of 0.1 M NaCl a direct comparison cannot be drawn with the system in this study. The hydrodynamic radii for the complex at each SDS/PEO value were obtained at the limit where the PEO concentration was zero using the Stokes-Einstein equation. There was a peak in that data corresponding to the position at which binding reached saturation. This data suggested a maximum at a concentration ratio of SDS to PEO of approximately 5; (*i.e.* 0.5 % w/w SDS to 0.1 % w/w PEO). This is higher than the value obtained from the phase diagram of Cabane *et al*[19] although those measurements, like the measurements in this study were performed in the absence of salt. The maximum in the plot of hydrodynamic radius as a function of ratio of SDS concentration to PEO concentration corresponded to a hydrodynamic size of around 600 Å. This is larger than the value obtained in this study, but the molecular weight of the polymer used in that study nine times the molecular weight of the polymer used in this here, (although it is known that polymer molecular weight has little or no influence on the aggregation number of SDS bound to it).

A recent paper has also measured the diffusion and scaling behaviour of the PEO/SDS aggregate[20] by pulse gradient spin echo NMR. Those results also showed that individual coils underwent significant complexation with surfactant

reflected by a decrease in the self-diffusion coefficient. In that study the PEO was of molecular weight 85,000 and at 0.05 % w/v. The values of self-diffusion coefficient were inserted into the Stokes-Einstein equation and the hydrodynamic radius extracted. In the absence of polymer, the hydrodynamic radius was 129 Å whilst at saturation was 222 Å which compare well with the data obtained in this study for the PEO of molecular weight 114,000.

7.2.3 Mixtures of all three components.

7.2.3.1Self-diffusion of SDS

Shown in **figure 7.14** is the effect of silica and PEO on the self-diffusion coefficient of SDS. The silica is at 4.0 % w/w and this corresponds to sufficient surface area for the PEO to provide full coverage, but without significant bulk polymer. The trend is similar to that seen with PEO/SDS but with a further lowering in the surfactant self-diffusion coefficient. However, the overall reduction is not as marked as between SDS alone and SDS with PEO. Again there is no distinct break in the curve. At low concentrations of SDS, the value of the self-diffusion coefficient is much lower than for SDS in the presence of just PEO. *For example*, at the lowest surfactant concentration the self-diffusion coefficient is almost half that in the absence of polymer or surface. There is no distinct break in the value of self-diffusion coefficient. At the higher surfactant concentrations (above 0.5 % w/w) the self-diffusion coefficient is very similar to that of SDS in the absence of the silica surface. Under such conditions the surfactant may exist in several different forms.

- As discrete monomer units within the bulk solution.
- As micelles within the bulk solution
- Bound to bulk PEO as aggregates.
- Bound to PEO at the silica interface - as aggregates
- Bound to bare silica.

Figure 7.14

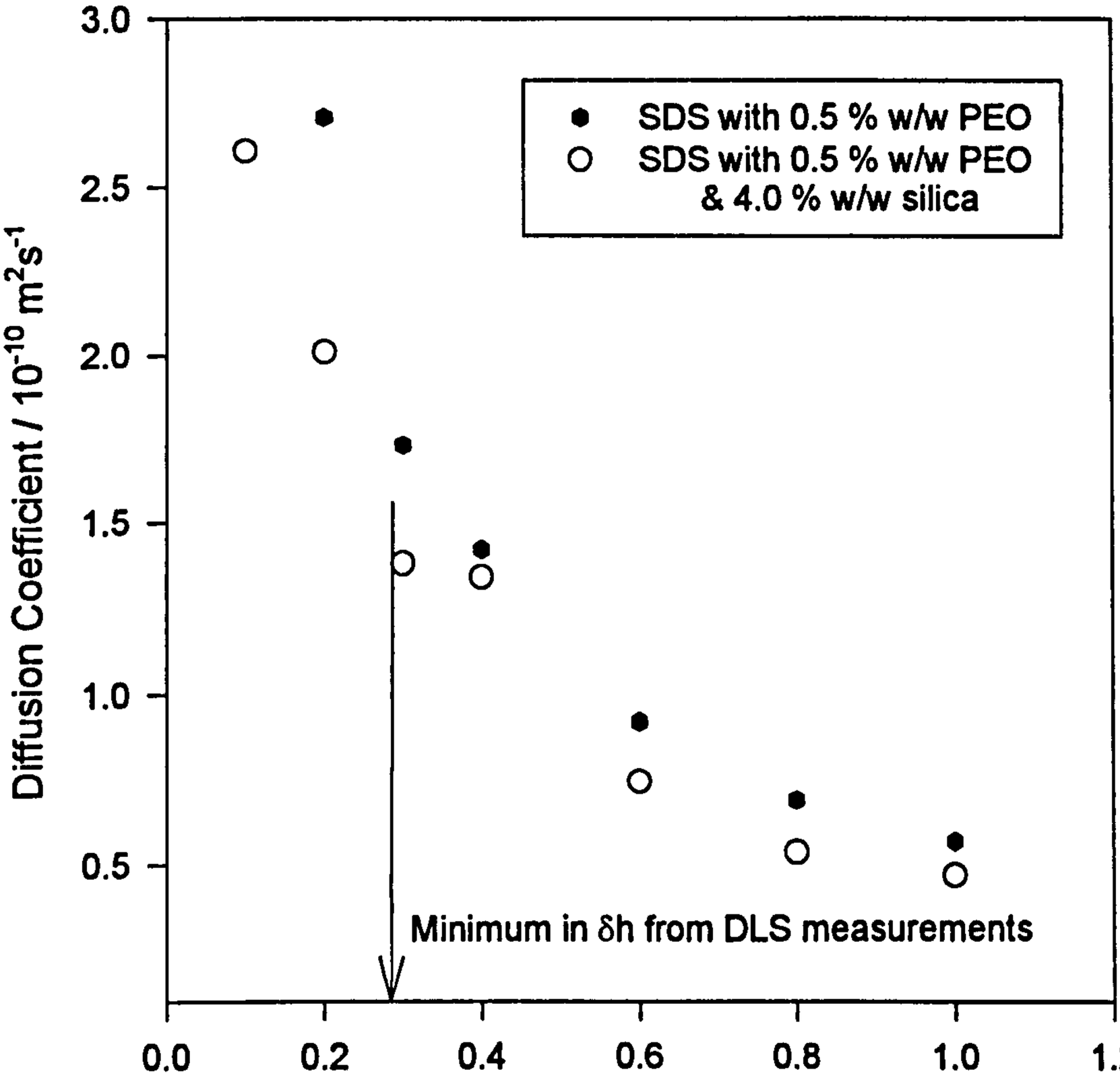

Hence, the origin of the average self-diffusion coefficient becomes very complicated indeed. However, if we assume that the phase diagrams are not dissimilar for PEO and SDS in the presence and the absence of the silica substrate then at all of the SDS concentrations in this study there are no free SDS micelles in the bulk; *i.e.* all of the SDS micelles are bound to polymer either in the bulk or at the interface. Molecular SDS at a concentration C_1 will be present If it is taken that the initial concentration of free PEO is low, then this may also be neglected. With these two assumptions, the description of the self-diffusion coefficient may be simplified somewhat. If it is taken that the SDS may exist either as a monomeric entity or 'bound' in some manner, then, equation 7.8 may be represented as

$$D_{meas} = \frac{C_{free}}{C} D_{free} + \frac{C_{bound}}{C} D_{bound} \qquad [7.15]$$

where the subscript 'bound' corresponds to SDS in some environment, where the limits are between the self-diffusion coefficient of the polymer alone in solution and the silica particle.

If is taken that the PEO desorbs around the normal CMC of SDS (as indicated by the DLS and solvent relaxation measurements) then it could be expected that the value of self-diffusion coefficient in the presence of silica and in the absence of silica would be similar. This is indeed the case and as can be observed in **figure 7.14** the measured self diffusion coefficient of SDS remains constant between 0.3 % w/w SDS and 0.4 % w/w SDS; the value at 0.4 % w/w being almost identical to that in the absence of silica particles. Beyond this SDS concentration since the self-diffusion coefficient is very similar in the presence and the absence of silica particles, this suggests that at these concentrations the SDS is in the same (or a very similar) environment as in the absence of silica. However, it must not be forgotten that is the PEO is desorbing or re-adsorbing that the viscosity will be changing constantly across the whole SDS concentration range, which will also make any effects difficult to model.

Fitting the data to equation 7.15 yielded a value of D_{free} 2.61 x 10^{-10} m^2 s^{-1} and C_{free} of 0.15 % w/w. The value of D_{free} is quite similar to the 'calculated' value obtained from equation 7.14 of 2.68 x 10^{-10} m^2 s^{-1} and the value of C_{Cree} is not unreasonable. Using the value of D_{bound} obtained from this fit, one obtains a hydrodynamic radius of 143 Å, but is must be remembered that this fit neglects any obstruction effects and assumes that D_{bound} is across the whole concentration range under investigation

7.2.3.2 Self-diffusion of PEO.

Figure 7.7

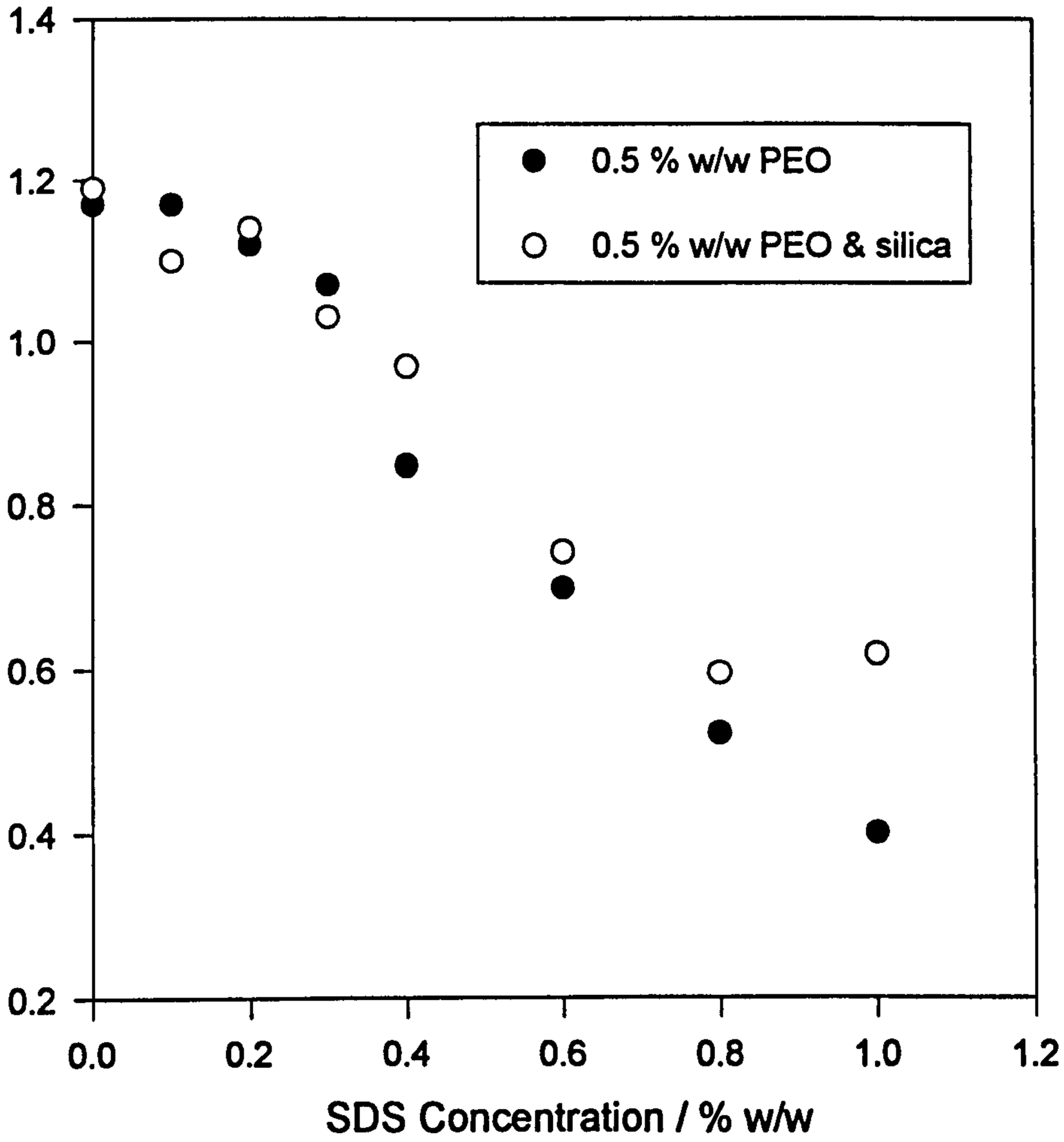

The effect of SDS on the self-diffusion coefficient of PEO in the presence of the silica surface is shown in **figure 7.15** Also shown on this figure are the data in the absence of particles. As in the previous case, the PEO concentration remains fixed at 0.5 % w/w. In the absence of SDS or particles, the PEO had a self-diffusion coefficient of 1.17×10^{-11} m^2s^{-1} (The radius of gyration of the polymer is 11.5 nm which is corresponds to an end-to-end distance of 14nm. Therefore, for this molecular weight the calculated self-diffusion coefficient at infinite dilution would be 1.27×10^{-11} m^2s^{-1}) Surprisingly, in the presence of silica, the measured self-diffusion coefficient did not appear to change, although DLS

measurements on these samples (similar to those reported in chapter 6) confirmed that adsorption had taken place. The calculated value of self-diffusion coefficient of the particle (ignoring any obstruction effects) is 1.96 x 10^{-11} m^2s^{-1}. The diffusion coefficient of the PEO and adsorbed silica was obtained from the DLS measurements on the same sample used for the self-diffusion measurements, **Figure 7.16**. This was obtained as 1.15 x 10^{-11} m^2s^{-1}, which is almost identical to that in the absence of particles. Therefore D_s bulk polymer ≈ D_s particle with adsorbed layer.

Under these conditions, the PEO may exist in three different forms.

- Bound to the SDS in solution.
- Bound to the silica
- Bound to the silica and SDS..

At zero and low concentrations of surfactant, the self-diffusion coefficient of the polymer is almost identical with and without particles. Since we know that D_s free polymer and D_s adsorbed polymer at full coverage are the same this indicates one of two scenarios,

- The polymer is all in the bulk *i.e.* there is no effect from the particle and the self-diffusion coefficient will follow that in the absence of silica.

- All of the polymer is adsorbed *i.e.* there is no effect from polymer in the bulk. This assumes that any SDS will bind to adsorbed PEO in the same manner as to free PEO. This is the case at zero SDS concentration where we know that there is only nominal free polymer.

However, at surfactant concentrations above 0.3 % w/w (around the normal CMC of SDS), the self-diffusion coefficient of the polymer in the presence of particles

no longer follows that in the absence of particles. Since, the self-diffusion coefficient increases this suggests that perhaps at least one of the entities is changing in size *i.e.* an increase in D_s is inversely proportional to a decrease in radius provided all other parameters remain constant (equation 7.9). Since we have the data in the absence of particles and know that the diffusion coefficient of the bare particle is 1.96×10^{-11} m^2s^{-1}, this increase in measured self diffusion coefficient may suggest that the 'polymer + particle' entity is getting smaller (than in the absence of surfactant). It is probable that this is as a result of desorption (which ties in with the results in Chapter 6 and the earlier part of this chapter) and the net result is that the weighted measured self-diffusion coefficient is larger in the presence of particles. However, it must be remembered that if desorption is taking place that the viscosity will increase which has the net effect of decreasing the measured self-diffusion coefficient. Therefore if it were possible to consider viscosity effects we may find that these effects are exaggerated further.

References.

1. Meiboom S, Gill D.; *Rev. Sci. Instrum.* **1958** 29 688
2. Cosgrove T., Griffiths P.C., Lloyd P.M.; *Langmuir* **1995** 11(5) 1457
3. Green N. D.; *B.Sc. Thesis, University of Bristol* **1994**
4. van der Beek G. P., Stuart M. A. C., Cosgrove T.; *Langmuir* **1991** 7(2) 327
5. Lloyd P. M.; *B.Sc. Thesis, University of Bristol* **1992**
6. Hammarström A., Sundelof L.-O.; *Colloid Polym. Sci.* **1993** 271 1129
7. Chari K., Antalek B., Lin M. Y., Sinha S. K.; *J. Chem. Phys.* **1994** 100(7) 5294
8. Hayter J. B, Penfold J; *Molecular Physics* **1981** 42(1) 109
9. van Stam J., Brown W., Fundin J., Almgren M., Lindblad C.; *ACS Symposium Series* **1993** 532 195
10. Söderlind E., Stilbs P., *Langmuir* **1993** 9 2024
11. Lindman B., Puyal M-C., Kamenka N., Rymden R., Stilbs P.; *J. Phys Chem* **1985** 88 5048D
12. Abrahamsén-Alami S., Stilbs P., *J. Phys. Chem* **1994** 98 6359
13. Faucompre B., Lindman B., *J. Phys. Chem* **1987** 91 383
14. Fricke H. *Phys Rev* **23** 575 1924
15. Cosgrove T., Griffiths P. C.; *Colloids and Surfaces A* **1994** 84 249
16. Mackie J. S., Meares P.; *Proc. R. Soc, London, Scr, A* **1955** 232 498
17. Cabane B.; *J. Phys Chem.* **1977** 81 163
18. Brown W., Fundlin J., Miguel M. da. D.; *Macromolecules* **1992** 25 7192
19. Cabane B., Duplessix R.; *Colloids & Surfaces* **1985** 13 19
20. Chari K., Antalek B., Minter J; *Phys. Rev. Lett* **1995** 74(18) 3624

Chapter 8.

SANS Results on PEO & SDS

8.1 Introduction.

In the first part of the SANS experiment the scattering from PEO and SDS in aqueous solution was investigated. The solvent was D_2O and through the use of deuterated SDS, the surfactant could be rendered effectively invisible to the neutrons. Next, the scattering arising from the adsorbed PEO layer for a series of PSL dispersions was examined as a function of SDS concentration. For some samples, hydrogenous SDS was used and in this case the SDS was visible, whilst for the remainder of the samples a mixture of hydrogenous and deuterated SDS was used to give the same scattering length density as the solvent and the particle. The polymer concentration was maintained at the concentration required to give full coverage if the particle and the respective equilibrium concentration in the absence of SDS. Similar experiments were performed with silica as the substrate.

The absolute values of the scattering intensities were determined by dividing the scattered intensity and transmission of the sample by the scattering intensity and transmission of water, thus removing the instrument variables[1]. All of the scattering data were fitted using a non-linear least squares analysis program.

"Phase Diagrams" of the aqueous PEO/SDS complex[2] show three distinct regions with increasing SDS concentration (**figure 1.1**). At the lowest SDS concentrations, free SDS monomers and PEO chains coexist discretely in solution. With increasing SDS concentration mixed PEO and SDS aggregates are formed which are not saturated with SDS. At very high SDS concentrations PEO/SDS aggregates are in equilibrium with regular SDS micelles. In all of the

experiments in the absence of particles reported in this chapter, the PEO concentration was maintained at 0.5 % w/w. The PEO concentration for the experiment involving silica particles was also 0.5 % w/w, whilst that involving PSL was 0.3 % w/w. The SDS concentrations ranged from 0 - 1.0 % w/w.

8.2 Pure Components

Initially, the components were investigated individually as backgrounds.

8.2.1 Silica Dispersions.

As shown in Chapter 4, the coherent scattering from discrete monodispersed particles obeys the form,

$$I(Q) = (\rho_p - \rho_s)^2 N_p V_p^2 P(Q) + B_{inc} \qquad [8.1]$$

where B_{inc} is the incoherent background level.

Thus, a minimum is observed in the scattering intensity when the scattering length densities of the particles and the solvent are matched, *i.e.* $(\rho_p-\rho_s)=0$. The scattering length density of the solvent and hence $\rho_p-\rho_s$ can be varied by changing the composition of the solvent mixture by altering the H_2O/D_2O ratio.

The effect of this is shown in **figure 8.1** which shows the scattering pattern arising from a series of silica dispersions all at 5.0 % w/w as a function of H_2O/D_2O ratio. This was varied from 80 % w/w D_2O down to 30 % w/w D_2O.

Figure 8.1

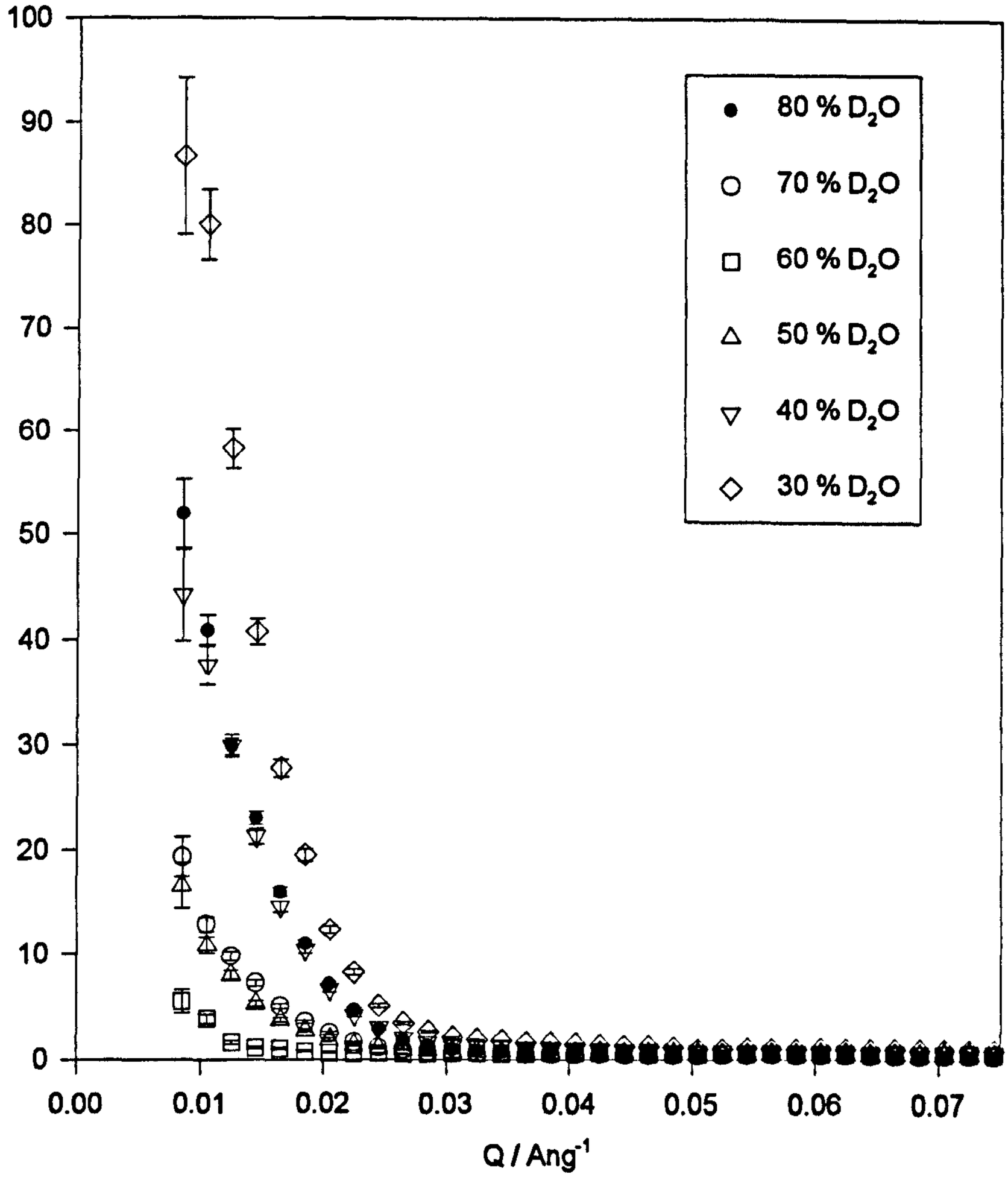

In order to subtract the incoherent background and therefore proceed with data analysis a plot of $Q^6I(Q)$ versus Q^6 is drawn.

The slope of this plot will give the incoherent background level. An example of this is given in **figure 8.2** which shows the scattering from a silica dispersion in a 70 % H_2O / 30 % D_2O solvent mixture. The slope of this plot (and therefore the incoherent background level) was determined as 0.80 cm^{-1}.

Figure 8.2

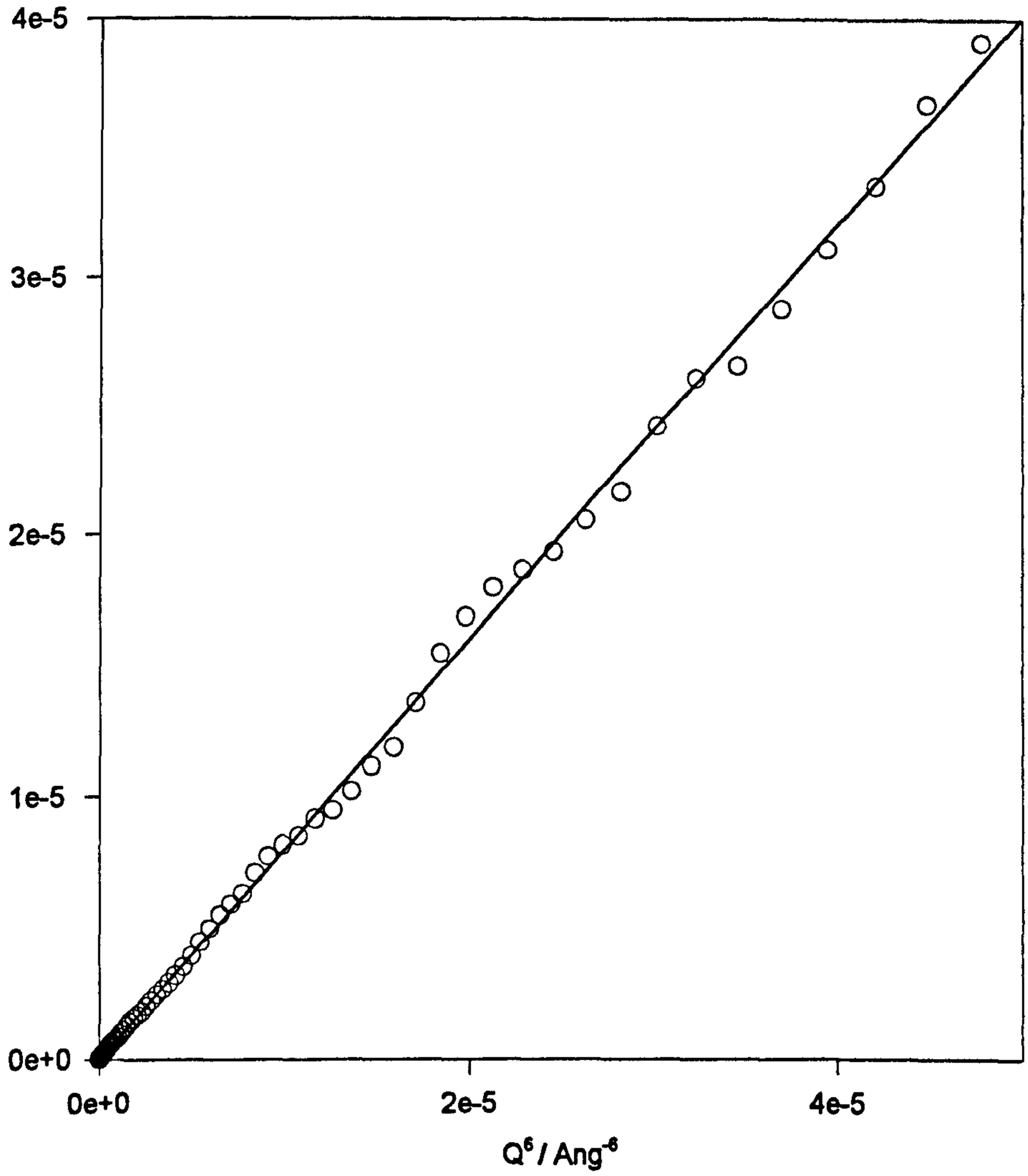

In order to determine exactly which H_2O/D_2O ratio corresponds to a minimum in the scattering, the initial intensities were plotted as $I(Q)^{½}$ as a function of H_2O/D_2O ratio [$I(Q) \propto (\rho_p - \rho_s)^2$]. Shown in this figure are the intensities obtained from the first measured data point for each data set. The result is a straight line which passes through zero - the intercept on the Q axis corresponding to what is termed "contrast match" for the particle, which is shown in **figure 8.3** and occurs at a H_2O/D_2O ratio of 58 % w/w D_2O.

Figure 8.3

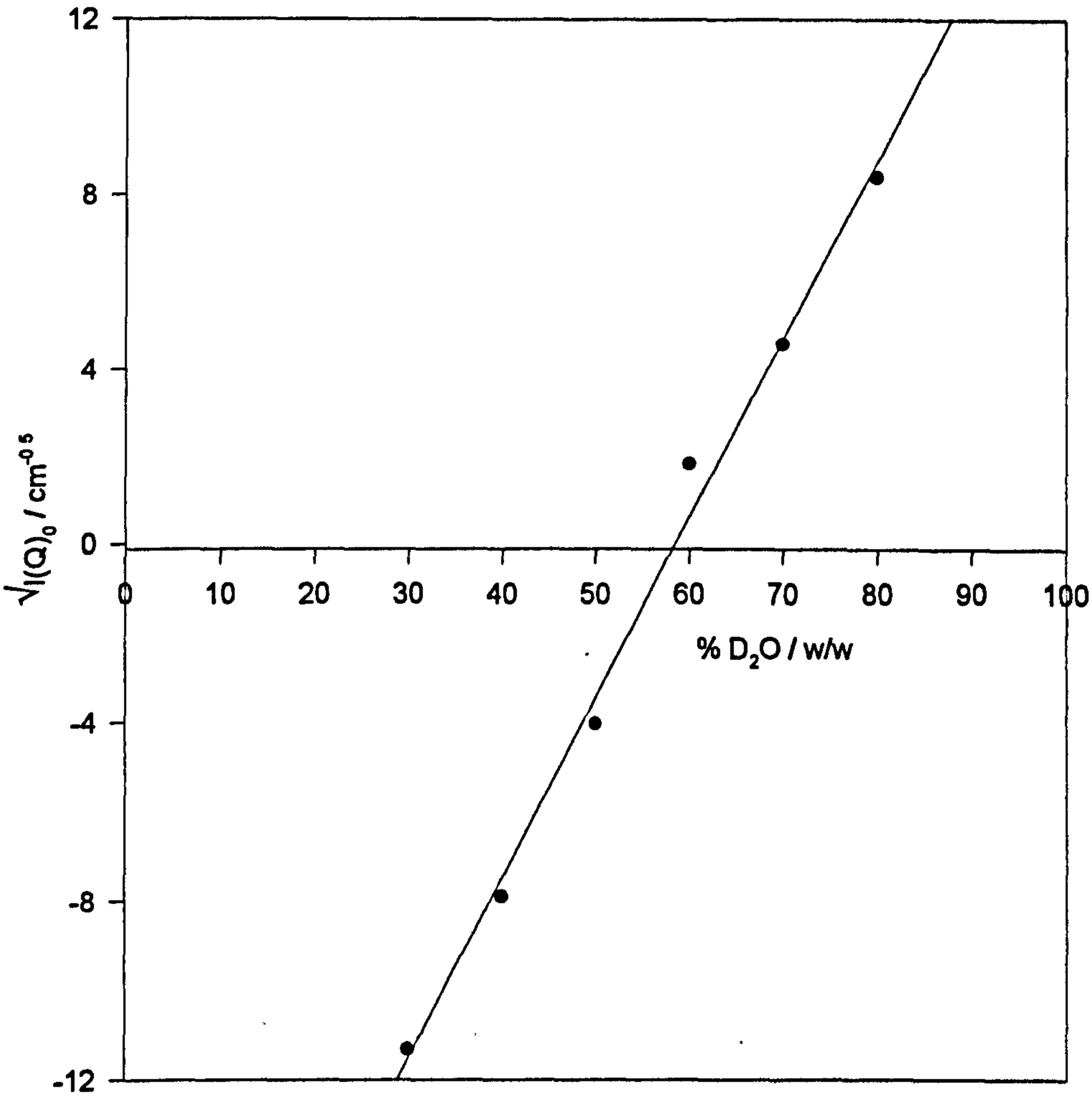

The scattering from a silica dispersion at a H_2O/D_2O ratio of 30/70 is shown in **figure 8.4.** These data are plotted on a log-log scale to accentuate differences in the slope of the scattering and have had the incoherent background subtracted. Since, the limit for the Guinier plot is $QR_g < 1$ this model cannot be used for these particular particles. Therefore, these data were fitted using the complete form factor for the scattering from spherical particles (equation 4.10)

Figure 8.4

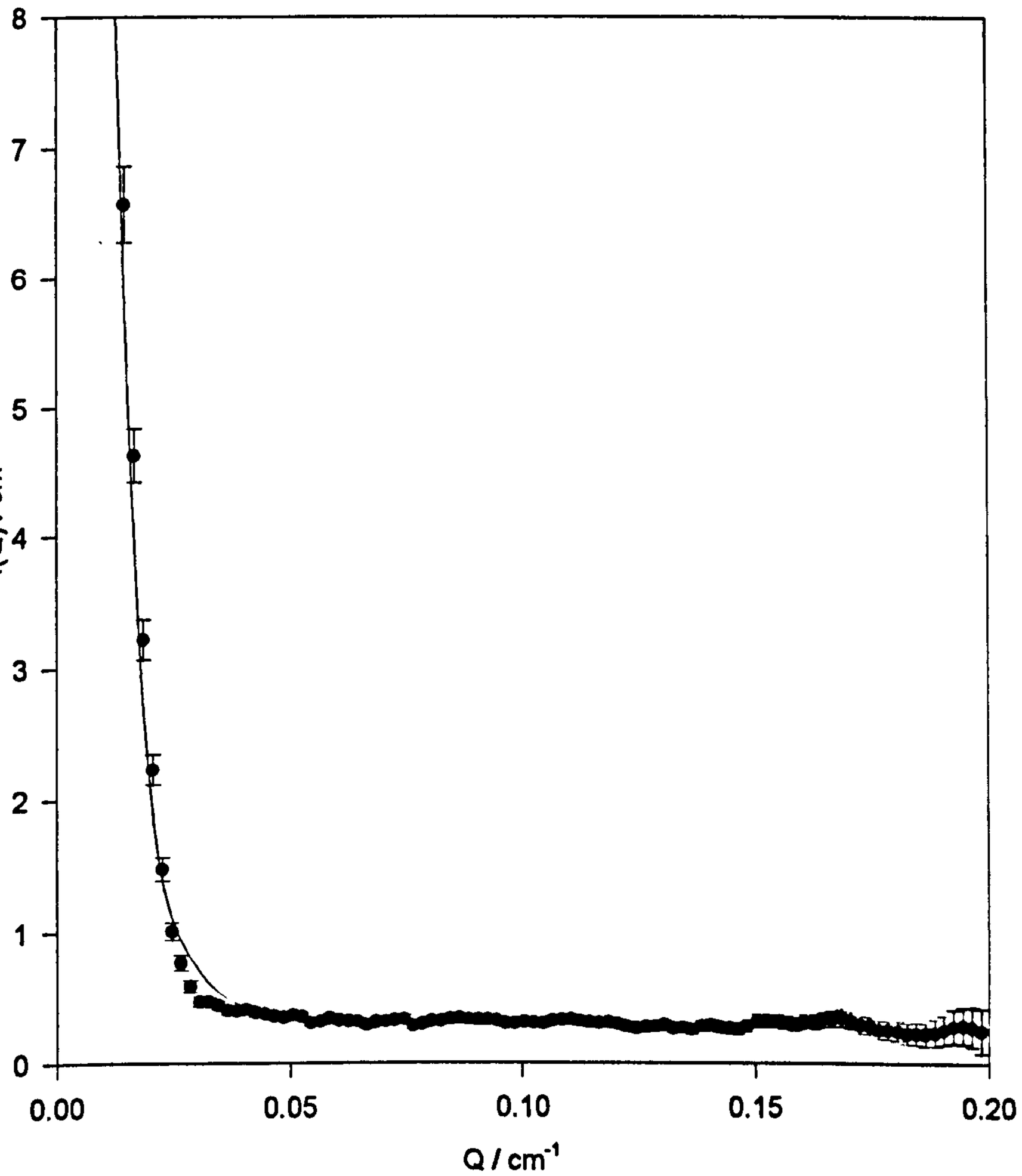

From these data in **figure 8.4,** the radius of the particles was obtained as 113 ± 20 Å. This compares with data sheets which quote the diameter of the particles as 200 -300 Å.

8.2.2 PEO in solution.

The polymer scattering in aqueous solution is presented in **figure 8.5.** Like the particle scattering presented in the previous section, different Q ranges of this data give different spatial information on the polymer coil structure[3].

The simplest model of a polymer in solution corresponds to a Gaussian segment density distribution. The form factor for this type of structure is given by,

$$P(Q) = \left(\frac{2}{Q^4 R_g^4}\right)\left[\exp(-Q^2 R_g^2) - (1 - Q^2 R_g^2)\right]$$

[8.2]

In theory, at very low values of Q, for dilute solutions, the Guinier approximation (equation 4.14) may be applied. However, the $QR_g << 1$ restriction often precludes the use of this approximation. On the other hand, at high values of Q which probe smaller distances, the scattering can be used to obtain information on a monomer scale. The power law can be used to characterise the scattering of given sample; *i.e.* plot $I(Q)^{-1}$ versus Q^a, where a is an exponent, until a straight line is obtained, alternatively the slope of a log-log plot would give the same information. The value of a gives information on the chain structure. For example, a truly Gaussian chain yields a value of a of exactly 2. Under these conditions the De Gennes theory[4] can be applied to obtain a characteristic correlation length of the polymer chain.

$$P(Q) = \frac{A}{1 + Q^2 \xi^2}$$

[8.3]

where P(Q) is the form factor, A is a constant and ξ is a characteristic correlation length, or mesh size.

Unfortunately, more often than not, an exact value of 2 is not obtained. Below are sample values of a and the type of structure they characterise[5].

SHAPE	VALUE OF a
Rigid Rod	1
Linear Gaussian Chain	2
Chain with Excluded Volume	$\frac{5}{3}$
Gaussian Chain-Randomly Branched	$\frac{16}{17}$

Figure 8.5

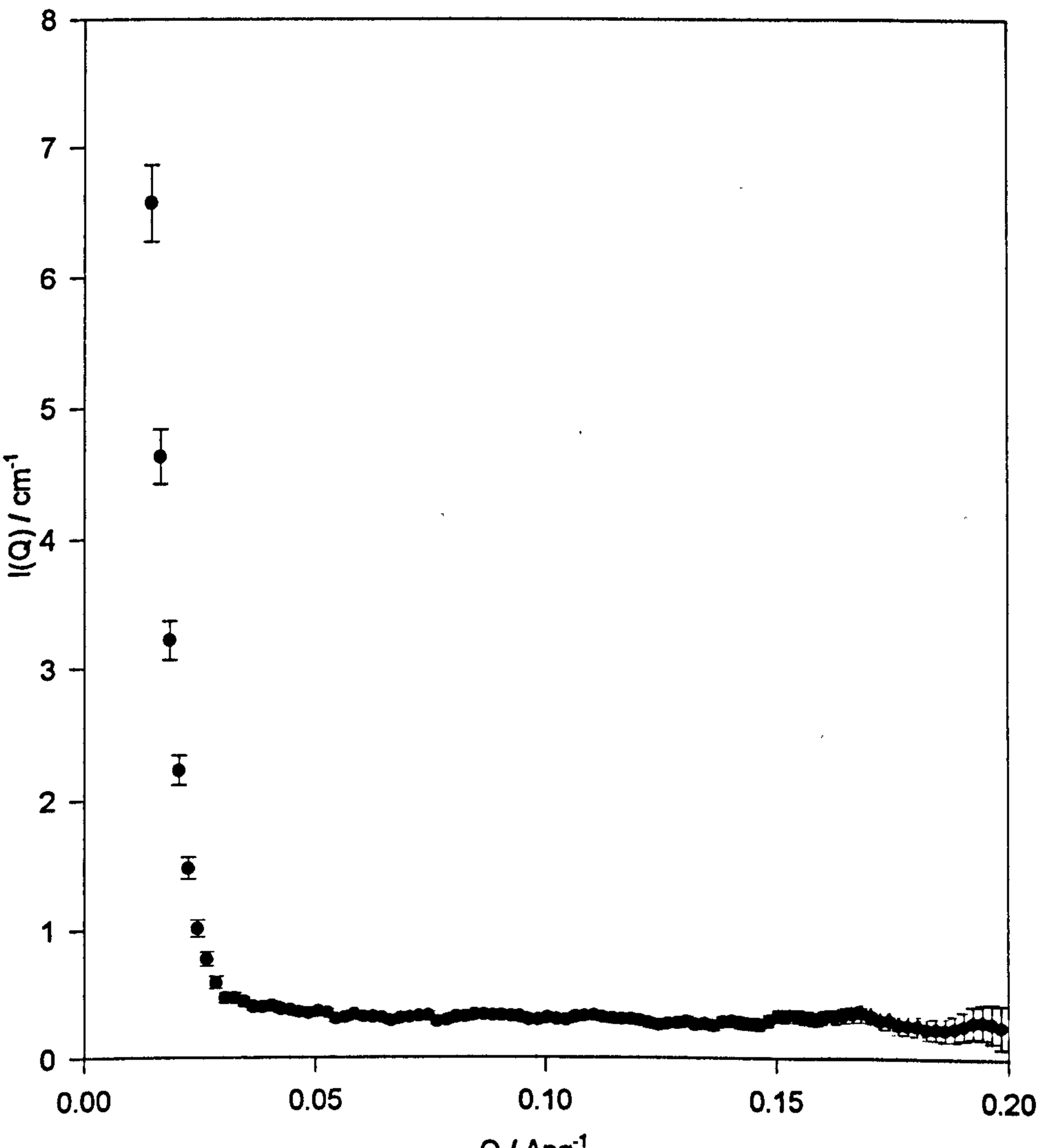

A value of a of 1.25 for this polymer sample was obtained indicating that we are in an intermediate value of Q where there is a transition from $a = 1$ to $a = 2$.

8.2.3 SDS in solution.

The next section discusses the scattering from SDS micelles in aqueous solution. As discussed in Chapter 4, the scattering from micellar solutions is dependent upon not only the form factor, P(Q), but also a structure factor, S(Q), arising from intermolecular interactions (equations 4.16 and 4.17).

Table 8.1.; **Parameters used to model the SDS scattering.**

Parameter	Value
Diameter	37.0 Å
Surface Charge	10.19
Debye Length	34.7 Å
Volume Fraction	0.01
$(\rho_{D2O}-\rho_{H\text{-}SDS})$	6×10^{-6} Å^{-2}

Hayter and Penfold[8] have shown that the structure factor for spherical micelles can be fitted by using a mean spherical approximation incorporating such parameters as micellar size, volume fraction and surface charge. This structure factor can be combined with the sphere form factor to fit the scattering intensity arising from the SDS micelles. **Figure 8.6** shows the modelled scattering for a 1.0 % w/w H-SDS in D_2O broken down into its form factor and structure factors. The parameters for this model are given in **table 8.1.**

Figure 8.6

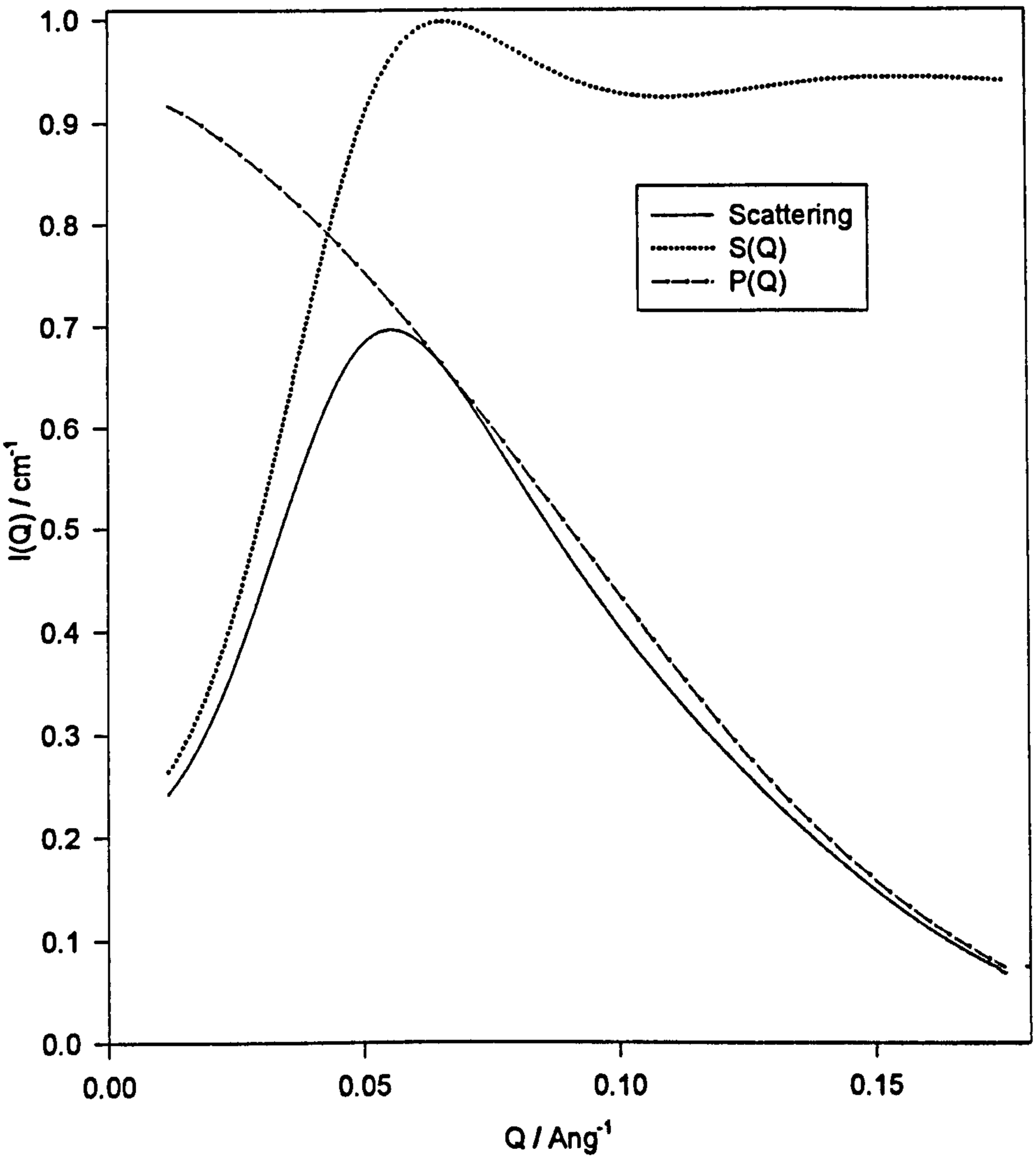

Figure 8.7 shows models of the scattering obtained for H-SDS in D_2O as a function of volume fraction (ϕ). As the solution concentration increases, the peak of the structure factor shifts to higher Q, indicating that the distance between micelles is decreasing. In reality, by the time SDS has reached a volume fraction of 0.05, it is believed to form more rod-like micelles and data will not adequately fit this model. Furthermore, on increasing the volume fraction the intensity of the scattering significantly increases.

Figure 8.7

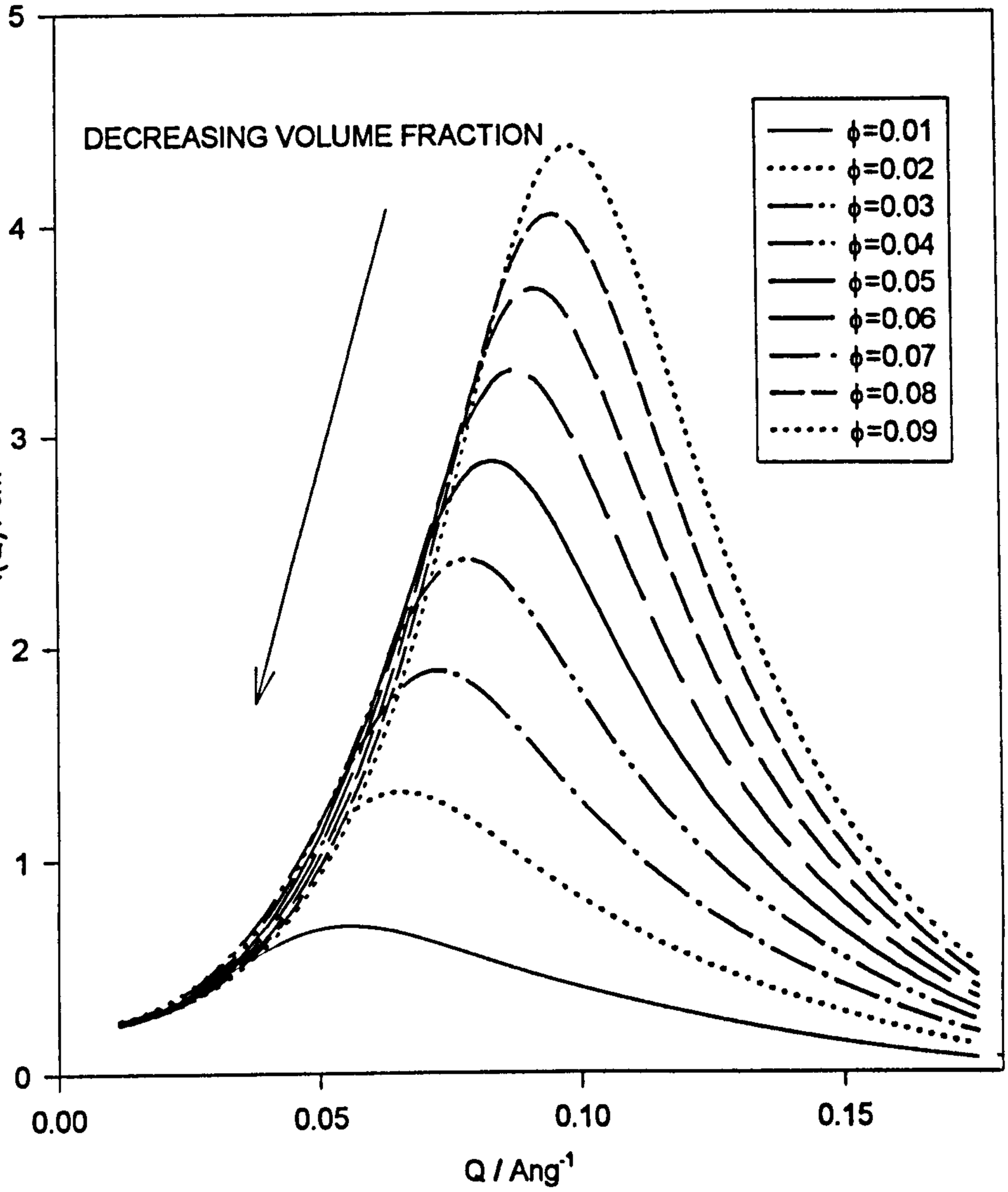

In **figure 8.8**, the scattering from SDS micelles as a function of micellar radius can be seen. Under these conditions both the P(Q) and the S(Q) are affected. Evidently, for the same volume fraction, larger micelles result in a greater separation between individual scattering centres, hence the position of the peak shifts to a lower value of Q.

Figure 8.8

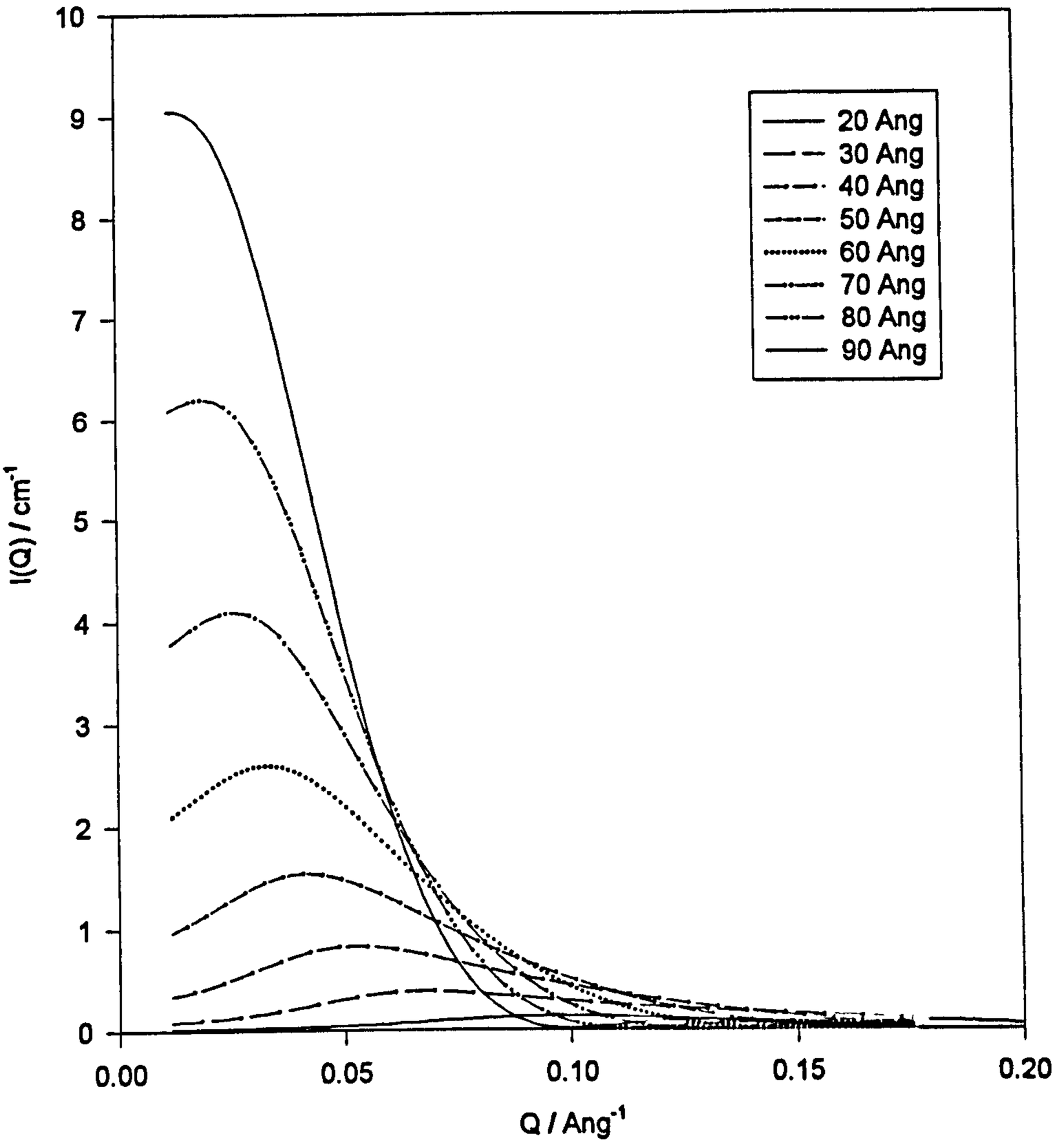

Figure 8.9 shows the scattering data from H-SDS in D_2O at 0.3 % w/w and 1.0 % w/w. Both of these concentrations are above the normal CMC of SDS (0.23 % by weight) and hence a structure peak is observed for both of these samples. The structure peak for the higher concentration sample occurs at a Q value of 0.05 $Å^{-1}$ and this corresponds to a centre-to-centre separation of the micelles of approximately 125 Å (separation $\approx 2\pi/Q$). The structure peak for the 0.3 % by weight SDS sample is much less pronounced (at an approximate Q value of 0.035 $Å^{-1}$), due to the fact that this particular solution is only just above the CMC of SDS and corresponds to a separation of approximately 180 Å. Calculating approximate values of separation from the volume fractions one

obtains a centre-to-centre separation of 150 Å for the 1 % w/w case and 380 Å for the 0.3 % w/w case. These separations are based on values of the CMC and aggregation number of SDS being 8.3 mMol and 58 respectively[7]. Also shown on **figure 8.9** are the fits obtained from these data using the Hayter-Penfold model (section 4.5.4) and the parameters obtained are shown in **Table 8.2.**

Table 8.2: **Typical Fitted Parameters for SDS using the Hayter-Penfold Model**

Parameter	1.0 % w/w SDS	0.3 % w/w SDS
Diameter (Å)	37.30 ± 0.08	33.10 ± 0.16
Debye Screening Length (Å)	33.40	33.40
Background Intensity (cm^{-1})	0.052 ±0.003	0.023 ± 0.004

These scattering patterns are very similar to those found elsewhere in the literature[8] which report a 42 Å diameter and a Debye Length of 25 Å for a 2.0 % w/w SDS solution. Since, the model fitting was not very sensitive to the Debye screening length (within this range), an approximate value of the Debye screening length was calculated from the ionic strength (as 33.4 Å for both samples based on the assumption that the CMC does not change significantly) and this value remained fixed for the model fitting. An important note is that the scattering from protonated SDS in D_2O and deuterated SDS in H_2O yield data which gives micelles of the same size and shape[2]. It is also known that the CMC of H-SDS is the same in D_2O as H_2O[9].

Figure 8.9

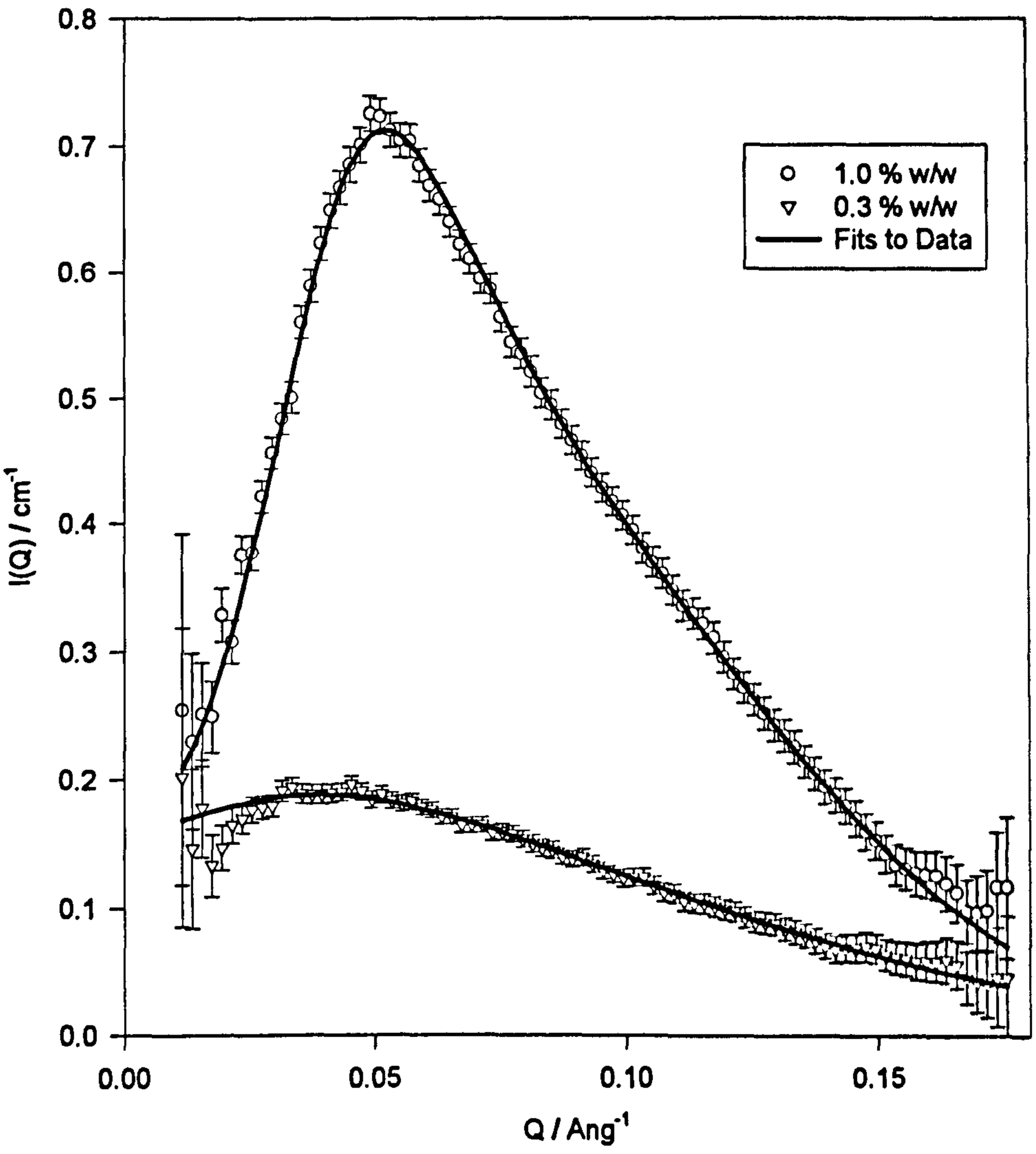

8.3 Binary Mixtures

8.3.1 Mixtures of PEO and Particles.

Figure 8.10 shows the SANS data for a silica particle with an adsorbed PEO layer under "contrast match" conditions for the particle. Under these conditions the particle is effectively invisible to the neutrons and only the scattering pattern arising from the adsorbed layer can be seen. The incoherent background and any residual particle scattering have been subtracted.

Figure 8.10

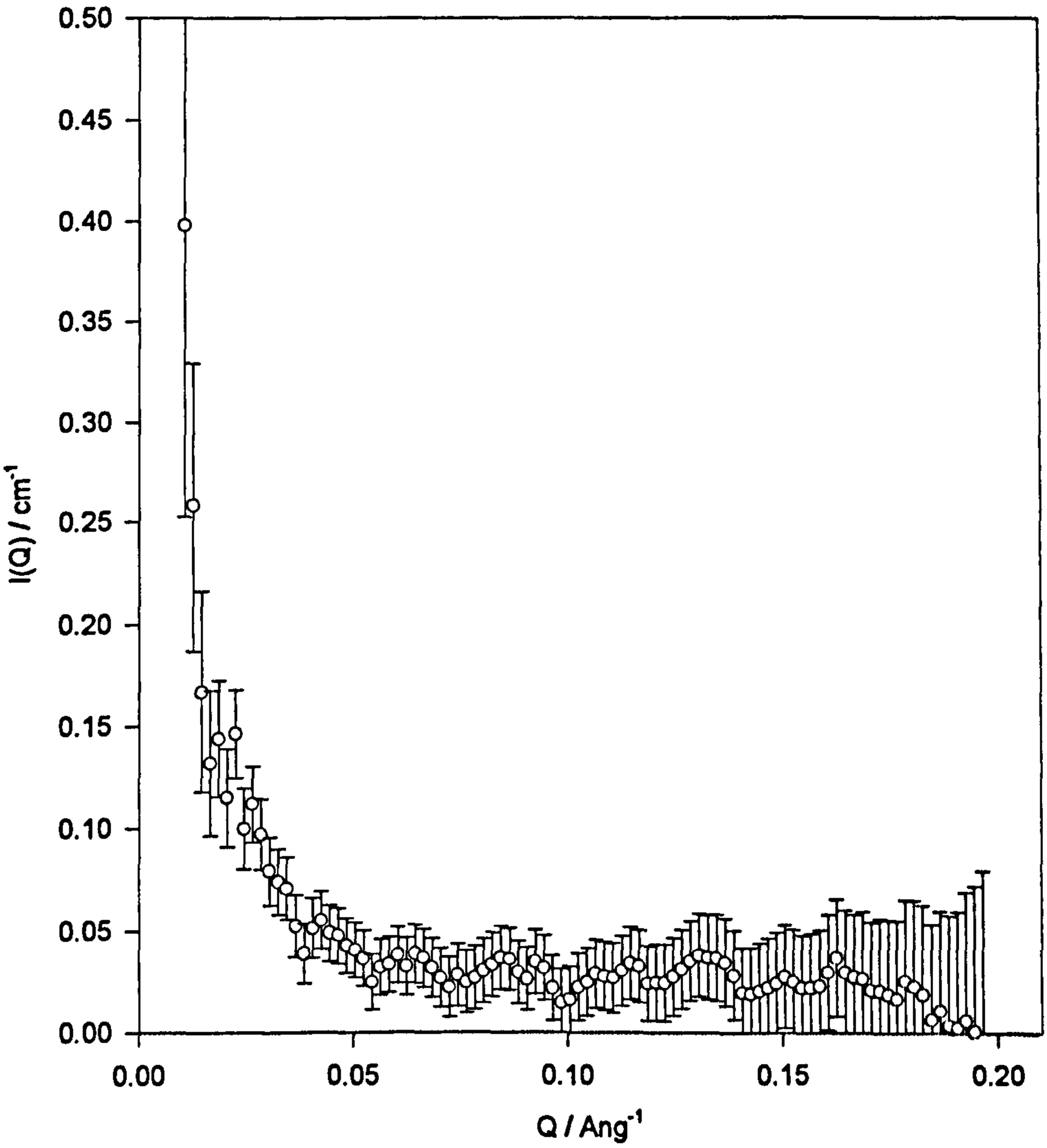

Figure 8.11 shows similar data for PEO adsorbed onto PSL. Also shown on this figure is the fit to this data set, according to equation 4.22 given in the SANS theory chapter (Chapter 4).

This fit was obtained by fixing the Q dependency of the fluctuation term to -⅓ (equations 4.21 - 4.23). Fits were repeated with various volume fraction profiles until a minimum in the standard deviation of the fit was obtained. The fluctuation intensity was determined from a plot of $Q^{-⅓}I(Q)$ against $Q^{⅓}$. The slope of this

plot corresponds to the incoherent background level and the intercept on the $Q^{4/3}I(Q)$ axis to the fluctuation intensity.

The plot for PEO on PSL is shown on **figure 8.12.** Similar plots can be drawn of $Q^{5/3}I(Q)$ against $Q^{5/3}$ if the fluctuations go as minus five-thirds. The error bars on this plot are very large and therefore care must be taken when interpreting these data.

Figure 8.11

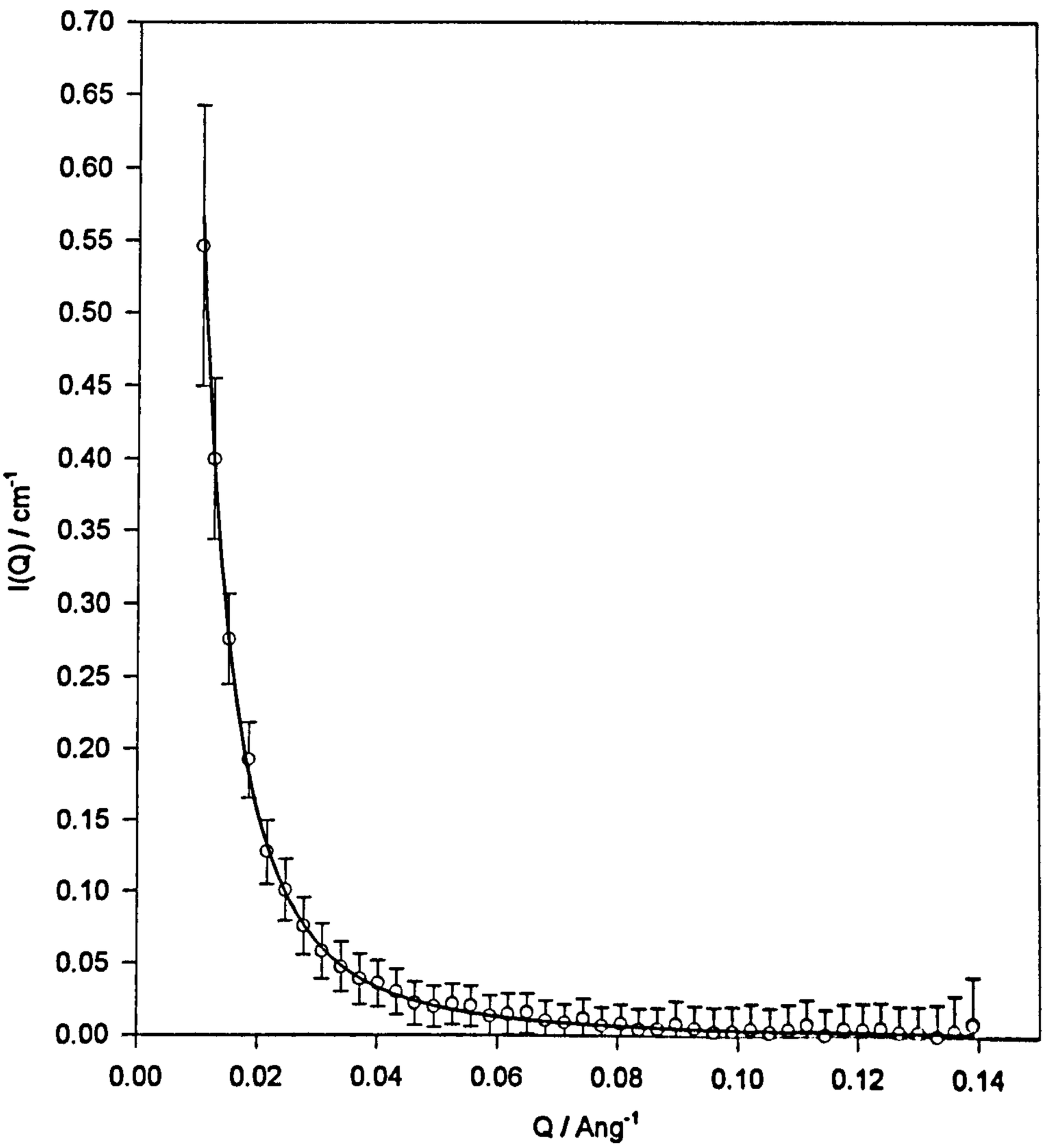

A best straight line has been drawn through the high Q data on **figure 8.12** and

this corresponds to a fluctuation intensity (intercept on the $Q^{4/3}I(Q)$ axis) of 5.6×10^{-4} Å$^{4/3}$ cm^{-1}.

Figure 8.12

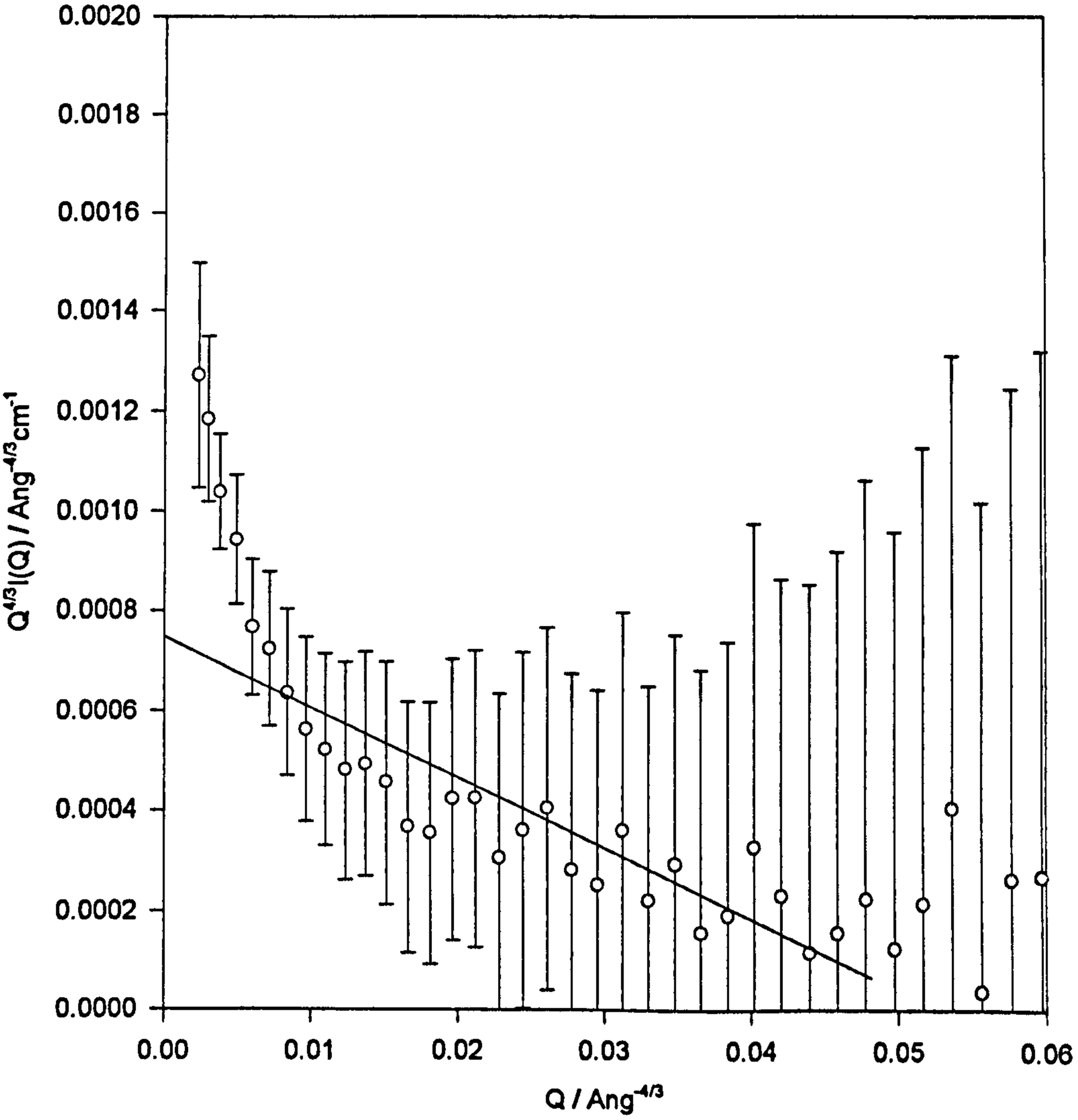

The corresponding volume fraction profiles, dependent upon the choice of fluctuation exponent are shown in **figure 8.13**. From **figure 8.13** it is evident that fluctuations play an important role in the resultant volume fraction profile, although there appears to be very little difference between fixing the fluctuation exponent at -⅓ or -⅔, but this may simply reflect the quality of the data. For these two values of the fluctuation exponent, the profiles extended out to

approximately 120 Å (12 nm) which compared well with the DLS measurements reported in Chapter 6 which indicated a hydrodynamic thickness of the adsorbed polymer layer in the absence of any surfactant of around 105 ± 10 Å. These two sets of data agree within experimental error. Data fitting in the absence of fluctuations yielded a maximum thickness of only around 80 Å. Moreover, the values of adsorbed amount from the adsorption isotherm measurements and the SANS data are in good agreement which suggests that the parameters used in the data fitting were correct.

Figure 8.13

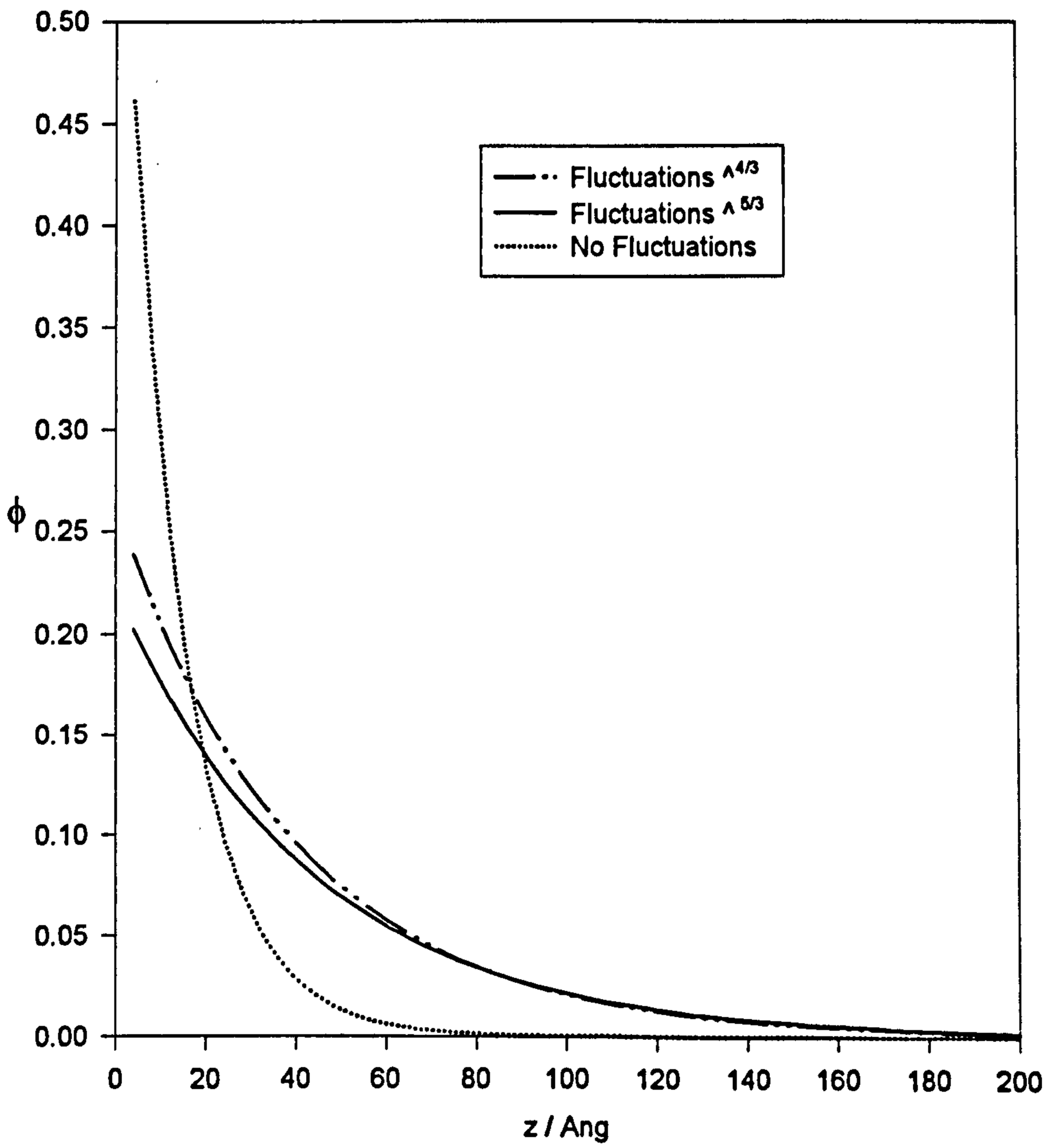

Table 8.3 gives the parameters obtained from these data fitting and a comparison between techniques.

***Table 8.3;* Comparison of techniques for the parameters obtained for an adsorbed PEO layer.**

Parameter	Isotherm Measurements	DLS Data	SANS Data
Adsorbed Amount	0.8 mg m^{-2}	--------	0.91 mg m^{-2}
Hydrodynamic Maximum Extent of the layer Thickness/	--------	105 Å	120Å
RMS. Thickness	--------	--------	32Å

From the volume fraction profiles obtained from the "off-contrast" data it is possible to obtain the fluctuation term explicitly, although experimentally this often proves difficult due to many subtractions leading to poor statistics of the data.

8.3.2 Mixtures of PEO and SDS in D_2O

The solution properties of the polymer-surfactant interaction were investigated in D_2O. The use of D-SDS allowed the scattering from the surfactant to be strongly suppressed and the polymer alone to be observed. **Figure 8.14** shows the scattering from the polymer in solution as a function of surfactant concentration plotted on a log-log scale. In comparing the scattering from the mixture to that of pure PEO, it can be seen that within the Q range under observation, the PEO in the absence of SDS has the highest scattering intensity. However, this may not be the case if the data were extracted to zero Q. All samples terminate in approximately the same level of incoherent background. At the highest surfactant concentration (1.0 % w/w), the scattering from the PEO shows a structure peak similar to that of SDS. Initially, this was believed to arise from residual SDS scattering (D-SDS and D_2O do not have exactly the same scattering length

density) and so the scattering from H-SDS at this concentration was scaled in order to resemble the D-SDS in D_2O according to equation 8.4.

$$I(Q)_{scaled} = \frac{(\rho_{D-SDS} - \rho_{D_2O})}{(\rho_{H-SDS} - \rho_{D_2O})} I(Q)_{unscaled} \qquad [8.4]$$

Differences in transmission between samples with high and low hydrogen content were also accounted for in the same manner. The resulting SDS scattering was over 2 orders of magnitude smaller than that of the observed peak in the PEO data. It was therefore concluded that the peak in the PEO data arises from some form of structure in the polymer rather than residual SDS scattering.

This effect has also been observed in the gelatin/SDS system[8] where the binding of SDS above the CMC causes a disruption in the gelatin mesh, resulting in the gelatin scattering following the structure factor of the SDS. Our effect is much smaller than that observed in the gelatin system, but nevertheless indicates that at high surfactant concentrations, the PEO structure begins to resemble that of the surfactant.

The sample containing PEO in the presence of 0.3 % w/w SDS showed a small structure peak. This confirms that even at low levels of binding the SDS disrupts the structure of PEO. The position of this peak (Q = 0.04 $Å^{-1}$) allows an 'interparticle' separation to be obtained (separation = $2\pi/Q$). This corresponds to a separation of 157 Å). These effects were not observed by Cabane *et al*[2], but those experiments were performed in the presence of salt which significantly screens charges between micelles and removes the strong interactions which give rise to the structure factor. Recent experiments performed in the absence of salt[10] have reported similar effects. In that paper SANS experiments were performed on mixtures of 1.0 % w/v (45,000 molecular weight) PEO with and without 0.15 M D-SDS in D_2O. The slopes of a log I(Q) versus log Q plots with and without surfactant were measured. The slope was equal to $-1/\nu$, where ν is

the excluded volume exponent. Therefore a larger value of ν corresponds to a larger excluded volume. In the absence of SDS the slope was equal to -1.70, whilst in the presence of SDS this was equal to -1.54.

Figure 8.14

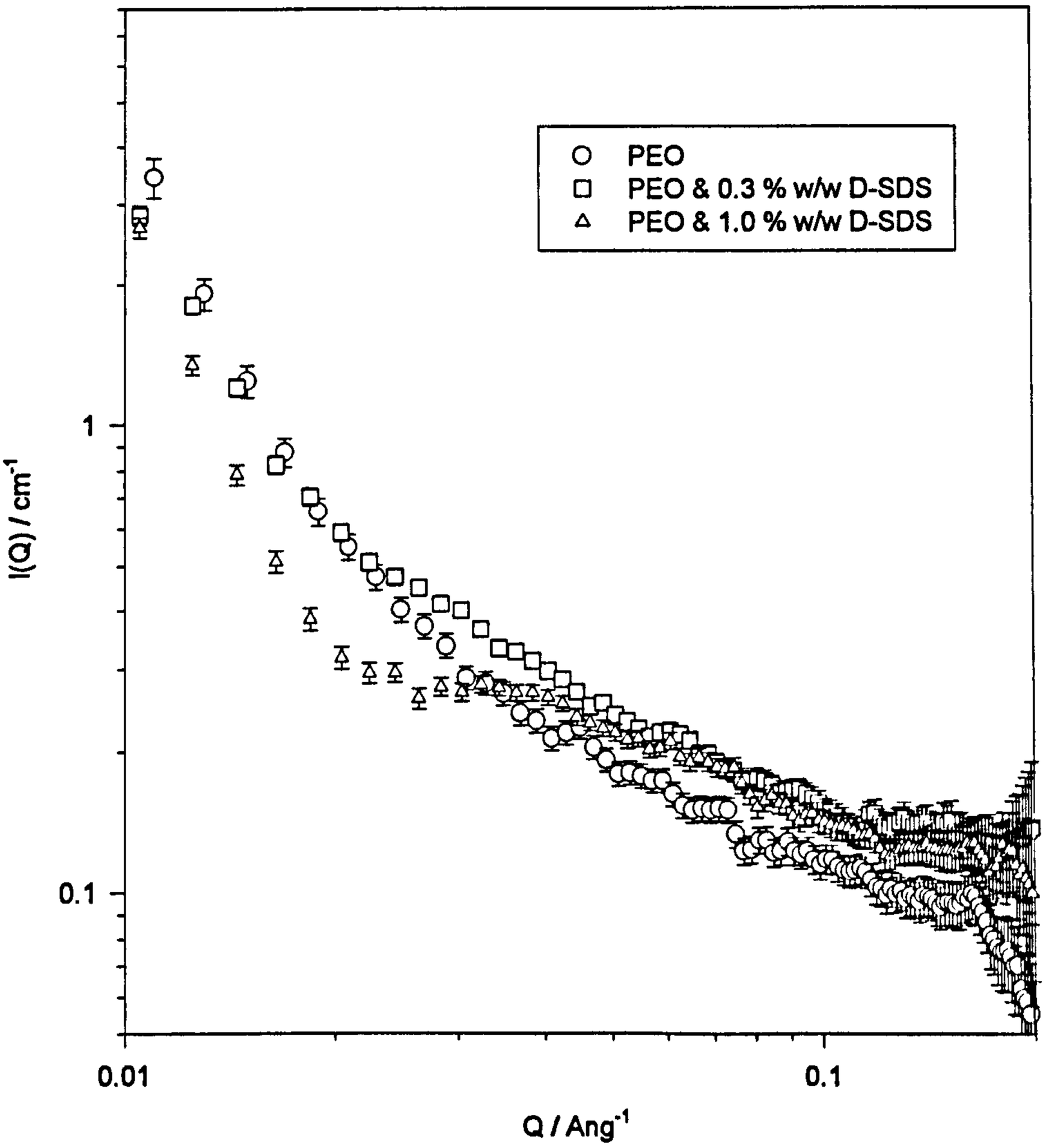

From this observation, Chari *et al*[10] proposed that PEO on approaching saturation was more like a swollen cage and not a necklace as suggested by Shirahama[11]. It was suggested that the backbone of the polymer formed hydrophobic microenvironments within the cage that could shield the hydrocarbon regions of the surface of a surfactant micelle from contact with water. Therefore the free energy of micellisation could be reduced. Furthermore,

in that paper, it was noted that the scattering of PEO in the presence of SDS exhibited a peak at low values of Q (although this was not discussed further).

Figure 8.15

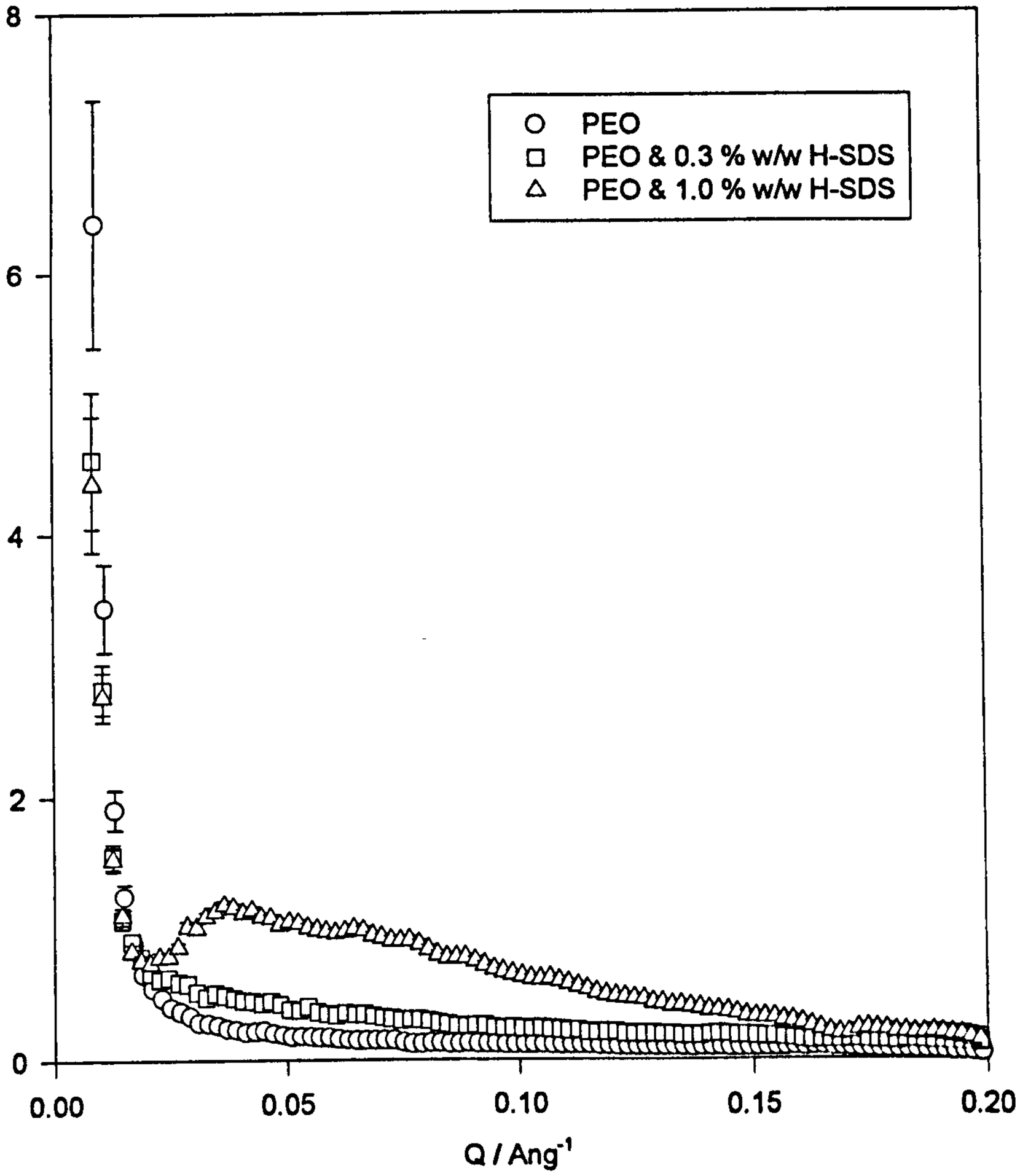

On replacing the deuterated surfactant with H-SDS the scattering from the SDS can also be observed. **Figure 8.15** shows the scattering pattern from H-SDS and PEO in solution as a function of surfactant concentration. Since both components are visible the scattering arises from a combination of the polymer, the surfactant and an interference term between the two. Therefore, intensities are much higher than for either the polymer or the surfactant alone. In the absence of PEO the SDS forms a well defined structure peak at a Q value of 0.05Å^{-1} and an intensity

of approximately 0.78 cm^{-1}**(Figure 8.9)**. Since Q is an inverse length an estimate can be made of the average interparticle separation (separation $\approx 2\pi/Q$). For the 1.0 % w/w SDS, this interparticle separation corresponds to approximately 125 Å. In the presence of PEO the structure peak has shifted to a slightly lower value of Q,(~ 0.04 $Å^{-1}$) which now corresponds to an approximate centre-to-centre distance of 157 Å. This is the same as that where the SDS was not visible (**Figure 8.14**). Chari *et al*[10] also obtained values of the intermicellar separation (from the position of the peak) for 2.1 % w/w SDS in the presence of 0.5 % PEO (molecular weight 85,000). The average distance between the micelles was 97 Å and the size of each micelle was taken to be 40 Å. It was calculated that for these concentrations there were roughly 28 micelles attached to each coil.

A measure of the effect of SDS on PEO can be obtained by subtracting the data in **figure 8.14** from that in **figure 8.15**. Unfortunately, no allowance can be made for any interference term between the SDS and the PEO but nevertheless the scattering may be examined qualitatively. These data are shown in **figure 8.16.** Also shown on **figure 8.16** are the fits obtained from the data fitting of the 0.3 % w/w and 1.0 % w/w SDS in D_2O.

At the lower SDS concentration it can be seen from **figure 8.16** that both the magnitude and shape of the SDS scattering are similar in the presence and the absence of PEO. This indicates that the SDS micelles when in the presence of PEO are of a very similar size and shape to those that exist in the absence of polymer. However, on the other hand, at the higher SDS concentration investigated, the shape of the SDS scattering is significantly different in the presence of polymer. It appears that the position of the peak has partially moved to a lower value of Q whilst there is still some residual peak at the original Q value. The shifting of the position of the peak suggests that the average micellar distance is further apart. Moreover, beyond these peaks the shape of the SDS scattering resembles that in the absence of polymer. However, it must also be remembered that the cross-term between the surfactant and the polymer may

cause some of the shifting of the peaks. Unfortunately, due to this and the quality of these data, a more qualitative (or indeed quantitative) description of the SDS micelles cannot be drawn.

Figure 8.16

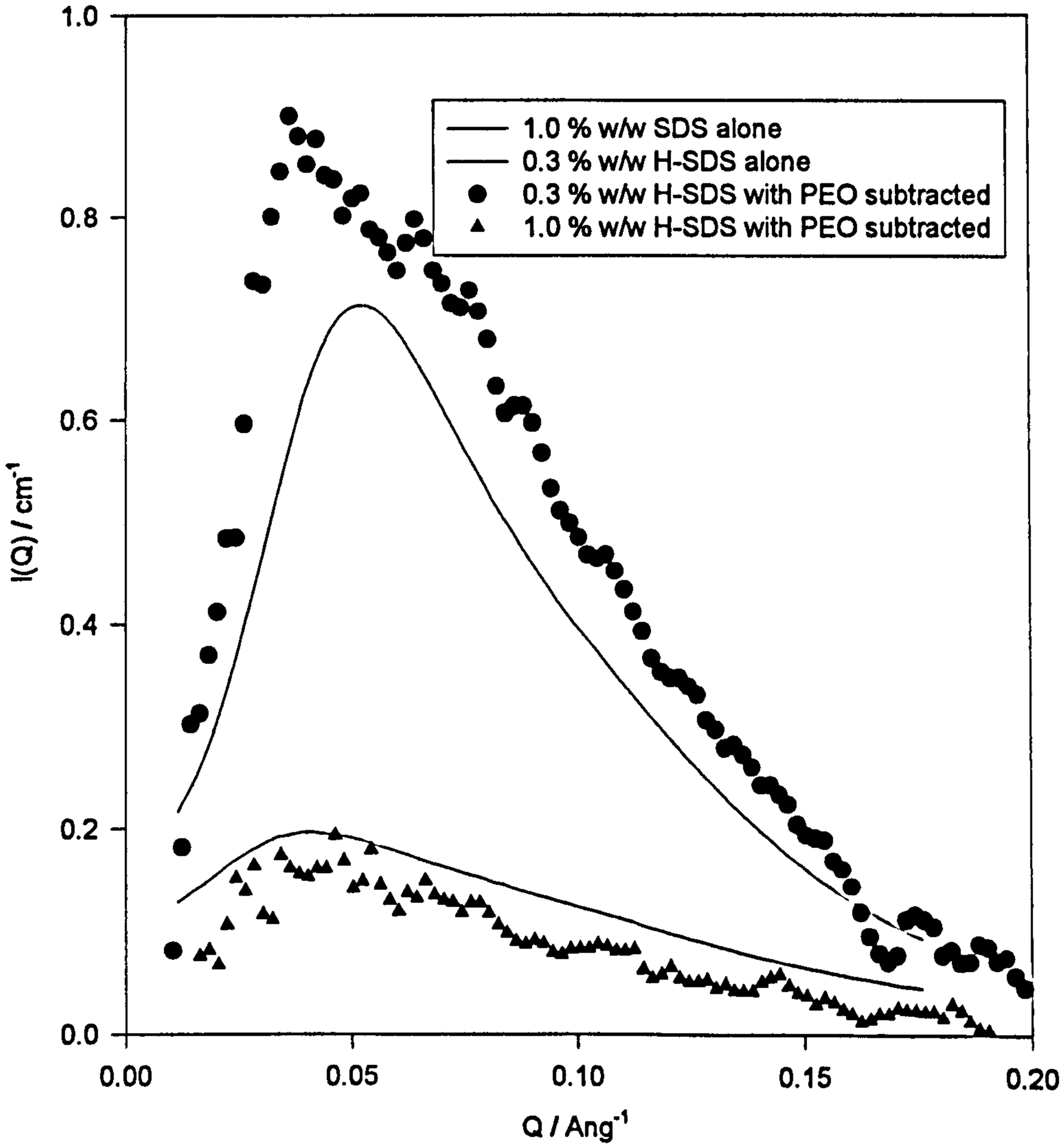

8.2.3. Dispersions of PSL and SDS.

Experiments were performed to examine the effect of a PSL substrate on SDS. At 0.15 % w/w H-SDS there is no observed structure peak, since SDS at this concentration is below the normal CMC of SDS. Also shown in **figure 8.17** is the scattering pattern from 1.0 % w/w SDS composed of a mixture of hydrogenous and deuterated SDS with the same scattering length density as the solvent.

Figure 8.17

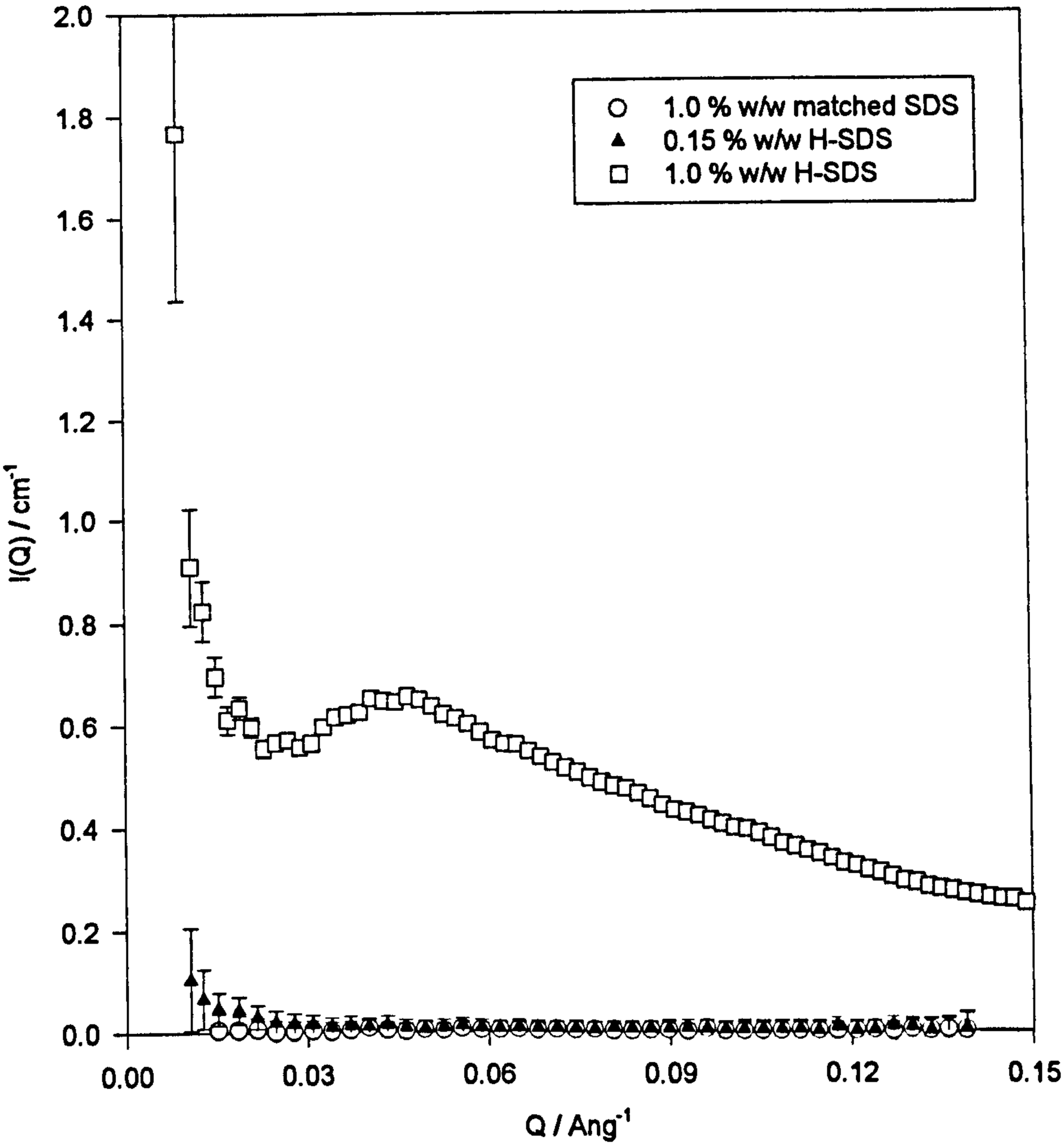

As can clearly be seen the scattered intensity is negligible, suggesting that indeed the SDS has been matched to the same scattering length density as the PSL and the solvent. The composition of SDS required for this contrast matching was used in many of the subsequent experiments. Finally, the scattering from 1.0 % w/w H-SDS in the presence of PSL was examined. A significant structure peak was observed at a similar value for that in the absence of PSL. Furthermore, the intensity at very low Q values was increased, showing some SDS binding to the PSL.

8.4 Mixtures of PEO, SDS and PSL.

8.4.1 PSL and SDS Matched, PEO Visible.

Figure 8.18 shows the SANS from the adsorbed polymer layer as a function of SDS concentration. The SDS used for these samples is a mixture of H-SDS and D-SDS with the same scattering length density as the solvent (and indeed the PSL); thus only the scattering from the layer is visible. The error bars are not shown on these plots in an attempt to clarify the chart data. The scattering at very low values of Q is shown in the insert.

Figure 8.18

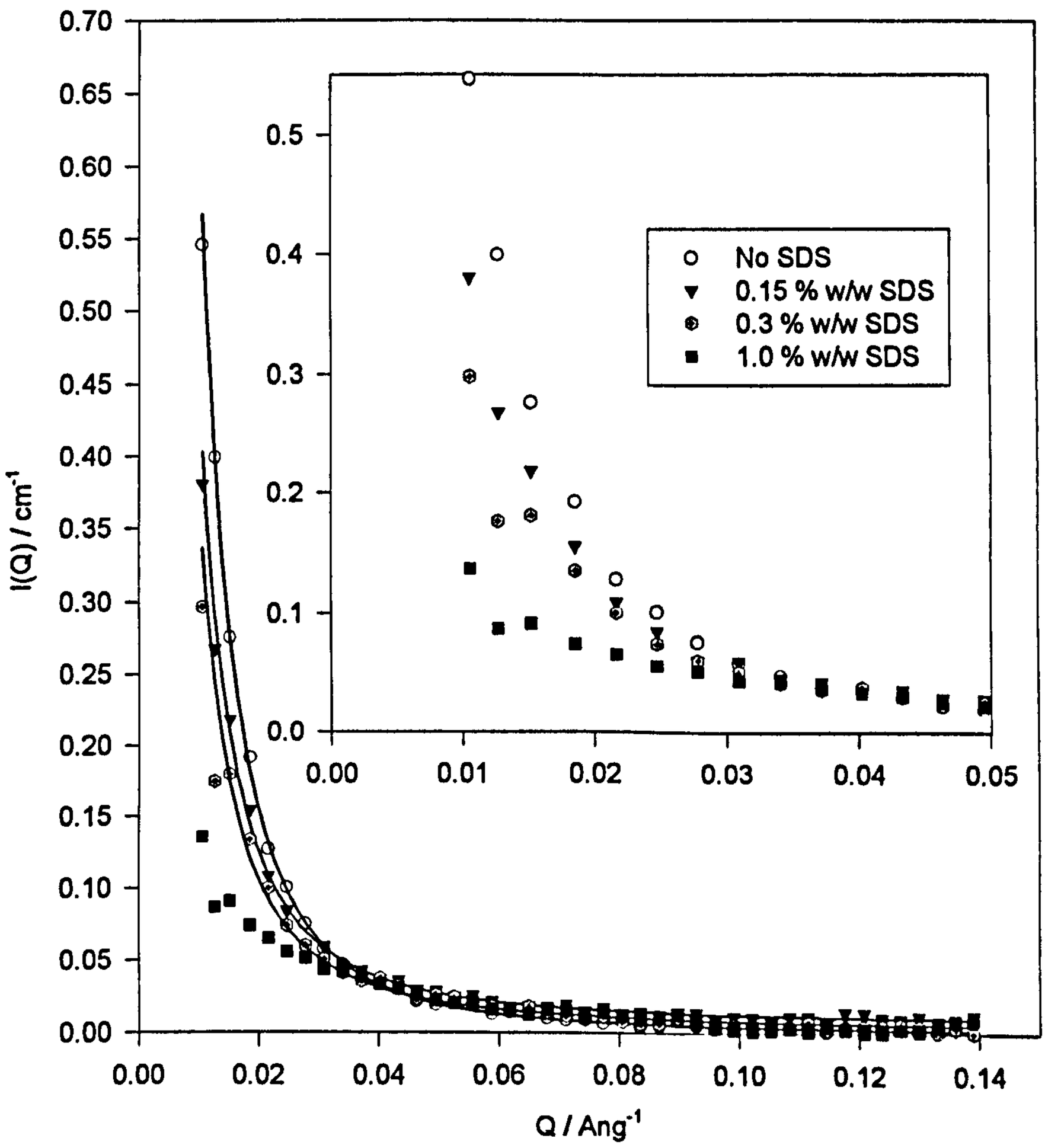

Also shown in the main figure are the fits obtained for these data. These fits were obtained in the same manner as for those in **figure 8.11** with the fluctuation exponent maintained at a value of $-\frac{4}{3}$. The sample in the absence of SDS has the highest scattered intensity and the sample with the highest SDS concentration having the lowest scattered intensity. All of these scattering patterns terminate in the same background level.

Figure 8.19

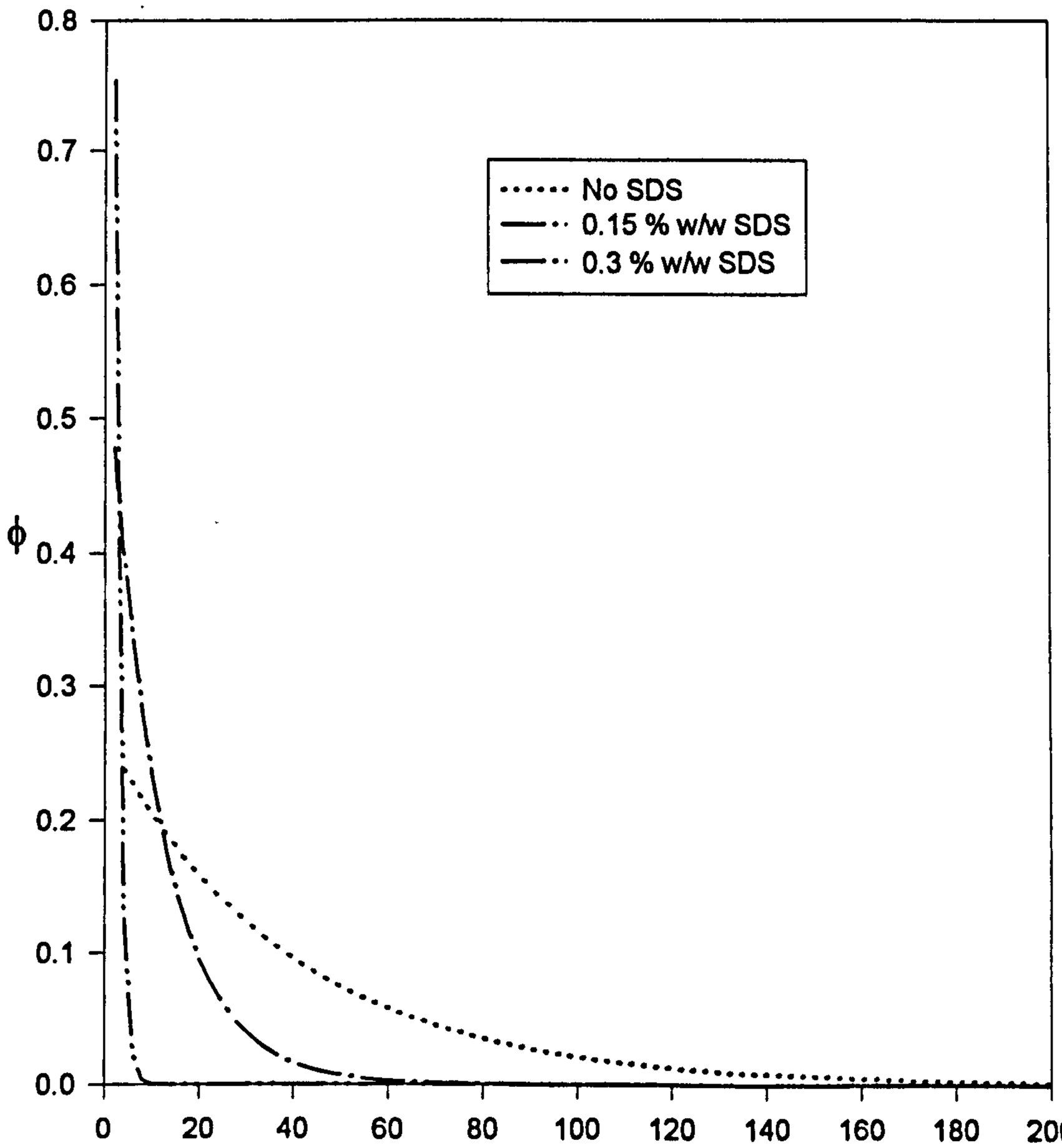

Figure 8.19 shows the corresponding volume fraction profiles for the scattering patterns in **figure 8.18.** Absent from this plot is the volume fraction profile for the sample with 1.0 % w/w SDS due to problems with fitting the data. In these

data a peak can clearly be seen at a Q value of 0.017 $Å^{-1}$. Therefore, as in the solution case, the adsorbed polymer is showing some form of structure similar to the SDS micelles. However, since the area under this curve is still significantly less than that in the absence of SDS; (the area under the curve is proportional to the adsorbed amount) it may be concluded that the adsorbed amount is less than the value in the absence of SDS (as may have been suggested from the DLS measurements). It is also debatable whether the adsorbed layer in the presence of 0.3 % w/w SDS is showing a similar structure peak. Furthermore, if desorption is indeed occurring, some of this scattering may result from solution PEO bound to SDS rather than adsorbed PEO - **figure 8.14**

However, these findings are not dissimilar to that of Shubin[12] who investigated the adsorption of the cationic polyelectrolyte Quatrisoft LM on mica as a function of SDS concentration by ellipsometry. In that paper[12], at high SDS concentrations, sparse highly extended layers decorated with SDS micelles were reported. Preliminary investigations into this system by SANS measurements will be reported in **Chapter 9** of this thesis.

The volume fraction profile in the absence of surfactant shows the classical exponential shape for a physisorbed polymer layer (Chapter 4, section 4.6). However, on the addition of surfactant both the shape and area under the curve (the adsorbed amount) changes. The profile for the 0.15 % w/w added SDS case indicates very much thinner layers than in the absence of surfactant, although the adsorbed amount is still relatively significant. On the other hand, at 0.3 % w/w added SDS (which is around the normal CMC of SDS), extremely thin layers (extending to only one or two nm) were formed in conjunction with only nominal adsorbed amounts. These data tie in very well with the DLS measurements on the same samples.

Table 8.4 **Comparison of parameters for adsorbed polymer layers in the presence of SDS**

SDS Concentration	δh / Å (DLS)	Max. extent / Å (SANS)
0.0 % w/w	107 Å	120Å
0.15 % w/w	49.5Å	52Å
0.3 % w/w	11.5Å	8Å
1.0 % w/w	88Å	------

Table 8.4 compares the parameters obtained from the SANS experiment to those obtained from DLS measurements. The surprising thing about these comparisons is that the enormous difference in substrate (and indeed polymer) concentration appears to have no effect on the adsorbed layer structure in the presence of surfactant.

The adsorbed amount for the sample containing 0.15 % w/w of surfactant was estimated at 0.64 mg m^{-2} and for that containing 0.3 % w/w of surfactant at 0.20 mg m^{-2}. Since PEO has the effect of reducing the concentration at which micelles are formed, micelles are formed on the polymer chains, even at surfactant concentrations below the normal CMC. From the "phase diagrams" of Cabane[2] (**figure 1.1**) a 0.3 % w/w PEO solution (the polymer concentration used in this part of this study) forms complexes with the SDS at surfactant concentrations beyond 0.18 % w/w. Saturation of the polymer occurs at 0.9 % w/w SDS. It must however be remembered that these values are for PEO and SDS in solution and not at the solid-liquid interface and since polymer concentrations at the solid-liquid interface may be an order of magnitude greater than in the bulk, it is probable that the SDS will interact with PEO at surfactant concentrations below 0.18 % w/w. Thus micelles can form on the polymer

chains, even at very low bulk surfactant concentrations. These polymer bound micelles effectively increase the hydrophilicity of the PEO chain (as reported in the solution data) and hence it is more favourable for the polymer to exist in solution than at the interface. Thus, the desorption observed here occurs. It is proposed that once the surfactant has bound to the PEO in a mixed micelle, this structure will not change, even if conditions take it to concentrations below that which interactions first occur (*i.e.* in the bulk). As the SDS concentration is increased, the spatial and electrostatic restrictions in the adsorbed polymer layer become more important reflected by the increased desorption at 0.3 % w/w SDS. Unfortunately, to date we have not managed to obtain a value of Gamma for the 1.0 % w/w sample due to the reasons outlined above, although the data do indicate a lowered adsorbed amount. If this system does in fact behave as that reported by Shubin[13] then at high surfactant concentrations very low coverage, highly extended layers indeed should be formed. Since the DLS measurements suggested highly extended layers and these SANS measurements have suggested low values of adsorbed amounts, it appears that in this system similar structures may be formed.

8.4.2 PSL Matched, PEO and SDS Visible

Figure 8.20 shows the scattering pattern from the surfactant in the presence of an adsorbed polymer layer. The surfactant concentration is 1.0 % w/w. The substrate has been "matched out" and the scattering from the polymer layer has been subtracted (data in **figure 8.18**). Also present in **figure 8.20** is the scattering pattern from SDS alone showing its characteristic structure peak.

It is evident from the scattering in **figure 8.20** that SDS in the presence of polymer and particle shows two peaks, not one as for SDS alone. The most probable reason for the occurrence of two peaks is that one arises from SDS in the bulk and one from SDS constrained at the interface. In this case the peaks are at Q values of 0.09 $Å^{-1}$ and 0.035 $Å^{-1}$. If we remember that Q is an inverse length, then it is reasonable to say that the peak at 0.09 $Å^{-1}$ is due to SDS micelles being

closer to each other than that peak occurring at 0.035 $Å^{-1}$. From interparticle separation ≈ $2\pi/Q$ then the peak at 0.035 $Å^{-1}$ corresponds to a separation of approximately 180 Å and the peak at 0.09 $Å^{-1}$ to a separation of 70 Å.

Figure 8.20

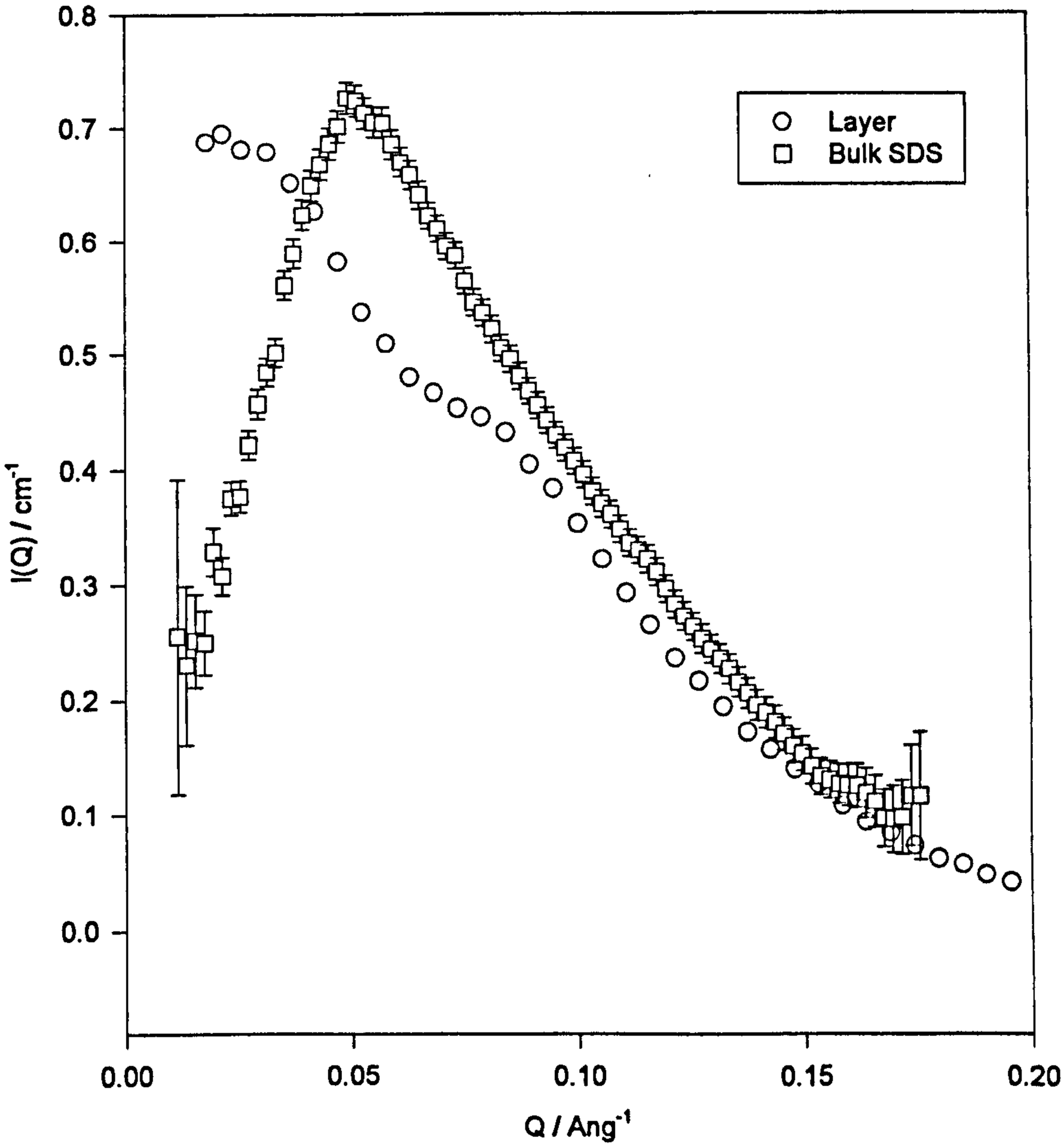

From the scattering from SDS alone, the interparticle separation was estimated to be approximately 125 Å. The diameter of an SDS micelle is approximately 40 Å and therefore micelles threaded along a polymer chain could quite conceivably give an interparticle separation of approximately 70 Å (at saturation in the bulk Chari *et al*[10] reported a intermicellar separation of 95 Å). There is no definite indication whether these micelles would exist on adsorbed polymer or on polymer

in the bulk solution. Until the adsorbed amount is known this cannot be determined qualitatively, although the mere existence of these two peaks suggest there is, to some degree, an adsorbed polymer layer. One important point to note is that in the absence of PSL only one peak was observed in the SDS scattering **(figure 8.16)**. This therefore confirms the existence of some form of adsorbed layer at high surfactant concentrations. Furthermore, the experiments in the absence of PEO **(Figure 8.17)** showed only one peak in the SDS scattering.

Figure 8.21

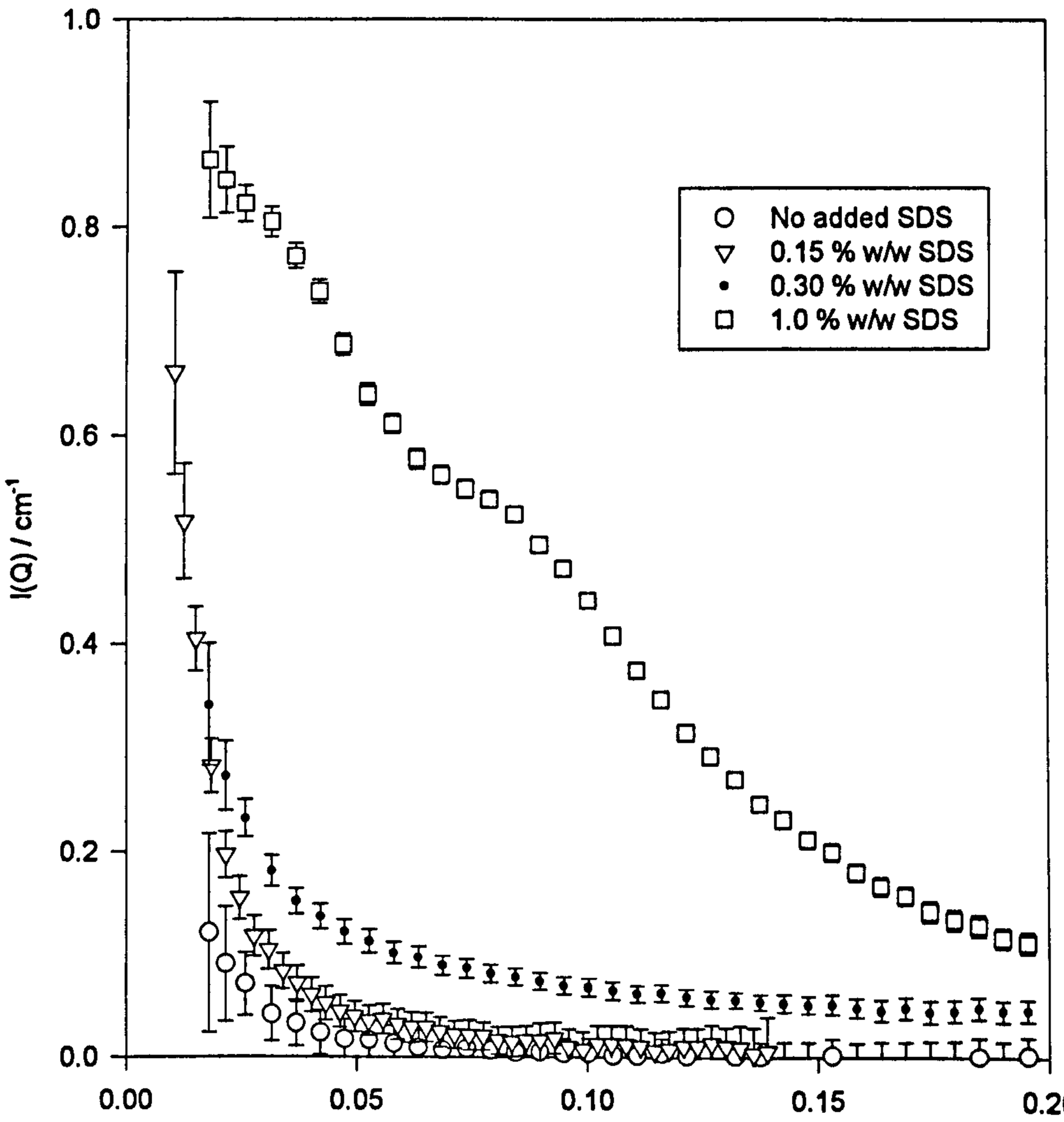

The corresponding data at 0.15 % w/w of SDS and at 0.3 % w/w of SDS are shown in **figure 8.21**. Also shown on this figure is the scattering in the absence

of any SDS and the data from **figure 8.20**. The data at the two lower SDS concentrations do not show any pronounced peaks, although we know that in the bulk both of these surfactant concentrations are above the critical aggregation concentration with PEO[2]. Therefore, this points to the absence of strong intermicellar interference in the adsorbed polymer layer at these surfactant concentrations. Since these surfactant concentrations are well below the saturation level of the PEO chains, it is likely that all of the SDS is bound to solution borne polymer in small aggregates which do not give rise to significant structure peaks.

8.4.3 PEO and PSL visible, with SDS

In the following section the solvent is pure D_2O. Therefore, the scattering from the PSL and the PEO is visible. The use of D-SDS allows the surfactant scattering to be "matched out". The data presented in this section have hadthe bare particle scattering subtracted and therefore the only components visible are the polymer layer and the interference term between the layer and the particle. Only a qualitative description will be made of the data presented in this section.

The scattering patterns as a function of D-SDS concentration are shown in **Figure 8.22**. These are analogous to those where in **figure 8.18** except the interparticle interference term is now also visible. Unfortunately, these data are of very poor quality and therefore data fitting and analysis was not possible.

Figure 8.22

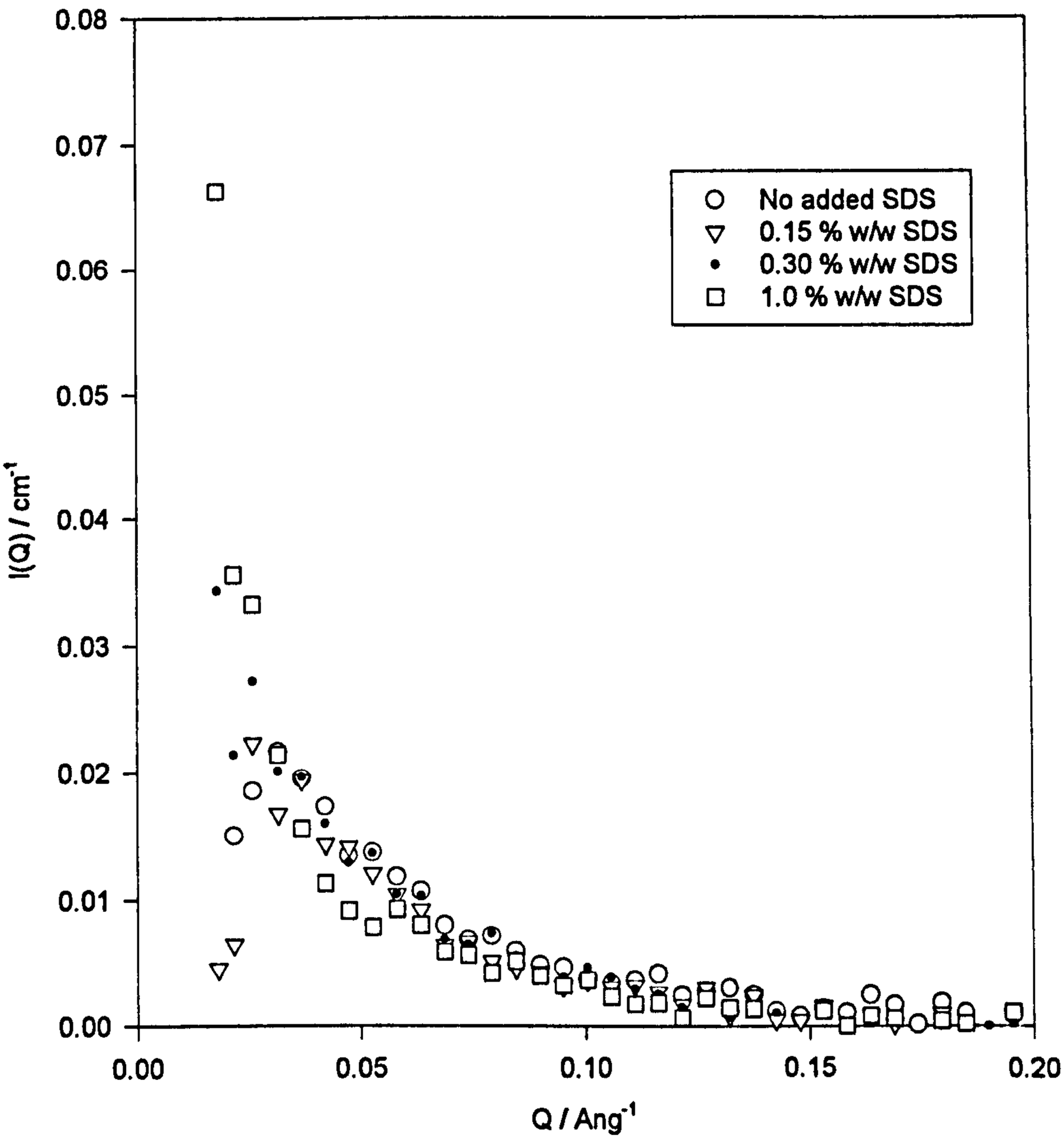

Figure 8.23 shows the analogous data to that in **figure 8.21**, but in this case, the interference term between the adsorbed layer and the particle is visible. The particle scattering has been subtracted from these data. The surfactant is H-SDS and therefore is visible. Again, at the highest surfactant concentration there is a significant structure peak arising from interparticle interactions within the SDS. As in the case where the particle/layer interference term was not present, two peaks are observed as compared with either SDS alone, or SDS in the presence of bulk PEO where only one peak is present.

Figure 8.24

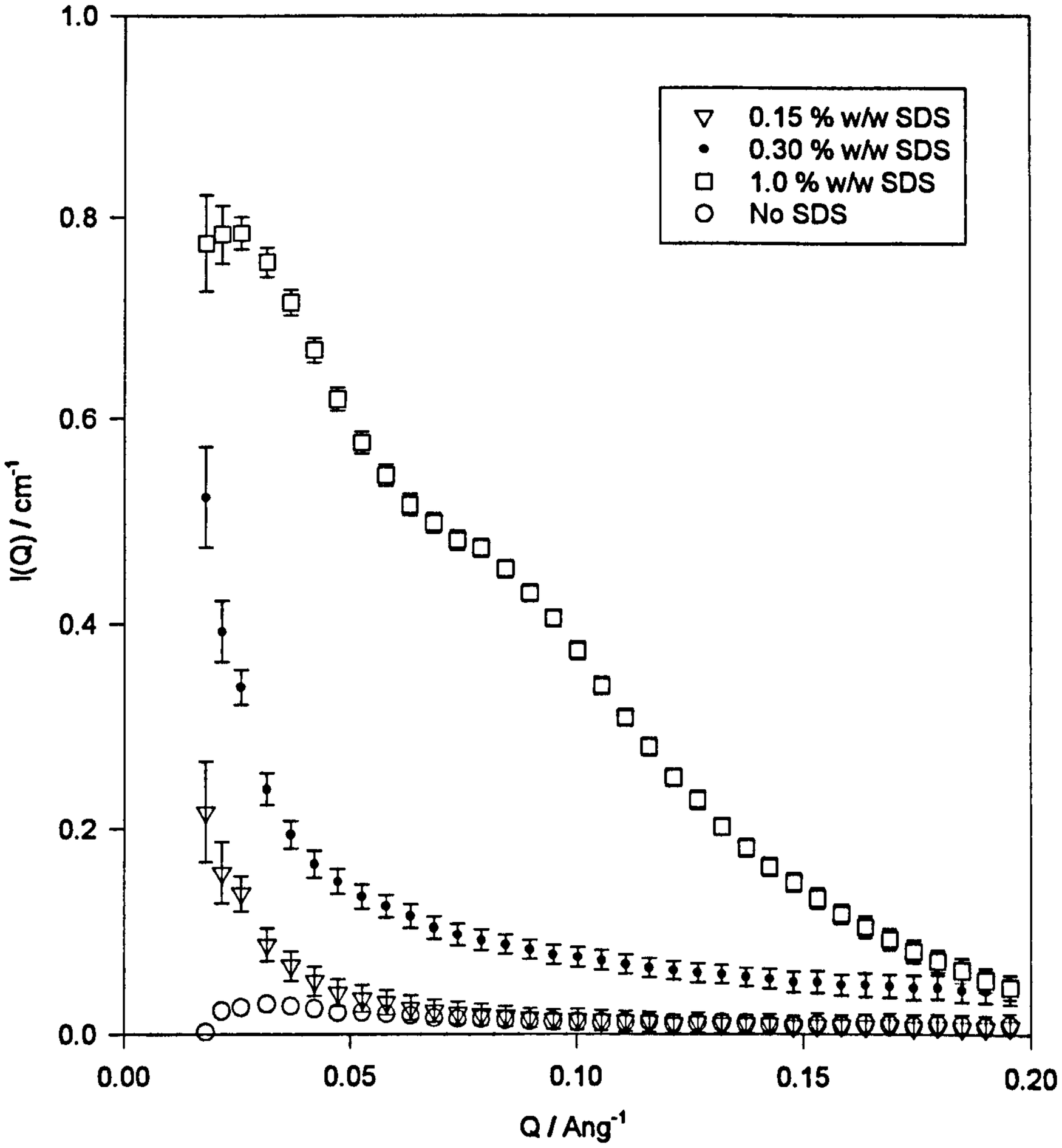

It was originally intended that the scattering patterns presented in **figure 8.22** and **figure 8.23** would be used to determine explicitly the interference term between the adsorbed polymer layer and the substrate. Unfortunately, the quality of the data was such that this was not possible.

8.5 Mixtures of PEO, SDS and silica

Figure 8.24 shows the scattering from aqueous dispersions of PEO, SDS and silica as a function of SDS concentration. Shown in the inset of this figure are the same data at very low Q values.

Figure 8.24

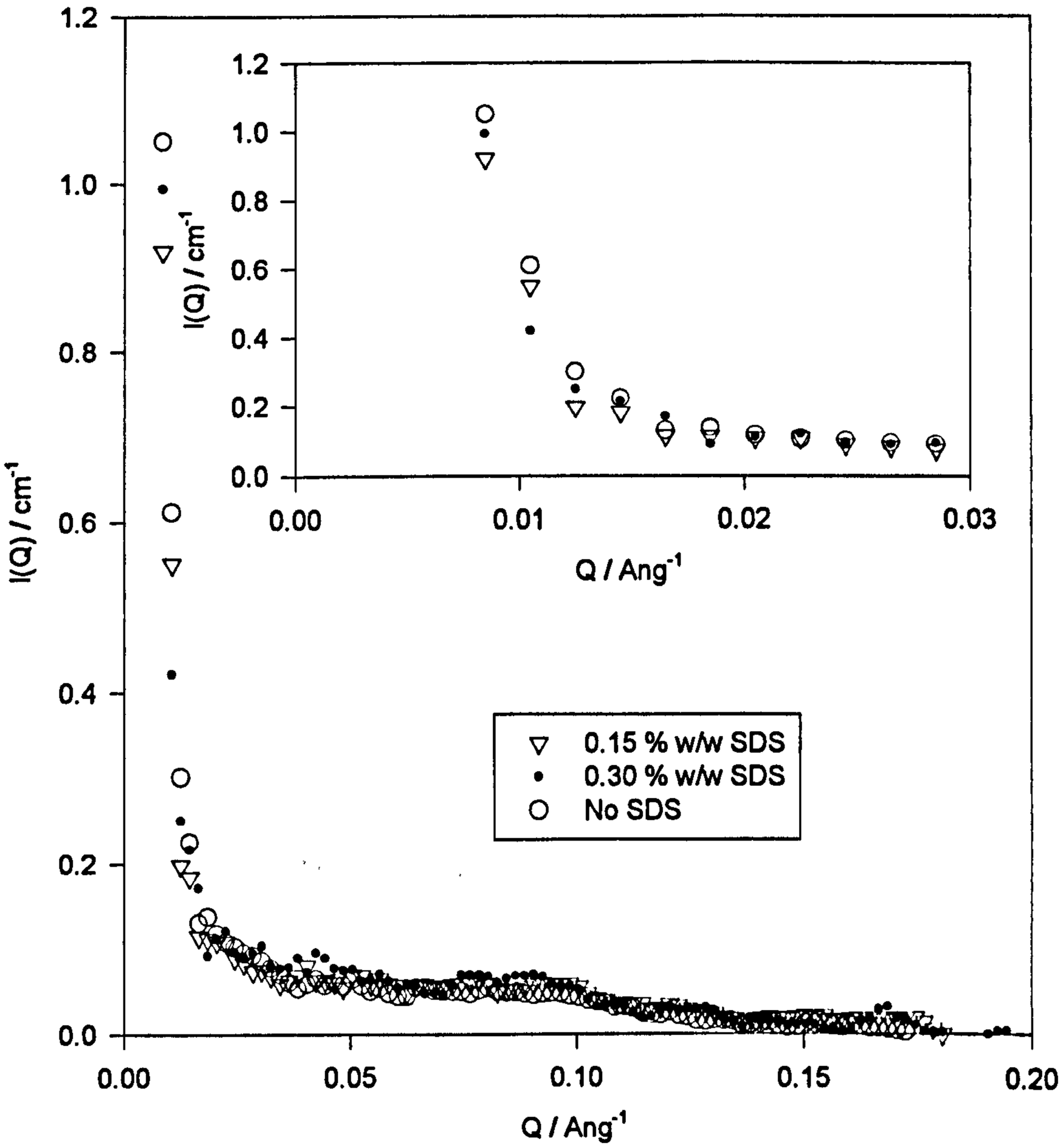

The incoherent background had been subtracted and the scattering length density of the solvent is the same as that of the silica dispersion. Furthermore, the SDS is a mixture of H-SDS and D-SDS to the same scattering length density as the solvent. Therefore, the only component which should be visible to the neutrons is the polymer itself.

Evidently from this figure, the data are of very poor quality and hence data fitting proved difficult. If the first point is neglected (due to instrumental inaccuracies), the general trend shows that an increase in surfactant concentration results in a decrease in scattering intensity. This is a similar trend as that reported in

figure 8.18 for the PEO/SDS/PSL system. Therefore, it appears that the adsorbed layer behaves in a similar manner on both substrates.

Figure 8.25

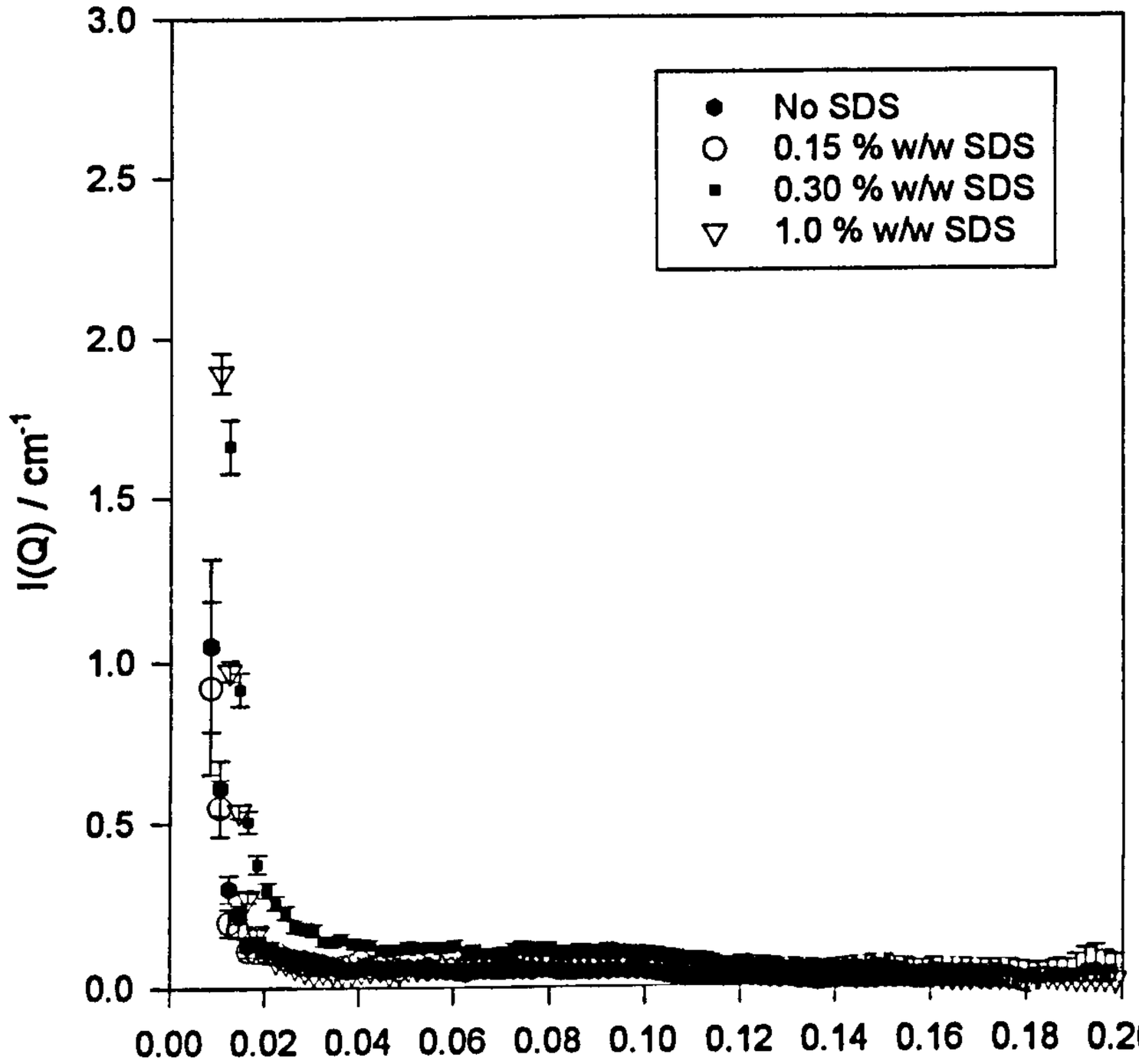

Due to the poor quality of these data (owing to only limited contrast between the polymer and the substrate), experiments were also performed where all of the components were visible. **Figure 8.25** shows the scattering from a series of silica dispersions at a solvent ratio of 30 % H_2O / 70 % D_2O. Each of these samples had polymer and varying concentrations of D-SDS. Under such conditions, the D-SDS is only partially visible.

In all cases the bare particle scattering has been subtracted. It can be seen that the sample in the absence of SDS has the highest scattering intensity and the sample with 1.0 % w/w SDS has the lowest scattering intensity. It is also evident that the

shape of the scattering pattern changes with increasing SDS concentration suggesting significant changes in the adsorbed layer structure.

8.6 Conclusions.

These small angle neutron scattering measurements have shown that the structure of PEO is significantly affected in the presence of SDS, with both the adsorbed amount and shape of the volume fraction profile altering dramatically. On a polystyrene latex substrate, the adsorbed amount is reduced by a factor of almost 5 in the presence of SDS around its normal CMC and the resultant layer thickness at this surfactant concentration is negligible. On increasing the surfactant concentration further, no quantitative information on the layer could be elucidated, but the DLS measurements (reported in Chapter 6) suggested a much larger hydrodynamic thickness of adsorbed layer. The SDS scattering at this concentration indicated two types of SDS moieties; one corresponding to solution SDS and one to SDS bound to polymer adsorbed at the interface.

References.

1. Higgins J. S., Benoît H. C.; *Polymers and Neutron Scattering*; Oxford Science Publications 1994 64
2. Cabane B.; *J. Physique* **1982** 43 1529
3. Higgins J. S., Benoît H. C.; *Polymers and Neutron Scattering*; Oxford Science Publications 1994 170
4. Auvray L., de Gennes P. G.; *Europhys. Lett.* 2 647
5. Higgins J. S., Benoît H. C.; *Polymers and Neutron Scattering*; Oxford Science Publications 1994 174
6. Hayter J. B, Penfold J; *Molecular Physics* **1981** 42(1) 109
7. Mukerjee P., Mysels K. J.; C in *Critical Micelle Concentrations of Aqueous Surfactant Systems*. Nat. Stand. Ref. Data System **1971**, Superintendent of Documents US Government Printing Office, Washington DC 20402 USA
8. Cosgrove T., White S. J., Zarbakhsh A., Heenan R. K., Howe A. M., *Langmuir*
9. Mukerjee P., Mysels K. J.; *"CMC's of aqueous surfactant systems"*. Nat. Stand. Ref. Data System **1971**. Superintendent of Documents. US Government Printing Office, Washington DC. 20402 USA.
10. Chari K., Antalet B., Lin, M. Y., Sintra S. K.; *J. Chem. Phys* **1994** 100(7) 5294
11. Shirahama K.; *Colloid and Polymer Science* **1974** 252 978
12. Shubin V.; *Langmuir* **1994** 10 1093

Chapter 9.

Comparisons with Other Systems.

9.1 Poly(NIPAM) microgel and SDS

Dynamic light scattering, small-angle neutron scattering and binding isotherm measurements have been performed on an aqueous poly(N-isopropylacrylamide) (poly(NIPAM)) microgel in the presence of the surfactant sodium dodecyl sulphate (SDS). Two surfactant concentrations (1.0 % w/w and 0.3 % w/w) were used for the neutron scattering experiments and through selective deuteration of the solvent, the different components, either the poly(NIPAM) microgel or the SDS were rendered 'invisible' to the neutrons. The microgel concentration was at 2.0 % w/w.

9.1.1 Scattering Theory Relevant to the Poly(NIPAM) microgel.

As discussed in chapter 4 of this thesis, the scattering intensity for a dilute dispersion as a function of Q comprises of an intraparticle interference factor, P(Q), and a factor dependant upon the chemical composition. The intraparticle interference is dependant upon the size and shape of the scattering bodies. For a dispersion of non-interacting spherical particles (p) of radius r, volume V_p the scattering intensity I(Q) may be given by

$$I(Q) = V_p^2 N_p (\Delta\rho)^2 \left[3 \frac{(\sin Qr - Qr\cos Qr)}{(Qr)^3} \right]^2 \qquad [9.1]$$

where N_p is the number of particles per unit volume, r is the particle radius and $\Delta\rho$ is the difference in scattering length density between the solvent and the particle.

Shibayama[1] *et al* performed small-angle neutron scattering measurements on poly(NIPAM) microgels. For the microgels in that study an excess scattering due to the presence of cross links was observed at very low values of Q. At low temperatures the scattered intensity function was fitted to a Lorentzian - Gaussian combination of functions such that,

$$I(Q) = I_{(G)}(0)\exp(-\varphi^2Q^2) + \frac{I_{(L)}(0)}{1+\xi^2Q^2}$$

[9.2]

where I_G is the Gaussian intensity and I_L is the Lorentzian intensity. The Gaussian intensity results from solid like inhomogenities having a characteristic size φ. The Lorentzian part of the scattering arises from the liquid like nature of the local concentration fluctuations of the gel (which are on a smaller scale than φ and hence are observed more at high Q values). These can be characterised with a thermal blob dimension, or mesh size, of ξ (the correlation length). A similar model, the Lorentzian - Debye model, has also been used successfully in characterising the bio-polymer gelatin[2] which also forms similar structures. Complex structures have also been probed by a combination of a Q^{-4} dependence and the Debye - Beuche equations[3,4,5]. In this thesis we shall use a combination of the Q^{-4} dependence (at low values of Q which is sensitive to larger scales) and the Lorentzian term in equation 9.3 (at high values of Q), such that,

$$I(Q) = AQ^{-4} + \frac{I_L(0)}{1+\xi^2Q^2}$$

[9.3]

where A is a constant.

9.1.2 Binding Isotherms

The degree of SDS binding to the poly(NIPAM) microgel was measured directly by equilibrating the gel in SDS solutions, centrifuging the dispersed gel and measuring the SDS concentration remaining in the supernatant. These measurements were performed by Dr. Y. Deng.* The results are shown in **Figure 9.1**.

Figure 9.1.

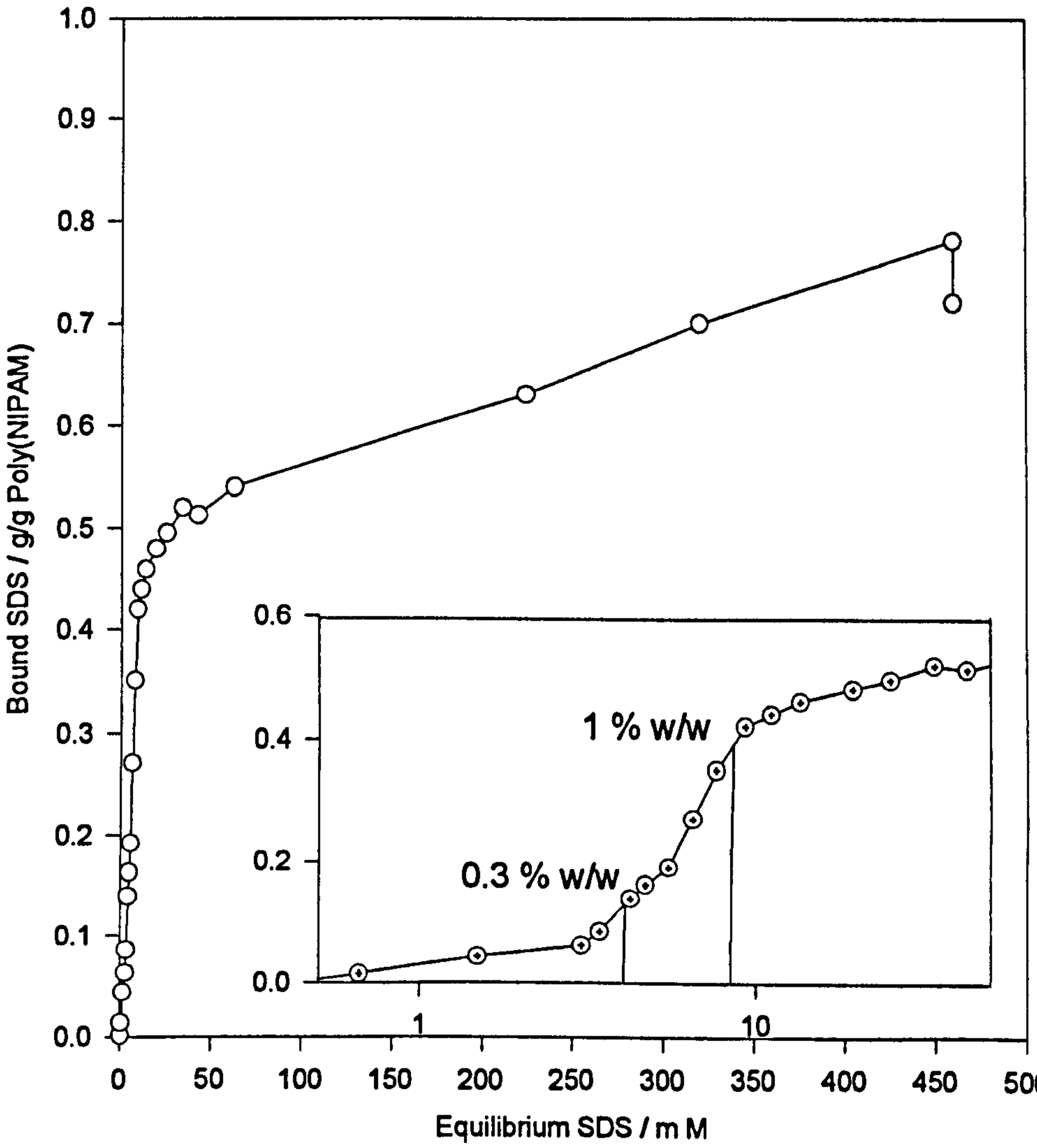

At 23 °C the SDS binding increased sharply above an equilibrium SDS concentration of 3 mM until the CMC (8.3 mM). The SDS binding to the

* Georgia Institute of Pulp and Paper Technology, Georgia, USA

poly(NIPAM) microgel slowly increased above the CMC with increasing surfactant concentrations. Thus, at room temperature there appeared to be two binding regimes with a crossover approximately at the normal CMC of SDS. The highest measured amount of bound SDS was about 0.8 g SDS per g of poly(NIPAM) microgel; this approximately corresponds to 0.3 surfactant molecules per amide repeat unit. From this binding isotherm two surfactant concentrations were chosen for the SANS experiment; one at 0.3 % w/w SDS (≈10 mM) and the other at 1.0 % w/w (≈ 36 mM). **Table 9.1** shows the binding data for these surfactant concentrations calculated from the data in **Figure 9.1**

Table 9.1: **Binding Data for the two SDS concentrations used in the SANS Experiments.**

Total Surfactant Concentration	**36 mM (=1% w/w)**	**10 mM (=0.3 % w/w)**
Bound SDS (mM)	27.24	6.05
Free SDS (mM)	8.76	3.95
Adsorbed Amount (g SDS / g poly(NIPAM) microgel	0.393	0.087

From **Figure 9.1** it is evident that the lower surfactant concentration corresponds to the onset of the high affinity binding regime whilst the higher surfactant concentration corresponds to a position on the knee of the isotherm. A bound amount of 0.393 g SDS/g poly(NIPAM) microgel (for the highest surfactant concentration) corresponds to a molar ratio of 0.151 SDS to poly(NIPAM) or approximately 6 poly(NIPAM) repeat units per SDS monomer. The lower SDS concentration corresponds to around 30 poly(NIPAM) repeat units per SDS monomer. These results are lower than those found by Schwuger[6] for the SDS/PEO system which indicated that at maximum binding 1.3 ethylene oxide units were bound per SDS molecule, but may simply reflect the smaller monomer

size of the ethylene oxide unit or the spatial restrictions imposed by the microgel structure.

9.1.3 SANS measurements on the Pure Microgel.

The first requirement of the SANS study was to find the scattering length density of the polymer latex in order to match the scattering length density of the solvent to that of the polymer microgel. This was determined, by using various ratios of H_2O and D_2O, to be at 18% D_20 (by weight) which corresponds to a scattering length density of the poly(NIPAM) microgel of 5.88×10^{-7} Å^{-2}. This H_2O/D_2O ratio was used for all subsequent 'on contrast' measurements. The scattering length density obtained by experiment is averaged over the whole particle and can be compared with the calculated value of 7.94×10^{-7} Å^{-2}. The difference in these values is due to the physical density of microgel being less than the pure homopolymer used for the calculation. The SANS measurements performed on SDS alone have been already discussed in Chapter 8, section 8.1.3

9.1.4 Mixtures of SDS and Poly(NIPAM) microgel - Poly(NIPAM) microgel visible, SDS invisible.

The scattering from the poly(NIPAM) microgel for two different SDS concentration is shown in **Figure 9.2.** The SDS is deuterated, the poly(NIPAM) microgel hydrogenous and the solvent is D_2O. Under these conditions the scattering length density of D-SDS and D_2O are almost identical and hence the scattering from the D-SDS is strongly suppressed.

Figure 9.2

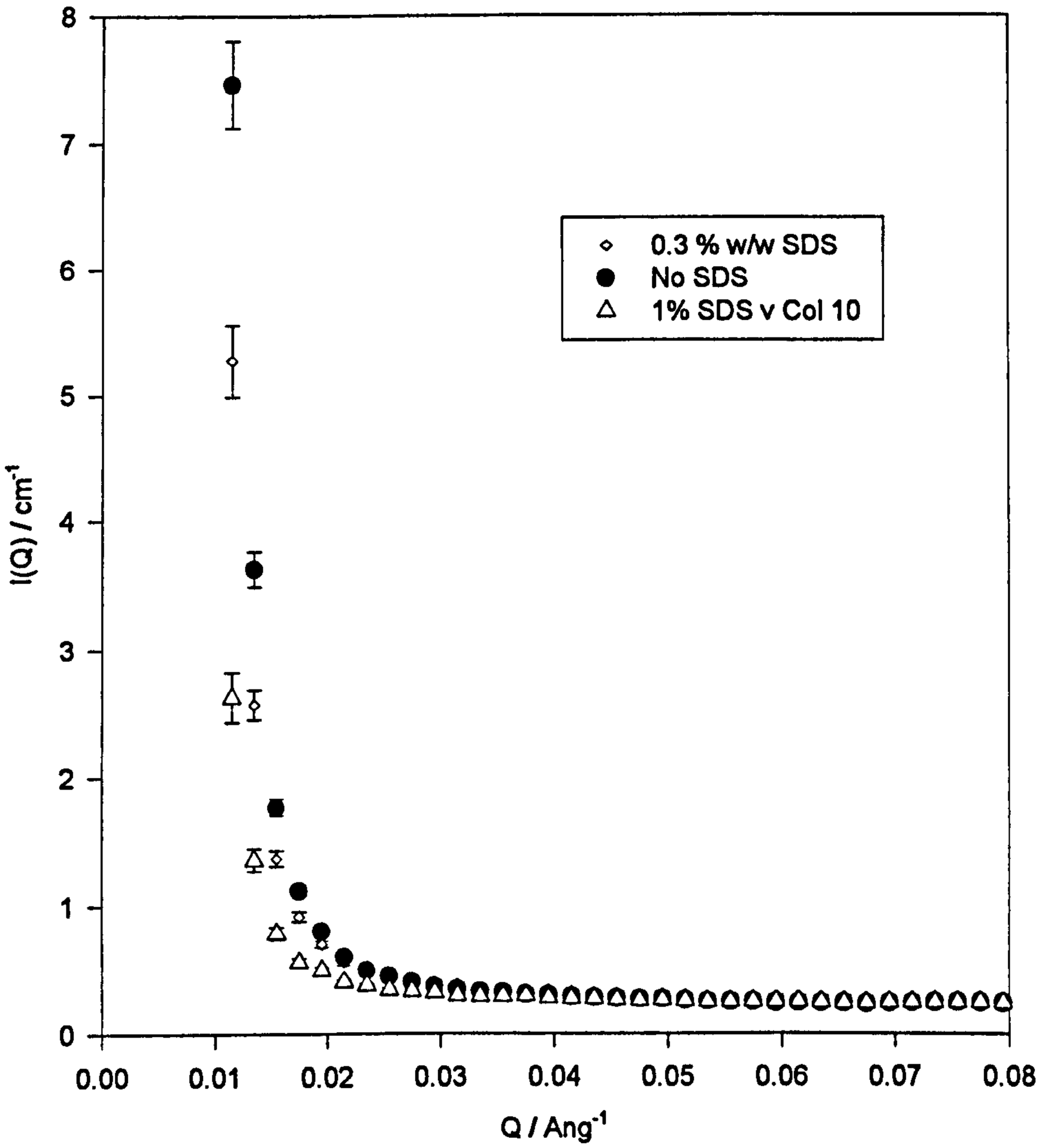

In comparing the scattering from the mixture to that of pure poly(NIPAM) microgel it can be seen that the poly(NIPAM) microgel in the absence of SDS has a much higher scattering intensity than either of the two samples with SDS. In order to extract qualitative data from these scattering patterns the background level was first subtracted. This was achieved by plotting $Q^6I(Q)$ against Q^6. The slope of this plot was the value of incoherent background. Next, the Q^{-4} dependence at very low values of Q was obtained and subtracted by fitting the first 10 points to an AQ^n+B dependence. n was fixed at -4 and B was the value obtained from the previous plot for the background level. This Q^{-4} dependence

and background level was then subtracted from the original data series. The data remaining showed a linear dependence with 1/I(Q) against Q^2 at higher values of Q. Therefore a plot of 1/I(Q) against the resultant Q^2 yielded a straight line with the correlation length being equal to the square root of the slope divided by the intercept. **Figure 9.3** shows data for poly(NIPAM) in the absence of SDS plotted as log I(Q) against log Q. Shown on this figure is the Q^{-4} and Q^{-2} dependence.

Figure 9.3

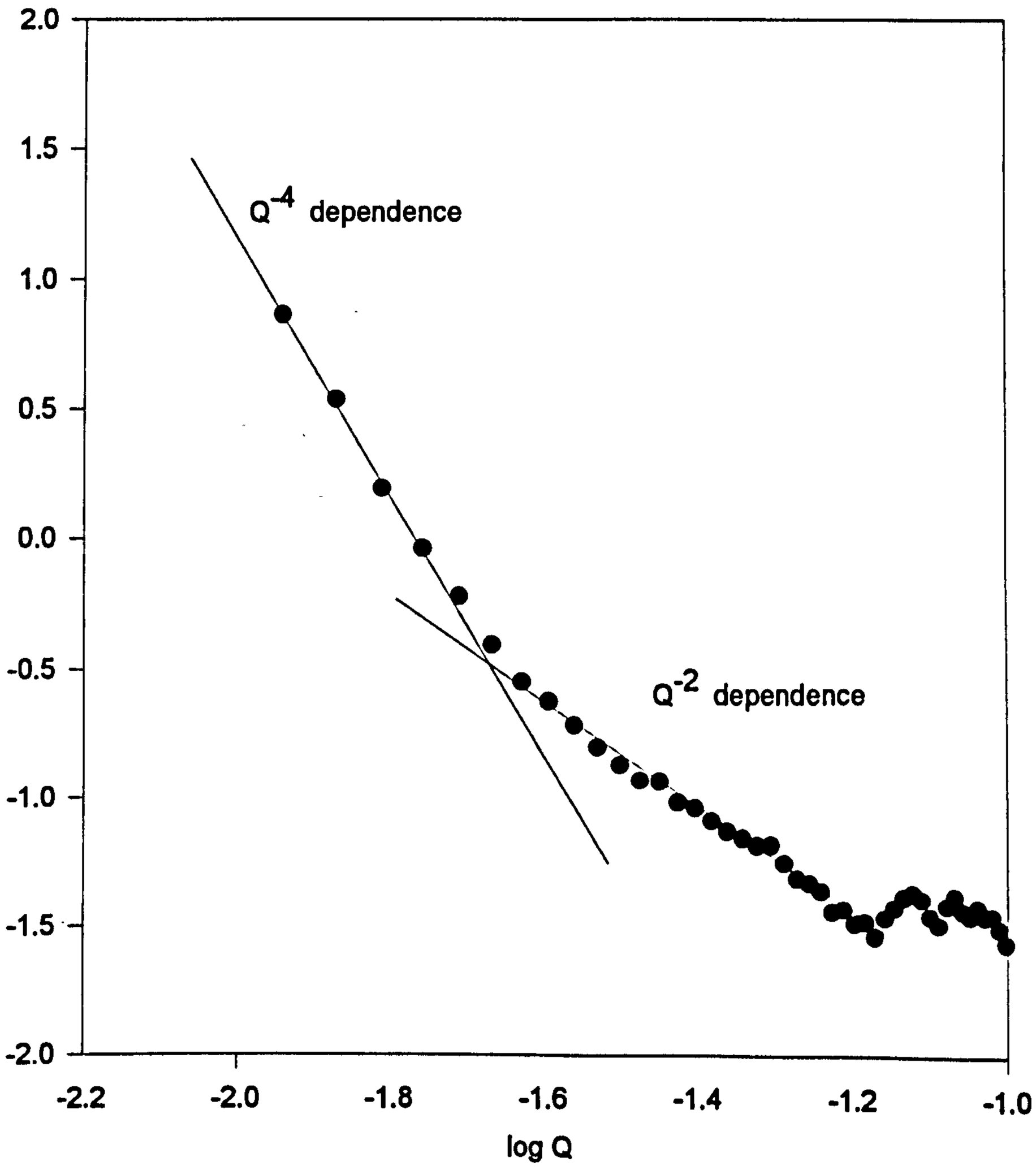

The parameters obtained for the poly(NIPAM) microgel as a function of SDS are given in **Table 9.2**. Also shown in **Table 9.2** are the data obtained from dynamic light scattering measurements.

Table 9.2: **Typical Fitted Parameters for poly(NIPAM) microgel using the Debye Model.**

Parameter	Amount of SDS		
	0	0.3 % w/w	1% w/w
Radius from DLS / Å	720 ± 50	935 ± 50	1040 ± 50
ξ / Å	18.17	27.52	31.93
ξ ÷ r	0.0252	0.0294	0.0307

The microgel swelling results from the DLS measurements in **Table 9.2** reflect the binding isotherm in **Figure 9.1**. The binding isotherm measurements showed that SDS binding increased over the whole range of SDS concentrations studied. Thus, it seems clear that surfactant binding continues to increase even above the normal CMC of SDS where, in normal circumstances, the activity of surfactant monomers is approximately constant. The value of ξ is a characteristic size related to the mesh of the microgel. From **Table 9.2** it is evident that this size also increases over the whole concentration range studied; at 1.0 % w/w the increase in ξ compared to that in the absence of SDS reflects five-fold increase in 'mesh volume'. The DLS measurements indicated that the volume of the microgel increased by a factor of about three on addition of SDS. In the absence of surfactant, the mesh size was approximately 18 Å whilst the addition of 0.3 % w/w increased the mesh size to approximately 27 Å which could hold aggregates of 2 or 3 SDS monomers bound together in small clusters. On the other hand, at the higher SDS concentration studied, the value of ξ has increased to 32 Å - large enough to permit the formation of small internal micelles.

9.1.5 Mixtures of SDS and Poly(NIPAM) microgel - Poly(NIPAM) microgel visible, SDS visible.

The effect of poly(NIPAM) microgel on 0.3 % w/w SDS can be seen in **Figure 9.4** and for 1.0 % w/w in **Figure 9.5.** For these samples the solvent was 18 % w/w D_2O/ 2 % w/w H_2O which has the same scattering length density as the poly(NIPAM) microgel. The SDS was deuterated and the difference in scattering length density between it and the solvent was 6.14 x 10^{-6} $Å^2$. Also shown for comparison is the scattering for SDS in the absence of poly(NIPAM) microgel. For the latter sample the SDS was hydrogenous and the solvent was D_2O; the difference in scattering length density between the solvent and the SDS was 6.00 x 10^{-6} Å . Therefore, the intensity of the scattering and transmission in the absence of poly(NIPAM) microgel has been scaled accordingly to allow for these changes.

Although the 0.3 % w/w SDS showed a weak structure peak at a Q value of 0.035 $Å^{-1}$ in the absence of poly(NIPAM) microgel, this disappeared upon the addition of the microgel, indicating that the polymer bound SDS was either too dilute, or in units too small to be detected by neutrons. Similarly, in the absence of any poly(NIPAM) microgel the 1.0 % w/w SDS showed a well defined structure peak at a Q value of 0.05 $Å^{-1}$ and an intensity of approximately 0.78 cm^{-1}. In the presence of poly(NIPAM) microgel this intensity is significantly reduced (to around 0.25 cm^{-1}) and the structure peak has shifted to a much higher value of Q,(~ 0.09 $Å^{-1}$) which now corresponds to an approximate centre-to-centre distance of 70 Å compared with a centre-to-centre separation in the absence of poly(NIPAM) microgel of 150 Å. Based on the binding isotherm (**Figure 9.1**) the concentration of free SDS in the bulk was 8.8 mMol (**Table 9.1**) which is close to the CMC of SDS. Therefore, free SDS micelles in the bulk should also be formed. Consider the scattering of SDS at 0.3 % w/w (from **Figure 9.4**), the structure peak occurs at a Q value and intensity of around 0.05 $Å^{-1}$ and 0.20 cm^{-1} respectively. Transferring these values to **Figure 9.5** it is evident that at a Q

value of 0.05 $Å^{-1}$, the intensity is very close to 0.2 cm^{-1} suggesting the existence of free micelles similar to those formed in the absence of poly(NIPAM) microgel at concentrations just above the CMC.

Figure 9.4

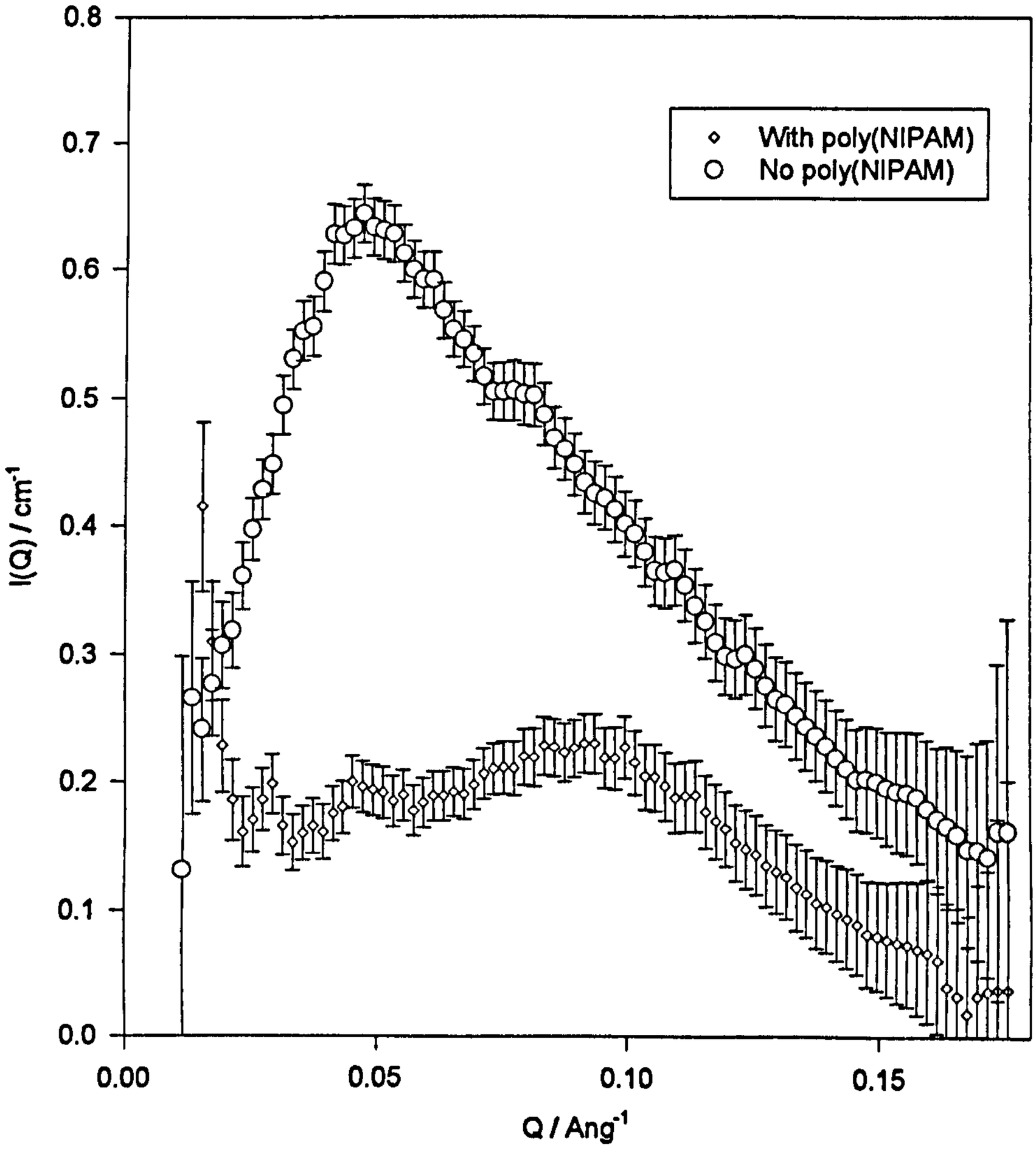

Figure 9.5

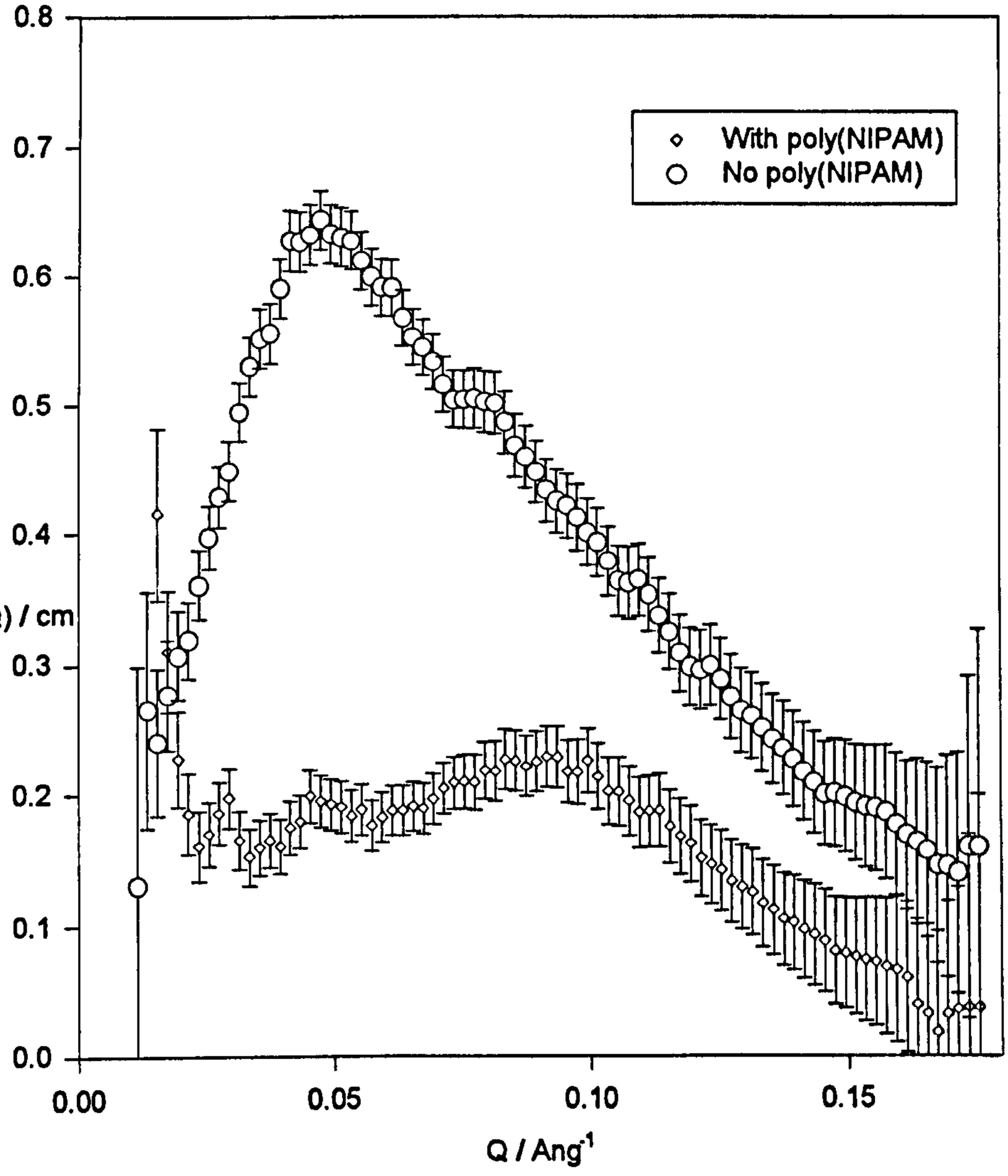

Moreover, the shift of the majority of the structure peak to a higher value of Q with the addition of poly(NIPAM) microgel indicates that the scattering centres are closer together, presumably bound to the microgel. The sharp decrease in the intensity of a structure peak with polymer addition suggests that the SDS scattering centres are either smaller, or that there are less of them. Therefore, it is proposed that the SDS is present as much smaller surfactant aggregates than conventional micelles.

These results are in stark contrast to those reported for other polymer/surfactant systems. For example in the gelatin/SDS system, the binding of SDS above the CMC causes a disruption in the gelatin mesh, resulting in the gelatin structure factor following that of the adsorbed SDS[7]. In the adsorbed state, the SDS micelles are larger (our micelles are smaller), even though the CMC occurs at a lower SDS concentration. As in our system, the bound micelles are closer together than those in the bulk, but this simply reflects the fact that the micelles are adsorbed. The PEO/SDS system, which is chemically closer to our system, shows very little change in the SDS scattering pattern on addition of PEO suggesting that bound SDS retains a very similar structure to that of the bulk. At high surfactant concentrations (above 1.0 % w/w) the PEO scattering follows that of the SDS, suggesting that the PEO structure begins to resemble that of the surfactant. This effect is similar to that observed with gelatin, but is not evident for the poly(NIPAM) microgel, again implying that the structure of poly(NIPAM) microgel bound SDS is very different to that in other polymer/surfactant complexes. One possible explanation for the lack of structure in the poly(NIPAM) microgel scattering pattern, is that poly(NIPAM) microgel, (in contrast to PEO or gelatin), is chemically cross-linked and therefore is less flexible than these polymers and hence less accessible to larger micelles.

9.2 Quatrisoft LM, SDS and Polystyrene Latex.

Adsorption isotherm and small-angle neutron scattering experiments were performed on a hydrophobically modified cationic cellulose derivative (Quatrisoft LM) physically adsorbed onto a partially deuterated polystyrene latex. The effect of high concentrations of surfactant (SDS) on the structure of the adsorbed layer was studied. These results will be compared and contrasted to those obtained on macroscopic surfaces[8] and those for the homopolymer system discussed in the earlier chapters of this thesis.

Figure 9.6

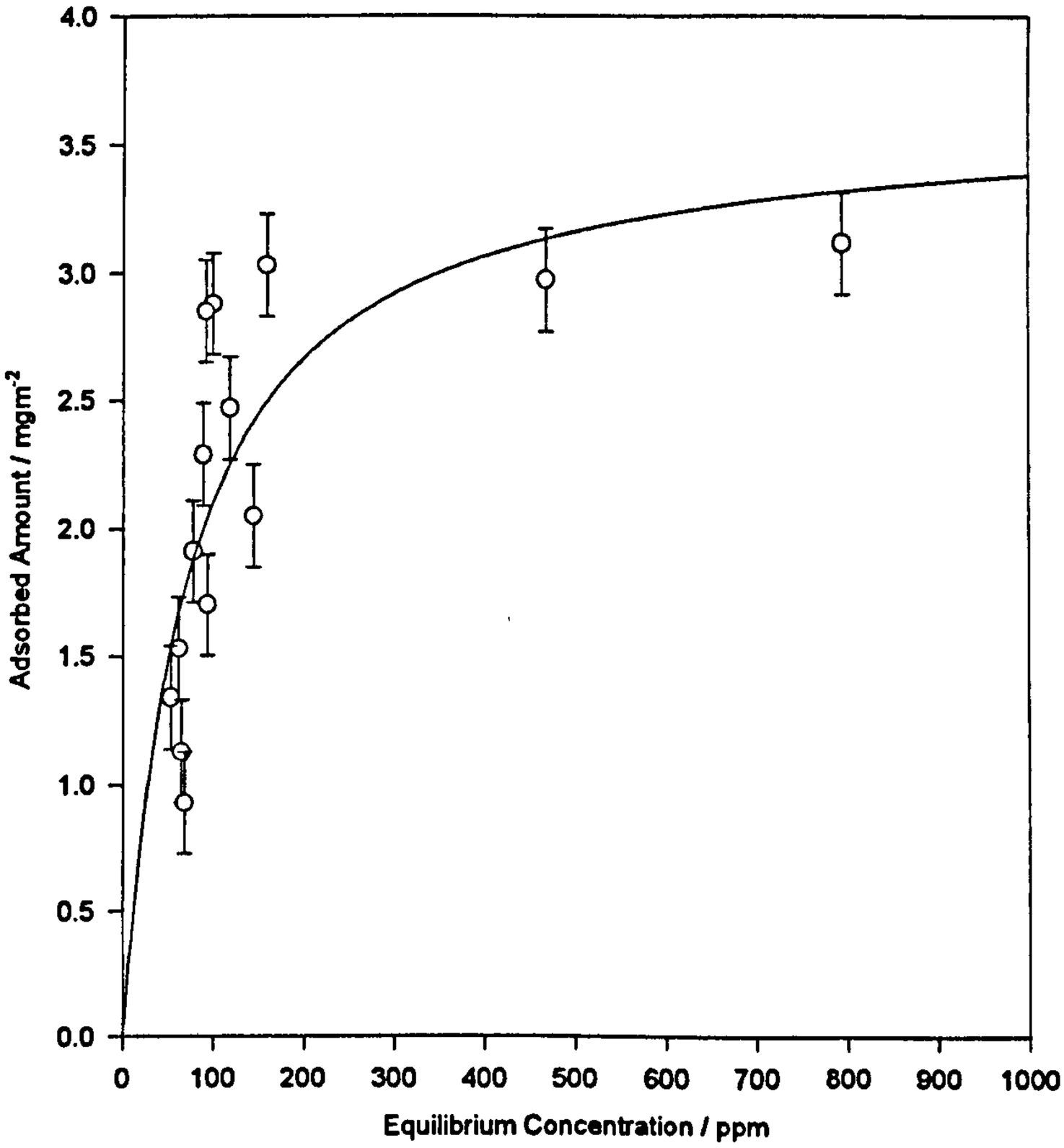

Figure 9.6 shows the adsorption isotherm of Quatrisoft LM physically adsorbed on polystyrene latex. The adsorption isotherm is of the high affinity type and yields an adsorbed amount of 3.0 mgm^{-2} + 0.1 mgm^{-2}. This adsorbed amount is higher than that reported by Shubin *et al*[8,9] on either a silica (1.6 mgm^{-2}) or a mica substrate. The most probable reason for this higher value of adsorbed

amount is that a polystyrene latex, in contrast to either the silica or mica, will have a large number of hydrophobic sites. Therefore, the binding will be through hydrophobic as well as electrostatic interactions. This value of the adsorbed amount was with an equilibrium polymer concentration of 500 ppm which was used for all of the SANS measurements.

For this experiment, samples were originally prepared covering a wide range of surfactant concentrations, but unfortunately it was found that phase separation occurred at all but the highest concentrations. Although the phase behaviour in the absence of a solid substrate was available[10] no information was available for the adsorbed system. The systems in the literature differ from the one in this thesis in that they used solid plates as substrates for which flocculation is not possible. Consequently, this discussion will be restricted to the effect of high surfactant concentrations on the adsorbed Quatrisoft layer.

Initially, experiments were performed on the latex as a function of the H_2O/D_2O ratio of the solvent in order to determine the solvent ratio for "contrast match" with the PSL. This was found to occur at a H_2O volume fraction of 0.014. This volume fraction of H_2O was used for all of the following "on contrast" measurements. Moreover, in order to examine further the structure of the adsorbed layer via the interference term between the adsorbed layer and substrate, experiments were performed under conditions where the scattering density of the solvent differed from that of the latex. It was chosen to perform these "off contrast" measurements in pure D_2O. Under these conditions the scattering from D-SDS is not visible since D-SDS has the same scattering length density as D_2O. Thus, problems in data analysis and sample preparation were lessened. For some of the "on contrast" measurements a mixture of D-SDS and H-SDS to the same scattering length density as the solvent, and indeed the latex. Under these conditions the scattering from the surfactant was also invisible. It was therefore possible to examine the scattering solely from the adsorbed polymer layer directly.

Figure 9.7

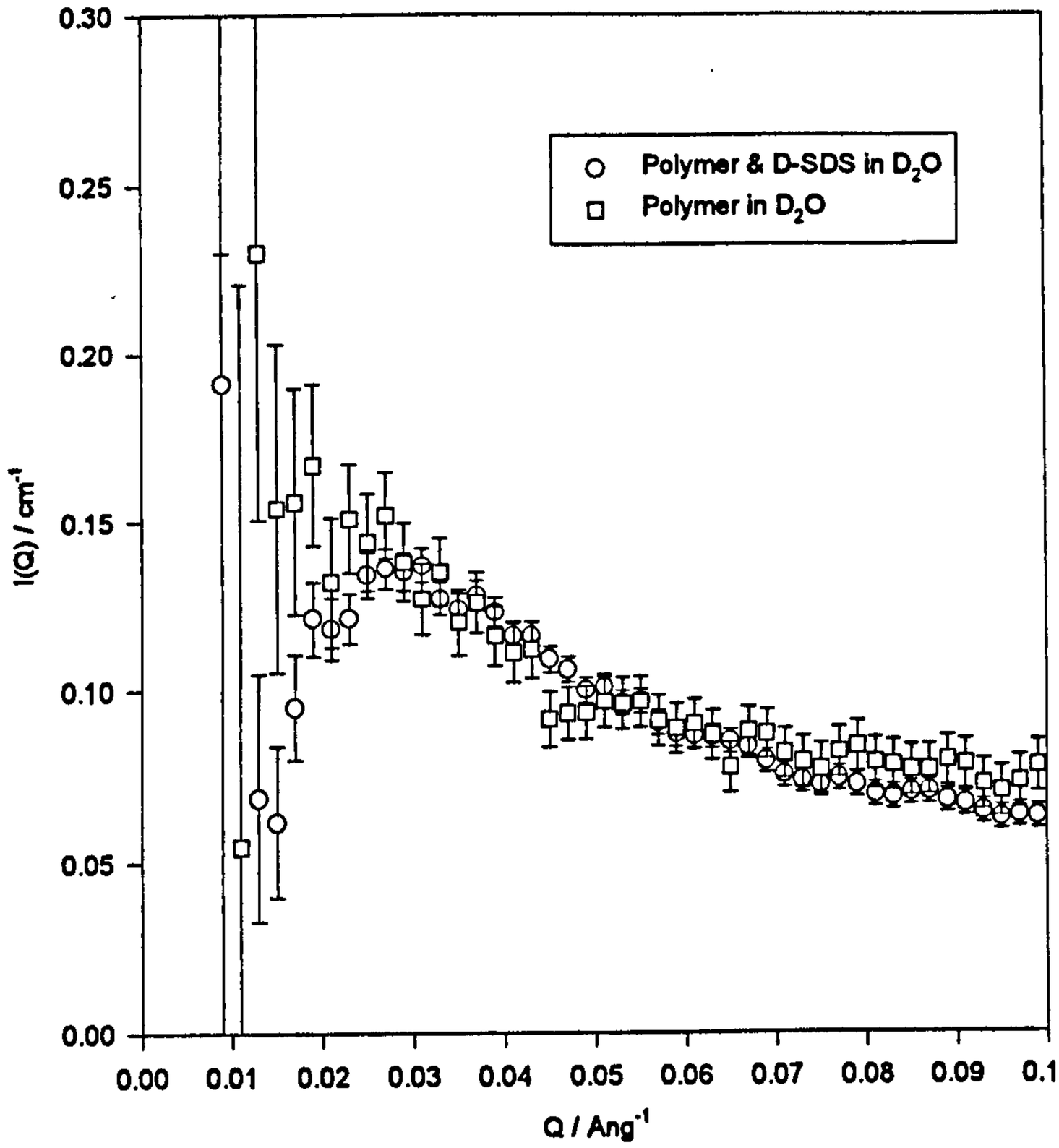

Experiments performed in the absence of polystyrene latex were performed in D_2O. The Quatrisoft LM concentration was maintained at 1.0 % w/w and either D-SDS or H-SDS was used. Experiments involving D-SDS enabled the scattering solely from the polymer to be observed, whilst those containing H-SDS enabled the scattering from both components to be investigated. Attempts to locate a "contrast match" point for the polymer in different H_2O/D_2O ratios were not successful owing to weak scattering from the polymer in solution and high levels of incoherent scattering.

The scattering from the polymer in solution with and without SDS is shown in **figure 9.7.** In the absence of surfactant the polymer scattering has an intensity of 0.3 cm^{-1} and decays to an incoherent level background level on around 0.03 cm^{-1}. This data has been treated to a Guinier approximation[10] and yields a radius of gyration of the polymer of 32 Å. In the presence of D-SDS (invisible) the

scattering at high values of Q is very similar to that in the absence of surfactant. However, at very low Q values a peak in this data can be observed at a Q value of 0.025 $Å^{-1}$. This can be attributed to the polymer wrapping itself around the surfactant and therefore taking on a degree of the micelle's structure. This behaviour is not uncommon and has been observed in the PEO/SDS system (Chapter 8) and the SDS/gelatin system[7]. The position of this peak corresponds to a centre-to-centre separation of the polymer chains of 250 Å.

Figure 9.8

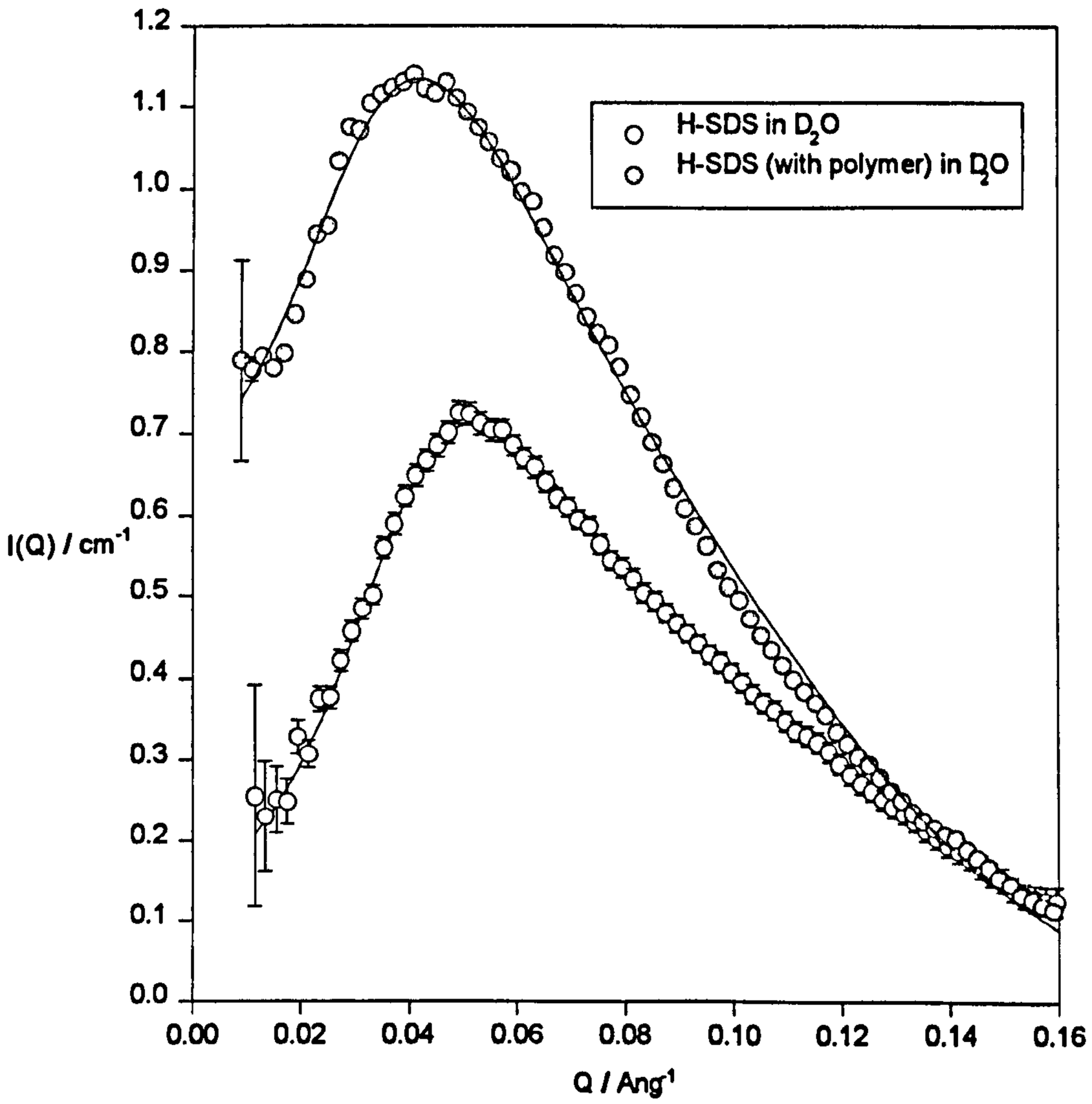

The scattering of H-SDS with and without Quatrisoft LM is shown in **figure 9.8.** The data in the presence of polymer has had the polymer scattering subtracted from it. As in the PEO/SDS case reported in Chapter 8, no allowance can be made for any interparticle interference term between the polymer and the

surfactant. The SDS concentration is maintained at 1.0 % w/w and both of these scattering patterns show a strong structure peak owing to interparticle interactions. Also shown on this figure are the fits to this data using the Hayter-Penfold model.

In the presence of Quatrisoft LM, the SDS scattering is now of a much higher intensity and the position of the peak has shifted to a slightly lower value of Q. The shift to a lower value of Q suggests that the centre-to centre separation of the micelles is larger in the presence of the polymer than for SDS alone. Attempts to fit the scattering in the presence of Quatrisoft LM to a double Hayter-Penfold model resulted in one set of parameters tending towards zero. In the presence of polymer, the micellar diameter was obtained as 43 Å, the Debye screening length as 44 Å and the number of surface charges as 17. This compares with a diameter of 33.7 Å in the absence of Quatrisoft LM. The increase in intensity is indicative of either more, or larger, micelles (see section 8.2.1 for modelled SDS scattering). In the SDS/gelatin system (which to a certain degree resembles this one) similar data were observed and again larger SDS micelles were reported., although the increase in intensity of the structure peak was larger than observed here. *For example*, a 2 % w/w SDS in the presence of 5 % w/w gelatin gave a micellar diameter of 48 Å, which compares with 42 Å for SDS alone at that concentration. This effect was not observed in the PEO/SDS case where the structure of the SDS in the PEO/SDS aggregate was very similar to bulk SDS micelles, or in the poly(NIPAM) microgel/SDS case reported earlier in this chapter, where much smaller SDS aggregates were observed.

The scattering pattern arising from the adsorbed polymer layer in the absence of surfactant is shown in **figure 9.9**. The solvent in this case is at the same scattering length density as the latex and hence only the scattering from the layer is visible. The adsorbed amount was measured at 3 mgm^{-2} and this, along with all other parameters in the fitting program, were allowed to float. The exponential volume fraction profile is also shown in **figure 9.9** which shows the adsorbed

layer with a span of 97.7 Å, which ties in well with previous measurements on adsorbed Quatrisoft LM layers[8,9] which give maximum layer thickness' on silica and mica of 85 Å and 70 Å respectively. This data fitting yielded an adsorbed amount of 2.38 mgm^{-2} and second moment of the layer of 12.93 Å The RMS thickness was 32.7 Å.

Figure 9.9

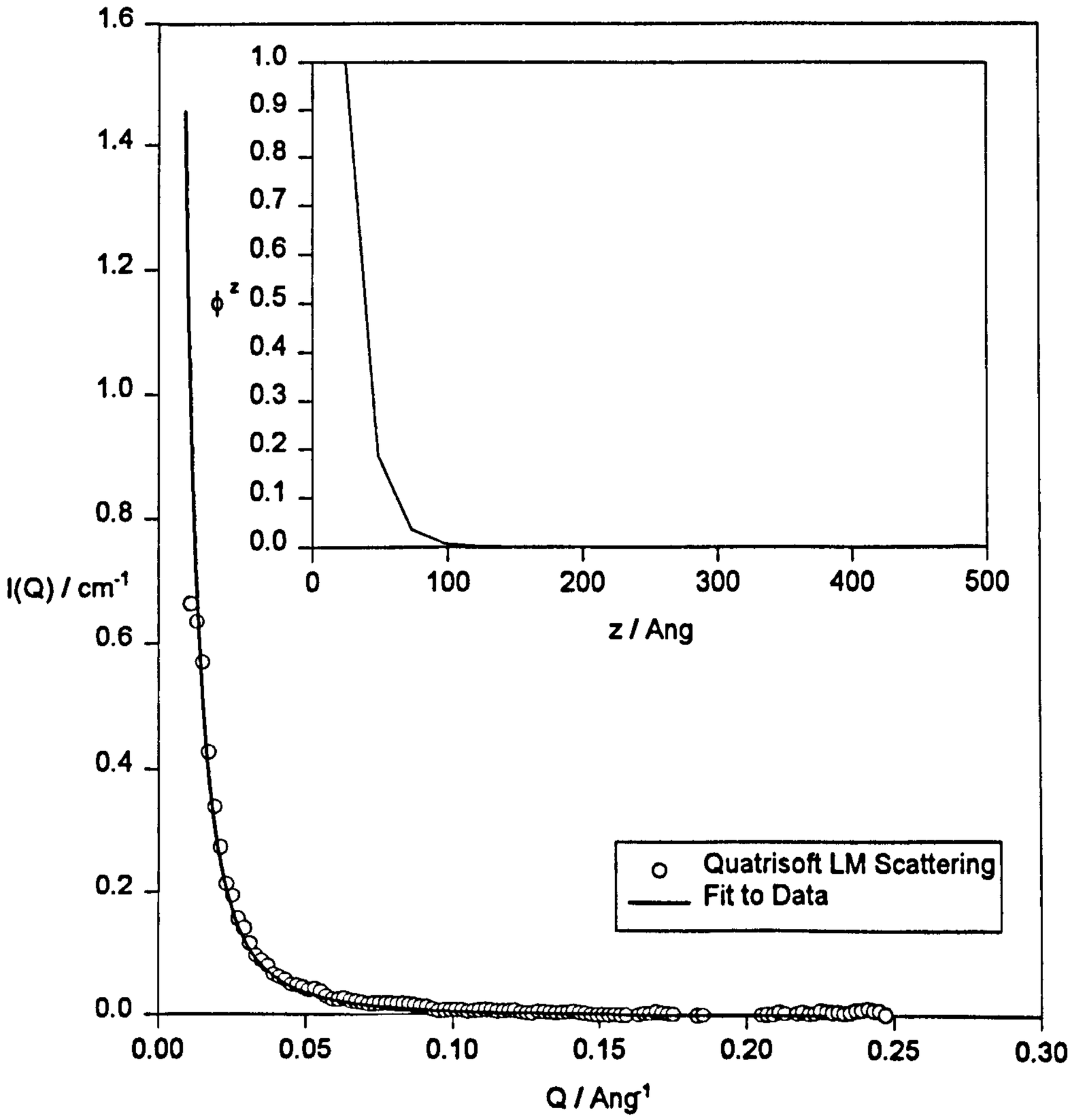

The effect of surfactant on the adsorbed Quatrisoft LM layer is shown in **figure 9.10**. The data using both and H-SDS (visible) and D-SDS (partially visible) is shown. Also shown is the data and fit for Quatrisoft LM in the absence of any surfactant.

Figure 9.10

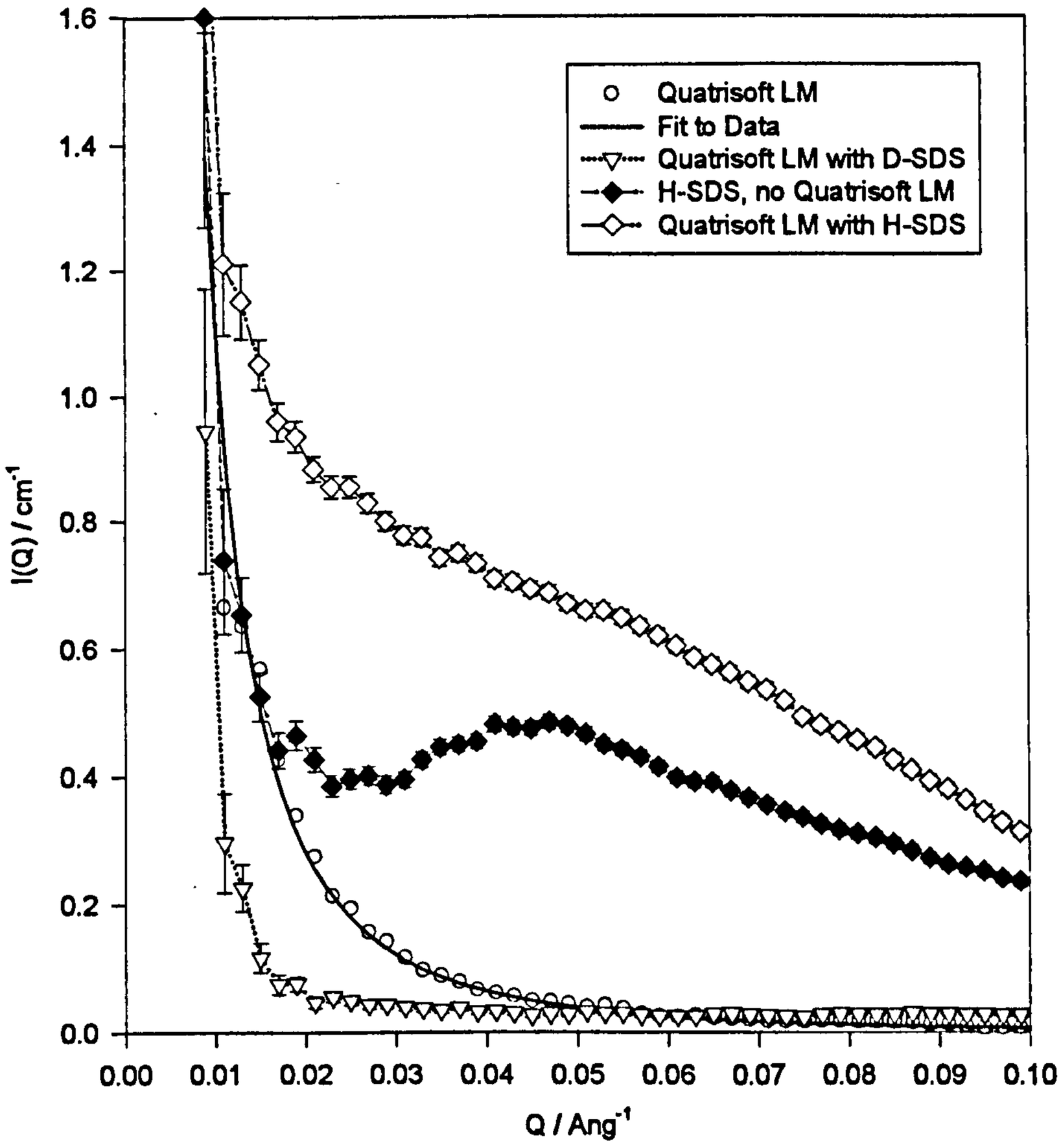

On addition of the D-SDS (where the scattering length density between the D-SDS and the solvent is very small), it is evident that the intensity of the scattering from the adsorbed layer is significantly reduced. This tends to suggest that the structure of the polymer is changing significantly. The scattering with H-SDS (which is visible) shows a very wide structure peak, which is significantly different to that of SDS in solution or adsorbed SDS without polymer. Attempts to fit this data to a either a Hayter-Penfold or a double Hayter-Penfold model were unsuccessful, but it still possible that part of this scattering arises from SDS bound to adsorbed polymer and part arises from SDS bound to free polymer.

9.3. Quaternised poly(vinyl pyridine) / SDS

Only a very limited study has been performed using this quaternised polystyrene-poly(vinyl pyridine) (PS-PVP$^+$). Many problems have been encountered mainly due to the lack of characterisation of the polymer. GPC's were difficult to obtain due to the charged nature of the polymer and microanalysis proved less than fruitful (mostly due to the high molecular weight of the iodine counter ion). High resolution NMR measurements were performed at and these were much more useful. These showed well defined aromatic and aliphatic bands. The aromatic bands corresponded well to library spectra of polystyrene and poly (vinyl pyridine). The relative peak heights were used to estimate the relative block sizes of the polystyrene and the poly (vinyl pyridine). Although only a rough estimate, these results suggested that the PS-PVP$^+$ ratio was greater than 1:7 and less than 1:10.

9.3.1. UV Absorbance Studies

Initially experiments were performed using UV spectrophotometry to ascertain firstly whether the polymer adsorbed in the UV region of the spectrum, whether this UV absorbance was directly concentration dependant and whether SDS interfered with this absorption. It was observed that in the region 0-150 ppm polymer there was a linear relationship between UV absorbance and polymer concentration at a wavelength of 266 nm. As the concentration increases the shape of the peaks (especially at lower wavelengths) became less well defined.

In order to check whether SDS interferes with this calibration a series of 50 ppm polymer samples were prepared, each one containing a different concentration of SDS ranging from 0 - 10,000 ppm. The UV absorbance of each of these was recorded and expressed as the (absorbance in the absence of surfactant)/(absorbance in the presence of surfactant). These results are shown in **table 9.3**

Table 9.3 **Effect of SDS on the UV absorbance of PS-PVP+.**

Polymer Concentration / ppm	SDS Concentration /ppm	$\frac{\text{Abs(nosurfactant)}}{\text{Abs(withsurfactant)}}$
50	0	1
50	2095	0.7266
50	4040	0.8699
50	6060	0.8163
50	7635	0.8527

The data in this chart appears somewhat erratic but definitely shows some effect with SDS concentration. It is possible that beyond the normal CMC of SDS that this effect appears to be constant. Since, presently in the adsorbed system, there is no way of telling where the SDS species are, it is unlikely that UV spectrophotometry would be a suitable method for adsorption studies in the presence of surfactant.

The adsorption isotherm for PS-PVP^+ was determined by adding a known surface area of Snowtex ZL particles to a known concentration of polymer. These samples were shaken and allowed to stand overnight to allow adsorption equilibrium to be reached. The sample was then centrifuged at 6,500 r.p.m. until no more solid was deposited (approximately 10 mins). To 200 μl of the supernatant, 2 ml of water was added to enable the supernatant concentration to fall within the linear region of the calibration plot. From the initial concentration and the final equilibrium concentration the amount of polymer adsorbed was determined and expressed in terms of mgm^{-2}. **Figure 9.11** gives the adsorption isotherm. The isotherm is of high affinity and gives and adsorbed amount of approximately 0.9 mg m^{-2}.

Figure 9.11

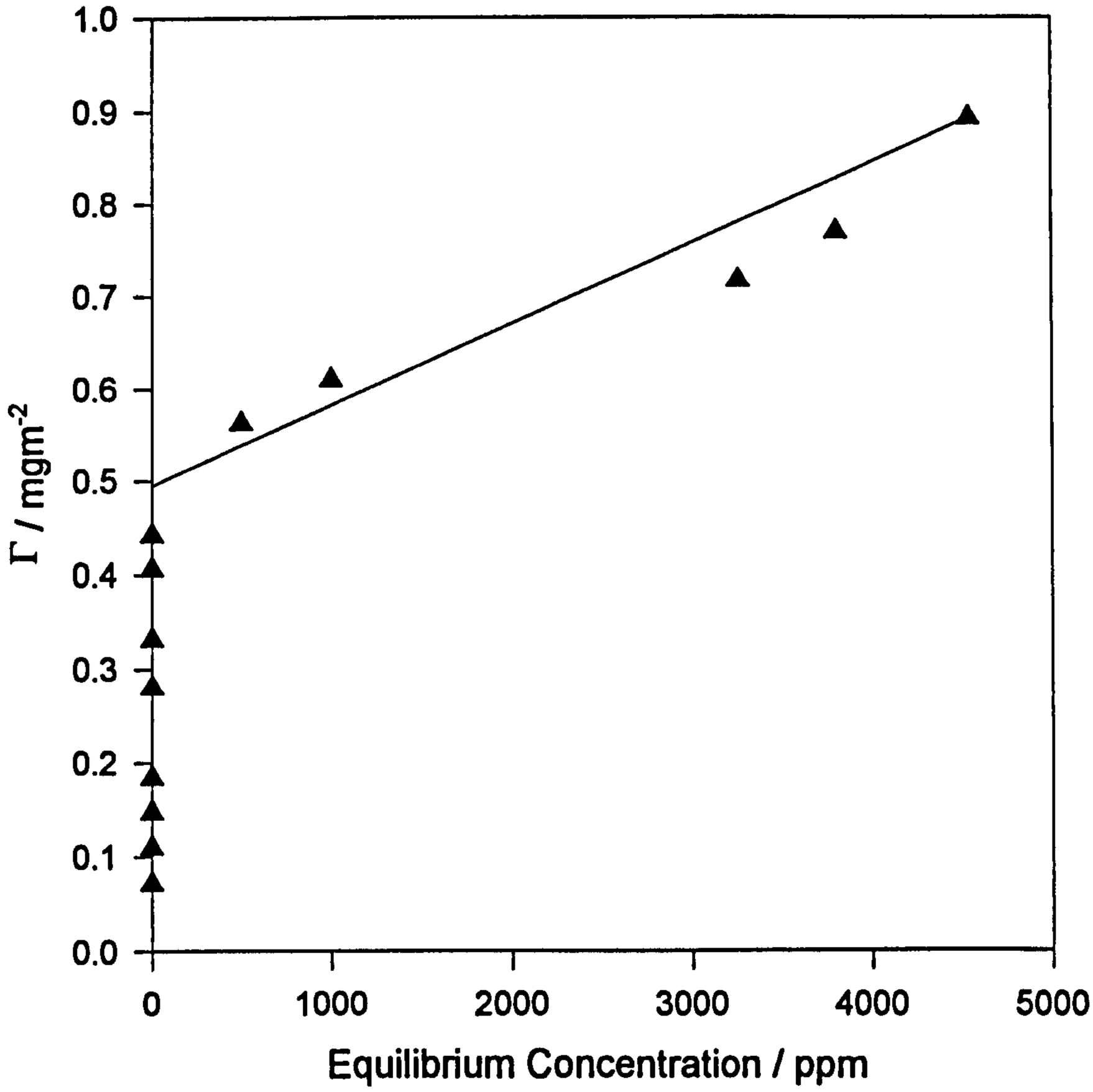

9.3.2 Photon Correlation Spectroscopy Measurements on the PS-PVP$^+$ / SDS System.

Initially the hydrodynamic thickness of PS-PVP$^+$ physisorbed on silica was investigated as a function of adsorbed amount in the absence of surfactant. The Snowtex ZL concentration was maintained at 500 ppm and the polymer concentration varied from 0 - 100 ppm. Assuming only negligible free polymer in solution, 30 ppm polymer would be enough to enable full coverage. These samples provided some unexpected results. Initially the hydrodynamic size

appeared to rise and then with increasing polymer concentration dropped again until it remained relatively constant at beyond 70 ppm of polymer (table 9.4)

Table 9.4; **Hydrodynamic thickness as a function of initial polymer concentration - measured by PCS.**

Sample	Polymer Concentration / ppm	(apparent)δ_h / nm
1	0	0
2	10	59.94
3	20	27.85
4	31	27.74
5	41	16.66
6	51	3.62
7	61	7.56

There could be two possible explanations for this. Firstly this may be an increased viscosity effect. Hence, if the viscosity of the background solution were to increase, then from the Stokes Einstein equation, the apparent radius would decrease. At a first glance it would seen unlikely that such a small concentration of polymer would produce such a appreciable change in viscosity. However, previous work on another polyelectrolyte, (a high molecular weight cationic polyacrylamide) showed that only a 50 ppm polymer solution was enough to double the relative viscosity (although it must be remembered that the PS-PVP$^+$ is much smaller than the polyacylamides being used). Consequently viscosity measurements were performed which showed that at 1000 ppm of polymer there was less than a 5 % increase in viscosity. The other possibility is that perhaps we are looking at polymer in solution rather than the adsorbed polymer. Since one end of the polymer is hydrophobic and insoluble in water it is therefore highly probable that the polymer will form some form of polymeric micelle. If the

hydrophilic charged segment of the polymer is fully extended then it is likely that the size of the "polymer micelle" may be of the order of that to which the PCS is sensitive. This experiment was repeated at lower polymer concentrations (in the range 2 - 20 ppm)and the results tabulated in **table 9.5**

Table 9.5; **Hydrodynamic thickness as a function of initial polymer concentration at low coverage's - measured by PCS.**

Sample	Polymer Concentration / ppm	(apparent)δ_h / nm
12	2	*
13	4	**
14	6	Flocculated
15	8	48.58
16	12	42.84
17	14	12.44
18	16	16.44
19	21	14.36

* Sample 12 appeared to have flocculated although when run the previous day (*i.e.* before equilibrium) had give a size of 330 nm, or hydrodynamic thickness of 104 nm. It is therefore likely that the sample was at this time flocculating and the value of 104 nm is meaningless.

** No decay or correlation function could be obtained for sample 13. This is most likely due to a huge variance in size of species within the sample, probably due to the onset of flocculation.

In order to investigate this phenomena further experiments were performed in the absence of a substrate. The size of the polymer as a function of concentration was measured. It was found that the size of the polymer was independent upon concentration (140 ± 10 nm) up to 7000 ppm and could still be detected at 20 ppm. Salt (NaCl) was added to the PS-PVP^+ solution, the addition of which screens adjacent charges and consequently the polymer may take on

homopolymer behaviour. A 0.25 M salt solution reduced the polymer size in solution from 140 nm to 94 nm. A 0.13 M salt solution resulted in a size of 99 nm.

Finally, SDS was added to the polymer solution. It was anticipated that the SDS could have two opposing effects. Firstly, that the SDS would bind to the polymer resulting in some form of mixed micelle causing an increase in effective size and secondly that the SDS would increase the ionic strength, screening out the charges and the polymer would collapse. All samples were prepared by adding water to a polymer solution and then by adding the SDS. The initial samples prepared covered the region 0 - 11250 ppm SDS in stages of 1125 ppm and all samples flocculated. This was not unexpected since the addition of surfactant would destroy any charge stabilisation of the polyelectrolyte. However, the lowest concentration sample appeared not to have flocculated to such an extent as all of the others. Samples were therefore prepared samples in the range 0 - 1000 ppm. Although these samples did not appear to have flocculated very large polydispersities were recorded suggesting that discrete structures which could be measured easily with this technique were not formed.

9.3.3 Small-Angle Neutron Scattering Measurements.

A very limited study was performed using SANS on these systems. Three samples were prepared.

- Polystyrene latex, PS-PVP^+, in H_20/D_2O contrast matched to the latex
- Polystyrene latex, PS-PVP^+, 3000 ppm mixed SDS in H_20/D_2O contrast matched to the latex
- Polystyrene latex, PS-PVP^+, 45000 ppm mixed SDS in H_20/D_2O contrast matched to the latex

Polymerization sample :
1 % monomer + D2O + 0.125% ammonia + 1% Tegopren 3012

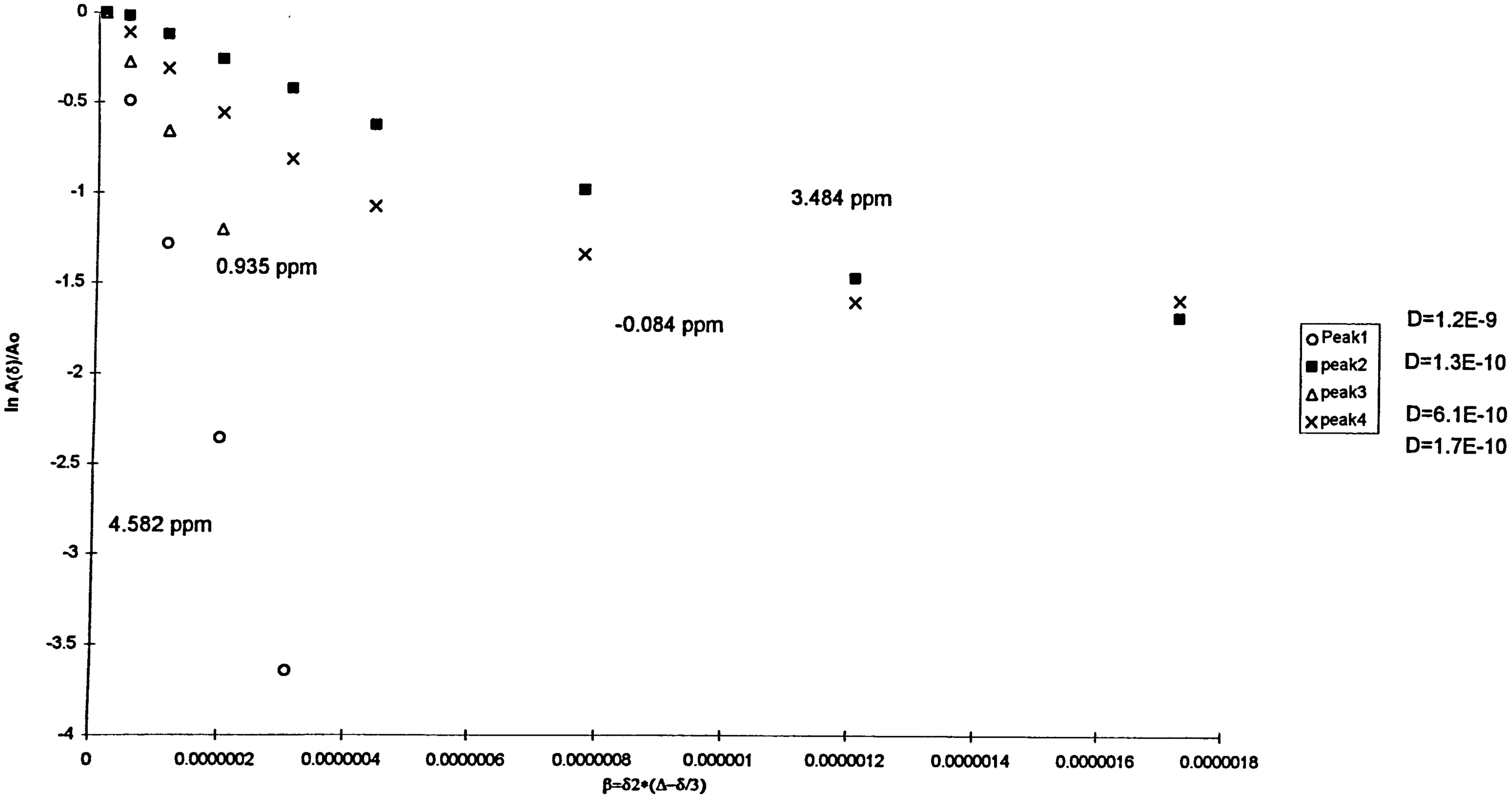

These SDS concentrations were chosen so that the sample with 3000 ppm SDS was close to the normal CMC of SDS and the sample with 45000 ppm SDS had significant excess SDS. These scattering patterns are depicted in **figure 9.12**.

Figure 9.12

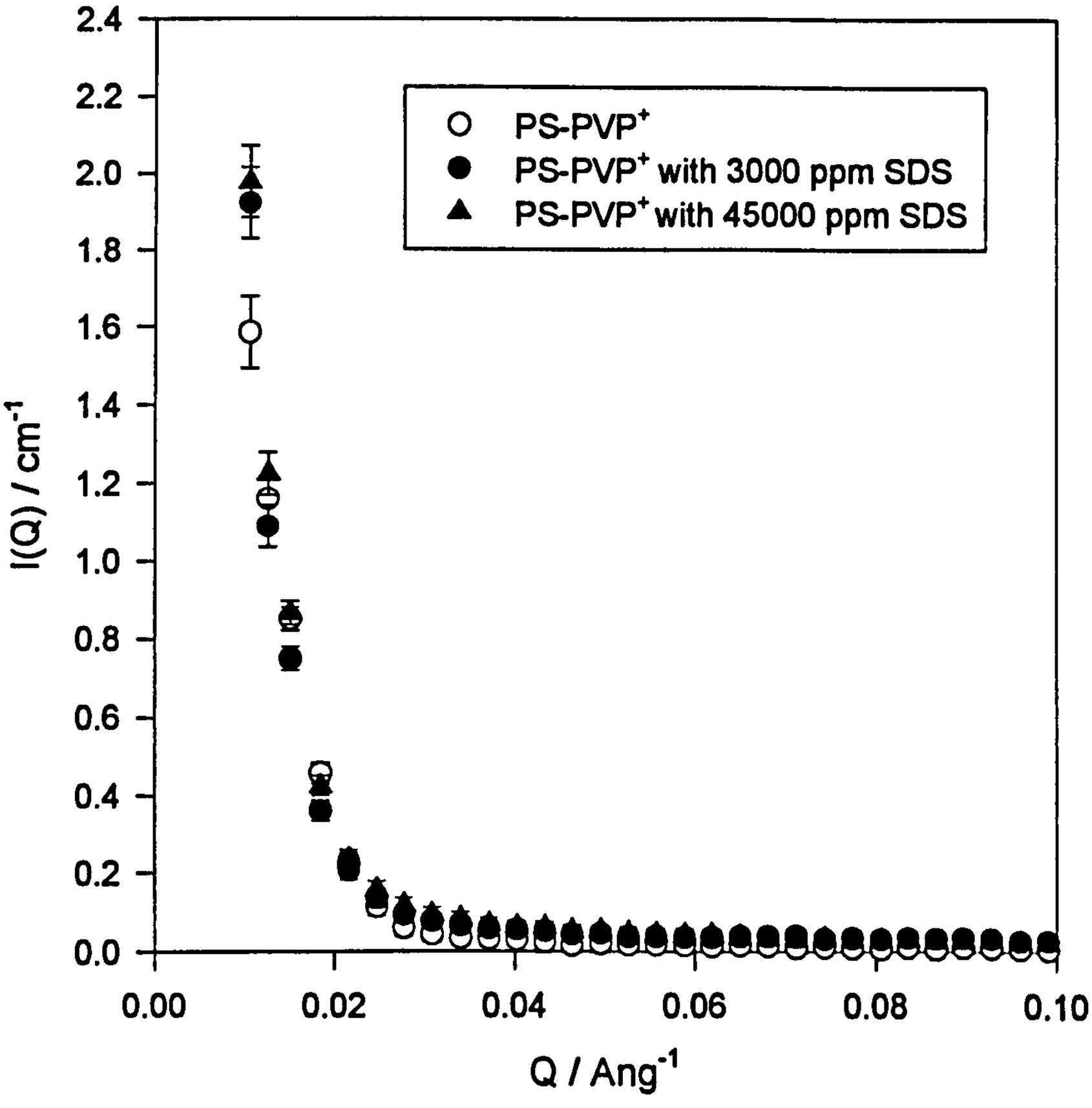

The sample with the highest SDS concentration has the highest scattering intensity and the sample without SDS the lowest scattering intensity. All of the samples terminated in similar incoherent background levels. These data were fitted to a gaussian profile[12] (**Figure 9.13**) and the parameters obtained are presented in **table 9.6.**

Figure 9.13

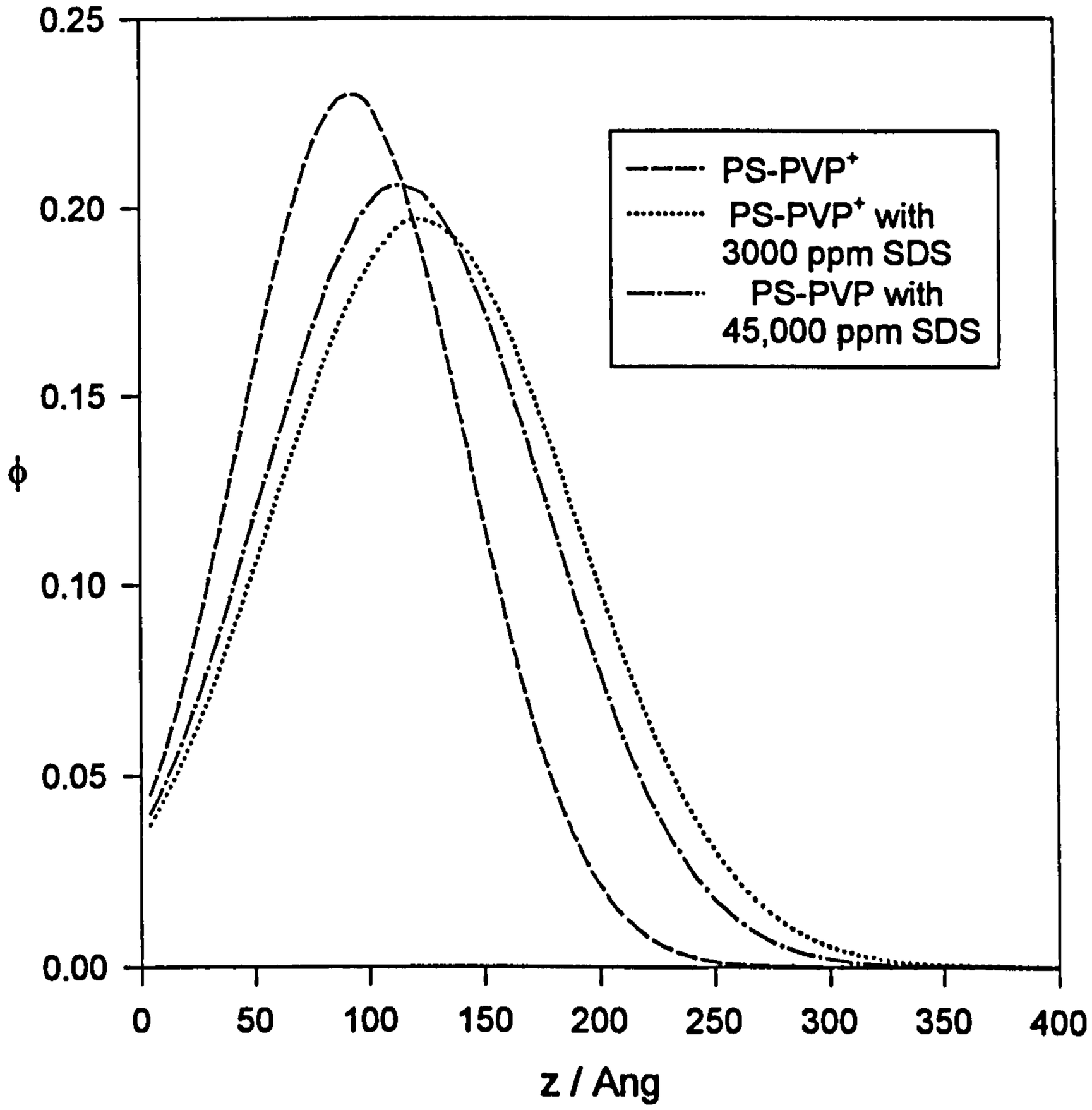

Table 9.6; **Parameters for adsorbed PS-PVP$^+$ as a function of SDS concentration**

SDS Concentration /ppm	0	3000	45000
Gamma / mgm^{-2}	2.9	3.4	3.3
RMS thickness / Å	106	142	131
Second Moment of the layer / Å	46	61	56
Span / Å	196	252	236

Evidently, there is some significant difference in the values of adsorbed amount obtained by UV absorbance measurements and these obtained by SANS, but nevertheless we are able to observe that although the shape of the profile changes significantly upon addition of SDS the adsorbed amount only changes from 2.9 mgm^{-2} to approximately 3.4 mgm^{-2}. There is little difference in the volume fraction profiles on increasing the SDS concentration from 3000 ppm (approximately the normal CMC of SDS) to 45000 ppm SDS (approximately 15 times the normal CMC of SDS) suggesting that the significant changes in the adsorbed layer take place predominately at lower surfactant concentrations. The thickness of the layer is also significantly affected by the addition of SDS, *for example*, the span increasing from 196 Å to 252 Å. If the SDS were to behave as background electrolyte, thus screening out any charges in the adsorbed layer, it may be expected that the layer would collapse. Thus, these data give an indication that the SDS is binding to the adsorbed layer, hence causing the observed expansion.

An alternative, although unlikely, explanation is that the PS-PVP^{+} is behaving as a grafted polyelectrolyte. Increasing the ionic strength can have two opposing effects. Firstly, adding electrolyte may increase the solvency of the polymer (and thus the layer would expand) and conversely adding electrolyte would screen out the charges between adjacent adsorbed chains and the layer may collapse. The net result is that with increasing ionic strength, the value of layer thickness passes through a maximum.

References.

1. Shibayama M., Tanaka T., Han C.; *J. Chem Phys* **1992** 97 6829
2. Cosgrove T., White S. J., Zarbakhsh A., Heenan R. K., Howe A. M.; *Langmuir* **1995** 11 744
3. Porod G.; *Kolloid Zeitschrift* **1952** 124 83
4. Debye P., Beuche A. M.; *J. Applied Physics* **1949** 20 518
5. Debye P., Anderson H. R., Brumberger H.; *J. Applied Physics* **1957** 28 679 1957
6. Schwuger M. J; *J. Colloid Interface Sci.* **1973** 43 491
7. White S. J. *PhD Thesis*, University of Bristol. **1994**
8. Shubin V.; *Langmuir* **1994** 10 (7) 1093
9. Shubin V., Petrov P., Lindman B.; *Colloid & Polymer Science* **1994** 272 1590
10. Guinier A., Fournet G.; *Small Angle Scattering of X-rays. John Wiley, New York* **1955**
11. Hayter J. B, Penfold J; *Molecular Physics* **1981** 42(1) 109

Chapter 10.

Conclusions

10.1 PEO/SDS Systems.

These measurements have shown that the structure of PEO is significantly affected in the presence of SDS, with both the adsorbed amount and structure of the adsorbed layer altering dramatically. The small-angle neutron scattering measurements indicated that the adsorbed amount is reduced by a factor of almost 5 in the presence of SDS around its normal CMC and the resultant layer thickness at this surfactant concentration is negligible. On increasing the surfactant concentration further no information on the layer from the SANS data could be elucidated but the DLS measurements suggested a much larger hydrodynamic thickness of adsorbed layer. The SDS scattering at this concentration indicated two types of SDS moieties; one corresponding to surface SDS and one to SDS bound to polymer adsorbed on the latex.

The proposed model is thus; in the absence of PEO the polymer adsorbs readily to PSL minimising hydrophobic contacts with the solvent. Both entropic and enthalpic factors govern the structure of the adsorbed layer. In the presence of low concentrations of SDS (below the normal CMC) there is an adequate surface concentration of PEO to facilitate the formation of a PEO/SDS complex. However, this is not entropically favourable, nor indeed enthalpically due to electrostatic intermicellar repulsion and the polymer desires. SDS micelles attached to the PEO chain will remain in this state. The shielding of the hydrophobic segments of the chain by the SDS molecules reduce the difference in enthalpy between adsorbed and free polymer and hence adsorption is not as energetically favoured. This sequential desorption increases with increasing SDS concentration. There still remains a nominal adsorbed PEO layer which is tightly

bound to the surface. At very high surfactant concentrations approaching saturation of the polymer the SDS will bind to both the free and adsorbed polymer. Since large concentrations of negative SDS micelles cannot approach the PSL, these micelles are threaded along highly extended, although sparse PEO layers as reflected by the DLS measurements. Significant re-adsorption does not occur. This model is presented schematically in **Figure 10.1**

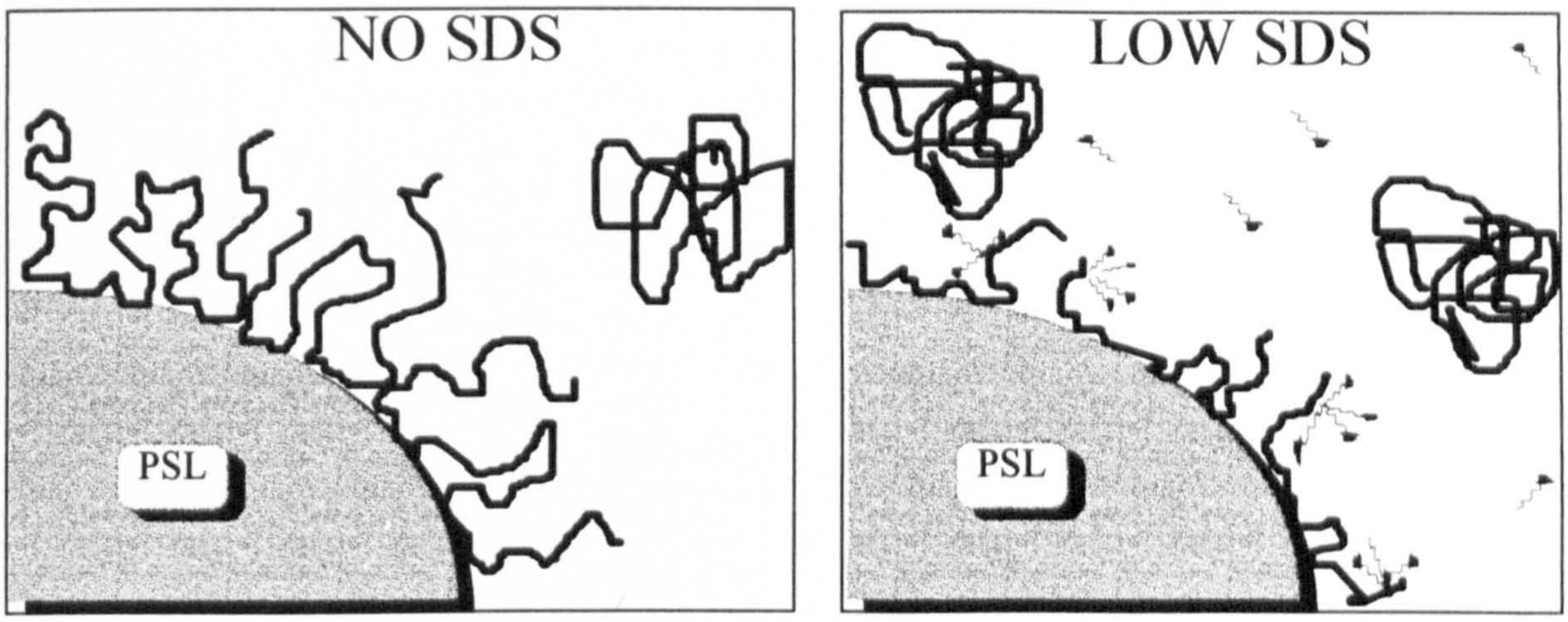

]

10.2 The Structure of SDS Bound to Poly(NIPAM)

Based on measurements of SDS binding, microgel swelling, and neutron scattering reported in this thesis we can speculate as to the structure of

poly(NIPAM) bound SDS. It is proposed that the SDS binds to the hydrophobic propyl groups on the poly(NIPAM) in units containing a small number of SDS monomer units. The aggregation number of the bound SDS depends on surfactant concentration. For 0.3% SDS, the bound surfactant was invisible to neutrons suggesting an aggregation number < 5 whereas for 1% SDS there was weak scattering from closely spaced centres perhaps containing 10-15 SDS molecules. In the case of 1% SDS the binding results showed that there were approximately 6 isopropyl groups for every bound SDS molecule. Thus, structures are possible in which assemblies of 2 to 10 SDS molecules are encased in isopropyl groups, perhaps with the poly(NIPAM) chain in a helical configuration.

Suggestions for further Work

Although we have gained significant insights into the field of polymer/particle/surfactant interactions there is still much to be learned. These are very complex systems and to a large extent the surface has only been scratched. Experiments could be performed at fixed ionic strengths, thus removing any ionic strength effects at high surfactant concentrations. Moreover, in the future several different polymers and surfactants (or indeed mixed surfactants) could be investigated in order to understand these type of systems fully.

More extensive DLS measurements could be performed investigating further the mode of addition of the separate components and the times taken for equilibrium to be reached. Furthermore, this could be complemented with more extensive PFG-NMR measurements involving several initial polymer concentrations and perhaps kinetic studies. The adsorption isotherms could possibly be measured using fluorescence techniques although this will have to be investigated further.

Finally, an interesting alternative could be to look at grafted polymers rather than purely physically adsorbed polymers in order to remove the possibility of polymer

desorption. This would enable the polymer surfactant interaction to be investigated in more detail.

Appendix A.

This appendix contains the raw NMR self-diffusion data on PEO and SDS. In all instances δ is in ms and the value of Δ is 50 ms.

Self-Diffusion of SDS alone

0.1 % w/w SDS

SAMPLE 0.1% SDS
FILENAME SARAH.090-.103
MSD REF NO.
DELTA (DA)= 50 MS
GRADIENT (G)=1000PL

DELTA	ATTN	d*d(D-d/3)
.5	.9784483	12.45833
1	.9310344	49.66667
1.5	.8793103	111.375
2	.8275862	197.3333
2.5	.7327586	307.2917
3	.637931	441
3.5	.5387931	598.2083
4	.4784483	778.6667
4.5	.3577586	982.125
5	.2801724	1208.333
5.5	.2155172	1457.042
6	.137931	1728
6.5	9.482758E-02	2020.958

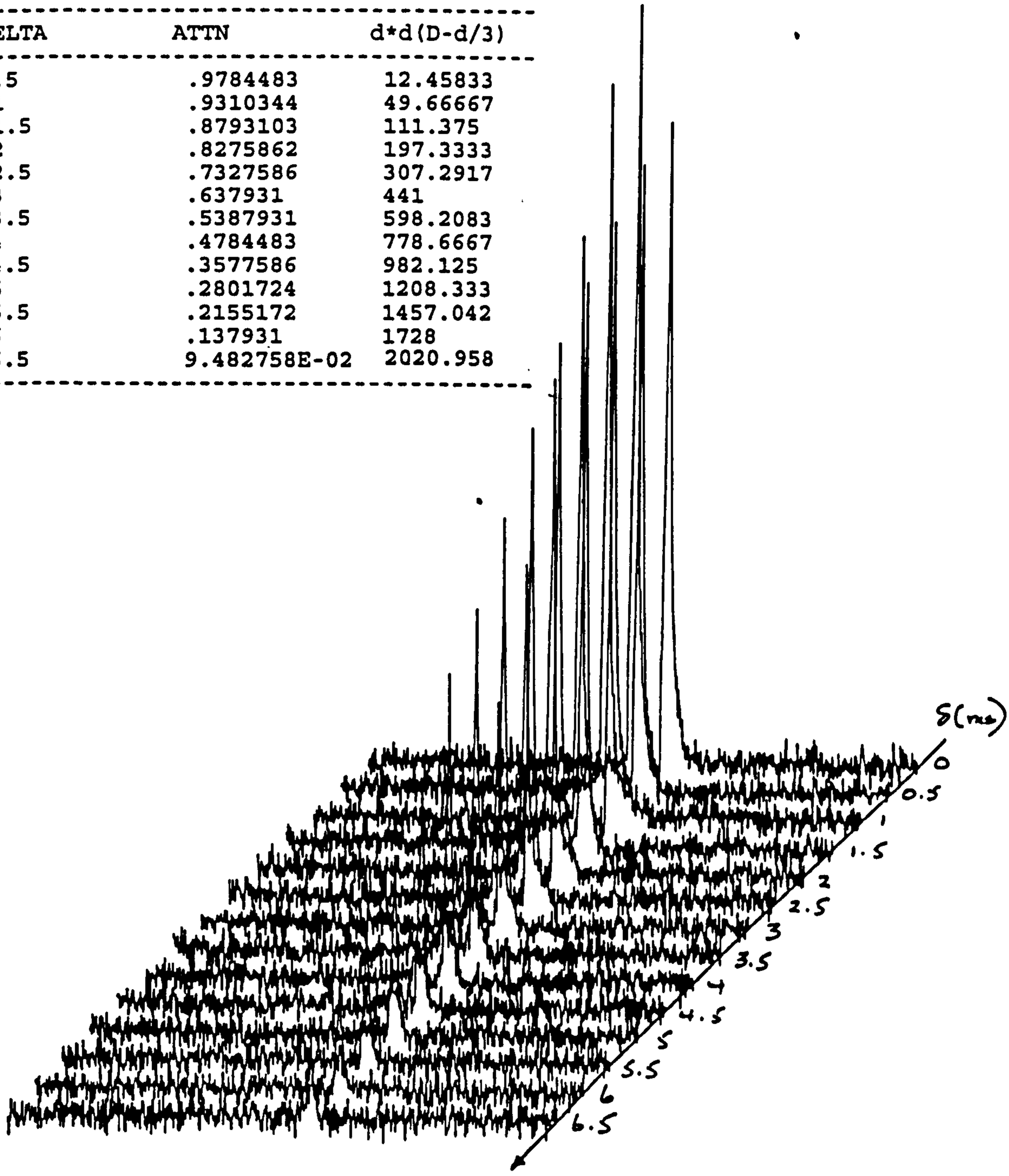

SAMPLE 0.2% SDS
FILENAME SARAH.076-.089
MSD REF NO.
DELTA (DA)= 50 MS
GRADIENT (G)=1000PL

0.2 % w/w SDS

DELTA	ATTN	d*d(D-d/3)
.5	.9779412	12.45833
1	.9338235	49.66667
1.5	.8602941	111.375
2	.8161765	197.3333
2.5	.7132353	307.2917
3	.6029412	441
3.5	.5	598.2083
4	.4191176	778.6667
4.5	.3382353	982.125
5	.2720588	1208.333
5.5	.1985294	1457.042
6	.1470588	1728
6.5	.1102941	2020.958

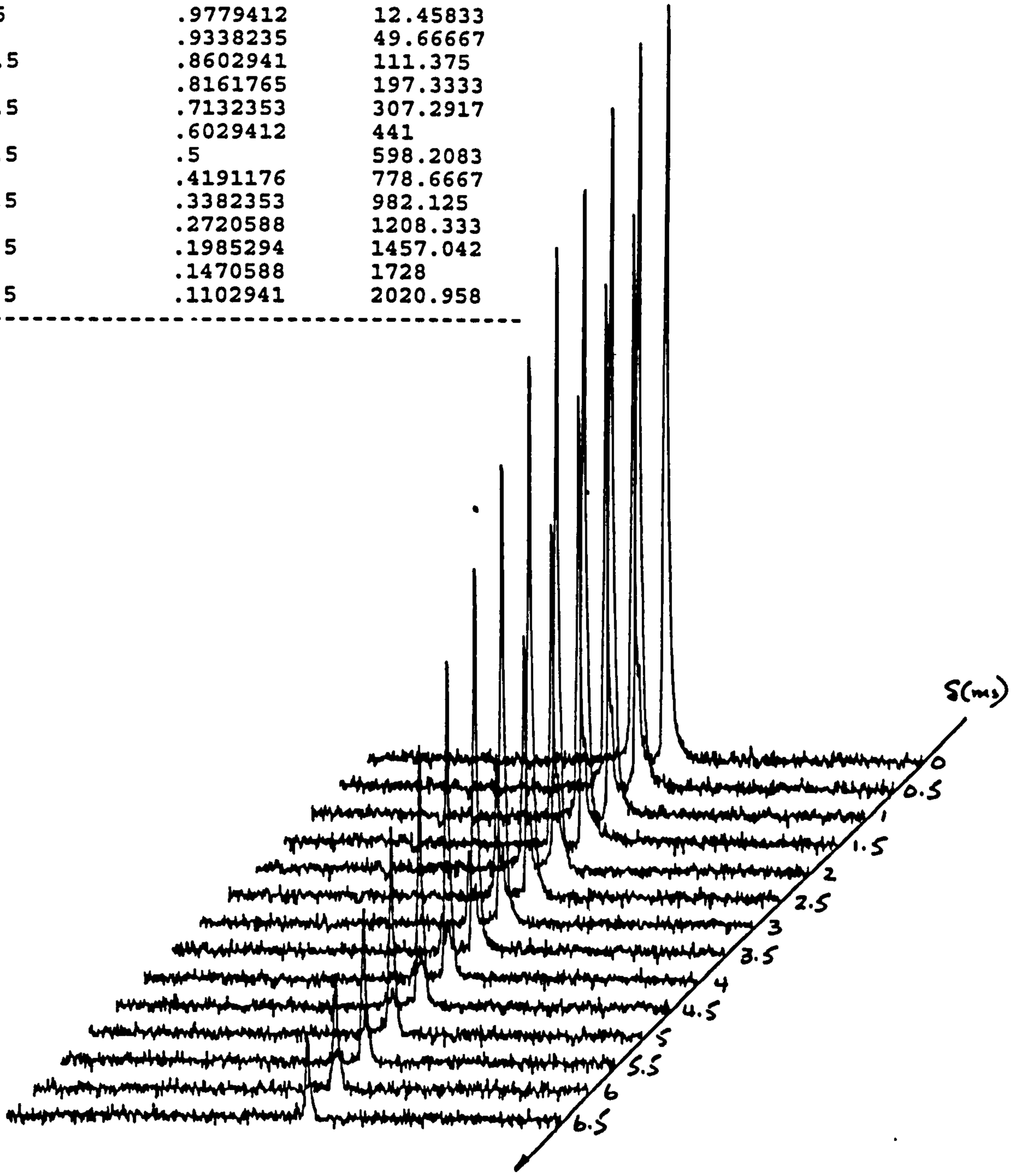

SAMPLE 0.3% SDS
FILENAME SARAH.061-.075
MSD REF NO.
DELTA (DA)= 50 MS
GRADIENT (G)=1000PL

0.3 % w/w SDS

DELTA	ATTN	d*d(D-d/3)
.5	.9705882	12.45833
1	.9313726	49.66667
1.5	.9019608	111.375
2	.872549	197.3333
2.5	.7941177	307.2917
3	.7156863	441
3.5	.6372549	598.2083
4	.5588235	778.6667
4.5	.4607843	982.125
5	.3921569	1208.333
5.5	.2941177	1457.042
6	.245098	1728
6.5	.1960784	2020.958
7	.1470588	2335.667

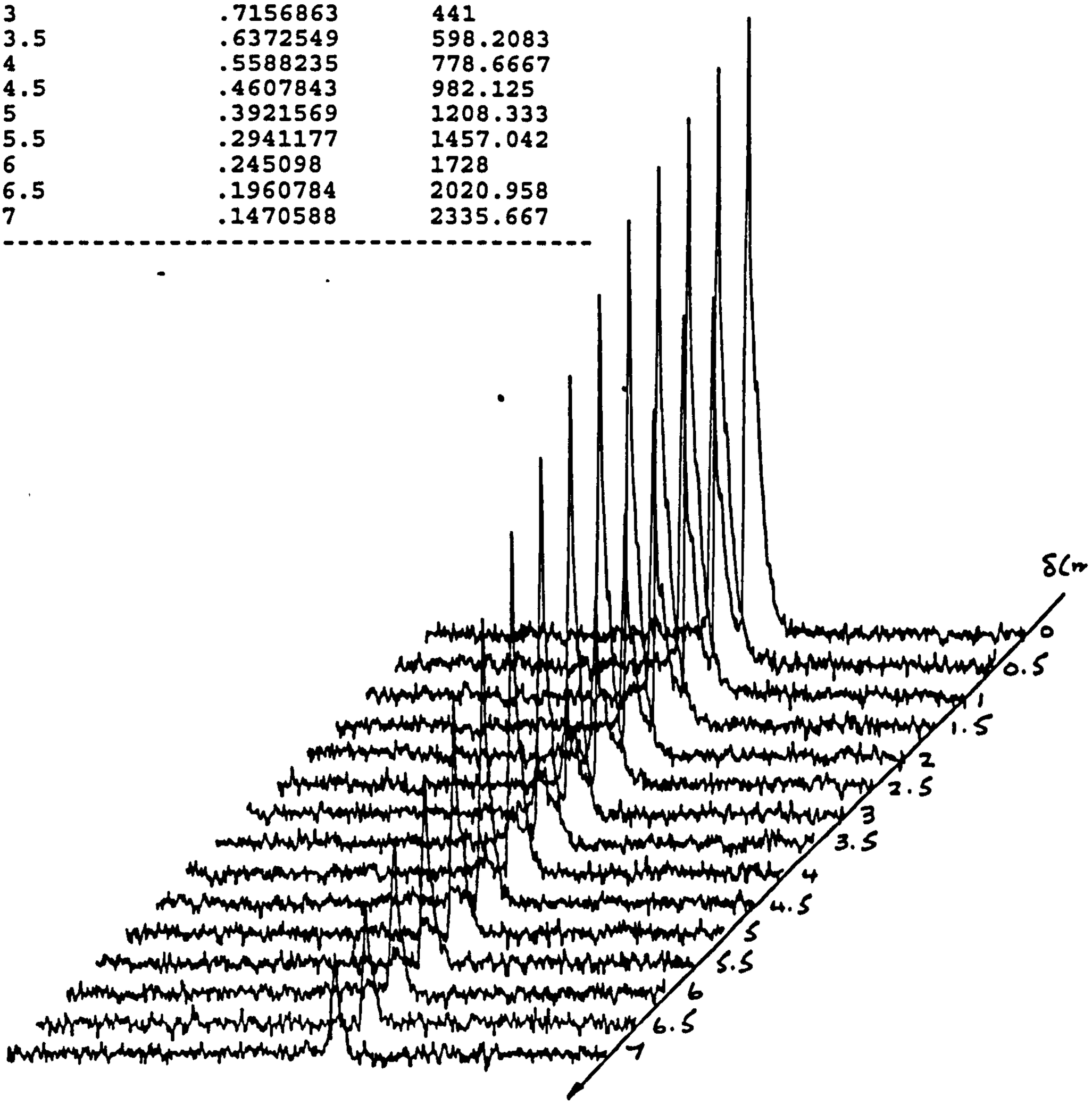

SAMPLE 0.4% SDS

0.4 % w/w SDS

FILENAME SARAH.051-.060
MSD REF NO.
DELTA (DA)= 50 MS
GRADIENT (G)=1000PL

DELTA	ATTN	d*d(D-d/3)
1	.9722222	49.66667
2	.9166666	197.3333
3	.787037	441
4	.6388889	778.6667
5	.462963	1208.333
6	.3425926	1728
7	.2407407	2335.667
8	.1574074	3029.333
9	9.259259E-02	3807

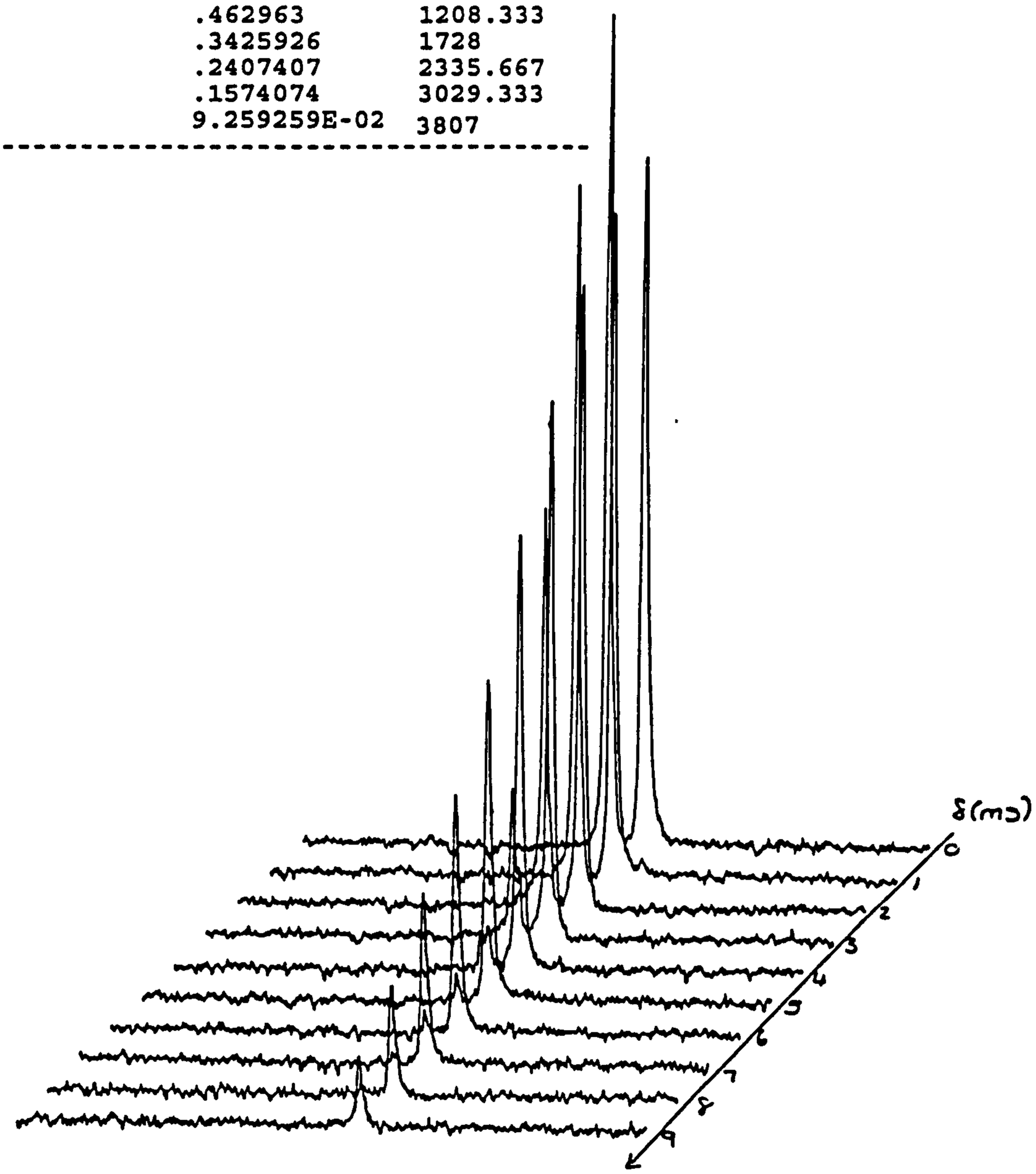

SAMPLE 0.6% SDS
FILENAME SARAH.038-.050
MSD REF NO.
DELTA (DA)= 50 MS
GRADIENT (G)=1000PL

0.6 % w/w SDS

DELTA	ATTN	d*d(D-d/3)
1	.9806201	49.66667
2	.9302326	197.3333
3	.8294574	441
4	.7209303	778.6667
5	.5891473	1208.333
6	.4961241	1728
7	.3720931	2335.667
8	.2713178	3029.333
9	.1937985	3807
10	.1395349	4666.667
11	.1007752	5606.333
12	5.813954E-02	6624

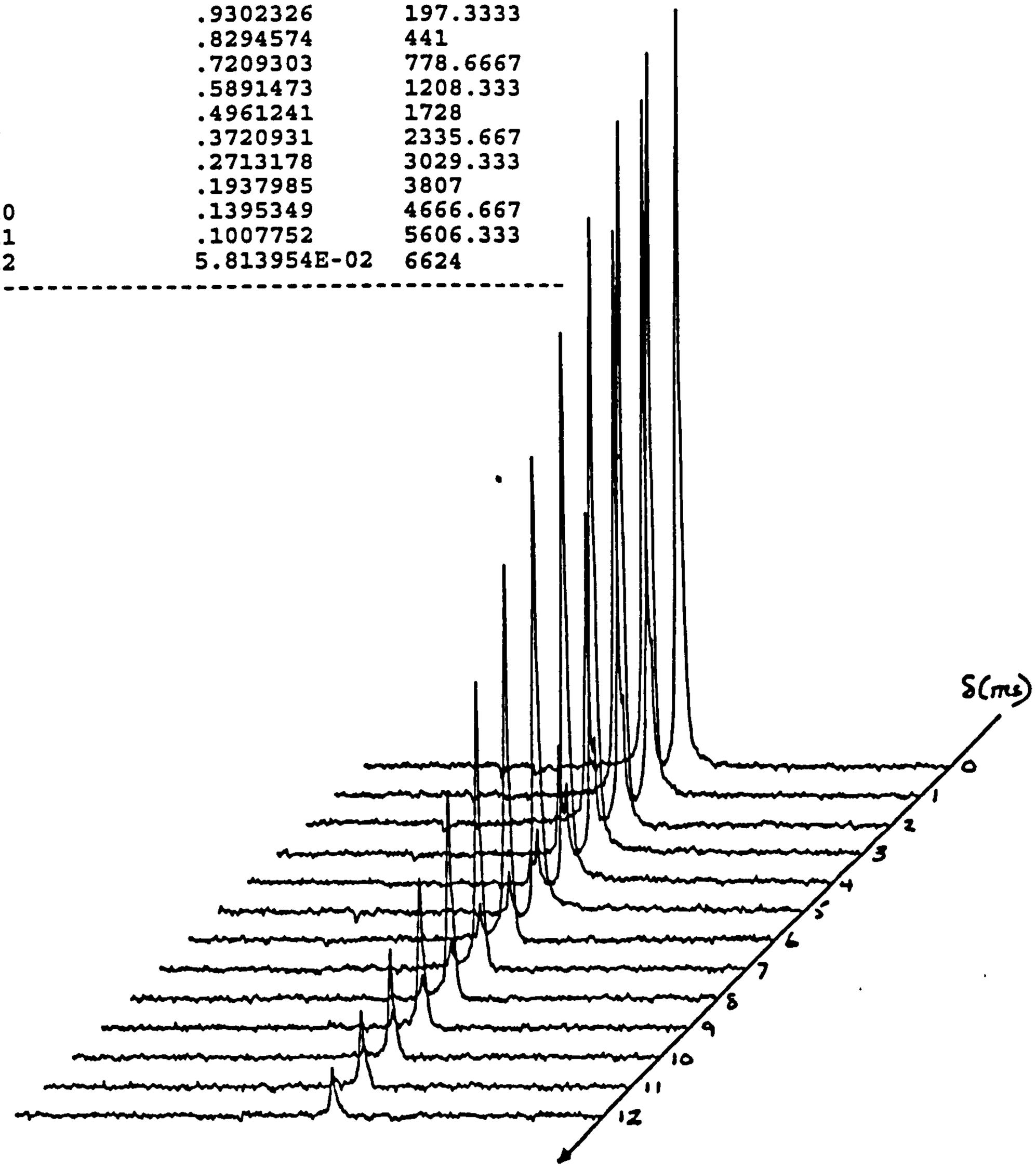

SAMPLE 0.8% SDS
FILENAME SARAH.025-.037
MSD REF NO.
DELTA (DA)= 50 MS
GRADIENT (G)=1000PL

0.8 % w/w SDS

DELTA	ATTN	d*d(D-d/3)
1	.9411765	49.66667
2	.9090909	197.3333
3	.855615	441
4	.7754011	778.6667
5	.6791443	1208.333
6	.5775401	1728
7	.4812834	2335.667
8	.3850267	3029.333
9	.2994652	3807
10	.2245989	4666.667
11	.1604278	5606.333
12	.1176471	6624

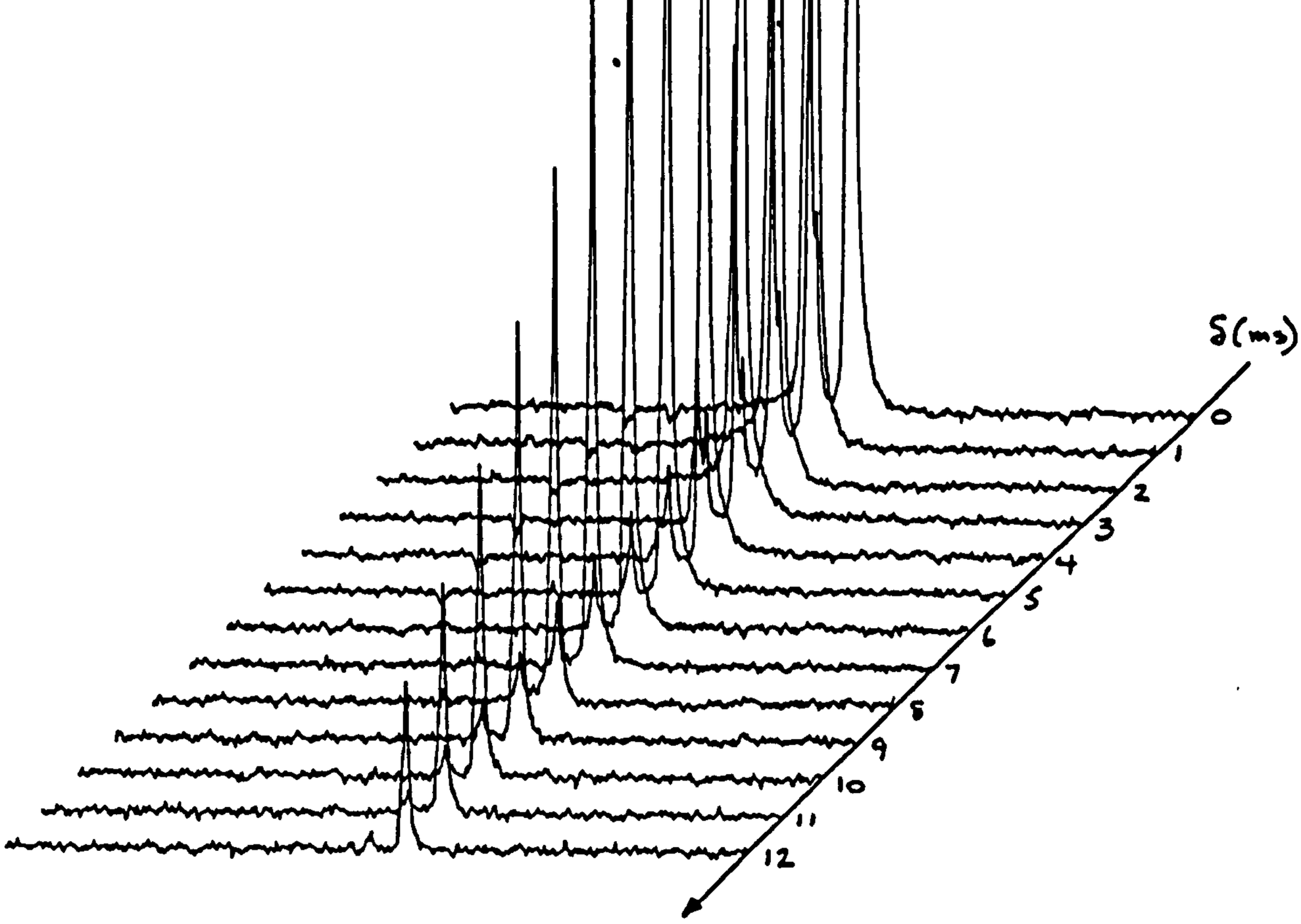

SAMPLE 1% SDS
FILENAME SARAH.012-.024
MSD REF NO.
DELTA (DA)= 50 MS
GRADIENT (G)=1000PL

1.0 % w/w SDS

DELTA	ATTN	d*d(D-d/3)
1	.9712644	49.66667
2	.9367816	197.3333
3	.9482759	441
4	.8275862	778.6667
5	.7413793	1208.333
6	.6436782	1728
7	.545977	2335.667
8	.454023	3029.333
9	.3678161	3807
10	.2873563	4666.667
11	.2241379	5606.333
12	.1666667	6624

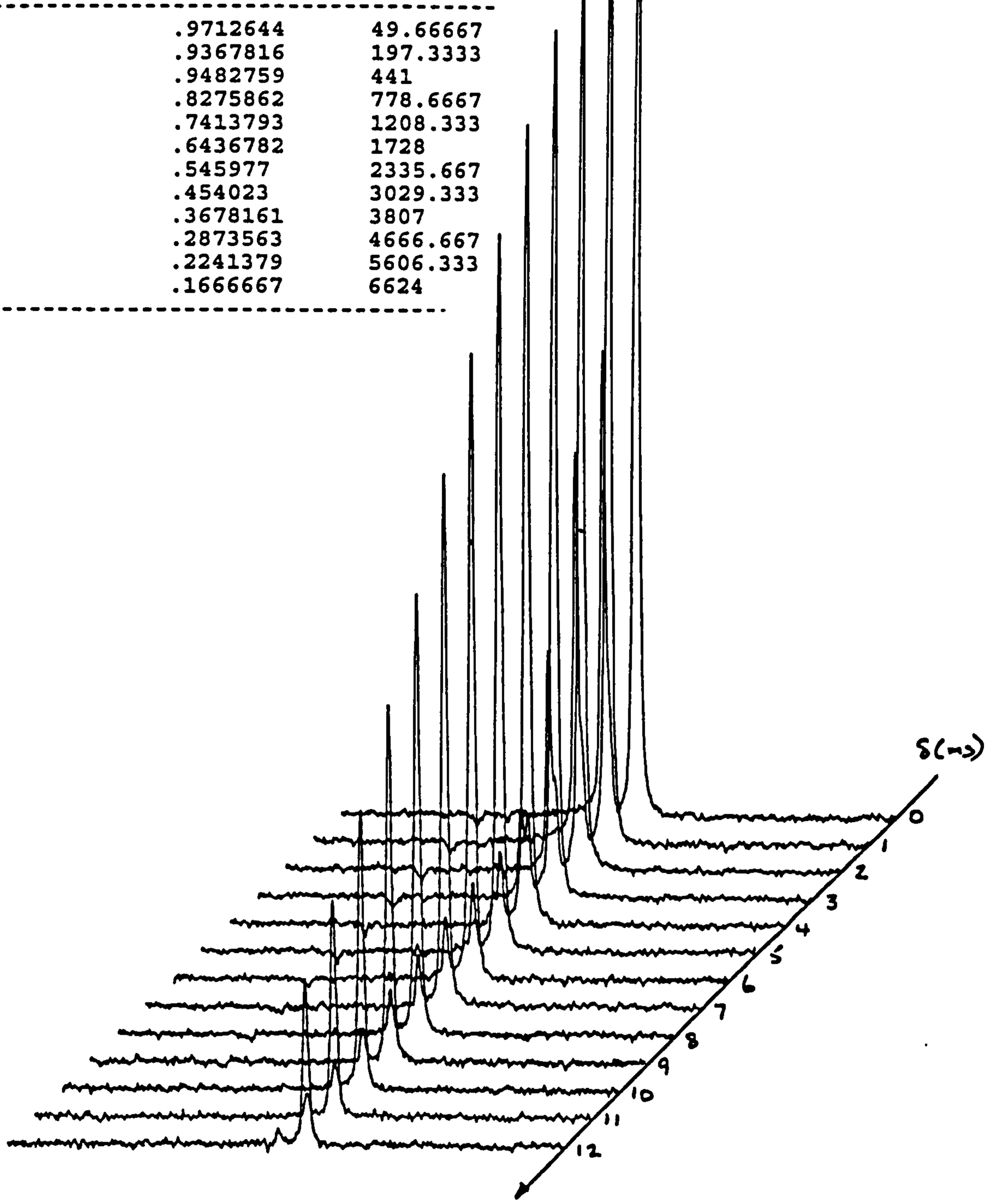

Self-Diffusion of PEO/SDS SDS Data.

0.1 % w/w SDS

SAMPLE 0.1% SDS + 0.5% PEO
FILENAME SARAH.207-.220
MSD REF NO.
DELTA (DA)= 50 MS
GRADIENT (G)=1000PL

DELTA	ATTN	d*d(D-d/3)
2	.86875	197.3333
4	.359375	778.6667
6	.090625	1728
8	.03125	3029.333

0.2 % w/w SDS

SAMPLE 0.2% SDS + 0.5% PEO
FILENAME SARAH.192-.206
MSD REF NO.
DELTA (DA)= 50 MS
GRADIENT (G)=1000PL

DELTA	ATTN	d*d(D-d/3)
2	.9032258	197.3333
4	.6129032	778.6667
6	.3225807	1728
8	.1419355	3029.333

0.3 % w/w SDS

SAMPLE 0.3% SDS + 0.5% PEO
FILENAME SARAH.177-.191
MSD REF NO.
DELTA (DA)= 50 MS
GRADIENT (G)=1000PL

DELTA	ATTN	d*d(D-d/3)
2	.8636363	197.3333
4	.6818182	778.6667
6	.4545454	1728
8	.2727273	3029.333
10	.1363636	4666.667

Self-Diffusion of PEO/SDS PEO Data.

Appendix A.

This appendix contains the raw NMR self-diffusion data on PEO and SDS. In all instances δ is in ms and the value of Δ is 50 ms.

Self-Diffusion of SDS alone

SAMPLE 0.1% SDS + 0.5% PEO
FILENAME SARAH.207-.220
MSD REF NO.
DELTA (DA)= 50 MS
GRADIENT (G)=1000PL

0.1 % w/w SDS

DELTA	ATTN	d*d(D-d/3)
2	.9951456	197.3333
4	.9951456	778.6667
6	.9854369	1728
8	.9466019	3029.333
10	.907767	4666.667
12	.868932	6624
16	.7621359	11434.67
20	.6359223	17333.33
24	.5048543	24192
28	.3883495	31882.67
32	.315534	40277.33
36	.2669903	49248
40	.2038835	58666.67

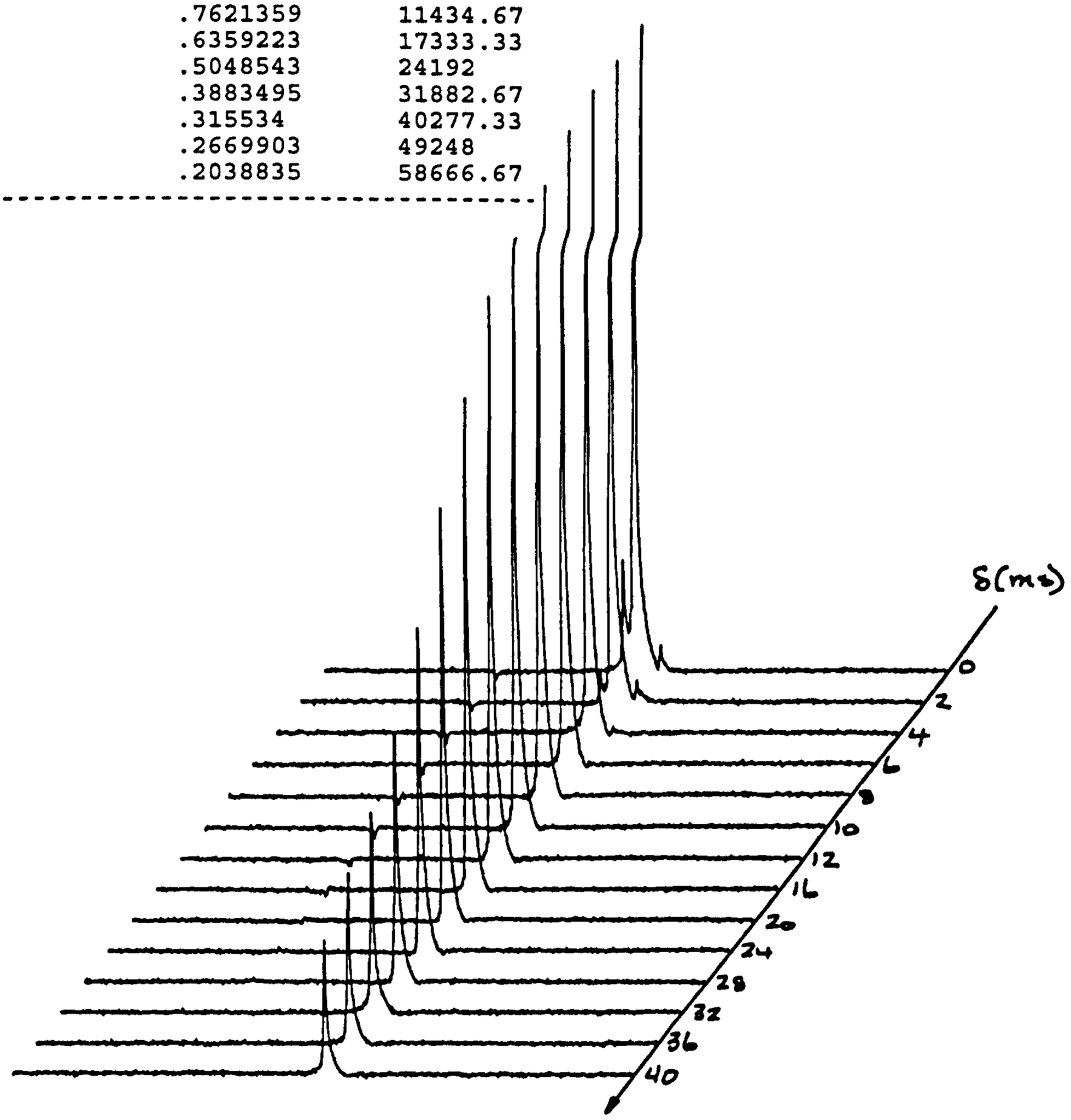

SAMPLE 0.2% SDS + 0.5% PEO
FILENAME SARAH.192-.206
MSD REF NO.
DELTA (DA)= 50 MS
GRADIENT (G)=1000PL

DELTA	ATTN	d*d(D-d/3)
2	1	197.3333
4	.9879518	778.6667
6	.9698795	1728
8	.9457831	3029.333
10	.9036145	4666.667
12	.8554217	6624
16	.7349398	11434.67
20	.6385542	17333.33
24	.5240964	24192
28	.4156626	31882.67
32	.3373494	40277.33
36	.2710843	49248
40	.2228916	58666.67
44	.1686747	68405.33

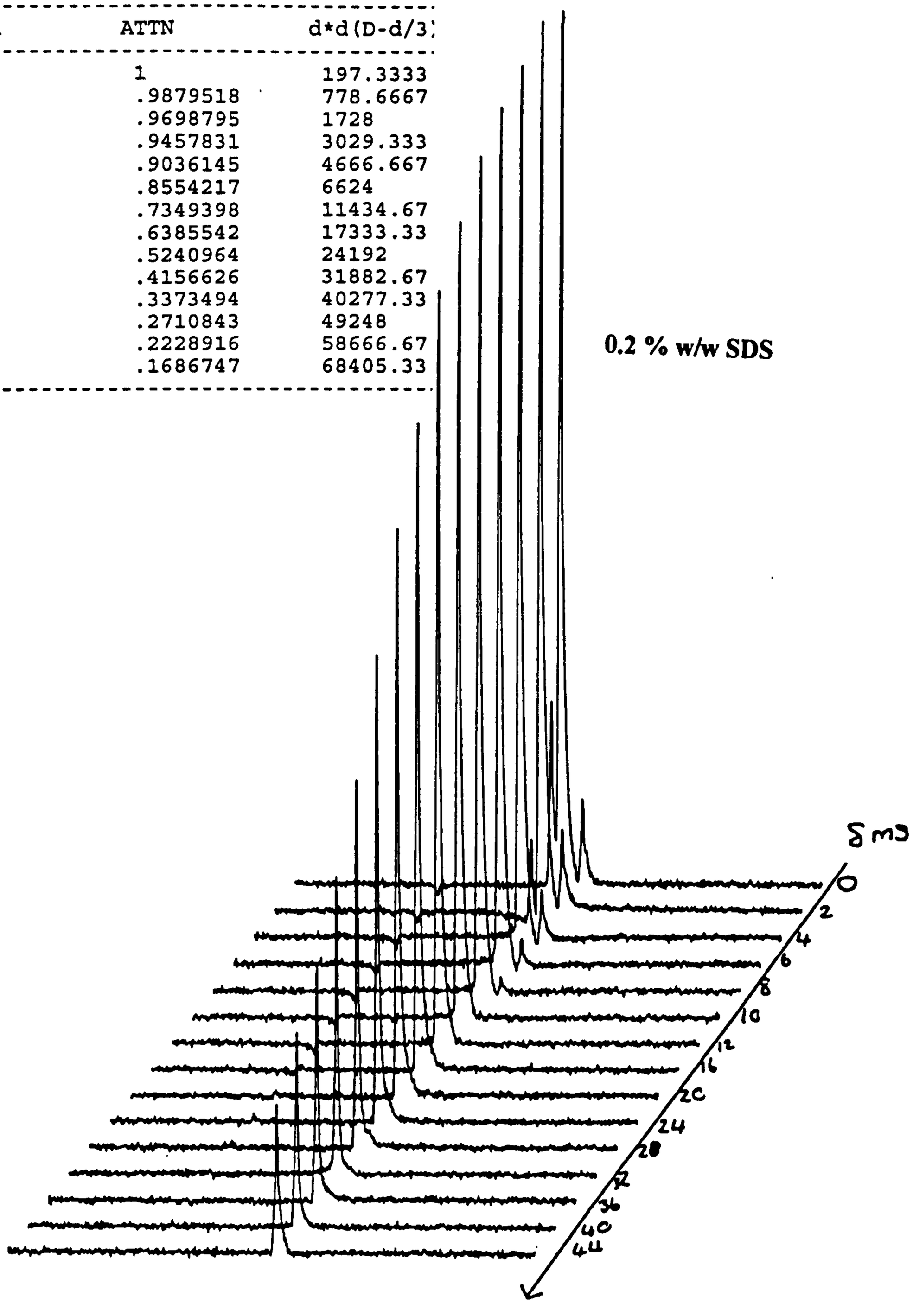

0.2 % w/w SDS

SAMPLE 0.3% SDS + 0.5% PEO
FILENAME SARAH.177-.191
MSD REF NO.
DELTA (DA)= 50 MS
GRADIENT (G)=1000PL

DELTA	ATTN	d*d(D-d/3)
2	.9617835	197.3333
4	.9299363	778.6667
6	.9235669	1728
8	.9108281	3029.333
10	.8789809	4666.667
12	.8343949	6624
16	.7324841	11434.67
20	.6178344	17333.33
24	.5095541	24192
28	.4076433	31882.67
32	.343949	40277.33
36	.2866242	49248
40	.2229299	58666.67
44	.1719745	68405.33

0.3 % w/w SDS

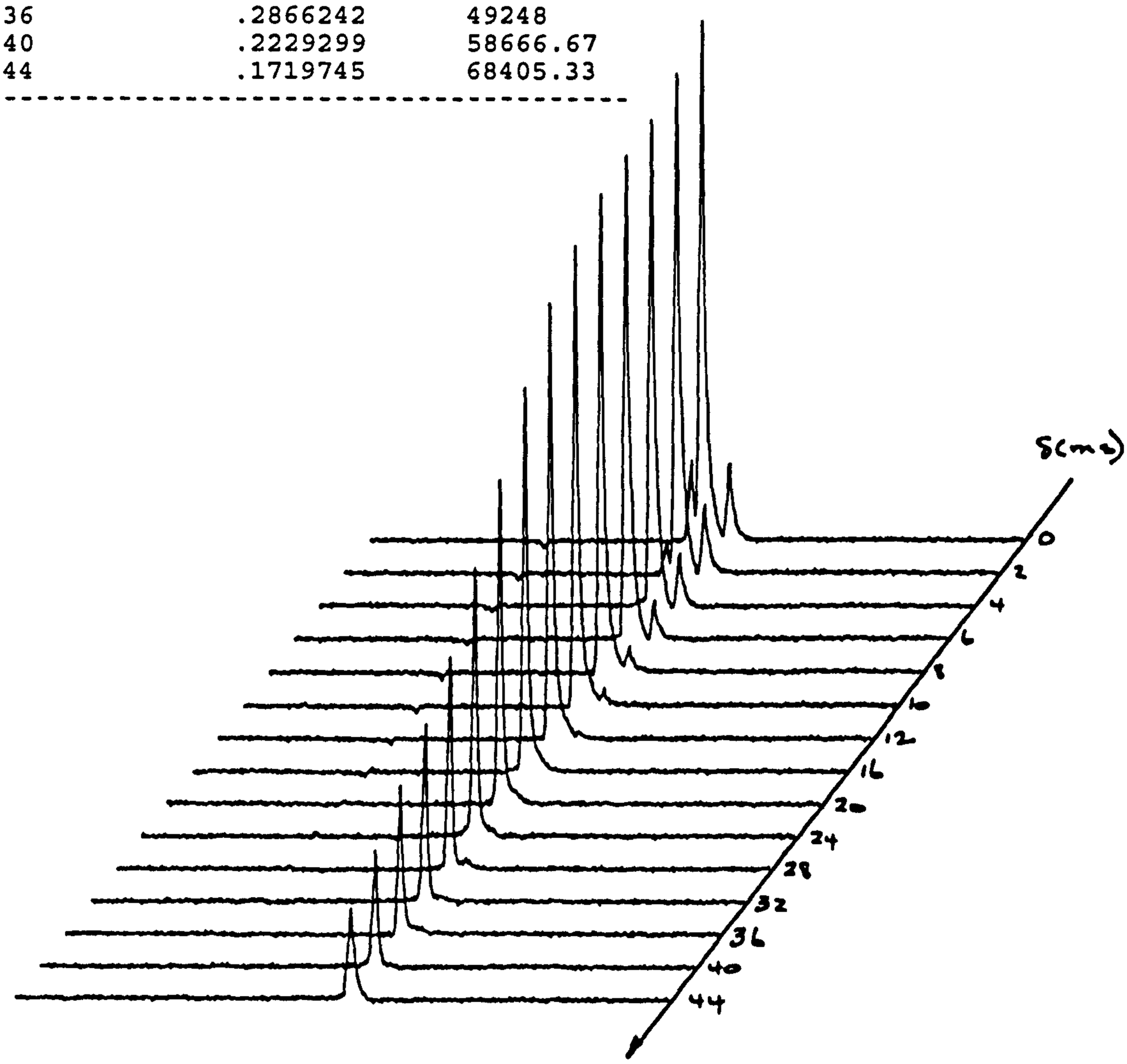

SAMPLE 0.4% SDS + 0.5% PEO
FILENAME SARAH.162-.176
MSD REF NO.
DELTA (DA)= 50 MS
GRADIENT (G)=1000PL

DELTA	ATTN	d*d(D-d/3)
2	.9103773	197.3333
4	.8867924	778.6667
6	.8490566	1728
8	.8160377	3029.333
10	.7877359	4666.667
12	.764151	6624
16	.6933962	11434.67
20	.6367924	17333.33
24	.5660377	24192
28	.5141509	31882.67
32	.4245283	40277.33
36	.3349057	49248
40	.2641509	58666.67
44	.2122642	68405.33

0.4 % w/w SDS

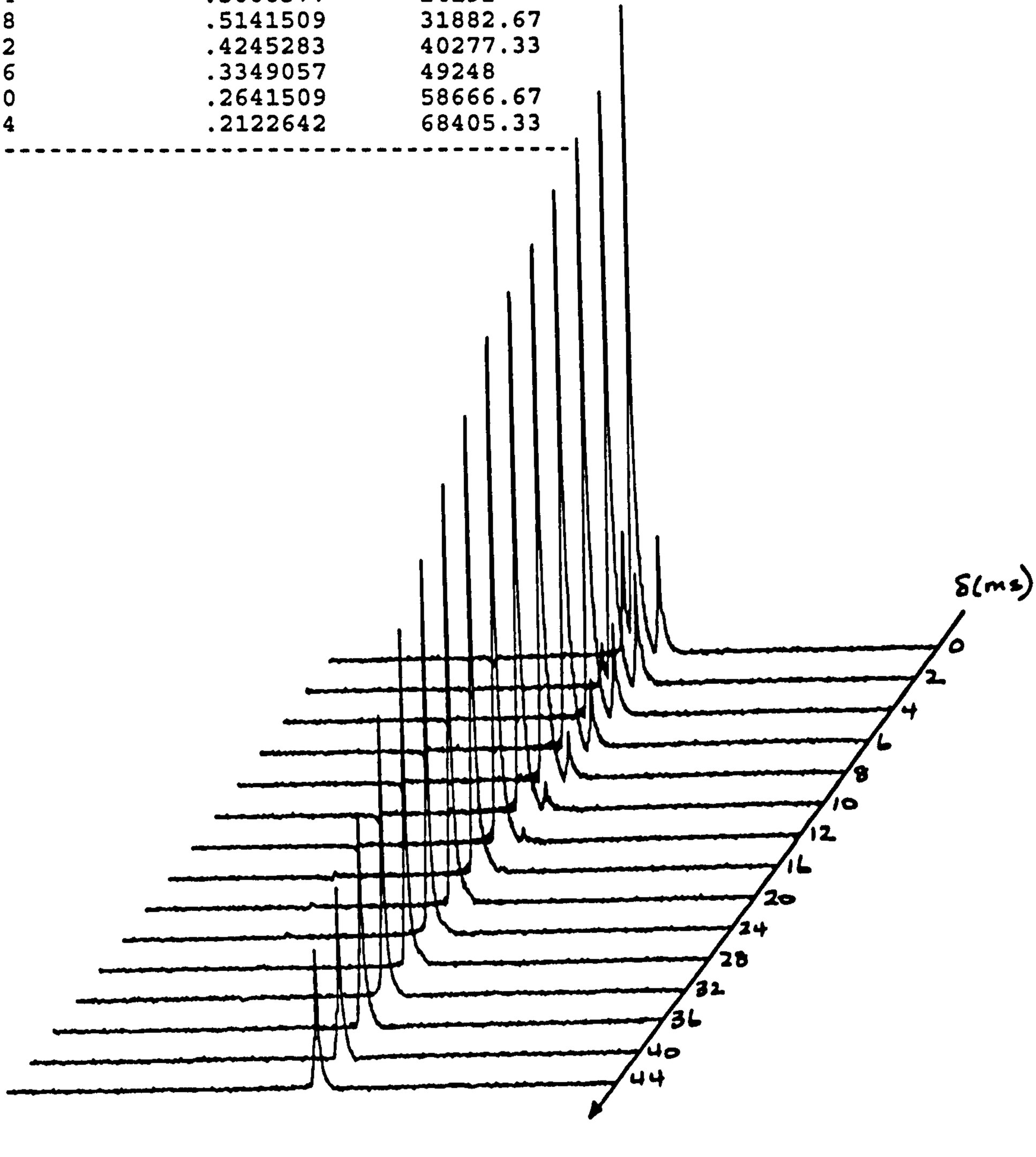

SAMPLE 0.6% SDS + 0.5% PEO
FILENAME SARAH.150-.161
MSD REF NO.
DELTA (DA)= 50 MS
GRADIENT (G)=1000PL

DELTA	ATTN	d*d(D-d/3)
4	.9365854	778.6667
8	1.02439	3029.333
12	.9658536	6624
16	.9170731	11434.67
20	.8292683	17333.33
24	.7414634	24192
28	.5853658	31882.67
32	.5463415	40277.33
36	.4878049	49248
40	.4195122	58666.67
44	.3512195	68405.33

0.6 % w/w SDS

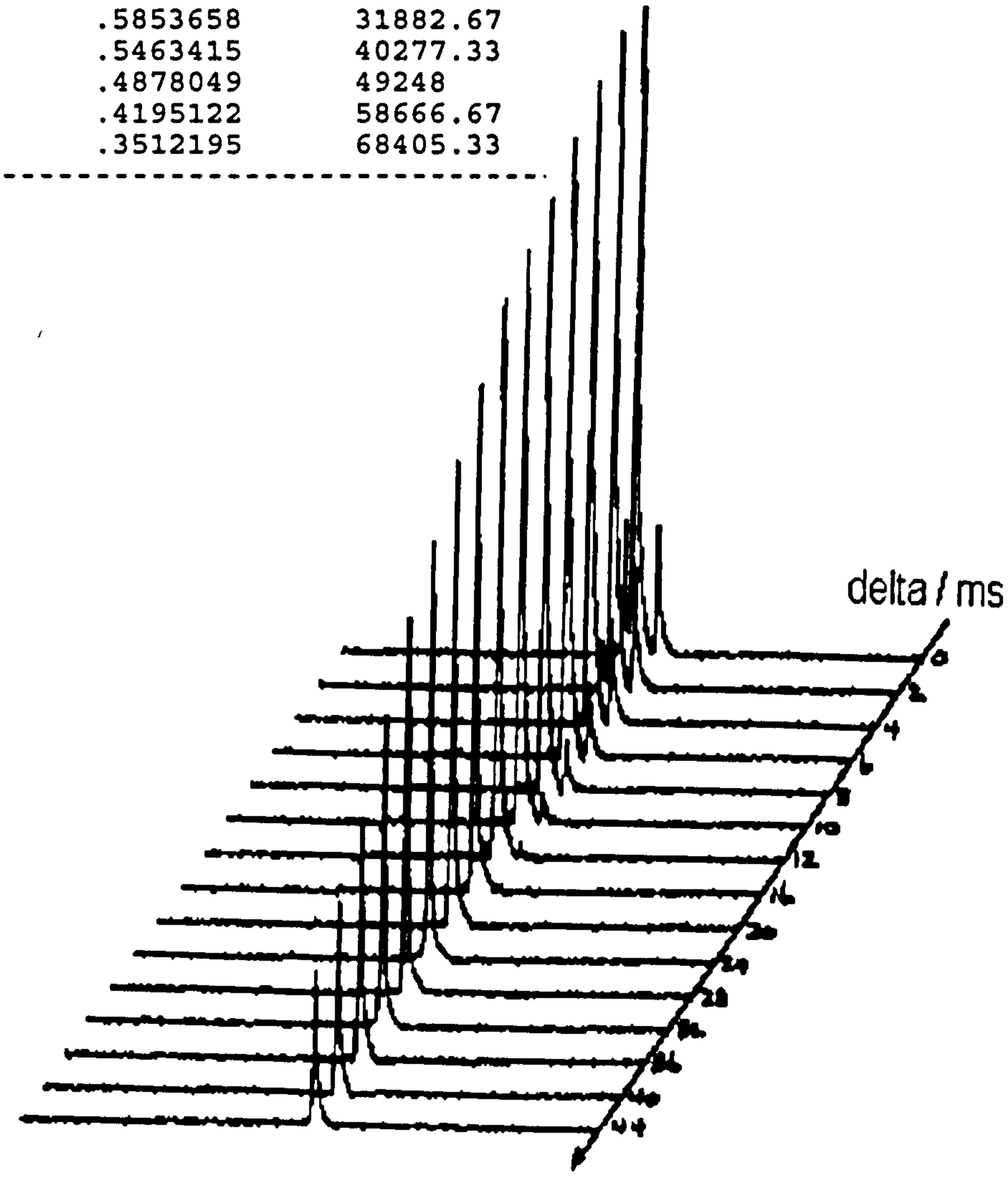

SAMPLE 0.8% SDS + 0.5% PEO
FILENAME SARAH.137-.148
MSD REF NO.
DELTA (DA)= 50 MS
GRADIENT (G)=1000PL

DELTA	ATTN	d*d(D-d/3
4	.98	778.6667
8	.94	3029.333
12	.8533334	6624
16	.7933333	11434.67
20	.6933333	17333.33
24	.5666667	24192
28	.6	31882.67
32	.5266667	40277.33
36	.5	49248
40	.4333333	58666.67
44	.3833333	68405.33

0.8 % w/w SDS

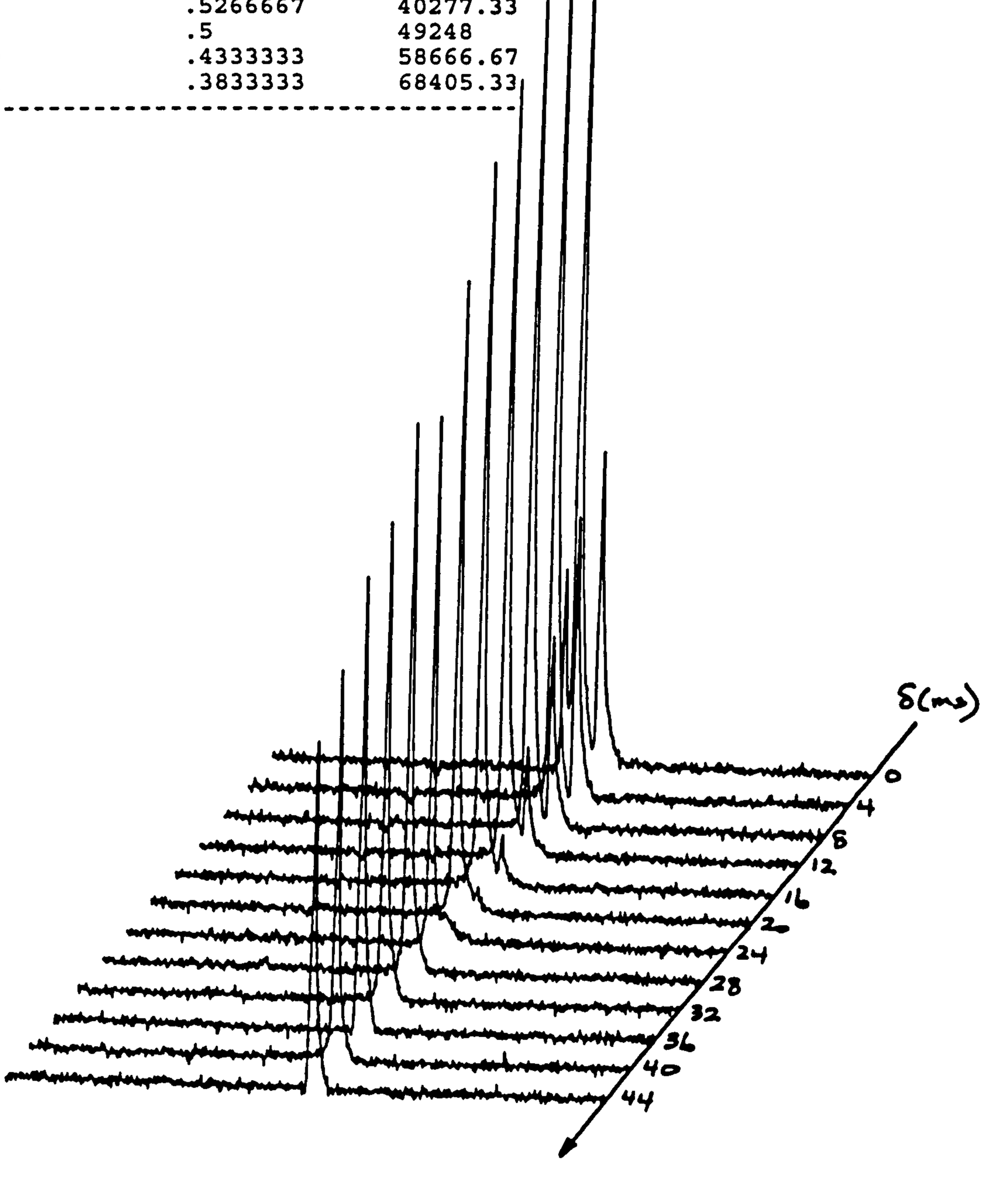

SAMPLE 1% SDS + 0.5% PEO
FILENAME SARAH.125-.136
MSD REF NO.
DELTA (DA)= 50 MS
GRADIENT (G)=1000PL

DELTA	ATTN	d*d(D-d/3)
4	.9859155	778.6667
8	.9859155	3029.333
12	.971831	6624
16	.9366198	11434.67
20	.8661972	17333.33
24	.8028169	24192
28	.7183099	31882.67
32	.6584507	40277.33
36	.584507	49248
40	.5457746	58666.67
44	.4612676	68405.33

1.0 % w/w SDS

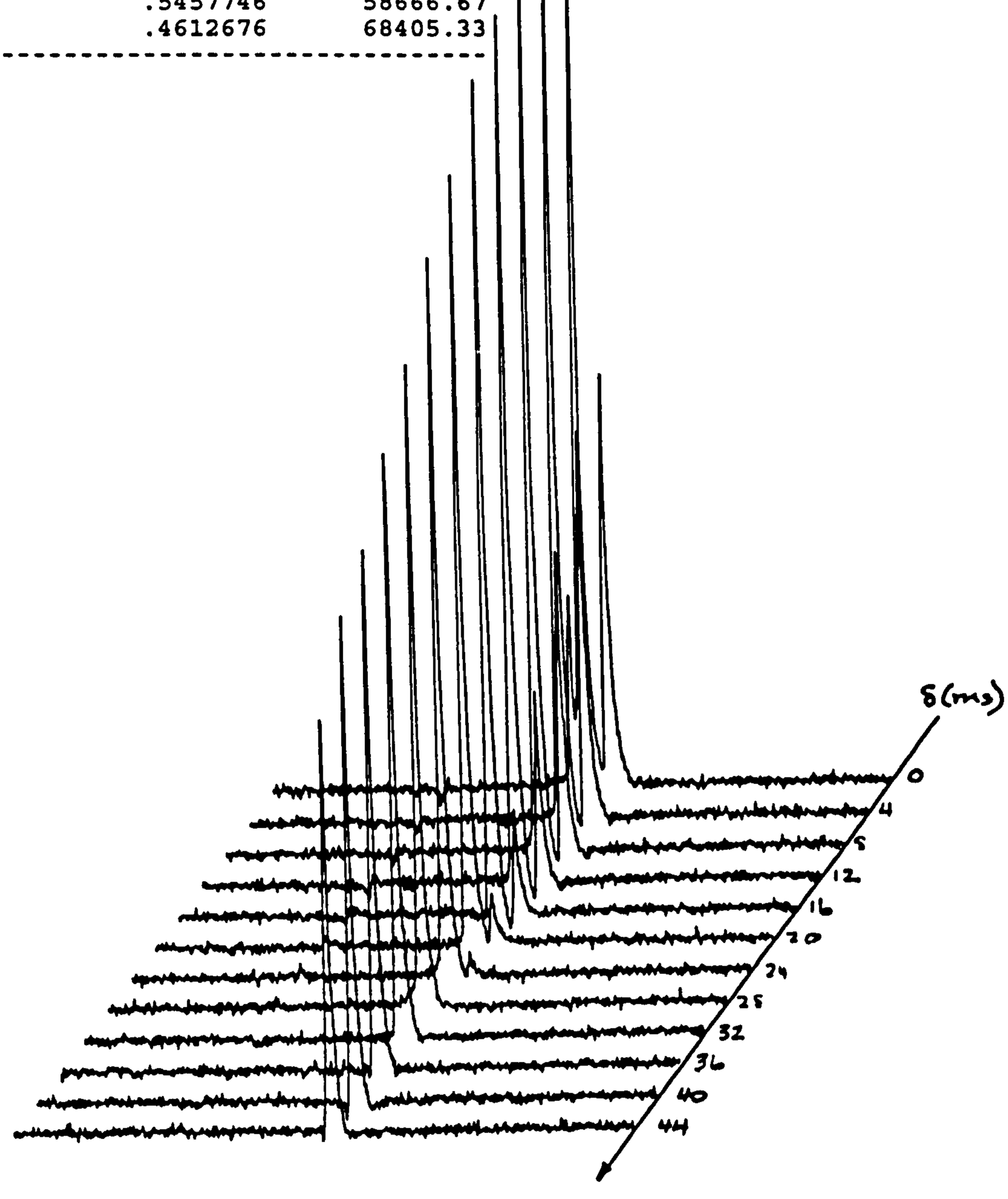

SAMPLE 0.8% SDS + 0.5% PEO
FILENAME SARAH.137-.148
MSD REF NO.
DELTA (DA)= 50 MS
GRADIENT (G)=1000PL

DELTA	ATTN	d*d(D-d/3)
4	.8823529	778.6667
8	.6078431	3029.333
12	.3431373	6624
16	.1470588	11434.67
20	5.882353E-02	17333.33

SAMPLE 1% SDS + 0.5% PEO
FILENAME SARAH.125-.136
MSD REF NO.
DELTA (DA)= 50 MS
GRADIENT (G)=1000PL

DELTA	ATTN	d*d(D-d/3)
4	.9384615	778.6667
8	.7230769	3029.333
12	.4615385	6624
16	.2461538	11434.67
20	.1076923	17333.33
24	4.615385E-02	24192